

***Environmental Systems  
Research FY 2001 Annual  
Report***

*David L. Miller, Program Manager  
Peter M. Castle, Deputy Program Manager*

*January 2002*



# **Environmental Systems Research FY 2001 Annual Report**

**David L. Miller, Program Manager  
Peter M. Castle, Deputy Program Manager**

**January 2002**

**Idaho National Engineering and Environmental Laboratory**

**Idaho Falls, Idaho 83415**

**Prepared for the  
U.S. Department of Energy  
Office of Environmental Management  
Under DOE Idaho Operations Office  
Contract DE-AC07-99ID13727**



# Environmental Systems Research FY 2001 Annual Report

## INTRODUCTION

Welcome to the annual report of the Environmental Systems Research and Analysis (ESRA) program for FY 2001. The ESRA program was initiated in mid-FY 1998 to perform science and engineering research that supports the technical needs of DOE Headquarters' Environmental Restoration (EM) program, as well as other DOE complexwide integration and analysis issues. The Environmental Systems Research (ESR) program portion of ESRA is working to help EM accomplish its mission by establishing the needed technical foundation to deal with both current and anticipated disposition, remediation, and waste management issues.

The ESR program is structured to perform both core and applied research and achieve balance and interaction between these two areas. Core research focuses on understanding environmental processes, developing new tools, and collecting data; applied research is more problem-driven. An increased emphasis on subsurface science at the INEEL accelerated the need for restructuring the ESR portfolio for FY 2001. Instead of five research area themes, there are two major areas—Subsurface Science and Waste Management Science—with supporting tasks (see Figure 1). Figure 1 also includes the Environmental Systems Research Candidates (ESRC) program, which had a one year supplement to the regular ESRA program.

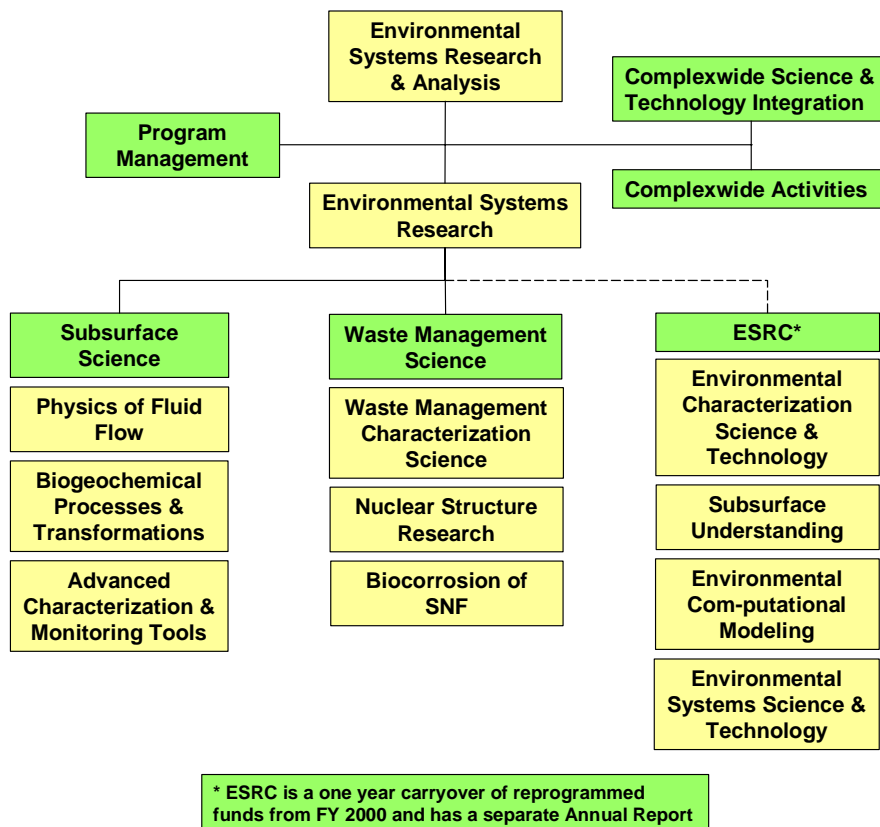


Figure 1. Organization chart of the Environmental Systems Research and Analysis program.

Both ongoing and new research activities were productive for the ESR program during FY 2001. New staff, who focused on applying their particular research expertise to environmental problems, were added to the existing INEEL skill mix, and capabilities in computational modeling and tools for studying contaminant surface interactions were expanded. Research conducted under the ESR program in FY 2001 has resulted in 19 technical papers in print or in press, and a number of others in review or in preparation. The publication activity for FY 2001 was less than for FY 2000, but this was anticipated because the new research activities initiated during FY 2001 are still maturing. Fifty-six presentations were made at professional society meetings.

The Advanced Tensiometer is in demand at numerous sites around the DOE complex and is being deployed by the U.S. Geological Survey and the Department of Agriculture to determine hydrologic gradients in variably saturated vadose zones. An ion trap secondary ion mass spectrometer (IT-SIMS) was designed, fabricated, and deployed at the Test Reactor Area on the INEEL for the purpose of measuring the chemical speciation of radionuclides and toxic metals on the surfaces of environmentally significant minerals. A prompt fission neutron probe and a neutron/gamma probe were developed and deployed into a U.S. Geological Survey

monitoring well and a Pit 9 monitoring well on the INEEL. These probes are designed to determine subsurface radionuclide contents and a range of elements of importance in understanding the fate and transport of contaminants. ESR program researchers are working with three other INEEL programs (Environmental Restoration, Waste Management, and Spent Nuclear Fuel) to understand particular programmatic science needs.

As a result of our continuing relationship with the Subsurface Contaminant Focus Area—started in FY 1999 for the purpose of determining high priority Environmental Management Science Program (EMSP) projects that might be carried forward through the ESR program in FY 2001 and later years—the ESR Candidates program continues to fund one of the EMSP projects, which is working to demonstrate a subsurface remediation technique at the INEEL. There will be ongoing tests to validate this process.

This annual report is an extended summary of the work carried out in the nine research activities that fall under the Subsurface Science and Waste Management Science themes. More detailed discussions of the work can be found in the publications that have resulted from this work, which are listed in the accomplishments section of each report, or by contacting the individual researchers.

# CONTENTS

Environmental Systems Research FY 2001 Annual Report .....	iii
Subsurface Science.....	1
Mesoscale Investigations of Vadose Zone Carbon Cycles .....	3
“Next Generation” Predictive Models of Vadose Zone Flow and Transport .....	29
Temporal and Spatial Characterization of the Vadose Zone .....	53
Investigation of Interfacial Chemistry of Microorganisms.....	65
Geomicrobiology of Subsurface Environments.....	79
Upscaling, Averaging, and Modeling of Coupled Subsurface Processes .....	107
Waste Management Science.....	125
Nondestructive Assay .....	127
Nuclear Structure Data Relevant to the INEEL Mission .....	141
Biocorrosion.....	153



# **Subsurface Science**



# Mesoscale Investigations of Vadose Zone Carbon Cycles

Larry C. Hull and David N. Thompson

## SUMMARY

A better understanding of the physical, chemical, and microbiological processes that affect the movement and transformation of contaminants in the vadose zone is needed to provide more reliable predictions of long-term performance of remedial actions. The objective of this project is to provide a better understanding of the processes controlling the movement of reactive constituents in variably saturated subsurface media (e.g., vadose zone) leading to a higher level of confidence in predictions of the long-term fate of contaminants and design of systems to monitor contaminant migration in the vadose zone. Inorganic carbon is selected as the integrating variable for multiphase and multicomponent vadose zone processes. Inorganic carbon serves as a coupling component among microbial productivity, solution pH, control of mineral-solute interactions, gas phase transport, and dissolved phase transport.

During FY 2001, relations for adsorption of uranium on INEEL sedimentary materials were derived using surface complexation theory. Laboratory adsorption isotherms collected at Clemson University were used to derive thermodynamic constants for the adsorption model. The model was used to predict the range of adsorptive conditions to be expected at the Radioactive Waste Management Complex (RWMC) on the INEEL, but more data are needed to validate the model over the range of expected conditions.

A mesoscale column (3 m high, 1 m diameter) was packed with sediment representative of the RWMC, and instruments to measure moisture and chemical parameters were installed. Carbon dioxide (CO<sub>2</sub>) production was measured in the column during initial dry conditions, and gas diffusion experiments were conducted using the tracer gas sulfur hexafluoride. Water is being

added to the column to increase the moisture content to approximately 70% of saturation. Once the system reaches steady state, one parameter at a time will be perturbed (such as moisture content), and the response of other system parameters (such as gas phase CO<sub>2</sub> concentration) monitored. Contaminants will be introduced to the column, and migration monitored over time.

Methods and equipment to derive a constitutive relation for the dependence of microbial activity on soil matric potential were the subject of work during FY 2001. An unsaturated flow apparatus was used in a range of studies to measure soil hydraulic properties and to dose soil with isotopically labeled food for microbes. Extraction techniques for collecting isotopically labeled CO<sub>2</sub> were developed.

## PROJECT DESCRIPTION

Past industrial practices at DOE facilities included the discharge of liquid wastes to infiltration ponds and cribs, burial of solid wastes in landfills, and inadvertent spills and leaks of contaminants. These planned and unplanned disposal activities have resulted in contamination of the vadose zone. Over the past 12 years, DOE has been working to remediate the contaminants in these areas so they no longer pose a risk to future generations. The only remediation options for much of the radionuclide and metal contamination are to either leave it in place or excavate and move it to a subsurface repository. Either way, it is still buried in the vadose zone, which requires long-term stewardship. At the INEEL, a number of recent records of decision concerning subsurface contamination have chosen to either cap it in place or consolidate it into a subsurface disposal area (SDA; see Table 1). Our current understanding of the movement and transformation of contaminants in the vadose zone is inadequate to accurately predict the long-term performance of such remedial actions. A lack of understanding in

Table 1. Partial list of recent records of decision for the INEEL, which selected capping in place or consolidation of contamination and burial in the vadose zone.

Document and Date	Title	Action Taken
DOE/ID-10719 Oct 10, 1995	Record of Decision for CFA Landfill I, II, and III, Operable Unit 4-12	Cap three industrial waste landfills in place.
INEL-95/0282 Jan 1, 1996	Record of Decision for Stationary Low Power Reactor 1 and BORAX I Burial Grounds, Operable Unit 6-01 and 6-10	Consolidate contaminated surface soil into the existing SL-1 burial ground. Cap two buried reactors in place.
DOE/ID-10586 Dec 22, 1997	Final Record of Decision for Test Reactor Area, Operable Unit 2-13	Leave contaminated sediments under the Warm Waste Pond in place. Consolidate contaminated surface soils into the TRA warm waste pond. Cap the pond.
DOE/ID-10660 Oct 7, 1999	Final Record of Decision for Idaho Nuclear Technology and Engineering Center, Operable Unit 3-13.	Leave contaminated soils in place under buildings, construct a new SDA, and consolidate contaminated soils into the new disposal facility.

physical, chemical, and microbiological processes leads to the use of conservative assumptions in making remediation decisions. In addition to increasing the amount of money being spent on remediation, the conservative assumptions may limit remedial action options. A lack of understanding of vadose zone processes also increases uncertainty in monitoring remedial actions to detect failures in selected remedies quickly enough for action to be taken before contaminant migration becomes significant.<sup>1</sup>

## Project Objectives

The technical objective of this project is to improve our ability to predict the migration of contaminants in the vadose zone under chemically heterogeneous conditions. We can achieve more reliable predictions once we better understand the processes (physical, chemical, microbiological) that affect the movement and transformation of contaminants in the vadose zone, which in turn can lead to a higher level of confidence in predictions of the long-term fate of contaminants and improved system designs for monitoring contaminant migration in the vadose zone.

The long-term fate of vadose zone contaminants will depend on the geochemical environment. Significant system variables include redox potential, pH, mineral surfaces, and water

chemistry. The vadose zone microbial community plays a significant role in defining the geochemical environment, particularly with respect to redox potential and pH. Microbes depend on the physical properties of the vadose zone such as gas-filled pore space. Thus physical, geochemical, and biological components of the system are interrelated. In this project, we employ inorganic carbon as the integrating variable for multiphase and multicomponent vadose zone processes. Inorganic carbon serves as a coupling component among microbial productivity, solution pH, control of mineral-solute interactions, gas phase transport, and dissolved phase transport.

The results of this project will apply directly to DOE needs. Two of the key radionuclide contaminants buried in the SDA at the RWMC on the INEEL are carbon-14 and uranium. Both have been identified as potentially impacting the performance assessment for the burial grounds.<sup>2,3</sup> Experiments being conducted in the mesoscale column and supporting laboratory experiments are designed to better understand the migration of these two contaminants under conditions similar to those expected at the burial ground. Results of this experiment will be constitutive relations and thermodynamic parameters applicable to contaminant transport in the vadose zone. The results will have been validated using INEEL soil materials. Environmental restoration and waste

operations use predictive computer models to assess risk posed by inactive waste sites and active radioactive burial grounds. Once demonstrated as a viable technology, these operations organizations can begin to use this approach in the decision making process.

## Background

The vadose zone is a multiphase region of the subsurface where three phases coexist: a solid phase consisting of mineral grains, an aqueous phase consisting of water and dissolved solutes, and a gas phase. In addition to these three phases, a microbial community exists within the pores of the vadose zone contributing to the biogeochemical environment.

Understanding vadose zone transport and transformation processes requires understanding how contaminants move within these phases, how they partition among the phases, and the chemical reactions that occur within the phases.

## Conceptual Model

The long-term fate of contaminants in the vadose zone will depend on the geochemical environment. Significant system variables include redox potential, pH, microbial community, mineral surfaces, and water chemistry. Both advection of water and diffusion/advection of gases in the vadose zone can transport volatile reactive species. This project focuses on the role inorganic carbon plays in transporting contaminants through the vadose zone. A significant component of this effect will be in the control of pH of advecting vadose zone waters. Inorganic carbon often controls pH in natural waters through reaction with calcite to produce soluble calcium,  $\text{CO}_2$ , and water. Atmospheric levels of  $\text{CO}_2$  are on the order of 350 to 400 ppmv ( $\sim 10^{-3.4}$  atm). Shallow desert soils can have a partial pressure of  $\text{CO}_2$  of 1,000 to 3,000 ppmv ( $10^{-3}$  to  $10^{-2.5}$  atm), while soil gas around waste disposal trenches at the SDA, where organic debris has been disposed, can be as high as 10% by volume (100,000 ppmv or  $10^{-1}$  atm) or higher. This can change the hydrogen ion concentration in soil water by an order of magnitude (see Figure 1).

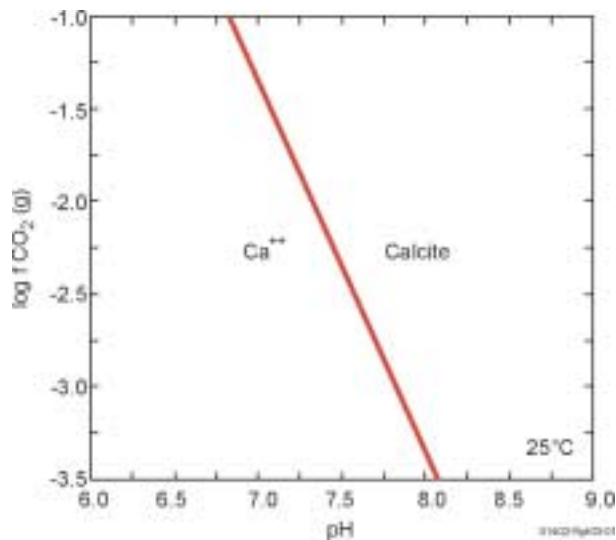


Figure 1. Effect of partial pressure of  $\text{CO}_2$  on the pH of a solution containing 0.001 molar  $\text{Ca}^{++}$  in equilibrium with calcite.

The importance of the increased  $\text{CO}_2$  levels is evidenced in Figure 2, which shows the adsorption of uranium[VI] onto iron oxide as a function of pH. Over the range of pH values readily achieved by the buffer system shown in Figure 1, the percentage of uranium[VI] adsorbed to soil minerals can drop from 95% to 30%. For uranium adsorbed to soil minerals near a waste disposal site, as microbial activity declines with a decrease in the food supply over decades, the partial pressure of  $\text{CO}_2$  will decline, the soil pH will rise, and the uranium may become mobilized. We have developed a simplified conceptual model of the vadose zone (see Figure 3) to illustrate our focus on the inorganic carbon cycle. Plant roots and microorganisms in the vadose zone produce  $\text{CO}_2$  gas by respiration, which enters the unsaturated pores in the vadose zone.  $\text{CO}_2$  is very soluble in water, and so the gas-phase  $\text{CO}_2$  will dissolve in the pore water. Calcium carbonate (the mineral calcite) is a common accessory mineral in soils, and the excess hydrogen ion generated by the dissolution of  $\text{CO}_2$  gas reacts with the calcite to be removed from the pore water solution. Thus, the distribution of  $\text{CO}_2$  among the three phases (solid calcite, gas phase  $\text{CO}_2$ , and aqueous phase dissolved carbonate) buffers the pH of the pore water. The mobility of a contaminant in the vadose zone will depend on the pH and aqueous chemistry of the pore water as well as the presence of surface

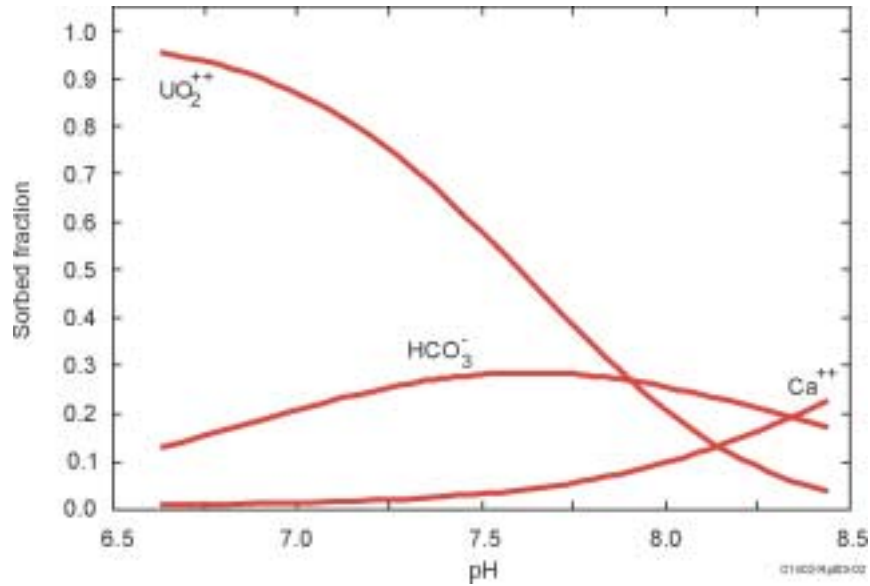


Figure 2. Fraction of system components adsorbed onto iron oxide as a function of pH.

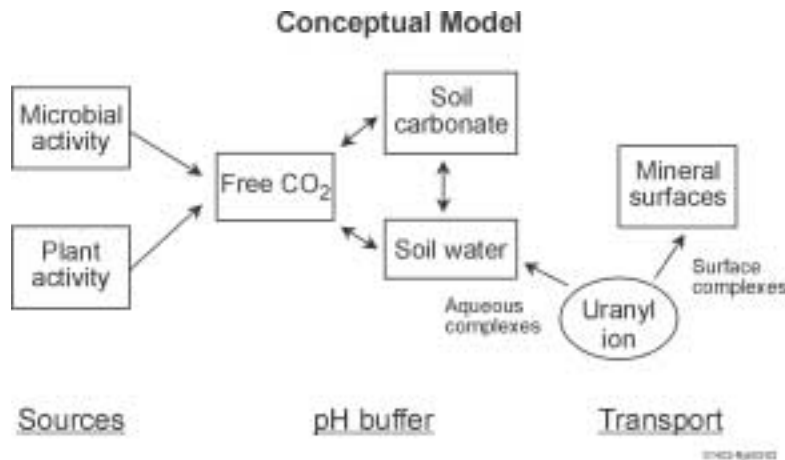


Figure 3. Conceptual model of vadose zone geochemical environment.

sites on mineral grains for adsorption. A uranium[VI] ion (uranyl ion) in the vadose zone will be distributed between surface adsorption sites on minerals and held in the pore water as aqueous complexes (mainly of carbonate ions). The mobility of uranium, therefore, will depend directly on the inorganic carbon cycle.

Significant progress has been made in understanding the production and transport of CO<sub>2</sub> for irrigated agricultural settings,<sup>4</sup> which permits an explicit calculation of CO<sub>2</sub> partial pressure in response to changes in the physical and geochemi-

cal state of the system. Residual contamination at DOE sites will generally be below the root zone; therefore, we will neglect plant roots as a source and sink of CO<sub>2</sub>, and focus on microbial production as affected by water and salt contents.

### Approach

Our general project approach is to start with a hypothesis of a constitutive or thermodynamic relation that defines how an important process within the conceptual model (such as CO<sub>2</sub> production or contaminant retardation) depends on

material properties (such as moisture content). Controlled experiments are conducted in laboratory microcosms, small laboratory columns, and a flow-through centrifuge to gather data from which parameters of the constitutive relations can be determined. While the laboratory work proceeds, computer algorithms are developed expressing the constitutive relations. The algorithms are used to modify or amend existing computer models such as PHREEQC, UNSATCHEM, or HYDROGEOCHEM, which currently incorporate many of the important processes. Mesoscale experiments are used to gather coupled data from systems where multiple processes occur at scales that approach the field scale, yet maintain controlled boundary conditions. Finally, field data are analyzed, so that conditions under which laboratory and mesoscale experiments are conducted represent field conditions.

Three activities were conducted in FY 2001: adsorption of uranium on sediments, microbial activity as a function of moisture potential, and multiphase transport of contaminants. Key environmental variables that control the activity of microorganisms in the subsurface are the availability of water and water borne nutrients. In addition to water stored in the gross interstitial voids between particles, significant volume may be accounted for in pores within the particles. We hypothesize that: (1) At very low water contents, water in unsaturated soil becomes unavailable for microbial use because the bulk of the remaining water is held in pores too small to be reached by microorganisms; and (2) At very high water contents, microbial activity is limited by the diffusion of oxygen through pores mostly filled with water. We are developing a constitutive relation between microbial activity and matric potential. This will be derived from the measured relationship between microbial activity and available water, which depends on the pore size distribution, and from the measured matric potential at each water content. This is a significant improvement over the current approach to modeling microbial activity in soil, which assumes that all soil water is available to the microbes.

Adsorption of reactive contaminants onto minerals is a surface area phenomenon and we

need to know how contaminants adsorb to the surfaces and how adsorption is affected by solution chemistry. Approaches to retardation based on empirical coefficients, either mass based  $K_d$  or surface area based  $K_A$ , still require significant assumptions concerning uniformity in soil properties and water composition. More sophisticated approaches are needed that allow us to relax the assumptions of constant geochemical conditions. Surface complexation models are based on the assumption that the formation of complexes with functional binding sites on mineral surfaces is analogous to the formation of aqueous complexes in bulk solution. The diffuse-layer model is one of the simplest of the surface complexation models that can still account qualitatively and quantitatively for the observed variation in experimental data.<sup>5-7</sup> The diffuse-layer model is also the model currently incorporated into the readily available geochemical computer simulation codes such as PHREEQC,<sup>8</sup> and Geochemist's Workbench®.<sup>9</sup>

Mesoscale experiments are being conducted in a 3-m-high  $\times$  1-m-diameter column packed with sediment. A vacuum applied at the bottom of the column induces water movement under unsaturated conditions. The column is instrumented with measurement devices and sampling ports to measure matric potential, water content, water chemistry, gas composition, and temperature. Additional instrumentation can be installed as needed or developed. The system will be brought to steady state, one parameter at a time will be perturbed (such as moisture content), and the response of other system parameters (such as gas phase  $\text{CO}_2$  concentration) monitored. Contaminants will be introduced to the column, and migration monitored over time. Uranium[VI] and carbon-14 will be the focus of the modeling and transport experiments because they are radionuclides of concern for waste operations and environmental remediation at the INEEL and other DOE sites.

## Adsorption of Uranium on Soils

Much of the work on adsorption to date has been conducted on single minerals in a laboratory setting.<sup>10-13</sup> Natural soils are made up of a number

of minerals, each of which can have multiple binding sites. It is not clear how complex mineral assemblages behave with respect to adsorption. One approach is to treat the soil as a black box, and measure an adsorption isotherm on the soil. The adsorption isotherm is fit to the specific adsorption model by empirically creating sites. This approach was applied successfully to zinc adsorption at a field test site on Cape Cod by the U.S. Geological Survey.<sup>14</sup> The alternative approach is to treat the soil as a mixture of individual minerals, and model adsorption as the physical mixing of the individual mineral phases (Reference 6). The approach we are currently attempting to implement is the first approach—to fit models to adsorption data without attempting to link adsorption to specific sites.

Using the theoretical equations for adsorption of metals onto mineral surfaces, a generalized equation can be derived to describe adsorption. Data on the adsorption of uranium onto INEEL sedimentary material, collected for the INEEL Environmental Restoration Program by Clemson University, was used to develop thermodynamic constants for the theoretical equation that could be used to model uranium transport at the SDA.

## Adsorption

Partitioning of dissolved constituents between an aqueous phase and solid minerals in soils and sediments is affected by three factors: a thermodynamic binding constant, the number of adsorption sites available, and the solution chemistry of the aqueous phase. Partitioning has commonly been described by a very simple empirical partition coefficient that simply relates the total concentration of a dissolved species to the total concentration of the adsorbed species:

$$K_d = \frac{C_{ads}}{C_{sol}} \quad (1)$$

where:

$K_d$  = empirical partition coefficient at equilibrium (mL/g)

$C_{ads}$  = concentration of parameter on the solid (mg/g, pCi/g)

$C_{sol}$  = concentration of parameter in solution (mg/mL, pCi/mL).

A site specific  $K_d$  partition coefficient can be measured under conditions appropriate to a specific location (solution chemistry and number of adsorption sites), and applied under those conditions to that location. The empirical  $K_d$  cannot be applied if conditions change, nor can it be applied at a different location. The  $K_d$  approach also does not account for the number of adsorption sites available.

The Langmuir adsorption isotherm was developed to include the concept that there are a finite number of adsorption sites on a sediment or mineral surface. The Langmuir isotherm is<sup>15</sup>:

$$C_{ads} = \frac{\alpha\beta C_{sol}}{1 + \alpha C_{sol}} \quad (2)$$

where:

$\alpha$  = an adsorption constant related to the binding energy (mL/g)

$\beta$  = maximum solute that can be adsorbed by the surface (mg/g, pCi/g).

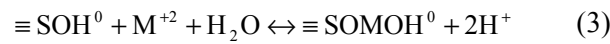
The Langmuir isotherm accounts for the limited number of adsorption sites available, but still includes an empirical adsorption constant that is dependent on solution chemistry. A mechanistic approach that incorporates a theoretical understanding of the factors that affect partitioning is needed so that changes in environmental conditions can be taken into account.

A class of adsorption models referred to as surface complexation models have evolved to describe adsorption of solutes to the surfaces of minerals. These surface complexation models incorporate the following principles:

- The sorbing mineral surface is composed of specific adsorption sites that react chemically with the solute to form chemical complexes analogous to the formation of aqueous complexes

- The adsorption reaction can be described by a chemical mass action expression
- The surface charge of the mineral surface is a function of chemical reactions with the adsorption sites
- An equilibrium constant expression can be written for the chemical reaction and is described by a thermodynamic equilibrium constant.

Adsorption can be described by a chemical mass action expression:



where:

$\equiv \text{SOH}^0$  = surface adsorption site (moles/L)

$\text{M}^{+2}$  = concentration of free metal ion in solution (moles/L).

An equilibrium constant expression can be written for the mass action expression given by Equation 3:

$$\frac{[\equiv \text{SOMOH}^0][\text{H}^+]^2}{[\equiv \text{SOH}^0][\text{M}^{+2}]} = K_{\text{int}} \exp\left(\frac{\Delta z F \psi}{RT}\right) = K_{\text{ads}} \quad (4)$$

where:

$$\exp\left(\frac{\Delta z F \psi}{RT}\right) = \text{Boltzman factor (unitless)}$$

$\Delta z$  = change in charge on surface during reaction (C)

$F$  = Faraday constant (J/volt equivalent)

$\psi$  = surface potential (volts)

$R$  = gas constant (8.3143 J/mole °K)

$T$  = temperature (°K)

$K_{\text{int}}$  = intrinsic thermodynamic equilibrium constant

$K_{\text{ads}}$  = effective thermodynamic equilibrium constant.

The Boltzman factor can be considered equivalent to an activity coefficient for the adsorption sites (Reference 15). For the purpose of developing this analytical equation, we will assume activity coefficients equal 1. For implementation within a geochemical reaction code, this simplification will be removed, and activity coefficients will be explicitly calculated using Debye-Huckel theory. For the adsorption reaction in Equation 3, there is no net change in surface charge, and so the Boltzman factor is zero in this particular instance. Equation 4 can be rearranged and solved for the concentration of the adsorbed metal ion:

$$\equiv \text{SOMOH}^0 = \frac{K_{\text{ads}} [\equiv \text{SOH}^0][\text{M}^{+2}]}{[\text{H}^+]^2} \quad (5)$$

The total number of adsorption sites on the soil is the sum of the uncomplexed surface sites and the sum of the surface sites that have formed surface complexes with cations ( $C_i$ ):

$$S_t = \equiv \text{SOH}^0 + \sum_i \equiv \text{SOC}_i \text{OH}^0 \quad (6)$$

Separating the surface complex for the metal of interest from the sum, Equation 6 gives:

$$S_t = \equiv \text{SOH}^0 + \equiv \text{SOMOH}^0 + \sum \equiv \text{SOC}_i \text{OH}^0 \quad (7)$$

Equation 7 can be used to replace  $\equiv \text{SOH}^0$  in Equation 5 giving:

$$\equiv \text{SOMOH}^0 = \frac{K_{\text{ads}} [S_t - \equiv \text{SOMOH}^0 - \sum \equiv \text{SOC}_i \text{OH}^0][\text{M}^{+2}]}{[\text{H}^+]^2} \quad (8)$$

Rearranging and combining terms for the concentration of adsorbed metal ion gives:

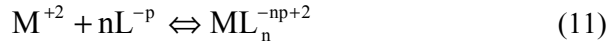
$$\equiv \text{SOMOH}^0 = \frac{K_{\text{ads}} (S_t - \sum \equiv \text{SOC}_i \text{OH}^0)[\text{M}^{+2}]}{1 + \frac{K_{\text{ads}}}{[\text{H}^+]^2} [\text{M}^{+2}]} \quad (9)$$

The concentration of metal in Equation 9 is the free metal ion concentration in solution, not the total metal concentration. Some of the metal may be bound up in aqueous complexes. The total metal ion concentration is given by the sum of the

concentrations of the free metal ion and the metal ion complexes:

$$M_t = [M^{+2}] + \sum ML_n^{-np+2} \quad (10)$$

The formation of each metal ligand can be described by the mass action expression:



An equilibrium constant expression for each ligand can be written:

$$\frac{[ML_n^{-np+2}]}{[M^{+2}][L^{-p}]^n} = K_L \quad (12)$$

so the ligand concentration can be calculated from:

$$[ML_n^{-np+2}] = K_L [M^{+2}] [L^{-p}]^n \quad (13)$$

The approach is generally applied to trace metals or radionuclides in solution, and so the metal ion concentration should generally be low. At low concentrations, the predominant metal-ligand complexes will contain only one metal ion. Substituting Equation 13 back into Equation 10 gives the following expression for the total metal concentration:

$$M_t = [M^{+2}] \left( 1 + \sum K_L [L^{-p}]^n \right) \quad (14)$$

rearranging to solve for the free metal ion concentration gives:

$$[M^{+2}] = \frac{M_t}{\left( 1 + \sum K_L [L^{-p}]^n \right)} \quad (15)$$

Equation 15 can be substituted back into Equation 9 for the free metal ion concentration:

$$[\equiv \text{SOMOH}^0] = \frac{\frac{K_{\text{ads}}}{[H^+]^2 \left( 1 + \sum K_L [L^{-p}]^n \right)} (S_t - \sum \equiv \text{SOC}_i \text{OH}^0) M_t}{1 + \frac{K_{\text{ads}}}{[H^+]^2 \left( 1 + \sum K_L [L^{-p}]^n \right)} M_t} \quad (16)$$

Equation 16 gives the concentration of an adsorbed metal in terms of a thermodynamic adsorption coefficient, solution chemistry (pH, metal ligand complexes in solution, and competing cations), and total number of surface sites. Therefore, Equation 16 can account for the important factors affecting adsorption.

If we make the following substitutions into Equation 16:

$$\alpha = \frac{K_{\text{ads}}}{[H^+]^2 \left( 1 + \sum K_L [L^{-p}]^n \right)} \quad \text{and} \quad (17)$$

$$\beta = S_t - \sum \equiv \text{SOC}_i \text{OH}^0 \quad (18)$$

we get the following equation:

$$[\equiv \text{SOMOH}^0] = \frac{\alpha \beta M_t}{1 + \alpha M_t} \quad (19)$$

Comparing Equation 19 to Equation 2, we can see that the analytical equation derived from the surface complexation theory (Equation 16) describes a Langmuir isotherm. More importantly, the adsorption coefficient of the derived Langmuir isotherm can be related to solution chemistry (pH, complexing ligands) and the thermodynamic binding constant between the metal and the surface sites on the sediment. The total number or adsorption sites can account for the effect of competing cations. Using Equation 16, laboratory data, and a thermodynamic model of aqueous solution chemistry, the thermodynamic adsorption constant can be obtained by nonlinear least squares fitting of lab data to the equation.

## Uranium Solution Chemistry

To study the adsorption of uranium on sediments, the aqueous chemical properties of uranium must be known. From Equation 16, the important properties of uranium are the formation of aqueous complexes in vadose zone water. A thermodynamic conceptual model of uranium aqueous geochemistry based on ion association theory is developed using a consistent set of thermodynamic equilibrium constants compiled by

Grenthe et al.<sup>16</sup> with corrections added by Silva et al.<sup>17</sup>

The important aspects of site-specific solution chemistry must be included in the adsorption model. Water samples collected from the vadose zone at the SDA at the INEEL were used to develop the aqueous solution model. Water samples have been collected from the SDA using perched water monitoring wells and porous cup samplers. Important anions that could form ligands with uranium are fluoride, with a typical concentration on the order of 0.1 mg/L, sulfate, with a typical concentration of 100 mg/L, and bicarbonate, with a wide range of concentrations from 92–1,700 mg/L. The distribution of species expected to occur in vadose zone water were calculated to determine which species are important. Figure 4 shows the uranium species present in typical SDA waters expected to be present at greater than 1% of the total uranium. Uranium carbonate complexes predominate, and these calculations indicate that hydroxide and carbonate are the only two ligands that need to be considered in the adsorption model for uranium at the SDA.

There is one species in the geochemical model with more than one uranium atom in the formula  $[(\text{UO}_2)_2(\text{CO}_3)(\text{OH})_3]^-$ . Figure 5 shows the stability fields of uranium species as a function of carbonate and uranium concentrations. The species  $(\text{UO}_2)_2(\text{CO}_3)(\text{OH})_3^-$  is favored by higher uranium concentrations and lower carbonate concentrations. The generally low uranium concentrations expected for release of a trace radionuclide from waste would not favor the formation of the complex, and so it is not included in the reduced model.

### Experimental Data

Adsorption experiments were conducted on seven INEEL sediments collected from the SDA. Experimental details and results are presented in Grossman et al.<sup>18</sup> A Langmuir isotherm was fit to the experimental results using a nonlinear least-squares algorithm. The fit of the Langmuir isotherm provided estimates of  $\alpha$  (Equation 17) and  $\beta$  (Equation 18). From the fitted parameters and the equations, the total number of surface sites and the thermodynamic equilibrium constant were calculated in Table 2).

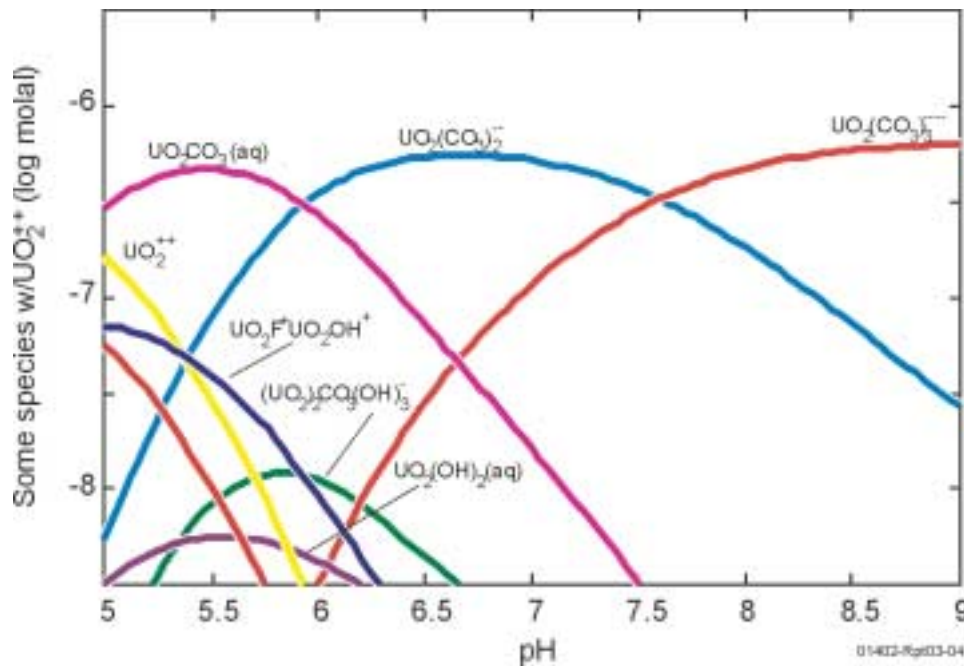


Figure 4. Distribution of aqueous uranium species in solution as a function of pH for a water composition typical of the SDA [  $\text{F}^- = 0.1 \text{ mg/L}$ ;  $\text{SO}_4^{2-} = 100 \text{ mg/L}$ ;  $\text{HCO}_3^- = 200 \text{ mg/L}$ ].

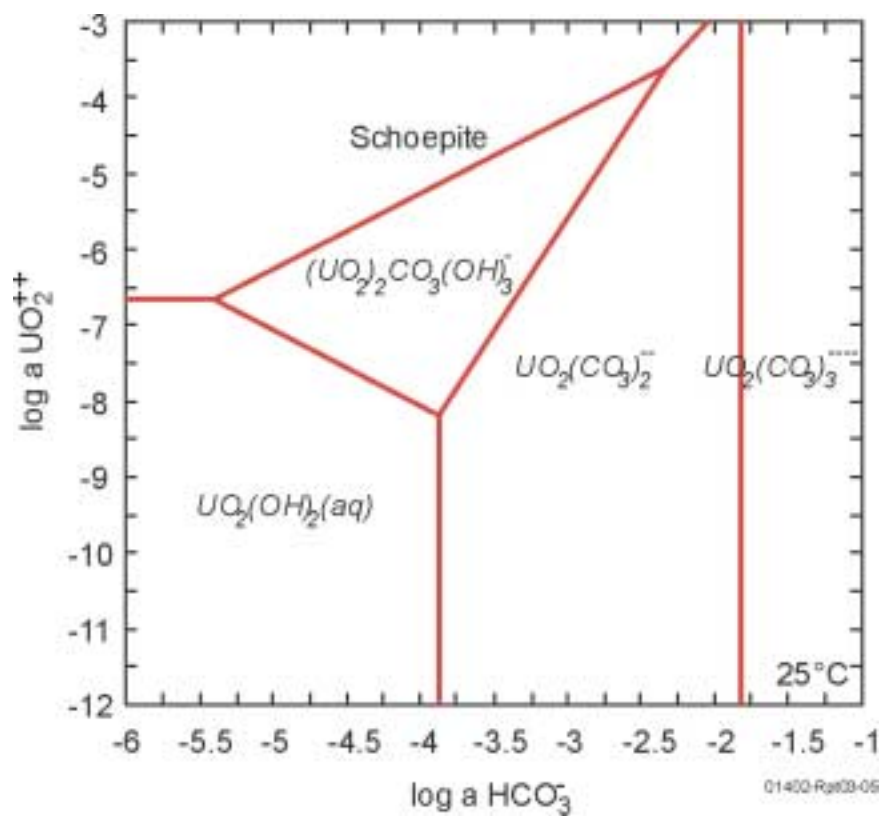


Figure 5. Stability fields of uranium species as a function of total dissolved carbonate concentration at a pH value of 7.5.

Table 2. Estimates of adsorption sites and thermodynamic adsorption constants for SDA sediments.

Sample	log (Alpha) (L/mole)	log (Kads) (L/mole)	Adsorption sites (mole/g sediment)
7DS00101KD	6.25	-2.13	3.60 E-8
7DS00301KD	6.19	-2.20	2.78 E-8
7DS00501KD	5.84	-2.54	3.86 E-8
7DS00701KD	5.88	-2.50	2.77 E-8
7DS00901KD	6.12	-2.27	2.54 E-8
7DS01701KD	6.11	-2.27	2.27 E-8
7DS02301KD	5.99	-2.39	2.73 E-8
Mean ± 2 S.D.	6.05 ± 0.31	-2.33 ± 0.31	(2.94 ± 1.15) E-8

From the definition of alpha and knowledge of the carbonate concentration and pH of the test solutions, the value of  $K_{ads}$ , the thermodynamic adsorption coefficient, can be calculated. The values cover a narrow range with an average  $\log K_{ads}$  of -2.33 L/mole. Equation 16 was then used to calculate the expected adsorption for the experiments, which was compared to the experimental results. The comparison between the predicted and measured adsorption of uranium for one of the experiments is shown in Figure 6. The agreement is very good. The aqueous uranium mainly consists of the two carbonate complexes as shown by the green and orange lines.

Having calculated all of the parameters needed to use Equation 16 to calculate adsorption, the effect of pH, dissolved carbonate concentration, and other parameters on adsorption can be calculated. Figure 7 shows the aqueous distribution of uranium in contact with SDA sediment over a pH range of 4.0 to 10.0 at a total dissolved carbonate concentration of  $3.6 \times 10^{-3}$  molar. This is the concentration of total dissolved carbonate used in the Clemson laboratory experiments. Adsorption onto a solid phase is included in the calculation. From the definition of the  $K_d$  partition coefficient

(Equation 1), the  $K_d$  is just the ratio of the total dissolved uranium concentration to the adsorbed uranium concentration. In Figure 7, the adsorbed uranium concentration exceeds the dissolved uranium concentration from pH 4 to about pH 8.5. Using the data illustrated in Figure 7, an effective  $K_d$  can be calculated as a function of pH. The results of this calculation are shown in Figure 8. The effective  $K_d$  is at low pH as the hydrogen ion competes with uranium for adsorption sites. Adsorption increases as pH rises and peaks at a pH of about 5.5. As pH increases above 5.5, carbonate complexing in solution inhibits adsorption of uranium onto the solid mineral surfaces. The distribution of uranium species shown in Figure 7 shows that formation of uranium carbonate complexes in solution begins to dominate the dissolved uranium starting at a pH value of about five. The results of the laboratory experiment are also shown in Figure 9. The laboratory experiments were conducted on seven sediments, but at one pH value and one total dissolved carbonate concentration. Additional laboratory measurements are needed over a range of pH values and dissolved carbonate concentrations to further validate this model.

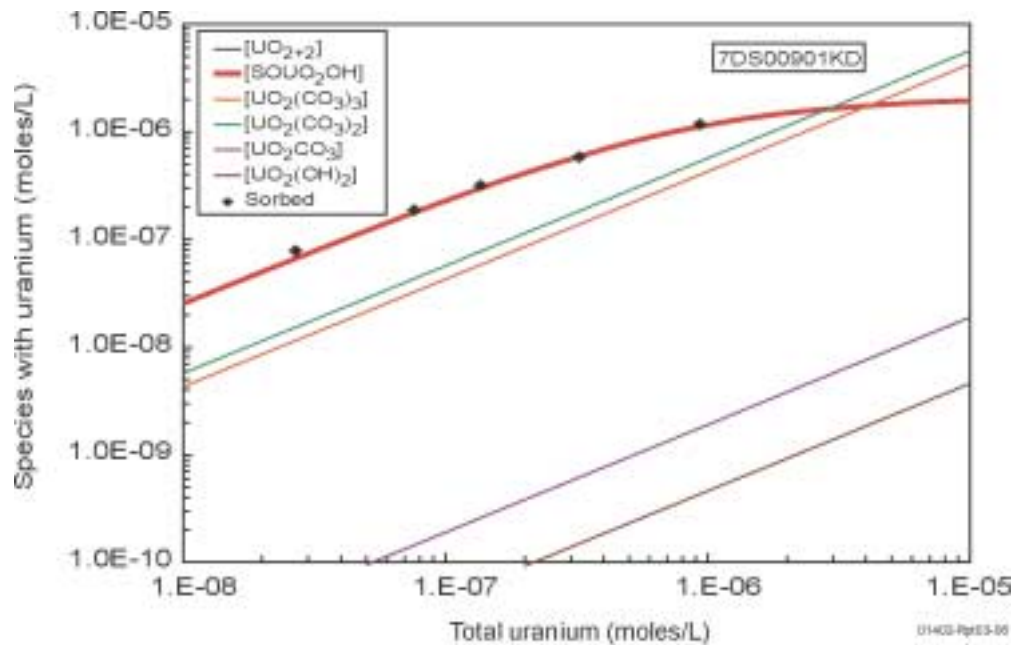


Figure 6. Fit of analytical adsorption model (Equation 16) to a uranium adsorption isotherm measured in the laboratory.

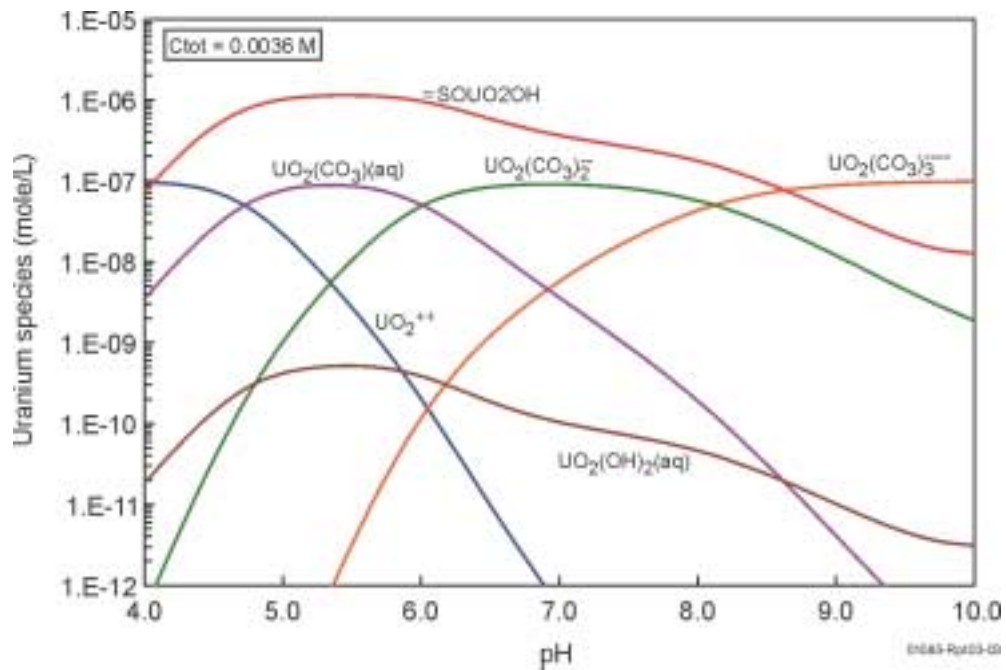


Figure 7. Distribution of uranium among aqueous species and adsorbed uranium calculated using the analytical adsorption equation.

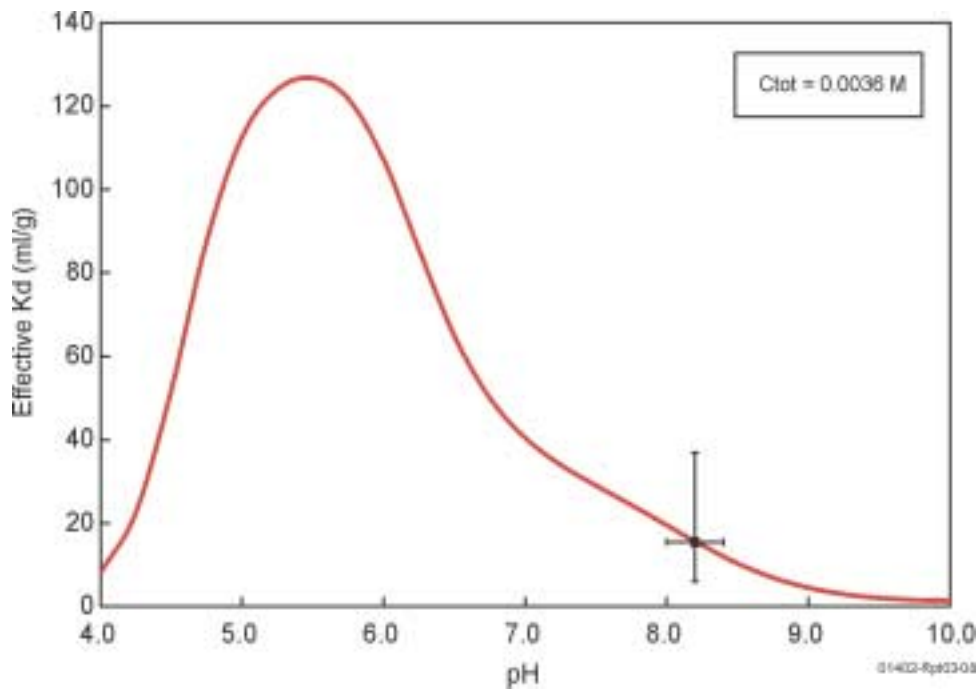


Figure 8. Calculated effective partition coefficient ( $K_d$ ) as a function of pH using Equation 16. Laboratory adsorption measurements are indicated by the cross.

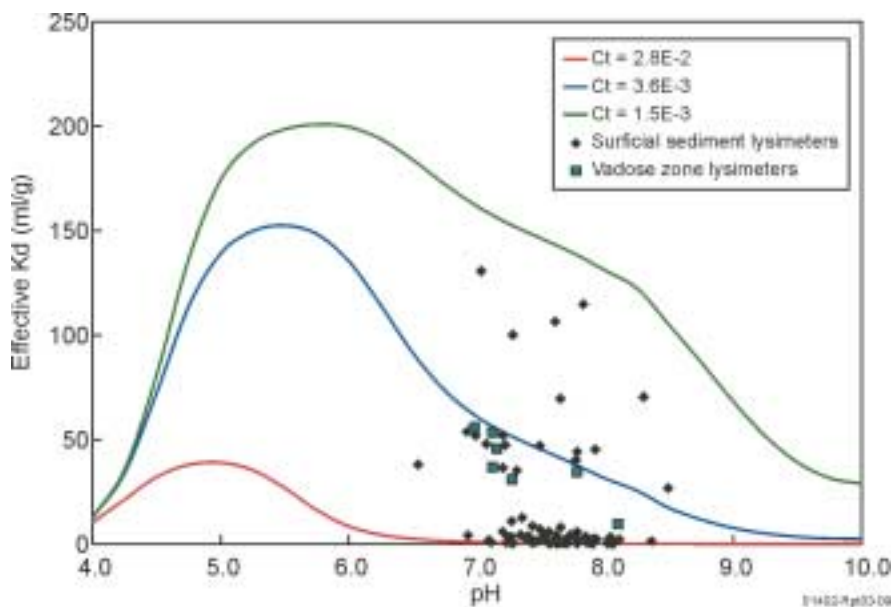


Figure 9. Plot of the range of effective  $K_d$  values for surficial sediment and deep vadose zone pore waters at the SDA as a function of pH using Equation 16.

## Multiphase Transport in Sediments

To study the interaction of processes in the vadose zone, a mesoscale column has been constructed to conduct laboratory experiments. The column is 3 m tall  $\times$  1 m in diameter (see Figure 10). The column has been instrumented with sensors and sampling ports. Sensors include tensiometers to measure sediment moisture tension, time domain reflectometers (TDR) to measure moisture content, and thermocouples to measure temperature. Sampling ports are installed to measure gas phase and water phase chemistry.

The column was filled in the summer of 1998 with sediments similar to those used to cap the SDA. The column was monitored periodically for gas phase chemistry. A natural gradient developed in the column from the native microbial community. The profile of  $\text{CO}_2$  that developed in the column is shown in Figure 11. The computer code UNSATCHEM (Reference 4) was used to simulate the microbial activity and develop the  $\text{CO}_2$  gradient.

During FY 2001, two gas-phase tracer tests were conducted using sulfur hexafluoride as the

tracer gas. Sulfur hexafluoride was injected into the column at a depth of 1.53 meters. The gas initially diffused both up and down the column until the lower portion of the column was filled with the tracer gas. This occurred after about 36 hours (see Figure 12). From that point on, a concentration gradient developed from the bottom of the column to the surface, and gas diffusion was upwards out of the column. Data from this test will be analyzed in FY 2002.

On July 16, 2001, we began to add water to the top of the column at a rate of 5 L/day. Until that time, no water had been added. This addition will continue until the column is wet to the bottom. Raw measurements from the TDR probes shows the downward migration of the wetting front (see Figure 13).

The rate of water movement has increased over time, even though the rate at which water is being added has not changed. From 0 to 0.45 m depth, the rate of advance was 0.023 m/day. To advance from 1.05 to 1.36 m, the front traveled at a rate of 0.039 m/day. At the most recent calculated rate, the wetting front should reach the bottom of the column the first week in October 2001 (see Table 3).



Figure 10. Photograph of mesoscale column showing the water application system consisting of four sets of reservoirs, UV sterilizers, and syringe pumps.

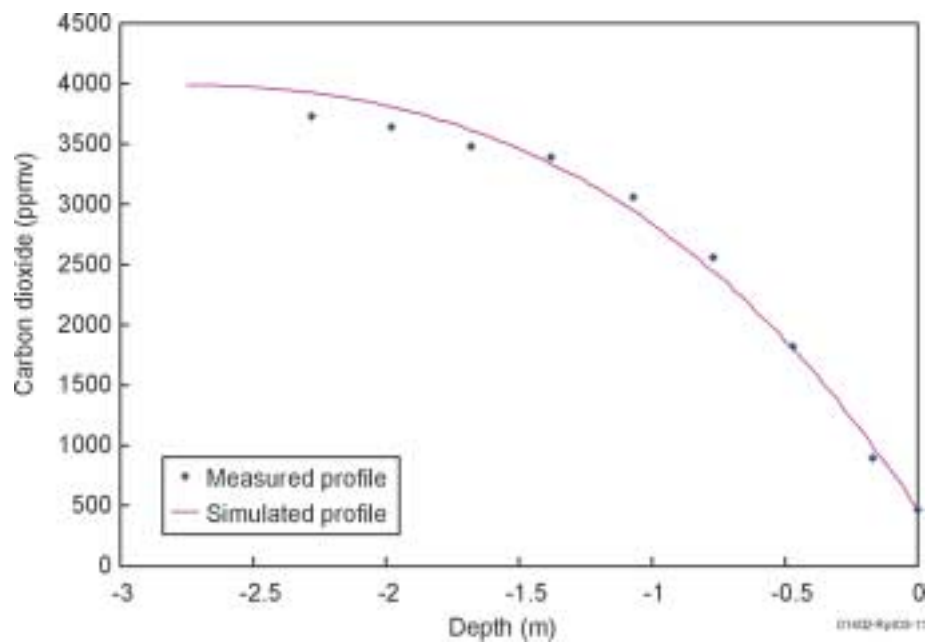


Figure 11. Vertical profile of CO<sub>2</sub> concentration developed in the column from microbial activity. The development of the profile was simulated using the UNSATCHEM computer code.

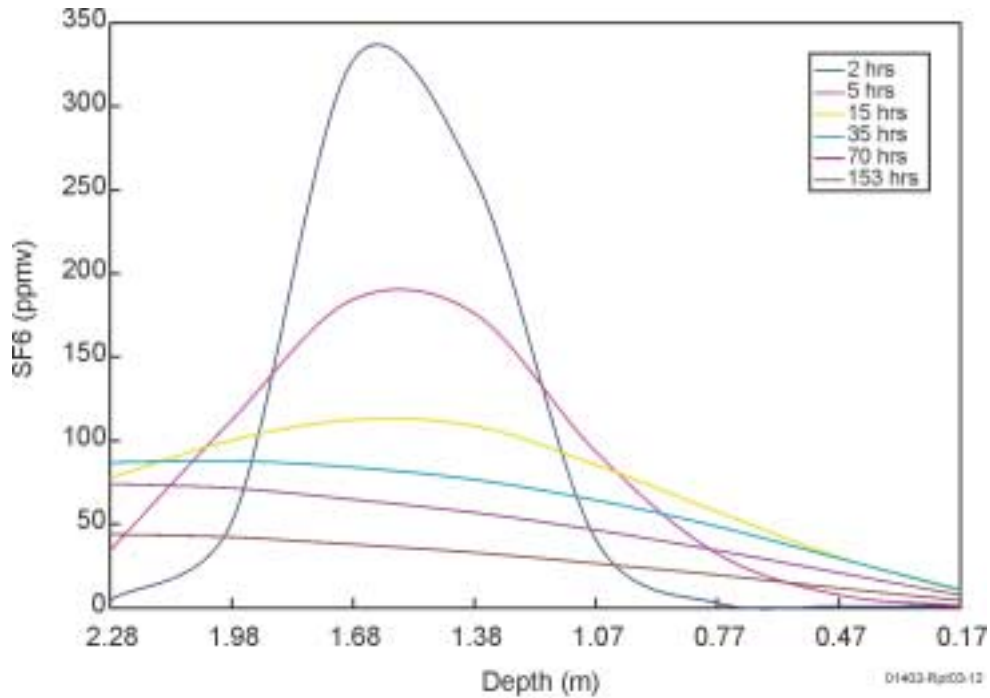


Figure 12. Change in sulfur hexafluoride profile in the column over time as the tracer gas diffused through the column and out of the surface of the sediment.

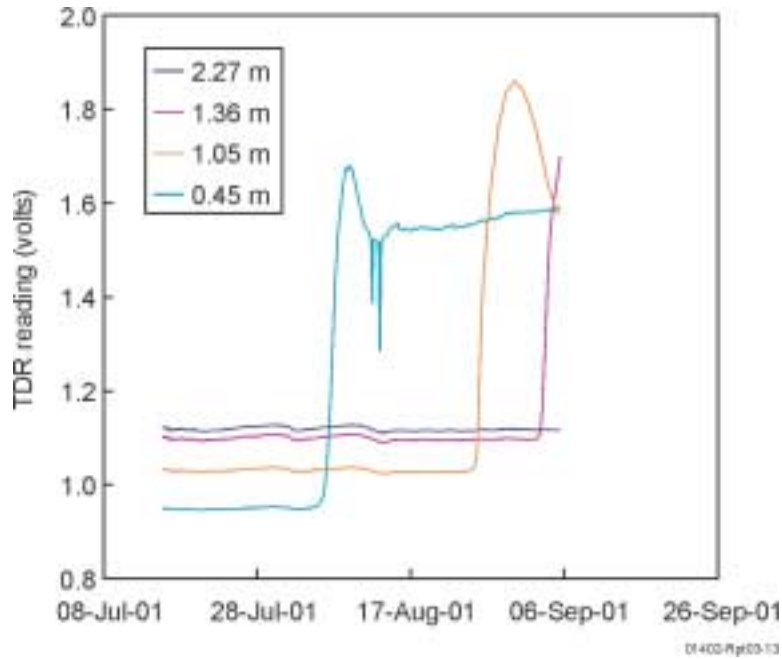


Figure 13. Output from time domain reflect-ometers, measuring moisture content, show the downward migration of the wetting front since July 16, 2001.

Table 3. Dates at which the wetting front in the column has reached the TDR probes, and the calculated rate of advance of the front.

Date	Depth (m)	Rate (m/day)
7/16/01	0	—
8/5/01	0.45	0.023
8/25/01	1.05	0.030
9/2/01	1.36	0.039

Once the wetting front reaches the bottom of the column, a vacuum will be applied at the bottom of the column to extract water. The rate of water addition at the top of the column will be reduced to 1 L/day. The column will then be run until steady-state flow conditions are approached. This will be determined by mass balance between input to and outflow from the column, and the stability of moisture content and matric potential measurements in the column. When steady-state conditions have been established, tracer tests will be conducted in the column.

## Relationships Between Moisture Content, Tension, and Biogeochemical Activity in the Vadose Zone

The objective of this task is to examine the role that available water content plays in soil microbial activity. The availability of water and water-borne nutrients affects microbial activity in the subsurface, which in turn affects water availability and mobility in soil. This interrelationship, and interactions between surface area, total pore volume, and microbiologically available pore volume can be very important in determining the remediation potential in the subsurface. Many microorganisms produce biofilms that may modify flow paths. Furthermore, the production and migration of CO<sub>2</sub> significantly influences the migration of radionuclides in the vadose zone. This task uses the Unsaturated Flow Apparatus (UFA™) to homogeneously distribute uniformly labeled substrate throughout soil water in intact soil cores. Subcores are then sealed in serum bottles and incubated. At specified times, samples are sacrificed and acidified, releasing respired CO<sub>2</sub>

and soil carbonates to the headspace. The CO<sub>2</sub> is quantitatively recovered using an alkali trap, and analyzed for labeled CO<sub>2</sub>. Water available to the soil microbes is estimated from pore volume distributions measured by several methods. This is an ongoing task, but we are progressing toward the goal of examining the effect of available water on in situ microbial generation of CO<sub>2</sub>.

To test these hypotheses, we will correlate microbial activity with water content and available water in a model soil. Physical characterization of the soil and microbial activity in the soil will include measurements of several parameters. Pore size distribution data will be used to determine the pore volume available to the microbes and the total volume in pores. Pore surface area will be used to differentiate between surface area in pores too small for the microbes and total surface area available to the microbes (which would be expected to change substantially with water content depending on the soil). External surface area will provide an estimate of surface area that is always available to the cells. Assuming a minimum of monolayer coverage of water on the soil particles at all times, the total external coverage can be used to estimate volumes of water in the pores at given water contents and how deep the layer may be in the pores. Salt concentrations in the soil water at saturation will allow calculation of the salt concentrations at lower water contents, and will provide estimates of osmotic pressure in the remaining available water. Water content and water activity will be used with the pore and surface measurements above to estimate available water volume for the microbes. Microbial activity will be measured by CO<sub>2</sub> evolution. This is expected to change substantially with water available to the cells, and will be measured over a range of available water. Water content will be adjusted and substrate will be homogeneously distributed throughout the soil water using the unsaturated flow apparatus. Pore tortuosity will provide a feel for the complexity of the diffusional path that O<sub>2</sub> must take to reach the cells at the soil particle surface. Finally, the effective diffusion coefficient for oxygen in saturated soil will, together with the tortuosity and microbial activity, allow estimation of diffusion path lengths, or at least determine the limiting factor at high water contents. Measurement at

different salt concentrations may help account for the effect of dilution as water is added incrementally.

The relationship between water content and microbial activity is expected to be complex. We are conducting laboratory unsaturated experiments to test hypotheses and develop an understanding of the relationship between microbial activity and moisture characteristics. This study focuses on sandy loam soils common in southeast Idaho, but may eventually include a wider range of soil types ranging from sands to clays. The study will be generally limited to water potentials in the range -0.1 to -12 bars to include air entry pressure and in situ moisture content of soils often found in arid climates. Adequate correlation of water content with biodegradability will be important in assessing remediation potential at most DOE and other contaminated sites. This task supports ongoing work to develop vadose zone instrumentation including the Exfiltrimeter, dielectric soil water content sensors, and geocentrifuge studies.

In porous media, microbial activity decreases at both very high and very low water contents (see Figure 14). This has generally been attributed to

higher osmotic pressures at low water contents and to oxygen limitations at high water contents. We hypothesize that this behavior also depends on the amount of water that is *available* to the microbes (see Figure 15). In effect, at very low water contents, water in unsaturated soil becomes unavailable for microbial use because the bulk of the water is held in pores smaller than or similar in size to the bacteria. Thus, not all of the water in unsaturated soils is available, and the amount available would depend directly on the pore size distribution of the soil (see Figure 16). This project is divided into two subtasks, soil characterization and aerobic microbial activity. Physical and chemical properties of a sandy loam soil, obtained from the USDA Sheep Experiment Station near Dubois, ID were measured to gain an understanding of the distribution of the water in the soil at the various water potentials. These properties included pore size distributions, percentage carbonate, percentage organic matter, soil chemistry, surface area, interstitial pore volume, intragranular pore volume, and a full range of pore volume distributions from 0.003  $\mu\text{m}$  to 360  $\mu\text{m}$ . Knowledge of how soil physical properties limit microbial activity will be useful in estimating the potential microbial activity in a soil

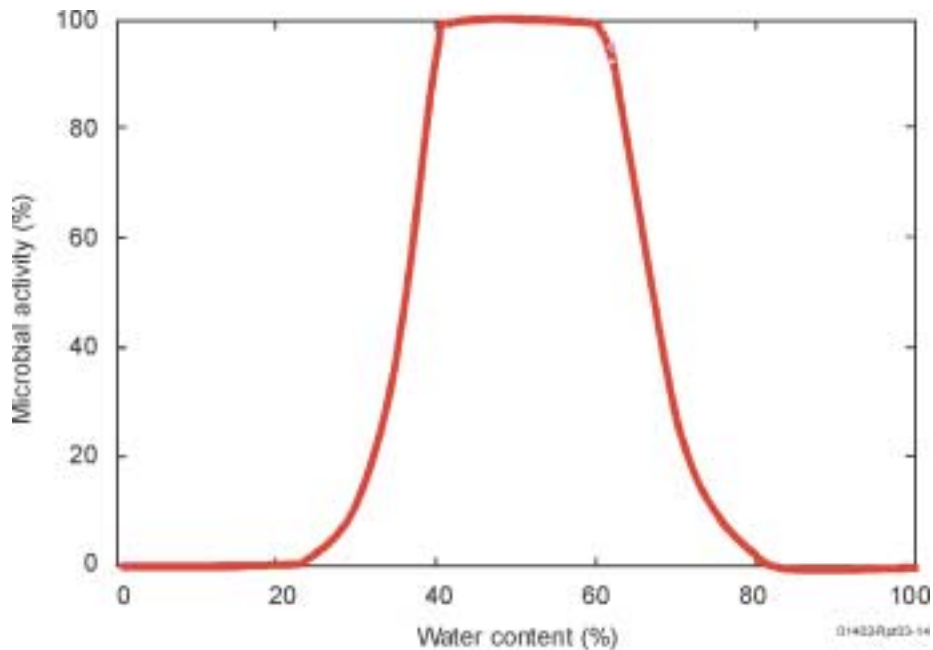


Figure 14. Observed variation of microbial activity with water content. This behavior is similar for various microporous supports, including soils and compost.

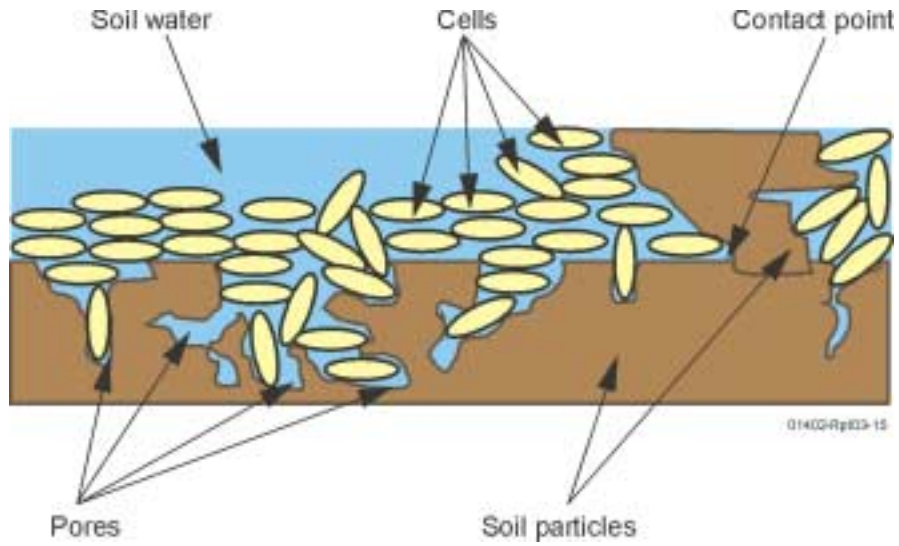


Figure 15. Diagram of a control volume of saturated soil. As depicted, not all of the soil water is in pores large enough for cells to enter.

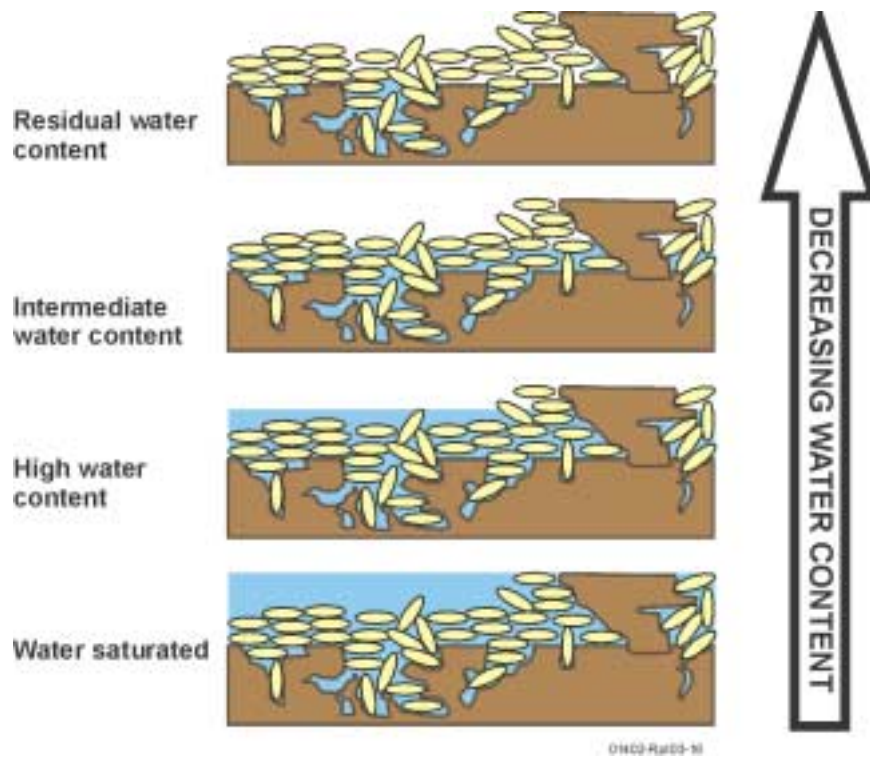


Figure 16. As the control volume dries out, the fraction of water that is unavailable to the cells increases. Even before reaching residual water content, very little of the soil water may be available to the bacterial cells.

over a wide range of water contents. For example, measured soil physical properties including pore volume, pore size distribution, percentage sand/clay, etc., along with the relationships developed in this project could be used to predict the range of microbial activities that would be seen at different water contents based on the physical distribution of the water in the soil and its availability to the microbes. Thus, the process of in situ biodegradation can be better understood, and a method that is based on soil physical properties and local water contents can be devised to predict biodegradability. This result would directly benefit bioremediation efforts.

Soil water content is adjusted by centrifugation<sup>19,20</sup> using a UFA™ rotor, manufactured by UFA Ventures, Inc., Richland, WA.<sup>21,22</sup> This method of desorption is expected to maintain a uniform substrate distribution throughout the sample during drainage, which is necessary to quantitatively observe the effects of decreasing water content on degradation of the added substrate. The UFA™ subjects the sample to large fluid driving forces up to 10,000 ×g in an open-flow centrifugation device, or in separate drainage cells. Because of the large driving forces, steady state is reached within hours to days even at hydraulic conductivities as low as 10<sup>-10</sup> cm/s, removing the traditional time barrier (days to weeks for traditional methods) often required for these types of experiments.<sup>23</sup> Wetting solutions include both <sup>13</sup>C-UL-glucose and a solution of <sup>12</sup>C-glucose spiked with <sup>14</sup>C-UL-glucose in two separate studies to examine the optimum solution for monitoring CO<sub>2</sub> evolution. Microbial activity in the soil is then measured by <sup>13</sup>CO<sub>2</sub> and <sup>14</sup>CO<sub>2</sub> evolution under aerobic conditions. These experiments are done in sealed batch systems at water potentials ranging from -0.1 to -12 bars. Cells are maintained in maintenance metabolism by adding very small amounts of substrate.

### **Summary of Results for FY 2001**

The goals for work during FY 2001 were to complete method development for microbial activity measurements, which included:  
(a) designing and testing methods for coring intact

soil samples with minimum disturbance; (b) completing the pore volume distribution measurements using solute exclusion and mercury porosimetry; (c) developing and testing methods for saturation of the cores with labeled substrate and draining them to the desired water content in the UFA; (d) designing and testing an efficient and quantitative recovery system for respired CO<sub>2</sub>; and (e) developing and testing methods for measuring microbial respiration in intact soil cores, using <sup>13</sup>C- and <sup>14</sup>C-uniformly labeled substrates. Each is discussed below.

### **Methods for Coring Intact Soil Samples**

Since a majority of the original soil cans obtained from the USDA Sheep Station in Dubois, ID were used to characterize the physical properties of the soil, a new batch of soil cores was collected from the Sheep station to complete this study. The cores were collected approximately 5 ft north of the previous sampling location (October 1999) at approximately the same depth and orientation. We collected 120 cores in 3 in. inside diameter × 2 in. high aluminum cans (about 230 cm<sup>3</sup> volume).

We made several attempts to determine optimum subcoring methods to preserve the integrity of in situ soil properties, such as bulk density, porosity, and sedimentary structure. To be consistent with an interfacing Environmental System Research Candidates (ESRC) project examining compaction of the soil from this study when measured in the UFA, 1 in. outside diameter plastic rings were required for subcoring. The small outer diameter of the ring made it difficult to obtain undisturbed cores using thick-walled rings, while thin-walled plastic resulted in deformation of the ring (and thus the soil) during the coring process. To overcome this problem, we designed a rigid stainless steel coring device allowing us to use thin walled rings. The coring device also allowed us to excavate the samples from the original soil cans with excess soil at the ends of the rings (the rings are 1.6 in. long while the coring device is 2 in. long). We then leveled off the soil at the ends of the rings, minimizing disturbance at the ends of the core (see Figure 17).

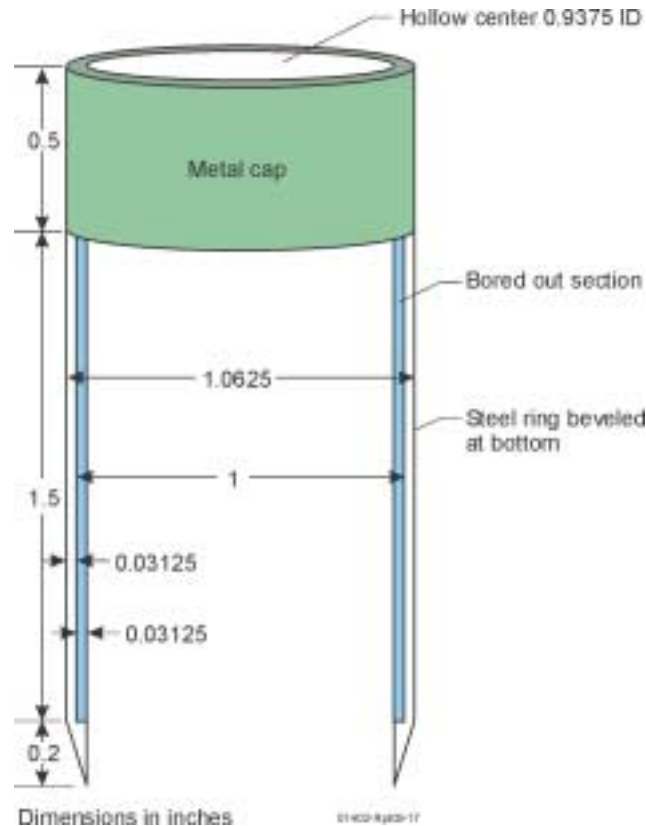


Figure 17. Soil coring device used to obtain undisturbed samples for hydraulic property analysis.

## Methods for Determining Pore Volume Distributions

**Solute Exclusion Technique.** In this technique, the dilution of solutes of different molecular diameters in water-saturated porous solid is measured and used to construct a micropore size distribution.<sup>24–26</sup> Three attempts to determine the micropore volume distributions in the soils were made. Each study used several simple carbohydrates and increasing molecular weight dextrans as solutes. In the first attempt, microbes present in the soil appeared to degrade the dextrans, resulting in incomplete mass balances. In subsequent attempts, we added sodium azide to the dextran solutions to control microbial degradation of the solutes. In the second attempt, the mass balances were better, and results using small molecular weight solutes (glucose,

maltose, raffinose, and Dextran 6K) were consistent. Results with the larger solutes (Dextran T10, Dextran 15–20K, Dextran T40, Dextran T70, Dextran 20–300K, Dextran T500, and

Dextran T2000) showed inconsistent mass balances and highly scattered data. To combat this problem, we increased the replicates from three to five, which further improved the results for the lower molecular weight dextrans, but there were still significant errors for the high molecular weight dextrans. For this method to produce valid results, the solutes cannot adsorb or otherwise interact with the solid surface, and the solute cannot be degraded by microbes present in the solid matrix. In plant matter such as lignocellulose, these assumptions are generally true despite the large number of free hydroxyl groups that could interact with dextrans, which are linear anhydroglucose polymers (References 23–25). Since silica in the soil is expected to have a chemically similar surface (many free hydroxyls), it was assumed that this assumption would be approximately true in soil as well. While we were able to minimize microbial degradation of the solutes by adding the sodium azide, it appears that the higher molecular weight dextrans (>6,000 g/mole) adsorbed significantly to the surface of the soil particles.

We will make further attempts at this measurement using increasing molecular weight polyethylene glycol (PEG) solutions, ranging in molecular diameters from 8–50 Å. PEGs are more hydrophobic than dextrans and so should not adsorb to porous materials with large amounts of free hydroxyls as easily as dextrans.<sup>27</sup> The size range afforded using PEGs is smaller than that available using dextrans (8–560 Å), due to solubility issues. However, the driver for using this method was as a check of pore size distribution measurements using nitrogen adsorption (BET method), which requires drying of the samples and potential collapse of pores. The pores most likely to collapse significantly are the smallest pores in the silt fraction, which have closely located hydroxyl groups. This range will still be covered by the solute exclusion technique using the PEGs.

**Nitrogen Adsorption.** Intraparticle (micropore) pore size and surface area distributions were measured during FY 2000 using nitrogen adsorption.<sup>28</sup> In these measurements, the BET method was employed,<sup>29</sup> with the following modifications to the standard procedure<sup>30</sup>: (1) organic matter and carbonates were not removed prior to measurement; and (2) the soil was dried under a vacuum at room temperature rather than oven-dried at 105°C. These modifications were made to preserve the pore structure seen by the bacterial cells as much as possible. The cumulative micropore volume and surface area distributions are available in Reference 27.

**Mercury Porosimetry.** Mercury intrusion porosimetry has been used as a reliable method for determining pore volumes ranging from 0.003 µm to 360 µm. Because mercury is a nonwetting liquid for most materials, the contact angle between liquid and solid is 90 degrees, thus it will enter the pores only if an external pressure is applied. Contact angle hysteresis may influence the accuracy of the mercury porosimetry measurements, but result in a greater mercury volume at a given pressure during extrusion than during intrusion. For this reason, both an intrusion and extrusion experiment is required to fully examine pore volume distributions affected by hysteresis (Reference 29). Daniel B. Stephens and Associates in Albuquerque, NM will be contracted

to perform these studies. The mercury porosimetry studies will be completed next fiscal year.

### **Methods for Saturation of the Cores Draining to the Desired Water Content in the UFA**

Determination of soil moisture equilibration times in the UFA for the undisturbed cores of the Dubois soil is necessary prior to sample saturation and desorption for microbial activity analysis. Measurement of these times are for single step UFA adjustment of moisture content of presaturated cores to the desired water contents. These measurements are necessary because nominal desorption time is required to prevent significant microbial release of CO<sub>2</sub> from added substrate during desorption.

We estimated the equilibrium times for draining the soil cores to the desired moisture contents in the UFA in conjunction with preparation of similar cores for an interfacing ESRC project, “Innovative Approaches to Characterize Vados Zone Hydraulic Properties,” in which the amount of compaction of the soil cores occurring in the centrifuge is being characterized. The interfacing ESRC project directly contributes to the goals of this project by providing a method for estimating the changes in interstitial pore volume (>25 µm pore diameter) in the centrifuge. Equilibrium times estimated in this part are the equilibrium times (and accompanying water contents) to be used in both projects. We estimated the equilibrium times at seven pressure heads, including 100 cm, 150 cm, 1/2 bar, 1 bar, 3 bars, 6 bars, and 12 bars. The results are shown, with the UFA rotor speeds, in Table 4. Equilibrium time was assumed to be reached once the change in volumetric water content was approximately equal to 0.5% (Equation 20), estimated to be the total measurement uncertainty in volumetric moisture content (based on precision of balance for measuring weight and caliper for measuring volume of sample). For a 20 cm<sup>3</sup> sample with an initial moisture content of 40%, the change in sample weight would amount to approximately ±0.04 g. At residual moisture content (~15%) the change in weight would amount to approximately ±0.005 g. The average of the two is approximately 0.02 g. To be certain that the sample was at

Table 4. Estimated equilibrium times at seven pressure heads.

Rpm	cm H <sub>2</sub> O pressure head	Bars Pressure	Approximate 'g'-force (m/s <sup>2</sup> )	Equilibrium Time (hours)
490	-100	-0.10	25	6
600	-150	-0.15	36	10
1,100	-510	-0.50	122	6
1,560	-1,020	-1.00	245	5
2,710	-3,060	-3.00	738	7
3,830	-6,120	-6.00	1,475	6
5,420	-12,240	-12.0	2,953	4

equilibrium, we assumed moisture equilibrium was reached once the change in sample weight was within  $\pm 0.01$  g at each rotational speed. Changes in sample weights were rarely smaller than this value within a 1 hour, monitoring-time interval primarily due to evaporation within the column during centrifugation.

$$(\theta_i - \theta_f) / (\theta_i) * 100 = 0.5\% \quad (20)$$

### Recovery System for Respired CO<sub>2</sub>

A CO<sub>2</sub> recovery system was developed to quantitatively recover biologically-produced CO<sub>2</sub> and CO<sub>2</sub> from soil carbonates in acidified soil

slurries. Several design variations were attempted before settling on a final design. Traditional methods for trapping CO<sub>2</sub> include insertion of a small container of strong alkali directly in a sealed container during soil respiration. However, <sup>14</sup>CO<sub>2</sub> and H<sub>2</sub><sup>14</sup>CO<sub>3</sub> produced by microbial decomposition may become trapped as Ca(H<sup>14</sup>CO<sub>3</sub>)<sub>2</sub> in calcareous soils. To remove all <sup>14</sup>CO<sub>2</sub> produced during incubation, calcareous soils require acidification.<sup>31</sup> The final design also includes a procedure which exhaustively recirculates gaseous CO<sub>2</sub> through a 5N NaOH trap until all of the CO<sub>2</sub> has been trapped (see Figure 18). Several pump types were tested, and we have settled on a

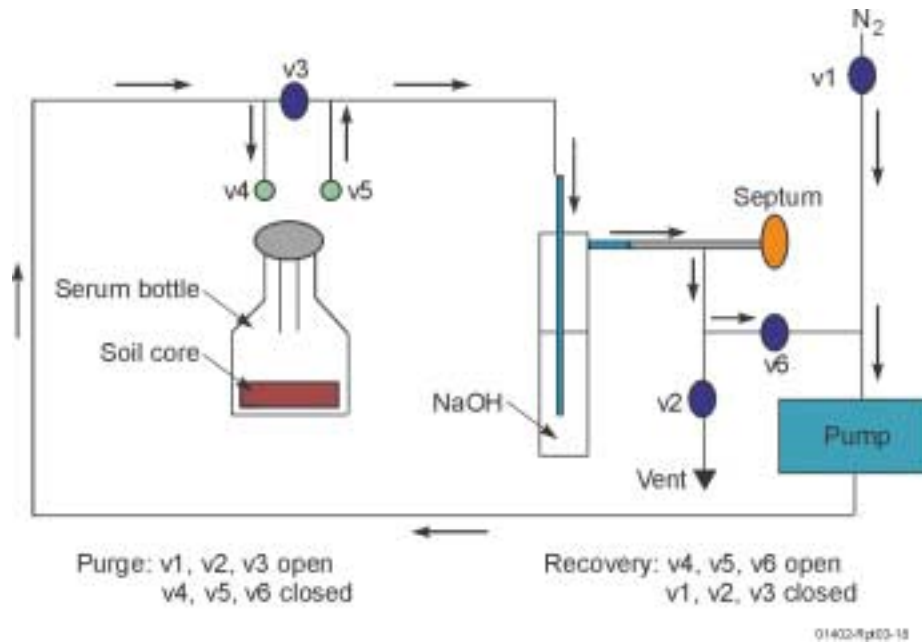


Figure 18. CO<sub>2</sub> recovery system.

diaphragm pump rather than a peristaltic pump because the tubing in the peristaltic pump head was overheating during extended use. The recovery system was validated using the  $^{13}\text{C}$ -microbial activity measurement samples (see below). The optimum pump rate was about 360 mL/min. A circulation period of 24 hours resulted in approximately 99.96% recovery of the  $\text{CO}_2$  initially in the serum bottles (confirmed by gas chromatography). This recovery will also suffice for  $^{14}\text{C}$ -UL-glucose-spiked experiments.

### **Microbial Activity Measurements: $^{13}\text{C}$ - and $^{14}\text{C}$ -uniformly Labeled Substrate Tests**

This study was conducted to determine whether  $^{13}\text{C}$  UL glucose can be used to measure microbial activity in variably saturated soils. Since  $^{13}\text{C}$  is a stable isotope, it is desirable for application in both a laboratory and field setting. Researchers typically use  $^{14}\text{C}$  as the labeled substrate because small concentrations can be detected with high precision using scintillation counters. Subcores from the Dubois soil cans were saturated and drained using standard laboratory methods at variable pressure heads (150 cm, 339 cm, 1,020 cm, 3,060 cm, and 6,120 cm head). Approximately 5 g dry soil plugs were extracted from the rings at moisture equilibrium and inserted into sterile serum bottles. A total of 0.20 mL of 200 ppm of  $^{13}\text{C}$ -UL-glucose was dripped onto the soil plugs in the serum bottles and the bottles were sealed. Three replicates and a blank were prepared for each pressure head examined, each of which were allowed to incubate for 30, 60, and 90 day time periods. At the end of the incubation periods, the samples were placed in a freezer until recovery. During harvesting, 20 mL of 2N HCL was injected into the serum bottles through the septum. The puncture hole was sealed with wax to prevent gas from escaping during soil respiration. After purging the circulation system with nitroge gas,  $\text{CO}_2$  from the serum bottles was allowed to circulate through 20 mL of 5N sodium hydroxide in a sparging tube for 24 hours at a flow rate of 390 mL/min (in a closed system) using a peristaltic pump. The sodium hydroxide was transferred from the sparger tube to culture tubes in a  $\text{CO}_2$  free environment chamber. The culture tubes were sealed and shipped to Coastal Science

Laboratories (CSL) in Austin, TX for stable isotope ratio analysis.

Instrument precision error reported by CSL was  $\pm 0.2$  per mil. This results in uncertainty in moles of  $^{13}\text{C}$  of approximately  $\pm 2.0 \times 10^{-9}$  per gram of dry soil. Data analysis indicates that each sample generated on the order of  $1 \times 10^{-6}$  to  $8 \times 10^{-6}$  moles of  $^{13}\text{C}$  (excluding background values) per gram of dry soil (see Figure 19). Variability between replicate samples was quite high, however, suggesting that measurement uncertainty was too great to detect concentrations of  $^{13}\text{CO}_2$  in these soils using gas chromatography techniques. It will thus be necessary to use  $^{14}\text{C}$  for the microbial activity tests. Scintillation methods for counting  $^{14}\text{C}$  concentrations are quite precise at very low concentrations and are therefore commonly used in these studies. The start of these tests is awaiting approval of IHR modifications and arrival of the radio-labeled substrate.

The measurement error was  $\pm 2.0 \times 10^{-9}$  moles/g dry soil (see Figure 19). Error bars represent standard deviation of three independent replicates. Values were calculated by subtracting the background (no  $^{13}\text{C}$  added) from each sample measurement. Thus, samples showing values less than 1.0 were lower than the background.

## **ACCOMPLISHMENTS**

During FY 2001, we initiated the experimental program to gather laboratory data to develop the thermodynamic and constitutive relations for the model. In the laboratory, we used the unsaturated flow apparatus (UFA) to uniformly distribute isotopically tagged food for microbes in an unsaturated sediment. We are building laboratory scale columns to measure microbial affects on carbon-14 transport and measure diffusion of  $\text{CO}_2$  through sediment. The mesoscale column is instrumented, and water is being added to the column to bring the water content of the sediment to desired levels prior to conducting tracer tests. Theoretical development of adsorption equations has been tested using laboratory data to develop an equation that could be applied in simulation of transport.

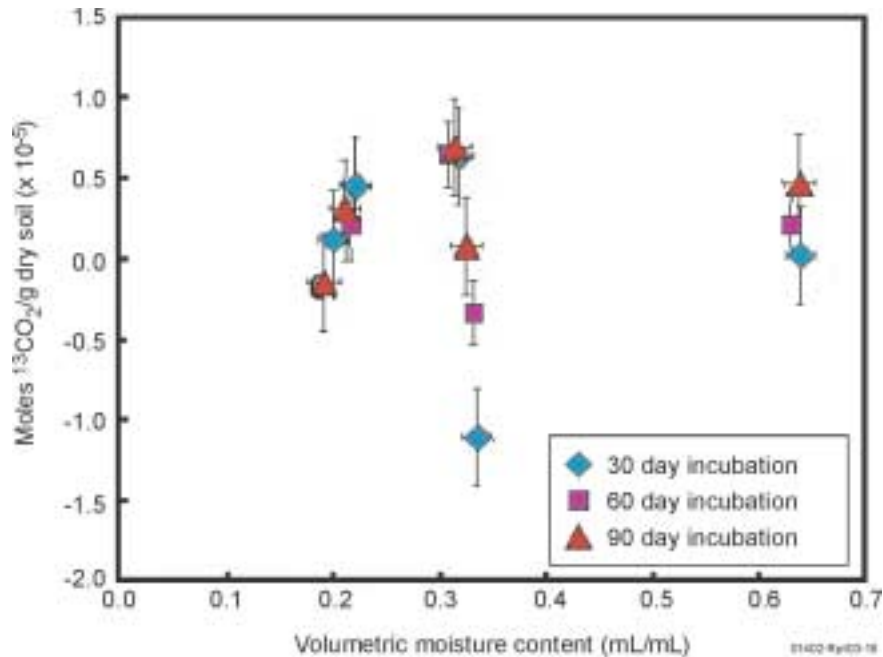


Figure 19.  $^{13}\text{C}$ -UL-glucose application results.

- Based on surface complexation theory, we derived an analytical model for the adsorption of uranium on sediments. Using measured uranium adsorption isotherms for SDA sediments, we obtained a thermodynamic adsorption constant for uranium by fitting the Langmuir isotherm to the lab data. Results of the modeling show that a large range in expected adsorption for SDA sediments, primarily because of the wide range in dissolved carbonate concentrations in vadose zone water.
- We tested the three-meter tall mesoscale column for gas phase composition and gas phase diffusion, and started the addition of water to bring the column up to planned moisture saturation conditions.
- We developed procedures for use of the unsaturated flow apparatus (UFA) and gained experience in sample acquisition, preparation, testing, and analysis. We developed techniques to core sediment samples and obtained representative intact soil cores small enough to use in the UFA. We measured soil moisture content equilibrium times at various pressures for soil core drainage in the UFA,

and evaluated soil compaction in soil cores that were run in the UFA.

- We developed methods for measuring microbial activity as a function of soil moisture potential, and developed a quantitative method for measuring soil respiration, including quantitative  $\text{CO}_2$  recovery apparatus and method for calcareous soils. We evaluated the use of  $^{13}\text{C}$  as a substrate to measure soil respiration in cores wetted using conventional methods and found that it lacked the necessary sensitivity.

## Presentations

Curtis, G. P., and L. C. Hull, "Estimates and Modeling of Uranium Mobility at the Idaho National Engineering and Environmental Laboratory," *American Geophysical Union Fall Meeting, San Francisco, CA, December 2000.*

Hull, L. C., R. A. Field, J. T. Coates, and A. W. Elzerman, "Surface Complexation and Actinide Migration in Soils," *Twenty-fifth Actinide Separations Conference, Boise, ID, May 2001.*

## REFERENCES

1. DOE, *A National Roadmap for Vadose Zone Science and Technology, Understanding, Monitoring, and Predicting Contaminant Fate and Transport in the Vadose Zone*, DOE/ID-10871, U.S. Department of Energy, Idaho Falls, Idaho, August 2001.
2. J. M. McCarthy, B. H. Becker, S. O. Magnuson, K. N. Keck, T. K. Honeycutt, *Radioactive Waste Management Complex Low-Level Waste Radiological Composite Analysis*, INEEL/EXT-97-01113, Bechtel BWXT Idaho, LLC, September 2000.
3. M. J. Case, A. S. Rood, J. M. McCarthy, S. O. Magnuson, and B. H. Becker, *Technical Revision of the Radioactive Waste Management Complex Low-Level Waste Radiological Performance Assessment for Calendar Year 2000*, INEEL/EXT-2000-01089, Bechtel BWXT Idaho, LLC, 2000.
4. D. L. Suarez and J. Simunek, "UNSATCHEM: Unsaturated Water and Solute Transport Model with Equilibrium and Kinetic Chemistry," *Soil Science Society of America Journal*, Vol. 61, 1997, pp. 1633–1646.
5. D. A. Dzombak and F. M. M. Morel, *Surface Complexation Modeling, Hydrous Ferric Oxide*, John Wiley and Sons, New York, New York, 1990.
6. D. R. Turner and S. A. Sassman, "Approaches to Sorption Modeling for High-Level Waste Performance Assessment," *Jour. of Contaminant Hydrology*, Vol. 21, 1996, pp. 311–332.
7. R. T. Pabalan, D. R. Turner, F. P. Bertetti, and J. D. Prikryl, "Uranium VI Sorption Onto Selected Mineral Surfaces," in: *Adsorption of Metals by Geomedia*, Everett A. Jenne, ed., Academic Press, New York, New York, 1998, pp. 99–130.
8. D. L. Parkhurst and C. A. J. Appelo, *User's Guide to PHREEQC (Version 2) —A Computer Program for Speciation, Batch-Reaction, One-Dimensional Transport, and Inverse Geochemical Calculation*, U.S. Geological Survey Water Resources Investigations Report 99-4259, U.S. Geological Survey, Denver, CO, 1999.
9. C. M. Bethke, *The Geochemist's Workbench, A User's Guide to Release 3.0*, University of Illinois, Urbana—Champaign, IL, 1998.
10. T. D. Waite, J. A. Davis, T. E. Payne, G. A. Waychunas, and N. Xu, "Uranium(VI) Adsorption to Ferrihydrite: Application of a Surface Complexation Model," *Geochim. Cosmochim. Acta*, Vol. 58, 1994, pp. 5465–5478.
11. M. Kohler, G. P. Curtis, D. B. Kent, and J. A. Davis, "Experimental Investigation and Modeling of Uranium (VI) Transport Under Variable Chemical Conditions," *Water Resources Research*, Vol. 32, 1996, pp. 3539–3551.
12. D. R. Turner, J. M. Zachara, J. P. McKinley, and S. C. Smith, "Surface-Charge Properties of UO<sub>2</sub>+2 Adsorption of a Subsurface Smectite," *Geochim. Cosmochim. Acta*, Vol. 60, 1996, pp. 3399–3414.
13. R. T. Pabalan and D. R. Turner, "Uranium (VI) Sorption on Montmorillonite: Experimental and Surface Complexation Modeling Study," *Aquatic Geochemistry*, Vol. 2, 1997, pp. 203–226.
14. J. A. Davis, J. A. Coston, D. B. Kent, and C. C. Fuller, "Application of the Surface Complexation Concept to Complex Mineral Assemblages," *Environ. Sci. Technol.*, Vol. 32, 1998, pp. 2820–2828.

15. D. Langmuir, *Aqueous Environmental Chemistry*, Prentice Hall, New Jersey, 1997.
16. I. Grenthe, J. Fuger, R. J. M. Konings, R. J. Lemire, An B. Muller, C. Nguyen-Trung, and H. Wanner, *Chemical Thermodynamics 1: Chemical Thermodynamics of Uranium*, North-Holland, New York, 1992.
17. R. J. Silva, G. Bidoglio, M. H. Rand, P. B. Robouch, H. Wanner, and I. Puigdomenech, *Chemical Thermodynamics 2: Chemical Thermodynamics of Americium*, North-Holland, New York, 1995.
18. C. J. Grossman, *The Sorption of Selected Radionuclides in Sedimentary Interbed Soils from the Snake River Plain*, Masters Thesis, Clemson University, Clemson, South Carolina, June 2001.
19. G. L. Hassler and E. Brunner, "Measurement of Capillary Pressures in Small Core Samples." *Trans. Am. Inst. Min. Metal, Eng.*, Vol. 160, 1945, pp. 114–123.
20. R. N. A. Hoffman, "Technique for Determination of Capillary Pressure Curves Using Constantly Accelerated Centrifuge." *Soc. Petrol. Eng. J.*, Vol. 3, 1963, pp. 227–235.
21. J. L. Conca and J. V. Wright, "Diffusion and Flow in Gravel, Soil, and Whole Rock." *Applied Hydrogeology*, Vol. 1, 1992, pp. 5–24.
22. FA Ventures, Inc, [http://www.UFAVENTURES.COM/ufa\\_ventures/tech\\_briefs/matric\\_potential.html](http://www.UFAVENTURES.COM/ufa_ventures/tech_briefs/matric_potential.html), 1996.
23. ASTM D18.21, "Test Method For Determining Unsaturated Hydraulic Conductivity In Porous Media By Open-Flow Centrifugation." *Annual Book of ASTM Standards*, Subcommittee on Ground Water, American Society of Testing Materials, Philadelphia, PA, 2000.
24. J. E. Stone and A. M. Scallan, "Structural Model for the Cell Wall of Water-Swollen Wood Pulp Fibers Based on Their Accessibility to Macromolecules." *Cellulose Chem. Technol.*, Vol. 2, 1968, pp. 343–358.
25. J. E. Stone, A. M. Scallan, E. Donefer, and E. Ahlgren, "Digestibility as a Simple Function of a Molecule of Similar Size to a Cellulose Enzyme." *Adv. Chem. Ser.*, Vol. 95, 1969, pp. 219–241.
26. D. N. Thompson, H.-C. Chen, and H. E. Grethlein, "Comparison of Pretreatment Methods on the Basis of Available Surface Area." *Bioresource Technol.*, Vol. 39, 1992, pp. 155–163.
27. J. K. Lin, M. R. Ladisch, J. A. Patterson, and C. H. Noller, "Determining Pore Size Distribution in Wet Cellulose by Measuring Solute Exclusion Using a Differential Refractometer." *Biotechnology and Bioengineering*, Vol. 29, 1987, pp. 976–981.
28. R.W. Smith, L .C. Hull, R. W. Johnson, E. D. Mattson, A. L. Schafer, J. B. Sisson, and D. N. Thompson, *FY 00 Annual Report*. Idaho National Engineering and Environmental Laboratory, Idaho Falls, ID, INEEL/EXT-01-01085, 2001, pp. 51–91.
29. S. Brunauer, P. H. Emmett, and E. Teller, "Adsorption of Gases in Multimolecular Layers."= *J. Am. Chem. Soc.*, 60, 1938, pp. 309–319.
30. A. Klute (ed.), *Methods of Soil Analysis*. Part 1, 2nd ed., Number 9 in the series AGRONOMY, ASG, Inc. and SSSA, Inc., Madison, WI, 1986, pp. 649–650.
31. L. Ström, D. L. Douglas, L. Godbold, and D. L. Jones, "Procedure for Determining the Biodegradation of Radiolabeled Substrates in a Calcareous Soil." *Soil Sci. Soc. Am. J.*, Vol. 65, 2001, pp. 347–351.

# “Next Generation” Predictive Models of Vadose Zone Flow and Transport

T. R. Wood,<sup>a</sup> D. L. Stoner,<sup>a</sup> R. A. LaViolette,<sup>a</sup> T. R. McJunkin,<sup>a</sup> R. K. Podgorney,<sup>a</sup> R. C. Starr,<sup>a</sup> K. Noah,<sup>a</sup> F. White,<sup>a</sup> G. Heath,<sup>a</sup> D. Peak,<sup>b</sup> R. J. Glass,<sup>c</sup> J. Fairley,<sup>d</sup> D. Lebreque,<sup>e</sup> B. Faybishenko,<sup>f</sup> C. Reardon,<sup>g</sup> C. Tolle,<sup>a</sup> P. Chiappini,<sup>h</sup> and H. B. Smartt<sup>a</sup>

## SUMMARY

The ability to accurately predict the transport of hazardous inorganic and organic compounds and radionuclides in the subsurface, particularly in the vadose zone, is inadequate for making key decisions in the DOE system. The usual assumption for this inadequacy has been that imperfect observations or lack of sufficient characterization data. It is commonly thought that the inaccuracies can be remedied by refining the input parameters for numerical simulations, increasing efforts to characterize the subsurface, or using faster, more powerful computers. We hypothesize that fractured-rock vadose zones are complex, dynamic systems, and that volume-averaged simplified concepts, such as percolation flux, cannot adequately describe contaminant transport.

In consideration, the objective of this project is to investigate the role of complex, interacting hydrological, geochemical, and biological parameters in producing the dynamic behavior of contaminants in subsurface environments. Mesoscale test beds are the unifying experimental framework upon which system identification tools, sensing methods, and conceptual models are developed. A fully automated mesoscale test bed with a time-lapse digital imaging system was developed. Smaller scale systems have been developed to test single fracture and fracture intersections unit processes that are believed to contribute to complex behavior. The mathematical

tools under development are to be used for the diagnosis of system characteristics, and will provide the basis for predictive modeling. Sensing methods ranging from macroscale electrical resistivity tomography measurements of wetting to microscale identification of microbial processes provide quantitative and qualitative assessment of system behavior.

## PROJECT DESCRIPTION

The ability to predict the transport of radionuclides, hydrocarbons, metals, and other pollutants in the subsurface, particularly in the vadose zone, represents one of the more important challenges facing DOE. Liquid flow and contaminant transport processes in the subsurface have been the subject of numerous experimental and modeling investigations. In spite of these efforts, it is still difficult to accurately predict future concentrations and distributions of contaminants in vadose zones because of subsurface heterogeneity and spatial and temporal variability of fluid flow.<sup>1</sup> Many experts believe that the shortcomings within the conceptual framework or science that underpins vadose zone hydrology results in the inability to accurately predict contaminant transport.<sup>2</sup> The conventional approach to simulating subsurface contaminant transport has been to take a volume average of the physical and chemical properties of a site. By assuming that these parameters vary in a deterministic manner and obey physical and chemical laws, the transport of contaminants can

---

a. Idaho National Engineering and Environmental Laboratory, P.O. Box 1625, Idaho Falls, ID 83404-2107

b. Department of Physics, Utah State University, Logan, UT 84322-4415

c. Flow Visualization and Processes Laboratory, Sandia National Laboratories, Albuquerque, NM, 87185-0735

d. Department of Geological Sciences, University of Idaho, Moscow, ID 83844-3022

e. Multi-Phase Technologies, LLC, Reno, NV

f. Lawrence Berkeley National Laboratory, Berkeley, CA

g. Idaho State University, Pocatello, Idaho

h. Ziccardi Productions, Blackfoot, ID

be expressed in the form of partial differential equations.<sup>3</sup> However, at the field scale, the properties affecting transport are subject to great uncertainty owing to their inherent heterogeneity and a general paucity of data.

We are therefore pursuing an alternative based on the observation that even under ordinary conditions, flow in fractured-rock vadose zones can be complex in nature, that is, the dynamics and characteristics of subsurface flow and transport emerge from the interaction of the physical, chemical, and biological properties of the system. Some of the essential features of complex systems include the presence of nonlinear feedback in time or space (or both), strong spatial fluctuations or inhomogeneities, and long-term transient behavior far from equilibrium. We suggest that contaminant transport associated with fluid flow in fractured rock vadose zones cannot be adequately described with averaged, simplified, continuum approaches. We are investigating whether conceptual models that incorporate self-organization and dynamical complexity in flow in fractured rock vadose zones will lead to improved transport codes for proper management of environmental waste and cost-effective remediation of contaminated areas. We suggest that developing scientifically sound, coupled experimental, theoretical, and mathematical arguments will better describe the impacts of complex system behavior on contaminant fate and transport. This research supports several major initiatives for understanding and predicting contaminant fate and transport in complex subsurface environments and for applying this understanding to long-term stewardship of DOE legacy waste.

Three goals were established at the outset of this project to focus the multidisciplinary team on the issue of nonlinear and complex phenomenon in vadose zone transport.

- *Characterize the causes and controls of nonideal behavior in vadose zone flow and transport, including the nonlinear feedback among variables.* This goal establishes the need for two general areas of experimentation—laboratory experiments and field experiments. The objective of the laboratory experiments is to isolate system or

environmental variables and test each for its contribution or control of the onset of nonlinear system behavior. These ongoing experiments are being conducted using large and small blocks to simulate single or multiple fracture networks. The objective of the fieldwork is to generate field data sets with sufficient data density to resolve important subsurface phenomena leading to complex behavior. At the field scale we are interested in the impact of how networks of fractures interact to create self-organized behavior. Furthermore, we are interested in the design, application and use of tools to identify and monitor transient, nonlinear and complex behavior in real vadose zones.

- *Develop generalizations, categorize common characteristics, and define associative relationships that lead to emergent patterns in real-world vadose zones.* Anomalies between predictions and subsequently measured values may be the first evidence of complex behavior at DOE Environmental Management sites. The objective of this task is to review applicable reports, texts, articles, and models of DOE vadose zone transport problems to find data sets that can be analyzed as complex systems. Data sets will be analyzed and categorized using diagnostic mathematical methodologies.
- *Generate a “new” conceptual model of vadose zone transport that accounts for feedback between transport variables and an alternative mathematical approach that better represents the effects of uncertainty and nonideal behavior in vadose zone transport.* Attainment of this goal falls into three general areas: computational analysis, complex systems analysis, and development of a conceptual framework. The objective of the computational analysis task is to evaluate time traces laboratory and field data as it is collected, and to provide input into the experimental design. The complex systems analysis will investigate the overlap between complex systems theory and chaos theory and its application to subsurface transport. Developing a conceptual framework will lead to the development of appropriate “new”

algorithms for subsurface flow with laboratory and field data.

## Experiments

### Assessment of Surrogate Fractured Rock Networks for Evidence of Complex Behavior

A series of laboratory studies is underway to assess whether complex behavior observed in the field is a fundamental characteristic of water flow in unsaturated, fractured media. As an initial step, a series of four duplicate experiments has been performed using an array of bricks to simulate fractured, unsaturated media (Figure 1). The array consisted of 12 limestone blocks cut to uniform size ( $5 \times 7 \times 30$  cm) stacked on end four blocks wide and three blocks high with the interfaces between adjacent blocks representing three vertical fractures intersecting two horizontal fractures. Water was introduced at three point sources on the upper boundary of the model at the top of the vertical fractures. The water was applied under constant flux at a rate below the infiltration capacity of the system, thus maintaining unsaturated flow conditions. Water was collected from the lower boundary via fiberglass wicks at the bottom of each fracture. An automated system acquired and processed water inflow and outflow data and time-lapse photographic data during each of the 72-hour tests. For all tests, the boundary conditions remained constant with 1 mL/min applied via needle to each of the three fractures. For Tests 3 and 4 the bricks were disassembled and allowed to air dry between tests. In Tests 5 and 6 the bricks remained in place and humid air was pumped through the system to keep moisture in the bricks for electrical resistance tomography (ERT) imaging.

From these experiments, we can make a few general statements on the overall advance of the wetting front in the surrogate fracture networks. For instance, flow generally converged with depth to the center fracture in the bottom row of bricks (Figure 2). In addition, fracture intersections appear to integrate the steady flow in overlying

vertical fractures and allow or cause short duration high discharge pulses or “avalanches” of flow that quickly traverse the fracture network below. Small changes in fracture aperture, initial moisture content, hysteresis, temperature and air pressure may account for the variation in wetting. Thus, smaller scale tests of single fracture and fracture intersections are underway to evaluate a wide array of unit processes that are believed to contribute to complex behavior. Examples of these smaller scale experiments include the role of fracture intersections in integrating a steady inflow to generate giant fluctuations in network discharge; the influence of microbe growth on flow; and the role of geochemistry in altering flow paths. Experiments are planned at the meso- and field-scale to document and understand the controls on self-organized behavior. Modeling is being conducted in parallel with the experiments to understand how simulations can be improved to capture the complexity of fluid flow in fractured rock vadose zones and to make better predictions of contaminant transport.

### Impact Of Microbial Activity On Fluid Flow Through Fractured Rock Systems

To simulate a vadose zone fracture, the experimental setup for microbiological studies consisted of two limestone bricks pressed together in a glass-faced support frame (Figure 3). To determine if microbial contamination would pose a problem in the system over time, the presence of bacteria was monitored using direct cell counts. Samples were taken daily from the discharge bottle, stained, and observed under a microscope. Initially, acridine orange, a nonviable fluorescent stain, was used, but was later replaced by the BacLight Live/Dead stain (Molecular Probes, Eugene, OR). Conversion to the BacLight stain provided a means to distinguish viable contaminant growth from residual, nonviable cells in the system. Because microorganisms are ubiquitous in the subsurface environment, future experiments will introduce the variable of stimulated microbial growth utilizing the knowledge gained from preliminary trials on limestone.

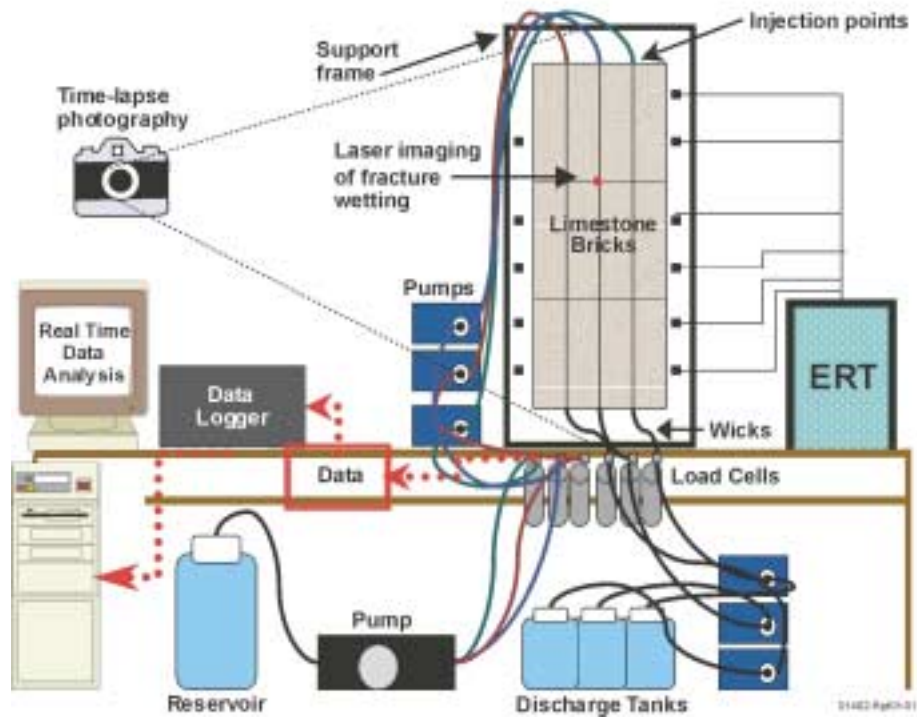


Figure 1. Schematic of experimental test bed.

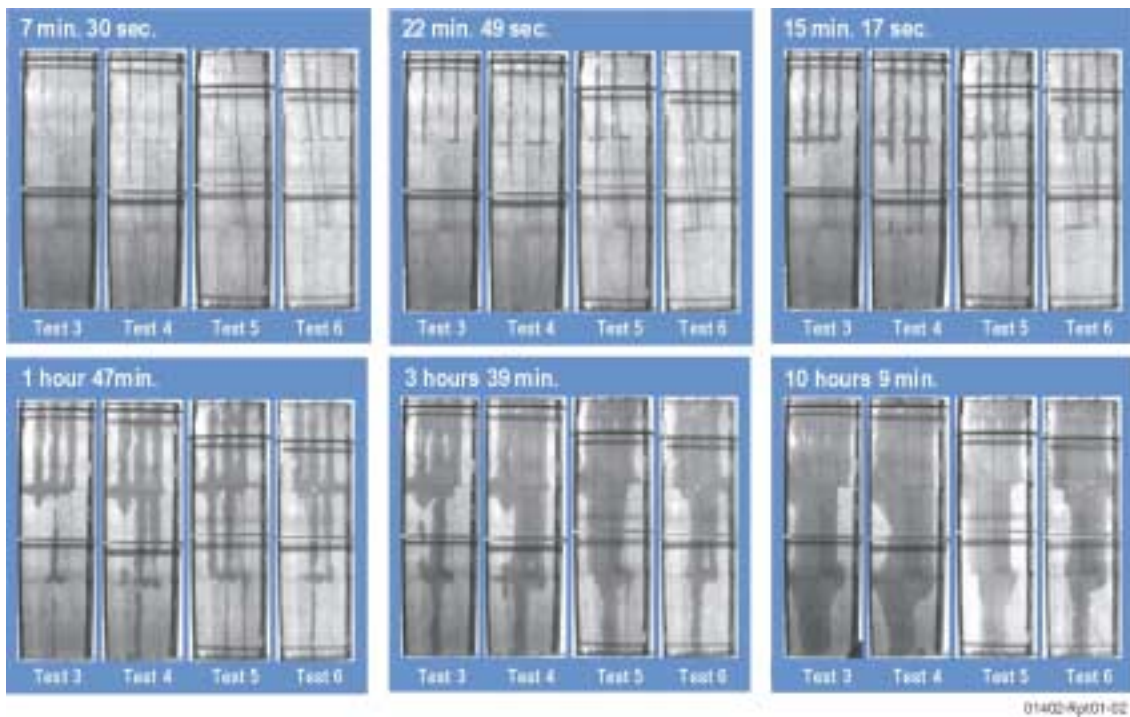


Figure 2. Time lapse photography of experimental system shows the variation in wetting front patterns for tests conducted under nearly identical conditions.

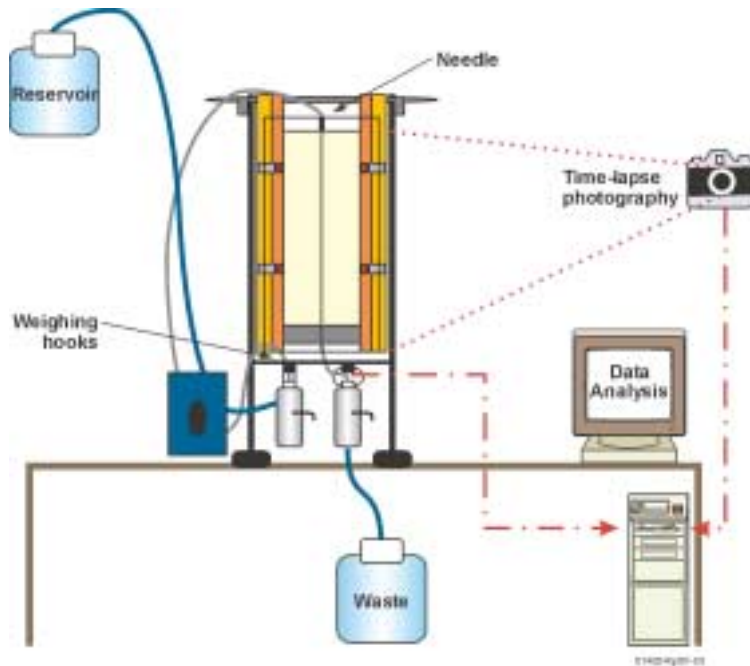


Figure 3. Schematic of microbial studies apparatus.

To determine how microbial numbers impact fluid flow through fractured media, biofilm formation and flow rates will be experimentally monitored. These experiments will use the approach described above with the exception of the incorporation of basalt, and the use of *Shewanella putrefaciens* cells genetically tagged with green fluorescent protein. Expression of green fluorescent protein by the bacterium (Figure 4) provides a noninvasive means for cell detection, visualization, and tracking.

### Electrical Resistivity Tomography

The use of electrical resistivity tomography (ERT) for imaging rock matrix and fracture moisture content was investigated in the laboratory experiments. The testing of various electrodes, electrode spacing, and imaging software routines (Figure 5) suggests that ERT will be useful during the course of our experiments for imaging relative moisture content of the brick network system. The right side of the figure shows the details of the various electrodes tested for imaging in the fractures. Based on signal to noise, ease of operation, and reliability, Type #3 was selected for use. Figure 6 is a difference plot of ERT image of

before and after the center area of the brick wall was wetted with a spray bottle. The area with low electrical resistivity is shown in blue and it corresponds to the area wetted with water. A series of experiments are under way that will compare geophysical images to time lapsed photographs of the wetting front advance.

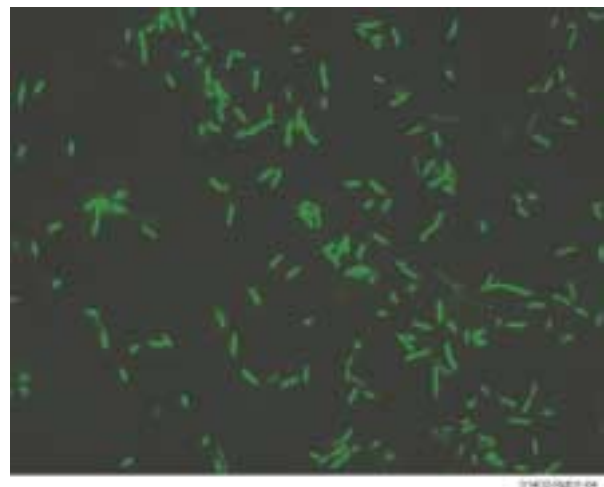
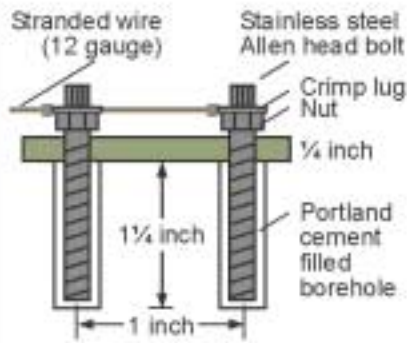


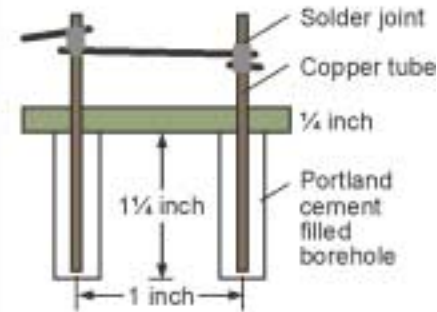
Figure 4. Epifluorescent photomicrograph of *S. putrefaciens* cells expressing green fluorescent protein.



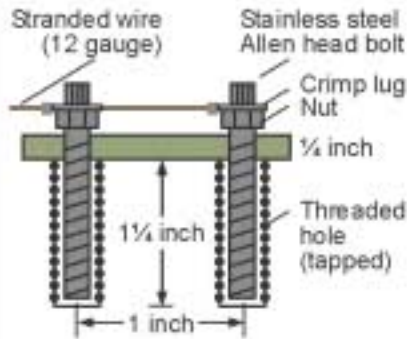
Type #1



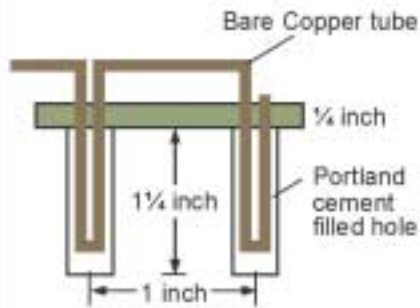
Type #2



Type #3



Type #4



01402-Rp01-05

Figure 5. Electrode type and placement for ERT tests.

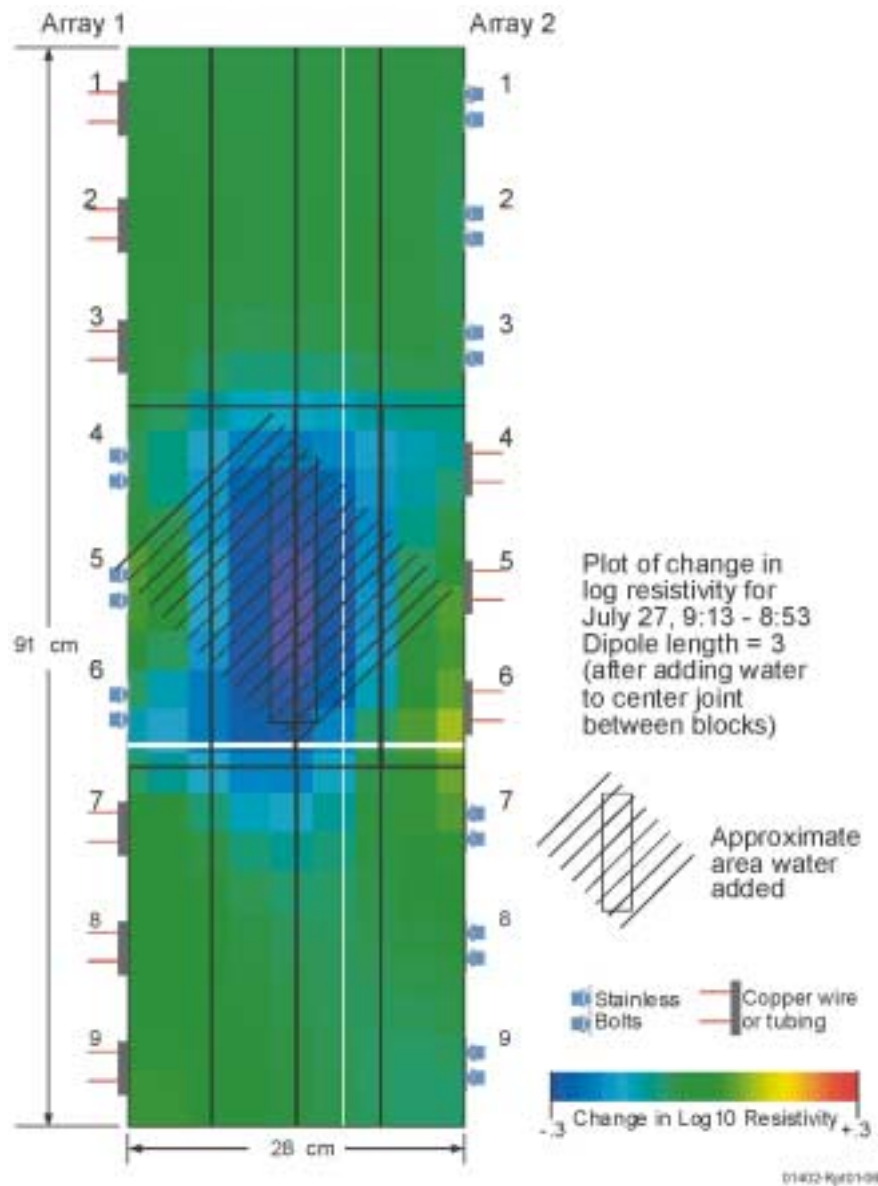


Figure 6. Results of ERT of experimental test bed.

### Fractured Rock Model Weighing Lysimeter

A weighing lysimeter experimental test bed was constructed and is currently being instrumented (Figure 7). The lysimeter is designed to allow measurement of small (<10g) changes in the weight of the laboratory model of the unsaturated, fracture rock system. The operating principal of the weighing lysimeter is similar to that of a triple beam balance with the mass of the model counter-balanced by weights at the beginning of the experiment. As water is added to the fracture model during an experiment, then the

model will become progressively more unbalanced. This change in weight can be correlated to the increase in saturation with great resolution. The fractured rock weighing lysimeter is equipped with high-resolution load cells that provide continuous monitoring of moisture content for the system.

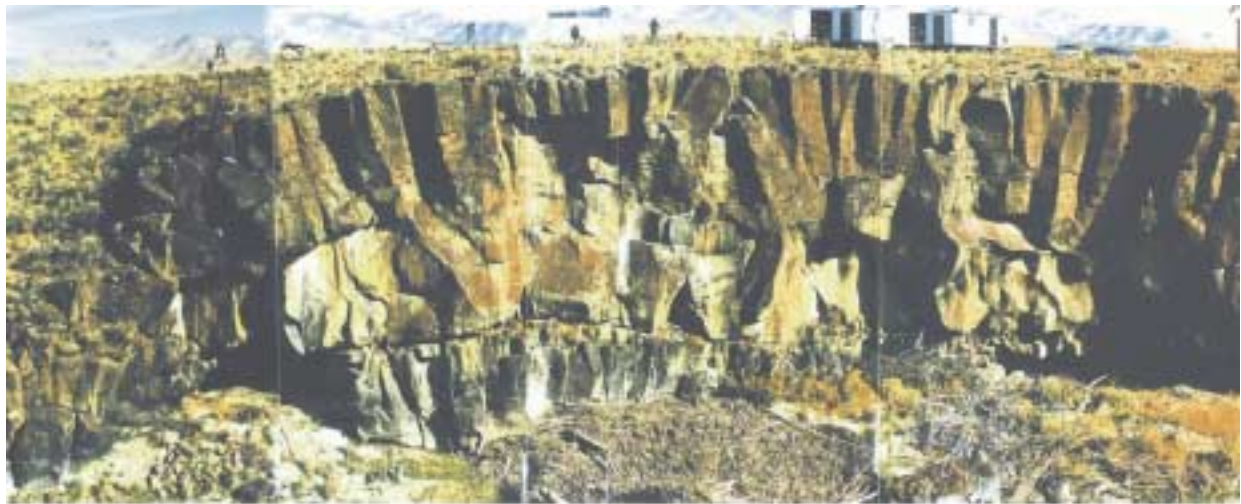
### Fieldwork

Several field excursions to the Hell's Half Acre (HHA) lava field and Box Canyon (Figure 8) yielded samples for experimental testing in the



01402-Rp01-07

Figure 7. Weighing lysimeter. The brick array is installed in the vertical section (white frame). The horizontal section and weights provides the counter balance.



01402-Rp01-08

Figure 8. Basalt fracture distribution on cliff at Box Canyon site.

laboratory and descriptive information on natural fracture apertures and orientation. Due to results generated in the laboratory testing, which found greater uncertainty in the causes and control of spontaneous complex behavior than anticipated, it was determined that actual field-testing would not take place in 2002. Rather, detailed testing under controlled laboratory

conditions of natural and artificially generated fractures in basalt would be conducted. These tests will examine the importance of air entry pressure and fracture topography in generating long-term behavior, typical of the Hell's Half-Acre data set. Plans for FY 2003 field testing will be generated in FY 2002 to look at field scale issues of fracture networking.

## Data Analysis

This task focused on examining existing data sets for the existence of complex behavior. We evaluated two subsurface data sets (Hell's Half Acre field data set and a brick wall experiment) and collected data, but did not interpret it. The evaluation of these two data sets is discussed below.

### Surrogate Analysis of Hell's Half Acre Dripping Data

We have applied a careful surrogate data analysis to flow rates measured in the 1998 and 1999 field experiments at HHA. The data consists of several records of drop intervals for the various sensors employed in the study, as well as mass flow rates at each sensor and total flow rates in and out of the test bed. The records are of varying lengths, but typically are a few thousand entries long. In order to conduct a careful iteratively refined Fourier transform (IRFT) surrogate analysis, it is necessary to use only data strings whose ends are similar. Using data strings with very different end values can introduce spurious high frequency contributions to the Fourier spectrum, which can lead to false rejections of the null hypothesis that the data are from a stochastic AR process. This requirement of end-value periodicity along with the requirement that useful data sets in the IRFT method have to be some power of two in length, severely limited what subsets of the measured data could be used for analysis. In fact, we were not able to find any flow rate stings that met both conditions that were longer than 128 entries. For the HHA data to exhibit a statistically significant difference from a stochastic AR process they would either have to be very low-dimensional (simple chaos) or wildly nonlinear.

For calibration purposes, we show (Figure 9) the flow rate data for one sensor taken from the HHA 1999 campaign along with an IRFT surrogate. The two are only subtly different, and a similar conclusion (in Table 1) was obtained for all useful data strings we managed to uncover. The data are from HHA99. In other words, based on the best analysis we

can perform at this point, it cannot be ruled out that the HHA data might be associated with a stochastic process with perhaps linear correlation. They are very unlikely to have resulted from low-dimensional chaos (as would be the case if each of the sensors were detecting droplets from independent chaotic faucets).

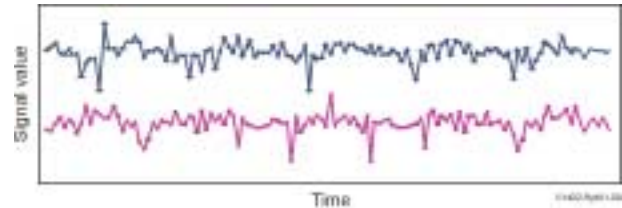


Figure 9. Flow rate data for Hell's Half Acre field data set (upper data string) compared to surrogate data set (lower data string).

Table 1. Significance level for data strings.

Data Source	Significance Level
Sum of Sensors	0.71
Sensor 4	1.39
Sensor 8	0.37
Sensor 15	0.51

### Evaluation of the Sandia Brick Wall Experiments

In 1995, Sandia National Laboratory, designed a laboratory-scale fracture-matrix network to explore the integration of single-fracture and single-fracture-matrix processes at the intermediate scale. However, the experimental data was not analyzed for this previous experiment, and was therefore deemed cost effective for our project to fund interpretation of the data because of the similarity of the tests with the proposed/needed experiments to evaluate complexity.

For the Sandia experiments, a thin, uncemented wall of porous bricks was constructed within a two-dimensional load frame. In a first experiment, water, chemically equilibrated with the bricks, was supplied to a fracture in the middle of the top of the initially

dry system, and subsequent system behavior was followed photographically over a 71 day period (Figure 10 and 11). Flow pathways evolved that were heavily controlled by processes acting within the fracture network, demonstrating the schizophrenic roles of fractures as both flow conductors and capillary barriers. Pathways formed primarily within the fractures, with minimal lateral matrix interaction across surrounding nonflowing fractures. Multiple pathways were also found to form over time. Finally, evaporation-precipitation (carbonate) processes led to a constraining of the flow field correlated with both pathway strengthening and starvation. A second more sophisticated experiment minimized the influence of external perturbations (principally evaporation) and included sensor arrays to measure pressure, temperature, and individual fracture outflow. On infiltration, the system once again showed the critical influence of fractures on the wetting process. Over time, the wetted structure took on

the look of a narrow plume without significant carbonate precipitation as might be simulated using standard single or dual permeability models; however, fracture outflow throughout the course of the 15-month experiment showed erratic temporal/spatial behavior both at short and long time scales. At long time scales, relative outflow contributions from each fracture varied and showed “switching” between flow pathways in time. At short time scales, we found that the erratic behavior could be synced through slight (0.1°C) oscillatory temperature forcing most likely through an evaporation/condensation mechanism within the experimental enclosure. The results of this second long-term experiment, under near constant temperature and inflow conditions, suggest flow processes within the fracture-matrix network, along with feedback from very small external forcing, to generate a time-local “unpredictable” behavior that is not simply random.

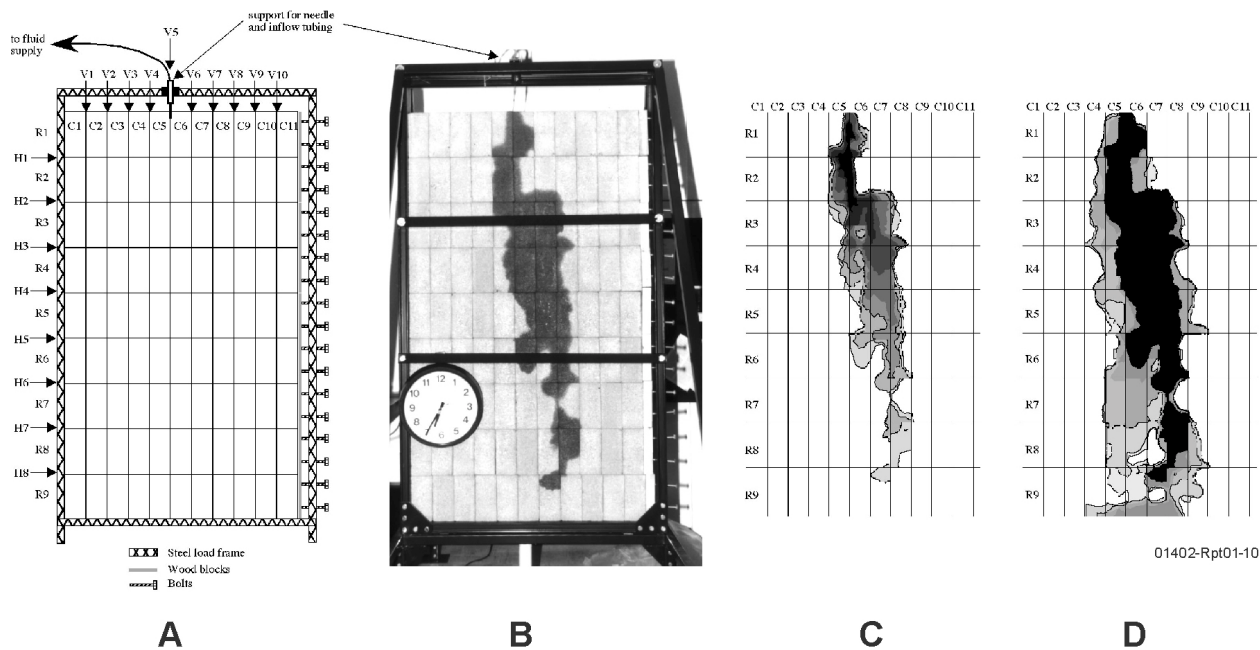


Figure 10. Experimental system and wetted structure development from 0 through 9 days. (A) Schematic of the experimental domain. Bricks and fractures are numbered from the upper left hand corner; V and H represent vertical and horizontal fractures respectively, while C and R represent column and row for the bricks themselves. (B) example wetted structure taken 42 hours after initiating flow. (C) Wetted structure development as a function of time, decreasing gray levels represent 2, 4, 8.5, 14.5, 20, 30, 42 hours after initiating flow. (D) continued development of the flow field, region shown in black represents the time span covered in C; remaining gray scale levels show wetted structure development at 52.5, 95.5, 149.5, 201.5, 225.5 hours after initiating flow.

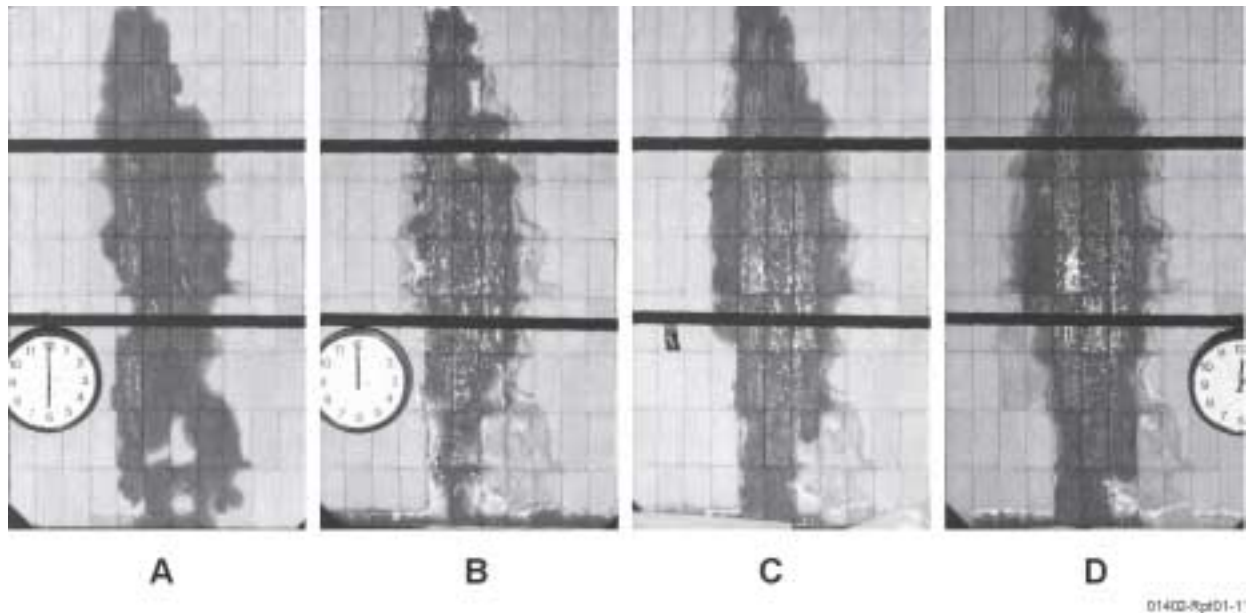


Figure 11. Wetted structure development and carbonate precipitation from 9 through 71 days: (A) 9 days, (B) 39 days, (C) 40 days, (D) 71 days.

## Theoretical and Modeling Tasks

Activities in this task focus on modeling nonlinear dynamics of vadose-zone flow using conventional approaches (continuum approaches), a method from complexity, and a new method based on theory developed under this project. The theoretical work on this project has centered on system observation and characterization of nonadditive, coupled, dynamical systems and detection of nonstochastic based dynamical systems via time series analysis for multidimensional spatial-temporal coupled distributed systems.

### A Surrogate Laboratory Experiment of Variably Saturated Fractured Rock

The applicability of current conceptual models of unsaturated fracture flow was explored by comparing laboratory tests and numerical simulations (Figure 12). An experimental domain

of a simplified fracture/matrix system was constructed from 12 limestone bricks stacked four wide and three high, separated by analog “fractures” whose apertures averaged from  $1.5 \times 10^{-4}$  m (vertical fractures) to  $1.7 \times 10^{-8}$  m (horizontal fractures). Water was introduced to the top boundary at a rate of about 1 mL/min to each of the three vertically oriented fractures (for a total of 3 mL/min), and collected by fiberglass wicks at the bottom boundary. These laboratory tests were simulated using four different conceptual models (isotropic and anisotropic equivalent continuum, dual porosity, and discrete fracture models). Despite the simple and well-characterized nature of the experimental system, all of the conceptual models tested failed to reproduce critical aspects of the observed behavior. This comparison implies that important physical processes are lacking from current descriptions of fracture flow in unsaturated media, and casts doubt on the ability of contemporary models to make useful predictions of subsurface flow and transport.

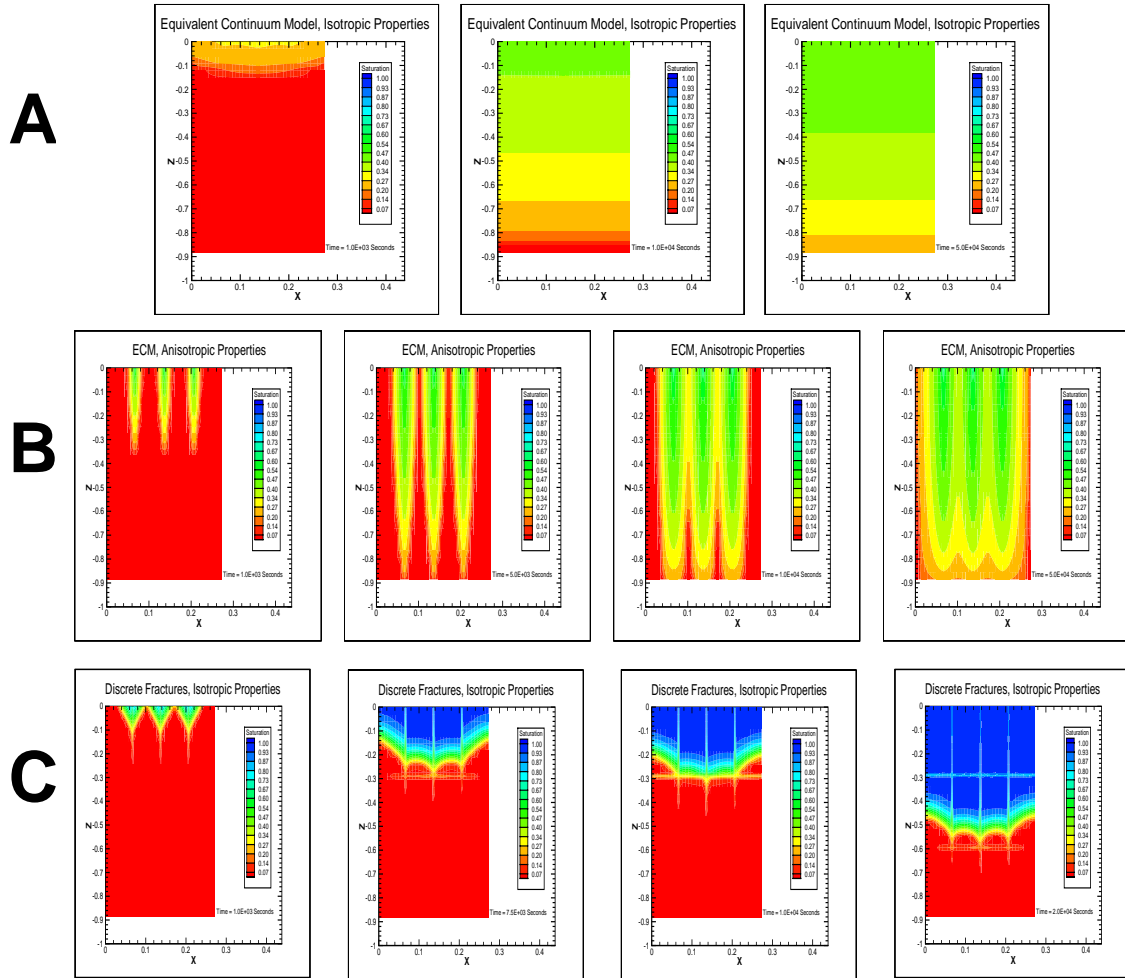


Figure 12. Results of modeling studies. (A) Equivalent continuum model with isotropic properties. The effects of fractures and matrix are lumped into a single material; properties are direction independent. (B) Equivalent continuum model with anisotropic properties; properties are direction dependent. (C) Discrete fracture model with isotropic properties; fractures and matrix each have their own independently specified properties sets.

### Effectiveness of ApEn and MI as Discriminating Statistics in Surrogate Data Analyses

The analysis of scalar time series for evidence of nonlinear dynamics frequently involves comparing the statistical properties of the measured data set with those of sets of “surrogate data.” The surrogate data are generated from the measured set in such a way that certain aspects of the original set are preserved while at the same time introducing elements of randomness. The most sophisticated surrogate method available at present, the IRFT method,<sup>4</sup> can produce data that

have exactly the same values as the original (meaning that they have the same mean, standard deviation, and frequency distribution) and almost the same Fourier spectrum, but whose order is scrambled relative to the original. Such surrogate data preserves whatever linear correlation exist in the measured data but destroys correlation that might arise from nonlinear dynamics. If the measured data are associated with such processes, then one would expect to be able to find a statistic that would discriminate between the measured data and a collection of related surrogates. In particular, it has been proposed by LaViolette, et al. (unpublished data) that ApEn (approximate

entropy)<sup>5</sup> is a good discriminating statistic. The reported results<sup>6</sup> are based on relatively large data sets (e.g., usually larger than 4,096 entries) and deal with relatively low-dimensional, weakly mixing, dynamical processes. To test whether ApEn yields a similar quality of discrimination for deterministic dynamics that are more strongly mixing, we calculated ApEn for 1,024 values of data generated by averaging the outputs of  $N$  one-dimensional chaotic “oscillators,” for different values of  $N$ . We then calculated ApEn for 100 realizations of IRFT surrogate data based on each of the originals. A level of significance was assigned to each comparison via the following equation:

$$significance = \frac{|ApEn_{measured} - \langle ApEn_{surrogate} \rangle|}{\sigma_{surrogates}} \quad (1)$$

Where:

**Error! Objects cannot be created from editing field codes.** =  
the mean value of  
ApEn calculated for the  
100 surrogates

**Error! Objects cannot be created from editing field codes.** =  
the standard deviation  
of the 100 surrogate ApEn  
values.

There are four different scenarios depicted in the Figure 13: (1) a straight sum of Tent Maps; (2) a sum of Tent Maps filtered through a power-4 observation function; (3) an AR(1,1) process with a sum of Tent Maps as the “stochastic term”; and (4) an AR(1,1) process with a sum of Tent Maps, then filtered through a power-4 observation function. The line on the plot in the figure represents a significance level of 5—at this level the ApEn for the original data is different from the average of ApEn for the surrogates by  $5\sigma$ , a typical criterion used for “significantly different.” Irrespective of which scenario is employed, ApEn fails to be an effective discriminator when the number of contributing oscillators exceeds *three*. In other words, when only 1,024 points are available for data from a reasonably mixing deterministic process, ApEn is likely not to be useful for discriminating between these data and data produced by a stochastically driven AR process (such as are generated by the IRFT surrogate method).

We have begun searching for a more sensitive statistic, but so far have not been successful. We speculated, for example, that mutual information (MI) might be more sensitive than ApEn (both statistics attempt to assay the presence of recurrent similarities in scalar data—as would be expected for data generated by nonlinear, deterministic dynamics)—but our numerical experiments have shown that MI is certainly no better than ApEn (and actually may be worse). This work continues.

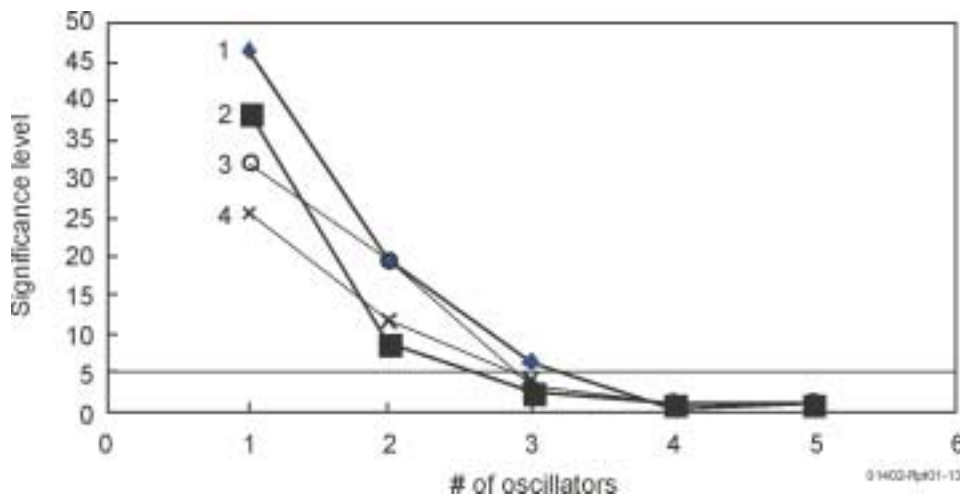


Figure 13. Results of ApEn Analysis.

## Modeling the HHA Experiments with Self-organized Dynamics

The HHA flow rate data exhibit strong fluctuations that are likely not due to some low-dimensional process. The HHA drop interval data show even greater variability. If one examines the frequency of occurrence of drop intervals of different sizes one finds an approximate power law relationship of the form frequency  $\propto$  interval<sup>*p*</sup>. Power law behavior of this kind is often symptomatic of an underlying process that lacks a characteristic length or time scale. One circumstance in which power laws can arise is when a spatiotemporal system is decomposable into a network of subsystems with a wide range of sizes. Because of the heterogeneity of cracks in fractured media, flow in fractured rock is a natural candidate for being such a system. In particular, we propose that flow of liquid through channels in fractured rock can be expected to episodically turn on and off as conditions of channel wetting, channel blockage, bubble formation, and the like vary. We expect that such fluctuations can result in flow networks with a self-organizing character. The simplest example of this is that flow that is stopped for whatever reason in one channel can stop flow both above and below that channel.

We have developed a simple pipe network (Figure 14.) that captures the essence of such self-organized fluctuations. The geometry of this simple model is shown to the right. In it, each pipe is labeled by a node (*i,j*) and a direction, + to the right, - to the left. Each has length *L* and a radius  $r_{ij}^{\pm}$ . Volume flow in each pipe obeys:

$$q_{ij}^{\pm} = \frac{\pi(r_{ij}^{\pm})^4 [p_{ij}^{\pm} + \rho g \Delta y]}{8\mu L} \sigma_{ij}^{\pm} \quad (2)$$

where:

$\mu$  = an average fluid viscosity (it could be pipe dependent)

$p_{ij}^{\pm}$  = the pressure difference

$P_{i,j} - P_{i+1,j \pm 1}$ . The quantities  $\sigma$  are either 1 (for an open pipe) or 0

(for a closed pipe). The pressure is assumed to be known at all top and bottom nodes.

Conservation of mass requires the following at each node:

$$q_{i-1,j-1}^{+} + q_{i+1,j-1}^{-} - q_{ij}^{+} - q_{ij}^{-} = 0 \quad (3)$$

If all pipes are open, the pressures at every internal node and consequently the flow rate into each node at the bottom can be found by a relaxation method. If some pipes are closed, one has to first identify the paths that fully connect the bottom of the network to the top before applying the relaxation calculation. In either case, we use the flow rates at output nodes to drive a set of ordinary differential equations of the dripping faucet kind<sup>7,8</sup> to yield an asynchronous, multidrop generator. Interesting dynamical behavior occurs when the various pipes are allowed to open and close randomly as time goes on. If we start with a sparse set of open pipes and apply open-closed reversals fairly infrequently we can obtain flow rates and drop intervals that are remarkably similar to those seen in the HHA data. That is shown in the following figures (15, 16, 17, and 18).

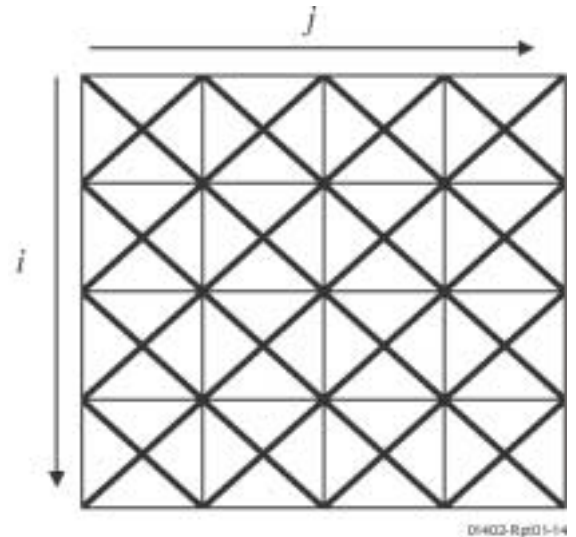


Figure 14. Simulated pipe network.

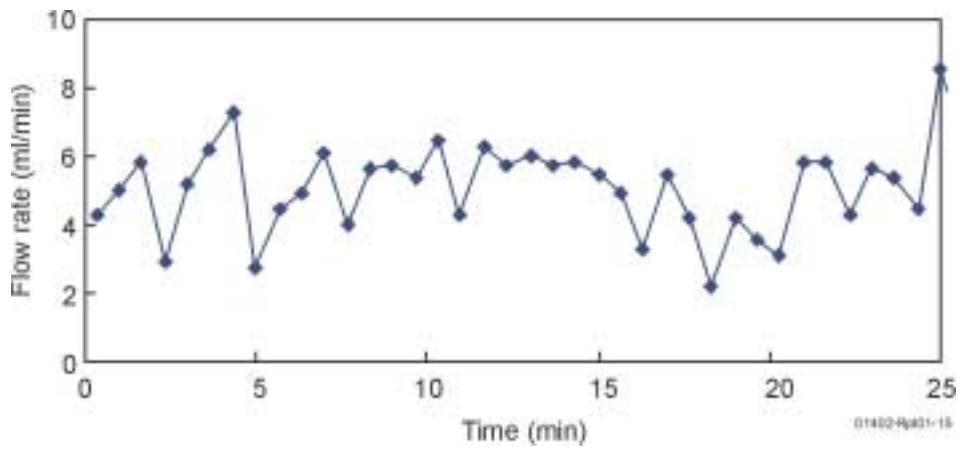


Figure 15. Total flow rate out of the network for Hell's Half Acre.

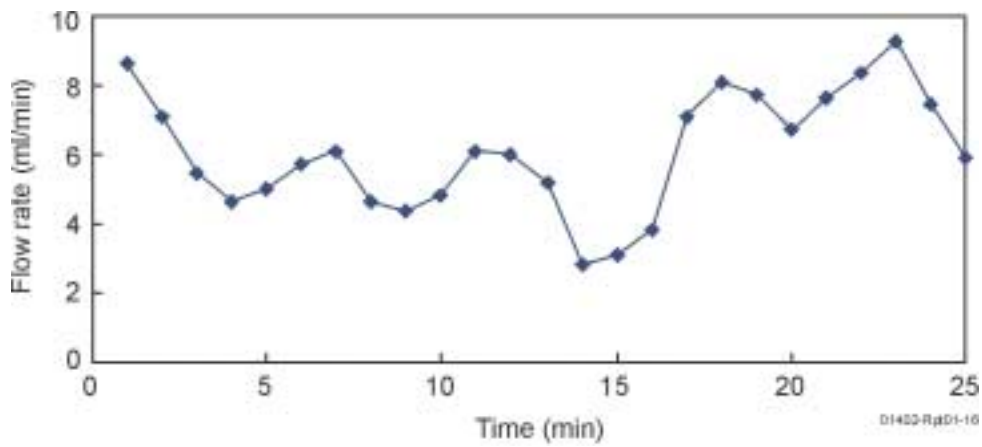


Figure 16. Flow for the simple pipe network.

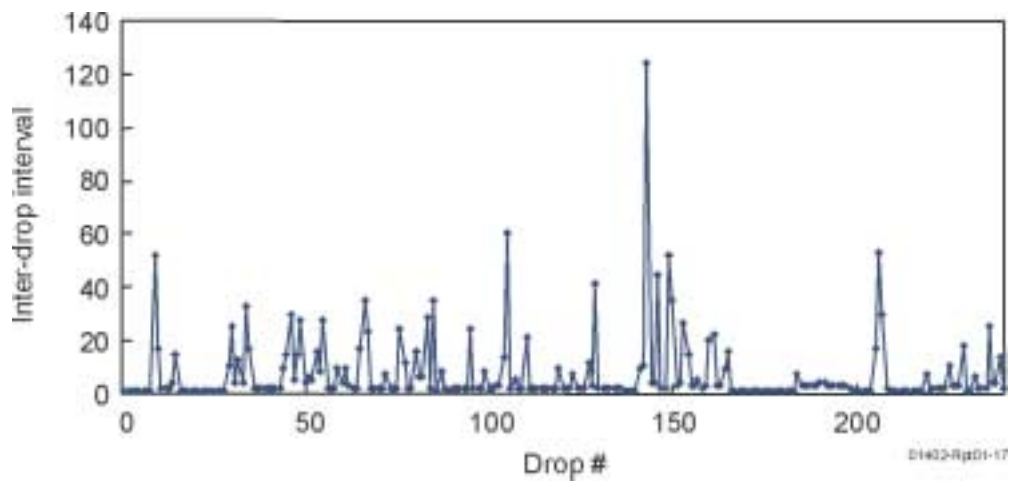


Figure 17. Drop interval data for Hell's Half Acre data set.

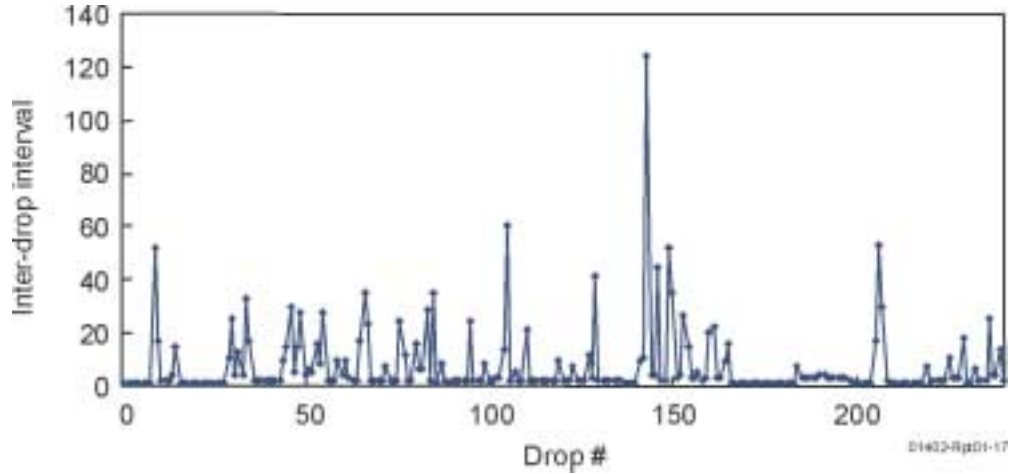


Figure 18. Drop interval for model data set.

The model described above is for fully saturated flow. In the case where flow is unsaturated, such as when internal dripping is the primary mechanism for the transport of liquid, a model that is very similar to a “sand pile” is likely to be more appropriate. Such a model will also show self-organized fluctuations. That is the focus of current work. While none of this proves that variability in flow in fractured rock is an example of self-organized dynamics, the similarities between model and measurement are certainly extraordinarily suggestive. In fact, these results lead us to believe that it is very likely that, under more or less ubiquitous conditions, large, power law fluctuations, which typically defy description by mean field hydrodynamics, will always be present whenever liquids flow through porous media. But, of course, that remains to be seen.

### Nonadditive Coupled Dynamical Systems

Complex, nonlinear dynamic systems are of fundamental interest because little is known at this point about how information propagates through such a system. Consider the rather simple case of two water droplet systems (e.g., two dripping faucets) where one system is the source for the second system. Under what conditions is it possible to observe the dynamics of the first system in data taken from the second system? It appears that the answer to this question is not presently known. How do nonlinear dynamic systems couple? Although we have just started investigation of these questions, we can offer some insight into at least the second question.

We can now have two Duffing oscillators:

$$x''[t] + 0.15x'[t] - x[t] + x[t]^3 = 0.3\text{Cos}[t] \quad (4)$$

Consider two dynamic systems. For ease of solution, we use a well-known Duffing oscillator:

$$x''[t] + 0.15x'[t] - x[t] + x[t]^3 = 0.3\text{Cos}[t], \text{ as shown in Figure 19.}$$

This is expressed as a third order differential equation with a cosine driving function. However, the cubic term makes this a nonlinear system; a numerical solution is shown below for initial conditions of  $x[0] = -1$ ,  $x'[0] = 1$ .

$$y''[t] + 0.15y'[t] - y[t] + y[t]^3 = 0.3\text{Cos}[t] \quad (5)$$

one in  $x$  and one in  $y$ . These oscillators are not coupled. However, we can easily couple them by adding a term to the second equation as:

$$x''[t] + 0.15x'[t] - x[t] + x[t]^3 = 0.3\text{Cos}[t] \quad (6)$$

$$y''[t] + 0.15y'[t] - y[t] + y[t]^3 + x[t] = 0.3\text{Cos}[t]. \quad (7)$$

By setting the initial conditions as

$$x[0] = -1, x'[0] = 1$$

$$y[0] = -1, y'[0] = 1,$$

we can generate numerical solutions as shown in Figure 20.

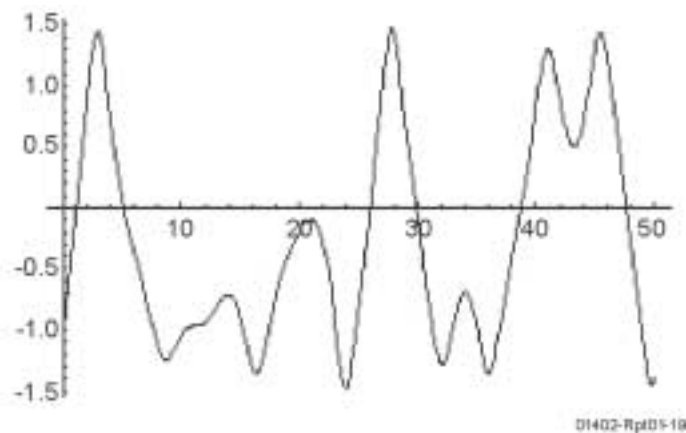


Figure 19. X as a function of t for a particular Duffing oscillator.

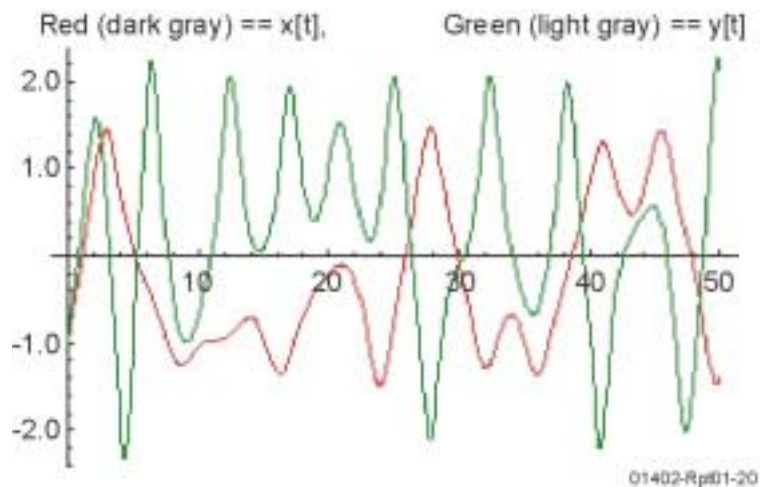


Figure 20. Solutions for x and y from the coupled oscillators.

The important issue to observe is that the coupling term acts as an additional term in the driving function in the second oscillator. Thus, there is not a simple addition of the dynamics of the two systems, but there is true dynamic coupling. This fact limits the use of super-position within the modeling and prediction efforts for such systems. In future work we plan to insert a variable integrator between the two systems, and then work on methods for observation of the dynamics of the first system, which are embedded in the dynamics of the second system.

### Multidimensional Spatial-Temporal Coupled Distributed Systems

There are many example systems that are multidimensional spatial-temporal distributed, such as: heat convection, electro-magnetic wave propagation, lasers, fibrillating hearts, and subsurface transportation. However, there exists almost no tools to quantitatively analyze these systems for nontrivial nonstochastic based dynamics. These efforts centered on developing a new method for this very purpose. The basic concept is to reduce the spatial information obtained from the system over time into a simple time series signal. The choice of this spatial reduction step is crucial. If you choose unwisely,

the system's dynamics being investigated can be integrated-out and lost. There are many possible choices: fractal dimension,<sup>9</sup> lacunarity,<sup>10</sup> capacity dimension,<sup>11</sup> etc. Once a traditional time series based on the system's reduced spatial information has been created; one can proceed with traditional time series analysis methods to infer nontrivial nonstochastic dynamics of the system. As a first cut, we choose to use surrogate data analysis as our method to infer nontrivial dynamics based on a spatial information reduction using fractal dimension (Reference 9), see Figure 21. Two surrogate generation methods were developed; type one consists of generating traditional time-series surrogates using the reduced spatial

information time series via iterated phase-randomized surrogates algorithm; type two consists generating spatial representation phase randomized surrogates in n-dimensional space before the spatial reduction into a spatially reduced time series occurs. The statistic that was used within this initial study was the nonlinear predictability statistic found within Kantz and Schreiber (Reference 11). Based on the decision to use the fractal dimension for our spatial information reduction process, we choose the complex Ginzburg Landau equation for our spatially distributed system to be tested (b=10):

$$A(1 - ib)A + \nabla^2 A - (1 - ib)|A|^2 A \quad (8)$$

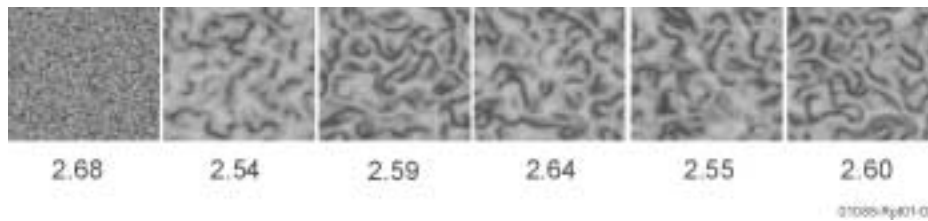
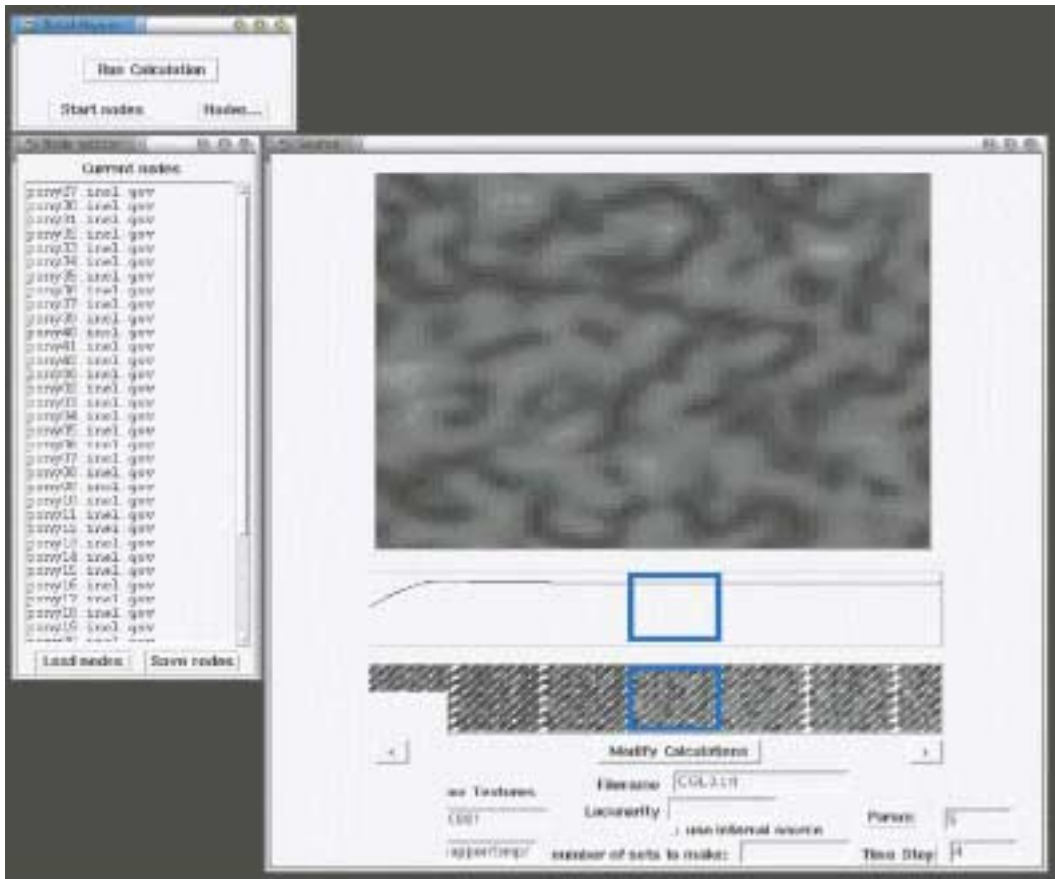


Figure 21: The Ginzburg Landau Equation (b=10) spatial information reduction via fractal dimension.

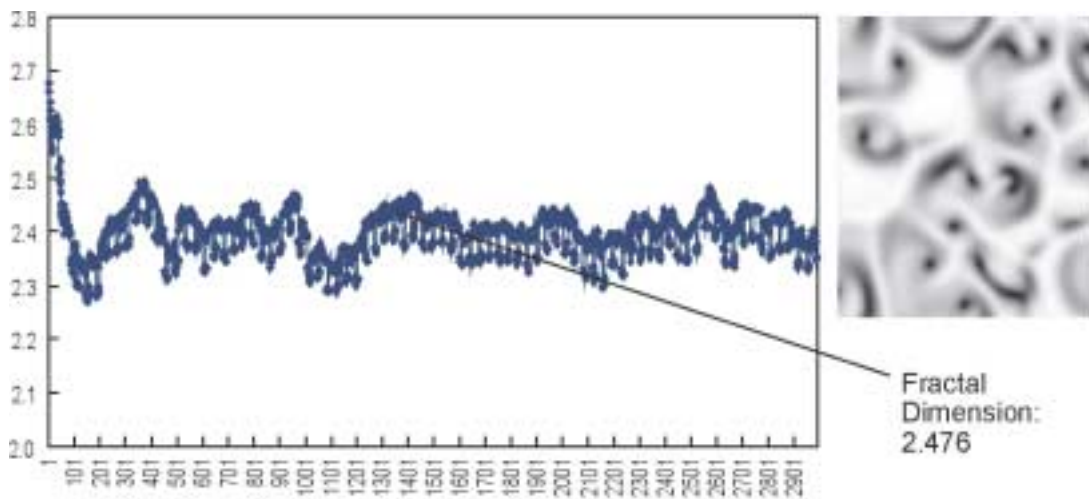
This equation is primarily used for modeling systems of traveling waves. The analysis code developed was designed to utilize parallel processing to minimize computation time. Parallel computational analysis are accomplished via an array of computers and data storage units networked with a conventional LAN. Such parallel arrays are managed by software systems that distribute the large computational workload across the various CPUs. The user interface is shown in Figure 22. Initial results for this analysis procedure are promising: the nonlinear predictability error's mean for the known nontrivial nonstochastic Ginzburg Landau system was calculated as 0.02575; while the type one surrogate mean for an ensemble of 99 was 0.2823 with a variance of

6.73E-08. Thus a separation of 9.6 standard deviations between the stochastic representative linear time invariant driven system and the original system was achieved. A sample of the reduced time series is given in Figure 23. The type two-surrogate generation method is still under development. In addition to the development of the spatial information reduction process and user interface, a method and algorithm for generation of n-dimensional phase randomized surrogate data, has also been developed. This algorithm is currently being tested, and is key to future examination of higher dimensional fused data sets being obtained through the experimental portion of this project.



01402-Rp01-22

Figure 22: Spatial-temporal to time series generation reduction user portion interface.



01402-Rp01-23

Figure 23: Example of spatially reduced time series based on the Ginzburg Landau Equation.

## ACCOMPLISHMENTS

We either made or submitted 20 technical presentations to upcoming meetings and are currently planning or preparing nine manuscripts.

For the experimental test bed, we have:

- Designed and built apparatus for measuring the change in mass of the unsaturated, fractured rock model. This weighing lysimeter has a resolution of +/- 0.01% of the total weight
- Designed environmental enclosure for maintaining constant temperature and relative humidity conditions=
- Designed and built smaller scale experimental systems to test single fracture and fracture intersections unit processes that are believed to contribute to complex behavior

For Sensors and Data Acquisition we have:

- Designed and built a fully automated data acquisition system with time-lapse digital imaging of wetting front advance
- Completed a Labview software module to automate time-lapse image acquisitionK
- Completed a Labview software module for integrating water flow data logging and pump control directly to PCI MIO card.
- Evaluated electrical resistivity tomography as a method to map system-wetting patterns
- Formed mathematical analysis and conceptual model
- Evaluated effectiveness of ApEn and MI as discriminating statistics in surrogate data analyses
- Modeled the Hell's Half Acre field data with self-organized dynamics=
- Developed prototype droplet detachment detection and logging software for future analysis work=
- Developed prototype spatial-temporal analysis tool for investigating determinism within

spatial-temporal systems using distributed computing resources

- Outlined the plan for single and coupled dynamics modeling and experimentation to discover boundary layer observation limitations.

## Publications

### In Preparation or Submitted

Glass, R. J., M. J. Nicholl, and S. E. Pringle, "Unsaturated Flow Through a Fracture-Matrix-Network: A First Experiment," In review for conference proceedings, "Bridging the Gap between Measurement and Modeling in Heterogeneous Media" *International Association of Hydrology, Groundwater Symposium, Berkeley, March 25-2, 2002.*

Glass, R. J., M. J. Nicholl, and S. E. Pringle, 2001, "Unsaturated Flow Through a Fracture-Matrix-Network: Dynamic Behavior of Flow Pathways," *Water Resources Research*, in preparation—target submittal end of September 2001.

Heath, G., D. Labreque, R. J. Glass, F. White and T. Wood, "Estimation of 2-D Moisture Content Using ERT Data On a Simulated Fracture Network," first data set completed and outline prepared.

LaViolette, R. A., D. Peak. C. R. Tolle, T. R. McJunkin and D. L. Stoner, 2001, "Combining the ApEn Statistic With Surrogate Data Analysis for the Detection of Nonlinear Dynamics In Time Series." *D. Physica*, in revision.

Peak, D. "Giant Fluctuations in Vadose Zone Flow," Data and figures completed.

Stoner, D. L., C. L. Reardon and others, "Impact of Biofilm Growth on Fluid Flow Through Fractured Media," planned.

Tolle, C. R. H. Smartt, R. LaViolette, K. Kenney, D. Pace, and J. W. James. "Chaotic Characterization of Droplet Detachments Within Aluminum Gas Metal Arc Welding," planned.

Tolle, C. R., D. Peak, T. McJunkin, and H. Smartt, "Characterization of Spatial-Temporal Chaos Using Traditional Chaotic Temporal Tools," planned.

Wood, T. R., D. Stoner, R. J. Glass, J. P. Fairley and R. A. LaViolette, 2001, "A Discussion of Complexity and the Prediction of Contaminant Transport in a Fractured Rock Vadose Zone," *Environmental Management*, in preparation.

### Accepted or Published

Faybishenko, B., P.A. Witherspoon, C. Doughty, J. T. Geller, T. R. Wood, and R. K. Podgorney, 2001, "Multi-Scale Investigations of Liquid Flow in a Fractured Basalt Vadose Zone in Flow and Transport through Unsaturated Fractured Rock," D. D. Evans, T. J. Nicholson, and T. C. Rasmussen, Editors, *Geophysical Monograph*, Vol. 42, Second Edition, pp. 161–182.

### Presentations

Fairley, J. A., T. R. Wood and T. R. McJunkin, "Comparison of Numerical Modeling Results with Laboratory Experiments of Flow in Unsaturated, Fractured Rock Abstract" Abstract submitted. *2001 Fall meeting of the American Geophysical Union, San Francisco, CA December 10-14, 2001*

Fairley, J. P., "Analysis of a fracture/matrix interaction test in low-permeability, welded tuff," *Spring meeting of the American Geophysical Union, Boston, MA, June 2001*.

Fairley, J. P., "Numerical simulation for the design of in-situ injection tests," *2001 International High-Level Radioactive Waste Management Conference, Las Vegas, NV, April 2001*.

Fairley, J. P., "Numerical simulation for the design of in-situ injection tests"; In: *Proceedings of the International Conference on High-Level Radioactive Waste Management, 2001, American Nuclear Society, La Grange Park, IL*.

Fairley, J. P., "Wetting front instability in unsaturated, fractured rock," Poster Presentation,

*Unsaturated Zone Interest Group meeting, Idaho Falls, ID, August, 2001*.

Fairley, J. P., "Wetting front instability in unsaturated, fractured rock," Poster presentation. *Annual meeting of the American Geophysical Union, San Francisco, CA, December 2000*.

Glass, R. J., and T. R. Wood., "Transport Within the Earth's Vadose Zone: Process Based Issues for Scaling" Abstract submitted. *2001 Fall meeting of the American Geophysical Union, San Francisco, CA December 10-14, 2001*

Glass, R. J., S. E. Pringle, and M. J. Nicholl. "Unsaturated flow through a fracture-matrix-network: Laboratory experiments at the meter scale," Abstract submitted. *Fall 2001 Annual Meeting of the Geological Society of America, Boston, MA, November 1-10, 2001*.

LaViolette, R. A. "Obstacles to Realistic Models of Contaminant Fate in the Subsurface." Abstract submitted. *2001 Fall meeting of the American Geophysical Union, San Francisco, CA December 10-14, 2001*

LaViolette, R. A., "Obstacles to Realistic Models of Contaminant Fate in the Subsurface," *Joint Northwest/Rocky Mountain Regional Meeting of the American Chemical Society, Seattle WA June 14-17 2001*.

LaViolette, R. A. "Exposing nonlinear dynamics in time series via surrogate-data analysis with a regularity statistic," Invited Seminar, *General Colloquium of the Physics Dept., University of Oklahoma, March 29, 2001*

Pringle, S. E., R. J. Glass, and M. J. Nicholl, Unsaturated Flow Through a Fracture-Matrix-Network: Dynamic Behavior of Flow Pathways, Abstract submitted. *2001 Fall meeting of the American Geophysical Union, San Francisco, CA December 10-14, 2001*

Reardon, C. L., T. R. Wood, J. M. Barnes, J. Fairley, K. S. Noah, and D. L. Stoner, Impact of Microbial Activity on Fluid Flow through Fractured Rock Systems, Poster presentation,

*Subsurface Science Symposium, Idaho Falls, ID  
September 6-7, 2001*

Stoner, D. L., T. R. Wood, D. Peak, R. J. Glass,  
and R. A. LaViolette “The Role of Complexity in  
the Prediction of Contaminant Transport in a  
Fractured Rock Vadose Zone Abstract” Abstract  
submitted. *2001 Fall meeting of the American  
Geophysical Union, San Francisco, CA  
December 10-14, 2001*

Wood T. R. McJunkin, R. K. Podgorney, R. J.  
Glass, R. C. Starr, D. L. Stoner, K. S. Noah, R. A.  
LaViolette and J. Fairley “Assessment of  
Surrogate Fractured Rock Networks for Evidence  
of Complex Behavior.” Abstract submitted: *2001  
Fall meeting of the American Geophysical Union,  
San Francisco, CA, December 10–14, 2001.*

Wood, T. R., D. L. Stoner and C. R. Tolle,  
“Communicating the Results of Modeled  
Predictions of Contaminant Transport in Fractured  
Rock Vadose Zones,” *Earth System Processes,  
Global Meeting, Scotland, Geological Society of  
America and Geological Society of England,  
Edinburgh, Scotland, June 24-28, 2001.* Wood, T.  
R., D. Stoner, C. Tolle, J. James, D. Peak, B.  
Faybishenko, and J. Crepeau, “Can a Fractured

Basalt Vadose Zone be characterized as a  
Complex System?,” *Summit 2000, Abstracts with  
Programs, Volume 32, Number 7, Geological  
Society of America, Annual Meeting and  
Exposition, Reno, Nevada, November 9–18, 2000.*

Wood, T. R., D. Stoner, C. Tolle, R. LaViolette, B.  
Faybishenko and R. K. Podgorney. “Alternative  
Analyses of Nonideal Water Movement in a  
Variably Saturated Fractured Basalt,” *38th U.S.  
Rock Mechanics Symposium, Washington, D.C.,  
July 7–10, 2001.*

Wood, T. R.” Implications of Conceptualizing a  
Basalt Vadose Zone as a Complex System,”  
*Fractured Rock 2001, Toronto, Ontario, Canada,  
sponsored by the US EPA, US DOE and Ontario  
Government (Ministry of the Environment). March  
26-28, 2001.*

Wood, T., D. Stoner, R. LaViolette, R. Glass, T.  
McJunkin, R. Podgorney, K. Noah, R. Starr, G.  
Heath, C. Reardon, M. Kerschbaum and D.  
Lebreque, 2001, “Integrated Experimental and  
Computational Analysis of Fluid Flow in  
Unsaturated Fractured Systems,” *Eighth Biannual  
Unsaturated Zone Interest Group Meeting, Idaho  
Falls, Idaho.*

## REFERENCES

1. R. K. Podgorney and T. R. Wood (1999). “Observations of Water Movement In Variably Saturated Fractured Basalt and Its Possible Implications On Advective Contaminant Transport.” *Dynamics of Fluids in Fractured Rocks: Concepts and Recent Advances, International Symposium in Honor of Paul A. Witherspoon’s 80th Birthday, February 10-12, 1999, Berkeley, CA.*
2. National Research Council. 2001, “Conceptual Models of Flow and Transport in the Fractured Vadose Zone,” Washington, D.C., National Academy Press.
3. Russo, D. (1998), “Stochastic Modeling of Scale-dependent Macrodispersion in the Vadose Zone. Scale Dependence and Scale Invariance in Hydrology,” G. Sposito, Cambridge University Press.
4. T. Schreiber and A. Schmitz. “Surrogate Time Series,” *Physica D*, 2000, 142: 346–382.
5. S. M. Pincus, “Approximate Entropy as a Measure of System-Complexity.” *Proceedings of the National Academy of Sciences of the United States of America*, 1991, 88(6): 2297–2301.
6. R. A. LaViolette, C. R. Tolle, et al. “Combining the ApEn Statistic With Surrogate Data Analysis for the Detection of Nonlinear Dynamics In Time Series,” manuscript in preparation.

7. A. D’Innocenzo and L. Renna, “Modeling leaky faucet dynamics.” *Physical Review*, 1997, E 55: 6776–6790.
8. A. D’Innocenzo and L. Renna, “Hopf Bifurcation and Quasiperiodicity In a Simulation Model of the Leaky Faucet,” *Physical Review*, 1998, E 58: 6847-6850 Part B.
9. C. R. Tolle, T. R. McJunkin, et al. (A).”Sub-Optimal MCV Cover Based Method for Measuring Fractal Dimension.” *IEEE Transactions on Pattern Recognition and Machine Intelligence*, in review.
10. C. R. Tolle, D. T. Rohrbaugh, et al. (B)”An Optimal Cover Based Definition of Lacunarity for Ramified Data Sets.” *Physica D*, in review
11. Kantz, H. and T. Schreiber (1997). *Nonlinear Time Series Analysis*. Cambridge, UK, Cambridge University Press: Chapter 4.



# Temporal and Spatial Characterization of the Vadose Zone

Earl D. Mattson (PI), James B. Sisson, and Joel M. Hubbell

## SUMMARY

The purpose of this project is to understand and quantify the phenomena underlying the fate and transport of organic and inorganic chemical species in the vadose zone to reliably predict their behavior under variable environmental conditions. To reduce the uncertainty of fate and transport model predictions, this research is examining three focus areas: temporal soil physics characterization, spatial geophysics characterization, and integrated data analysis and processing. This 3-year project focuses on developing innovative measurement tools, integrating temporal and spatial characterization approaches, and developing appropriate data interpretation techniques. Soil physical characterization tools have the advantage of providing continuous temporal data, but suffer from the fact that the measurement volume is small in comparison to the problem of interest. Alternatively, measurement techniques, such as geophysics, measure large volumes but do not provide direct measurements of state variables or parameters of interest, and are typically acquired at discrete points in time. The two measurement techniques are complementary and must be integrated and evaluated together to provide better conceptual and numerical models of contaminant fate and transport.

During the first year (FY 2001), this project has focused its efforts on temporal characterization, spatial characterization, and methodologies to interpret the data for model development. We have leveraged our resources in incorporating INEEL soil physics monitoring instrumentation with seven vadose zone research sites located within and outside the DOE complex. Based on two university collaboration efforts, we have (a) initiated methodology to collect sufficient data for geostatistical analysis and an indicator geostatistical approach to analyze this data set; (b) initiated development of a collaborative relationship with other (DOE, USGS, USDA, and

university) scientists through the sponsorship of a numerical model workshop and the organization of a vadose zone scientific meeting at the INEEL.

## PROJECT DESCRIPTION

Our inability to adequately describe the subsurface has been documented in numerous articles, books, and workshops.<sup>1-4</sup> A draft copy of a DOE sponsored book describes the primary characterization needs (listed in order of importance) as techniques that identify and describe heterogeneity, describe the contaminant and controlling geology, and improve sampling of the subsurface (Reference 1). Not only is the subsurface environment spatially variable, but recent studies also suggest that temporal variability of infiltration has a profound effect on the transport within the vadose zone. Data collection techniques have evolved from sporadic sampling to near continuous recording (e.g., quarterly monitoring of soil moisture with a neutron activation tool to permanently installed time domain reflectometry devices). The application of geophysical data collection techniques (electrical resistive tomography, ground penetrating radar, acoustic) within the vadose zone is rapidly expanding. Methodologies need to be developed to interpret these data sets and incorporate the results into numerical transport models. This 3-year project focuses on developing innovative measurement tools, integrating temporal and spatial characterization approaches, and developing appropriate data interpretation techniques (Figure 1). Understanding and predicting water movement and chemical transport at waste disposal sites requires measurement of four vadose-zone-state variables: water content, water pressure, temperature, and chemical concentration.

Richard's equation requires these variables as initial conditions in predictive models, and also to develop modeling parameters. Despite the

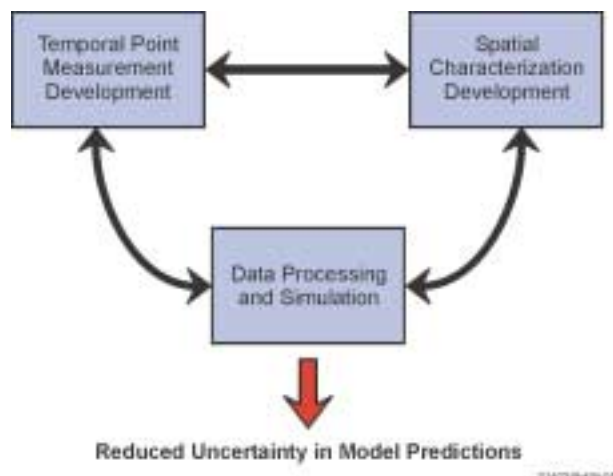


Figure 1. Relationship between temporal characterization, spatial characterization, and data processes to reduce numerical model uncertainties.

apparent simplicity of the concept of four state variables, we have yet to achieve a complete data set; appropriate measurement techniques are not available to provide the spatial distribution of these variables in a heterogeneous subsurface. In addition, parameters required by the numerical models are nonlinear and require temporal evaluation. As a result, modeling nonlinear effects requires the measurement of state variables, estimating multiple parameters at each spatial point in the vadose zone, and the changes in these variables and parameters over time.

The advective transport of water and gases is the primary mechanism that controls the distribution of contaminants, nutrients, and electron donors/acceptors in the vadose zone. The fluid pathways are determined by the distribution of the permeability distribution within the subsurface and the boundary conditions. Numerous controlled-boundary field scale studies (e.g., Las Cruces Trench site, New Mexico Tech Golf Course site, and Sisson and Lu's PNNL Borehole site) have indicated that the heterogeneity (distribution) of fluid transport properties is the controlling factor in the direction of fluid movement in the subsurface. Tools are needed to directly and indirectly describe subsurface processes and characterize these processes both spatially and temporally. In addition, methodologies are needed to process this data to ultimately describe spatial and temporal

chemical transport in liquids and gases in conceptual and numerical subsurface models.

We initiated a number of subtasks to integrate temporal and spatial characterization with flow and transport processes. These tasks are described below.

## Temporal Characterization of the Vadose Zone

### Vadose Zone Monitoring System

The INEEL Vadose Zone Monitoring System (VZMS) is a suite of borehole characterization instruments used to temporally characterize subsurface soil water flow and chemical transport. The VZMS measures vadose zone state variables; water potential, water content, and temperature, and allows extraction of moisture for chemical analysis. Data from the water potential, water content, and temperature sensors can be collected on a nearly continuous basis and stored in a data logger while soil water/gas sampling for chemical analysis is performed periodically. Data is typically retrieved remotely without having to access the sites. Instrument suites are placed at multiple depths within a borehole to develop a vertical profile of the temporal response of the flow system. Sensor configuration and individual types vary with specific site requirements.

The VZMS components are selected to measure the important state variables affecting contaminant transport in the vadose zone. These systems are typically customized for specific transport conceptual models, taking into account any additional constraints imposed by the specific site. Soil water potential is obtained using multiple Advanced Tensiometers,<sup>5</sup> which provide data for calculation of hydraulic gradients (direction of flow), allow evaluating of changes in water potential and to detect the presence or absence of perched water. Water content is measured using electronic sensors based on the dielectric constant of soil and water. Data is used to calculate changes in moisture content with time and depth. The configuration of the water content sensors varied for placement in various sized boreholes. Temperature is measured using thermistors or temperature sensitive resistors. Temperature data

is used to evaluate the depth of freezing, movement of wetting fronts, or at some sites, to determine if heat generated from decay of the waste may effect moisture transport. Solution/vapor chemical samplers are used to collect soil water and gas samples for specific chemical analyses.

The vadose zone monitoring system has been installed at four DOE sites this year: the B and SX Tank Farms at Hanford, and the Vadose Zone Research Park and Radioactive Waste Management Complex (RWMC) at the INEEL. All of these sites, except the SX Tank Farm had the complete suite of sensors, whereas the SX Tank Farm used only the tensiometer and water content sensors. The instrument design varied by location. The Hanford B Tank farm and Vadose Zone Research Park used the standard instrument suite as described above, while the SX site used specially designed small diameter instruments installed using the drive point technology. The instruments placed at the RWMC were installed using a sonic/cone penetrometer technique. The RWMC site also included a unique imaging system for visual examination of the material penetrated. Data from these sites are collected on a daily basis. Analysis of the data for long-term trends in soil moisture will begin in FY 2002.

## **CO<sub>2</sub> Monitoring**

The transport of contaminants in the vadose zone depends on hydrological, chemical, and biological processes. Although physical heterogeneities often control the initial spread of contaminants into the subsurface, chemical heterogeneities such as redox zones, organic rich layers, and sorbent-laden environments control the attenuation of many contaminants at depth. The presence of a gas phase in the vadose zone and the nonlinear relationships between material properties and moisture content make predictions of contaminant transport more complex than for the saturated zone. In situ measurement techniques to characterize contaminant distribution and chemical heterogeneities are lacking. Few methodologies for long-term monitoring of chemical processes in unsaturated soils have been developed. This task examines the impact of geochemistry on contaminant transport and

transformation in the vadose zone through the examination of CO<sub>2</sub> long term monitoring.

Chemical characterization of the vadose zone was initiated through the incorporation of CO<sub>2</sub> monitoring devices into the INEEL VZMS. The Vaisala GMM220 series transmitter is being evaluated as a long-term CO<sub>2</sub> sensor at the Jefferson Canal Research site. Five of these CO<sub>2</sub> transmitters were installed to depths of 10 meters to evaluate the long-term stability of the transmitters and to evaluate sensitivities to temperature, barometric pressure fluctuations, and soil physical variables. Preliminary data indicates that a high cross-correlation of the CO<sub>2</sub> sensor with temperature.

## **Spatial Characterization of the Vadose Zone**

### **Exfiltrometer**

We lack adequate site-characterization methods to predict unsaturated flow in porous media. Soil physical research initially focused on the nonlinearity of unsaturated water flow in soils, and has evolved to more recently include the description of spatial variability. The nonlinearity dependence on water content requires as many as seven parameters to estimate unsaturated hydraulic properties. Describing the unsaturated hydraulic properties spatial variation requires that the parameters be determined in a dense pattern over the area to be characterized. Currently available methods to determine these parameters are not efficient to employ. The characterization method must be fast, cheap, easy, low risk to employ, automated, easy to interpret, and provide direct measurements of the parameter of interest.

The INEEL has developed the exfiltrometer method for estimating unsaturated hydraulic properties of soils. The exfiltrometer method is a modified instantaneous profile method (IPM) used to estimate unsaturated hydraulic properties of soils in situ. Unlike current infiltration methods, this method relies on soil water leaving the measurement volume, coining the term exfiltrometer. Although the IPM has been successfully used over the years, it requires infiltration of large volumes of water covering the

surface, and subsequent weeks of monitoring for soil water potential and content. These requirements are often difficult to meet and do not provide a dense enough data set for geostatistical evaluation. The INEEL developed the exfiltrometer method in an effort to overcome the IPM requirements. The exfiltrometer is a steel cylinder equipped with a water content sensor and a series of tensiometers for monitoring soil water potential that is driven into the soil to a depth of 10 cm. Plots of the soil water content against water potentials are used to estimate the soil water retention curve. The changes in water content over time, along with gradients in water potentials, are used to estimate the hydraulic conductivity as a function of water content or water potential. The required calculations are the same as those for the IPM. When installed in dry soils, the relatively short column length (10 cm) allows water to be removed quickly from the exfiltrometer by the underlying dry subsoil.

Repeatability of the exfiltrometer method was demonstrated on a single column of soil. Four sequential measurements of the hydraulic

conductivity were made on the same soil unit. Figure 2, illustrates the repeatability of the exfiltrometer method. In general, the reproducibility was quite good (well within 50%) as compared to over an order of magnitude scatter in other characterization methods. Near saturation (less than 10 cm soil water pressure), the exfiltrometer hydraulic conductivity results were biased by temporal changes in the soil mechanical properties (soil density) as the test sequence progressed.

### Dielectric

The electrical permittivity of soils can be used to estimate the water content and electrical conductivity of vadose zone materials. The properties are related to the soil structure, and hence, the distribution of these properties can be used to describe the heterogeneity of the soil structure. The electrical permittivity of soils in the field is estimated from capacitance measurements, analysis of electromagnetic (EM) signals, or from the analysis of electrical signals obtained in specifically constructed waveguides. Operators of

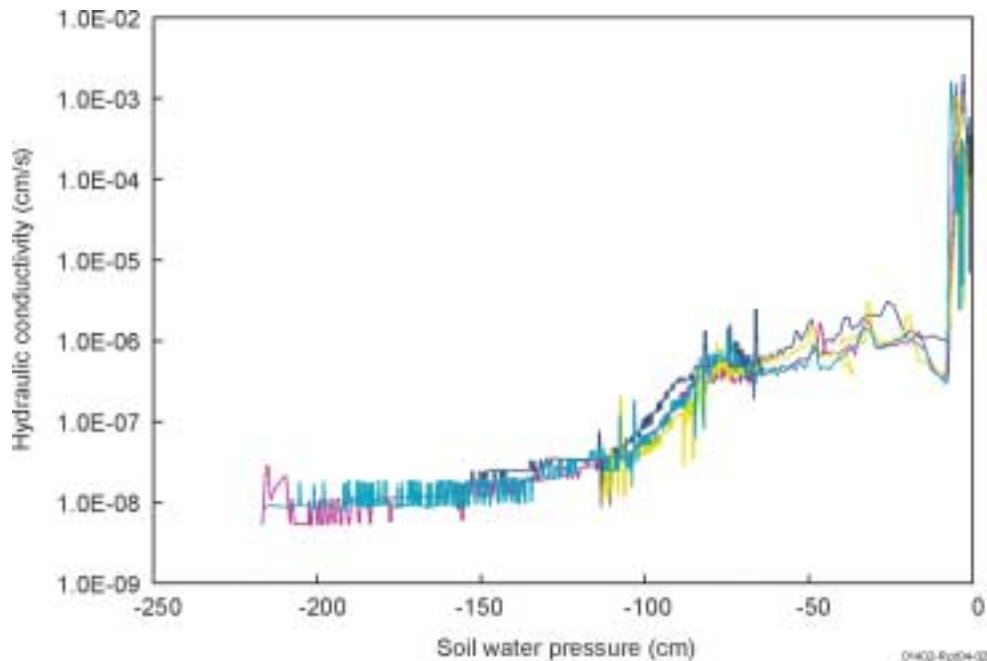


Figure 2. Exfiltrometer repeatability study results on a single soil sample. Lines illustrated the measured hydraulic conductivity as a function of soil water pressure from four sequential measurements on a single soil sample.

EM equipment prefer to investigate soil media at as high a frequency as possible to minimize the effects of ionic composition of the soil pore water. Unfortunately, EM signals rapidly attenuate, which reduces the depth of investigation with increasing frequency. The trade-off between signal attenuation and ionic effects is being approached as an optimization problem.

Ground penetrating radar (GPR) is becoming a common method in attempting to characterize saturated and unsaturated porous media. One problem in creating a tomographic image of the vadose zone with GPR data is the nonuniqueness of the inversion methods, which require additional data sets to constrain the GPR tomogram. However, these tools would allow estimating the electrical permittivity in the field during normal soil sampling and well installation activities. Field deployable permittivity instruments provide information that will be used to improve the calibration and design of water content—salinity sensors useful to long-term stewardship. A field deployable sensor will also be used to make in situ permittivity determinations at the frequency of the GPR that will be used to constrain numerical inversion models and sharpen the images of the subsurface.

Before we develop a field deployable permittivity sensor we developed a standard material and method procedure for calibrating field sensors. The standard method chosen was a shielded, open circuited, coaxial line sample holder connected to a microwave vector network analyzer (VNA). We use the VNA instrument to measure the signal reflection coefficient at the coaxial input to the sample holder, as the frequency of the signal is swept over a predetermined bandwidth. We were able to calculate the average complex permittivity of the material from the reflection coefficient data. The standard method was evaluated using deionized water and a series of NaCl solutions made up to a wide range of electrical conductivities. Since electrical permittivity is a complex variable, both the real and imaginary portions of the permittivity need to be considered. Figure 3 shows the real and imaginary parts of the complex permittivity plotted against frequency for a 0.005N NaCl solution, and the theoretical responses based on

the Debye model. The imaginary component of the measured and predicted permittivity varies by two orders of magnitude with the frequency of excitation and electrical conductivity of the solution. The real permittivity values are nearly constant until the excitation frequency exceeds 2 GHz. The measured permittivity using our method closely agrees with the Debye model results. The real permittivity and the predicted permittivity results almost lie upon one another. Only a slight bias in the measured and predicted imaginary permittivity is noted in our test sample (Figure 3). Testing our laboratory equipment to the theoretical models will allow us to design and build a series of field deployable wave guides and electronics for use in the field.

## Data Interpretation

### Flux Measurement

The detection of soil water transport in the vadose zone beneath hazardous waste disposal sites is important for monitoring and predicting contaminant transport in the subsurface. Water and contaminant transport in unsaturated fractured rock has become a concern over the past few decades. Vadose zone monitoring at disposal sites is gaining acceptance as a way to avoid the high cost of remediating contaminants in aquifers.<sup>6</sup> Nevertheless, long-standing attempts to monitor the vadose zone at disposal sites have been hampered by difficulties involving suitable instrumentation, suitable installation techniques, interpretation of results, and spatial variability. Natural recharge through fractured rock in deep vadose zone profiles is difficult to detect and quantify. Instrumentation has not been available to accurately detect and characterize water movement in the deep subsurface. Most vadose monitoring instruments evolved from agronomy/soil physics. As such, they were developed for shallow applications (less than 2 meters). Fortunately, instruments are now being adapted for deeper monitoring applications at disposal sites including some at fractured rock sites.<sup>5,7,8</sup>

Recharge through fractured vadose zones is more difficult to quantify than recharge through porous media vadose zones. Although water can move through either the fractures or the materials

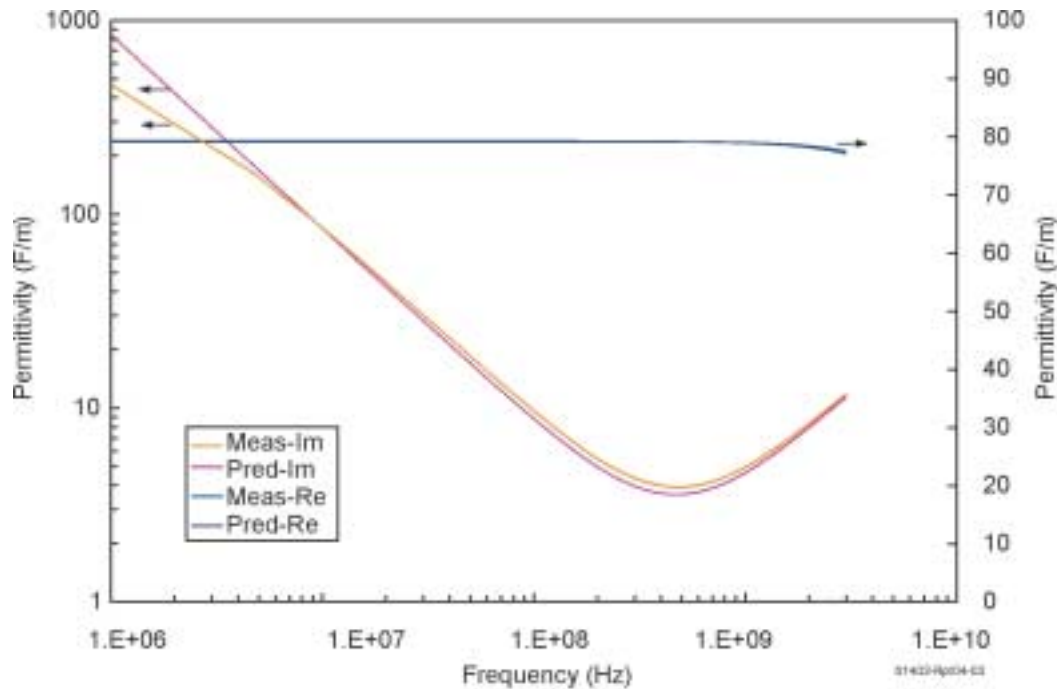


Figure 3. Measured and theoretical values of the complex permittivity plotted as a function of frequency, for a 0.005N NaCl solution. The left vertical scale represents the imaginary component; the right vertical scale the real component.

matrix, most researchers agree that localized partially saturated recharge through a fractured vadose zone occurs primarily through the fractures and not through the medium.<sup>9-11</sup> The magnitude of recharge, and hence the transport mechanism, is highly variable and is dependent on both local topography and plant cover.<sup>12</sup> Field and modeling results from a large-scale infiltration test conducted at the INEEL suggest that infiltration is primarily through the fractures, with the matrix flow having a minor influence on the advance of the wetting front.<sup>13</sup> The matrix flow may act to slow flow within the vadose zone by retaining fluids in slower flow pathways. The infiltration pathway becomes more difficult to conceptualize when the fractures become filled with porous material. At present, there is a lack of appropriate field monitoring data to distinguish between alternative conceptual fractured rock infiltration models.

A field study was conducted to determine if episodic recharge could be detected through fractured basalt at the Idaho National Engineering and Environmental Laboratory from spring

snowmelt events. Episodic recharge events were analyzed by examining long-term water potential from 2 to over 30 m below land surface over 3-1/2 years. Instruments (INEEL advanced tensiometers) were placed in both fractured and unfractured basalt media, which indicated values ranging from saturated (~+100 cm of head) to unsaturated conditions (-250 cm of water) throughout the year. Temporal analysis of the water potential data indicates a near steady-state unit-gradient downward flux within the fractured basalt for most of the year. However, episodic snowmelt infiltration events at land surface produced detectable changes in water potentials at depths to 15.5 m, in some cases, within a few days of the recharge events. These water potential responses varied both temporally and spatially during episodic infiltration events indicating preferential flow pathways through the fractured basalt. Large infiltration events were fairly easy to detect, but smaller infiltration events were difficult to distinguish due to fluctuations in water potential resulting from changes in barometric pressure.

Unit gradient analysis of the steady-state recharge flux indicates that unsaturated fracture flow is the major recharge mechanism through the fractured basalt during much of the year. Flux estimates were determined for the basalt matrix and sedimentary interbeds using steady state calculations and the change in depth of perched water from episodic infiltration within overlying surficial sediments and the basalt matrix. The estimates suggest moisture moves primarily in the fractures during episodic infiltration events and that the episodic events transport significantly more moisture than steady state flow through the basalt matrix. The results of this study indicate that advanced tensiometers can be used to measure water potentials in deep vadose zones, detect and monitor infiltration events, and estimate the contributions of episodic and steady-state recharge flux.

### **Geostatistical Analysis**

The exfiltrometer method was developed to provide information for geostatistical analysis of flow and transport parameters. Geostatistics is a mathematical method for interpolating values between known spatial points. The interpolating process requires estimating the semivariogram or the autocovariance function (cross correlation function for multiple variables) that describes the correlation structure. Once the autocovariance function is known, values are assigned to all points of interest within a volume of vadose zone materials.

A large data set is required to develop the autocovariance function. The cost to obtain these data sets has been prohibitive. For example, for a modern laboratory to estimate the van Genuchten parameters on a single soil sample the direct costs are on the order of \$2000/sample. The exfiltrometer can provide the van Genuchten parameters for a fraction of the laboratory cost. In collaboration with the University of Idaho, a student is currently in the process of collecting a sufficient data set to evaluate the covariance structure of all seven van Genuchten parameters using these standard geostatistical techniques.

In collaboration with Dr. Robert Holt of the University of Mississippi, we are developing an

alternative method for characterizing the spatial variability of hydraulic properties. This approach assumes that the classical geostatistical approach is not feasible due to measurement errors in obtaining the data sets. Typically, the transport parameter of interest, such as hydraulic conductivity, is not directly measured but calculated from surrogate measurements such as moisture content and soil water potential. If sufficient errors are contained in the surrogate measurements, these errors will be propagated to the transport parameter being determined. Errors in the transport parameter could bias the classical geostatistical approach.

In our alternative method, we use a nonparametric “indicator approach” to define the spatial patterns of the hydraulic properties. In this case, we propose not to interpolate for the value of the parameter of interest but to use the data to define zonal spatial patterns for the parameters. After the zones are determined, parameterization of these zones can be made. Both methods of geostatistical approaches will be evaluated and compared in numerical models and field experiments.

## **ACCOMPLISHMENTS**

The development of vadose zone contaminant transport conceptual models and the parameterization of numerical transport models have been problematic due to a lack of integration between temporal and spatial characterization approaches as well as methodologies to interpret the data. Soil physical characterization tools and geophysics are complementary and when used together can provide better characterization and monitoring data to develop conceptual models of infiltration and contaminant fate and transport.

The accomplishments of this project, which focus on temporal characterization, spatial characterization, and methodologies to interpret the data for model development, are summarized as follows:

- We have leveraged our resources in incorporating INEEL soil physic monitoring instrumentation with seven vadose zone

research sites within and outside the DOE complex.

- Between two university collaboration efforts, we have initiated methodology to collect sufficient data for geostatistical analysis and an indicator geostatistical approach to analyze this data set.
- We are collaborating with other (DOE, USGS, USDA, and university) scientists through the sponsorship of a numerical model workshop and the organization of a vadose zone scientific meeting at the INEEL.
- We have increased the scientific capability of the INEEL through the purchase a PowerProbe soil sampling unit and the hiring of a Ph.D. hydrologist and master level hydrogeochemist scientist.

A patent (U.S. Patent Number 6,263,726) was granted to Joel M. Hubbell and James B. Sisson, for a "Sidewall Tensiometer and Method of Determining Soil Moisture Potential in Below-Grade Earthen Soil," July 24, 2001.

A patent application was submitted to the U.S. Patent and Trademark Office for a "Self-Compensating Portable and Advanced Tensiometer design.

A patent application was submitted to the U.S. Patent and Trademark Office for a self-maintaining tensiometer for long-term monitoring at either shallow or deep depths.

A commercial license agreement was signed between the INEEL and North Wind Environmental Consultants July 24, 2001 to allow North Wind to construct and install advanced tensiometers and associated vadose zone monitoring instruments at Idaho Nuclear Technology and Environmental Center (INTEC).

Six invention disclosures were prepared and submitted to the Technology Transfer and Commercialization Officer of Bechtel BWXT Idaho LLC and the Chicago Intellectual Property Law Division (DOE). These intellectual properties include:

- *In situ vadose zone geochemical sensor.* This device is used for monitoring continuous, long-term geochemical constituents of fluids in the vadose zone or ground water. This device allows the measurement of geochemical parameters such as TDS, nitrate, carbon dioxide, pH, temperature, pressure, bromide, chloride, and other chemical constituents using commercially available sensors. This design will allow the in situ measurement of these variables at locations that were not previously possible, and will also allow other probes to be used in this device, as they become available. Either one or several probes (multiparameter) can be used at the same time. The probes can be removed, calibrated and/or replaced as required. This device's design is very flexible. It can be used to detect moisture movement, tracer movement, or a long-term in situ condition in the vadose zone or even in ground water.
- *Combination water content and water potential sensor.* This device is designed for monitoring continuous, long-term water potential and water contents in small diameter boreholes in the vadose zone. This device is designed for installation in small diameter boreholes such as the 1.25-in. (inside diameter) borehole formed by the AMS Power Probe, direct push drive rod, or in a hand augered borehole. This instrument will allow rapid deployment of sensors with minimal disturbance of the subsurface. These devices are planned to be installed at INEEL research sites, the University of Idaho's Troy research test site and at Hanford this fiscal year or early next fiscal year.
- *Sealed direct-push tensiometer.* This tensiometer is designed for placement in highly contaminated sites, and to operate for long time periods without the possibility of contaminants, such as radionuclides, moving through the instrument to land surface. The tensiometer, which can be calibrated in place, is designed to significantly reduce the noise in the data from changes in barometric pressure and so can detect very small changes in water potential in response to infiltration events. Additionally, the tensiometer has increased

strength and durability for emplacement using direct push or sonic drilling techniques. This instrument is one of a suite of instruments being installed in the SDA at the RWMC this fiscal year.

- *Horizontal advanced tensiometer.* This tensiometer is designed for placement beneath sites either by installing them prior to waste placement or by way of a horizontal access conduit. These designs are based on the original design of the advanced tensiometer and may be used at the RWMC for active waste monitoring, or at sites such as the mega-trench or slit trench at the Savannah River Site.
- *Techniques and devices to measure flux in the vadose zone (2).* These designs and associated techniques can be used to measure flux in the vadose zone.

Through collaboration with other sites we accomplished the following:

- *Hanford Tank Farm.* A vadose zone monitoring system was designed, constructed, and installed at the B Tank Farm in the 200 E Area of the Hanford Site using instruments and techniques developed for this project and adapted for use at the Hanford Site. Eight depths were instrumented with a combination of water content, temperature, water potential, shallow flux meter and solution samplers to characterize the soil moisture movement between the tanks at depths of 3 to over 200 ft. These instruments will provide a comprehensive data set of deep vadose zone properties to assist in understanding the dynamics of unsaturated flow at this site. This will be the first vadose zone monitoring installation measuring these parameters ever installed near the single walled tanks. These instruments are connected to a data logger for the unattended collection, storage, and transmittal of data using a cell phone system. Work is being conducted in conjunction with Glendon Gee of PNNL as part of the Subsurface Contaminants Focus Area (Subcon) EM-50 Project (RL31SS31), and in

collaboration with the RPP Vadose Zone Characterization Project.

- *INEEL, Vadose Zone Research Park (new INTEC Percolation Pond Monitoring).* Vadose zone instruments, borehole instrumentation techniques, and information obtained from monitoring the deep vadose were combined to support vadose zone instrumentation at the Vadose Zone Research Park being established at the location of the new INTEC percolation ponds. The research park will serve as a place to test hypotheses about water movement through the vadose zone and to compare new instrumentation to established methods of vadose zone characterization. Instrumented boreholes are being installed to depths of over 400 ft. Laboratory techniques were developed to calibrate the borehole water content sensor to allow measurement of moisture content within basalt. This will provide the first ever measurements of water content in situ within the basalt matrix. The calibration indicated a linear fit for moisture content versus output from the sensor.
- *INEEL, Radioactive Waste Management Complex (WAG 7).* A network of advanced tensiometers are monitored at the RWMC to characterize soil water potential in the deep vadose zone beneath the buried waste. Instruments are located from depths of 20 to over 220 ft below land surface. Data from this site was used in the ASTM paper and is being used to understand the flow and transport in this heterogeneous geologic media. Instruments invented for the V and V program (drive cone tensiometer, imaged drive tube and drive cone lysimeter) were used to develop a suite of vadose zone instruments for installation below, within and above the waste in pits 4, 5, 6 and 10 at the RWMC to characterize the distribution and movement of moisture and contaminants in these waste pits. To date over 50 instruments have been deployed and additional instruments will be installed in this FY 2002.
- *University of Texas, Engineered Barrier.* Ten advanced tensiometers were supplied to B. Scanlon and R. Reedy of the Bureau of

Economic Geology at the University of Texas for installation in an engineered barrier. These instruments will be used in conjunction with other vadose zone instruments to characterize the distribution and movement of moisture in the engineered barrier.

- *Mojave River Basin Recharge Study*. This work is being done in collaboration with J. Isbicki of the USGS in San Diego, who is using Advanced Tensiometers for a recharge experiment to be conducted near Victorville, CA in the Mojave River Basin. Advanced tensiometers were installed in a well at sedimentary interfaces to depths of 470 ft to track the movement of moisture in the subsurface in this alluvial fan material.
- *Rillito Creek Transmission and Evaporative Loss Investigation, AZ*. This work is being done in collaboration with K. Blasch, University of Arizona and the USGS in Tucson, AZ to evaluate recharge from the ephemeral Rillito Creek. Advanced Tensiometers are being installed in the arroyo to track the movement of moisture in the subsurface. The tensiometers will be used to monitor and analyze vadose zone flow events from summer monsoonal precipitation.

*Southeastern Kansas High Plains Recharge*. This work is being done in collaboration with M. Sophocleous, G. Kluitenburg (Kansas Geological Survey), and J. Healey (KSU), wherein vadose zone instrumentation is being used to characterize moisture and contaminant flow into the Ogallala aquifer. This investigation is being conducted with the USGS.

## **Publications**

### **In Preparation or Submitted**

Hubbell, J. M. and J. B. Sisson, "Measuring Water Potential Using Tensiometers," submitted to *Encyclopedia of Water Science*, Agropedia, Marcel Decker, Inc.

Hubbell, J. M., E. D. Mattson, J. B. Sisson, D. L. McElroy, "Water Potential in Fractured Basalt from Infiltration Events," in review for *Evaluation*

*and Remediation for Low Permeability and Dual Porosity Environments*, ASTM Special Technical Publication 1415.

Sisson, J. B. and A. H. Wylie, "Exfiltrometer Method for Estimating Unsaturated Hydraulic Properties in situ," Prepared for submittal to *Water Resources Research*.

### **Accepted or Published**

Mattson, E. D., E. R. Lindgren, and R. S. Bowman, "Electrically Induced Movement of Ions in Unsaturated Soil: 2. Field and Modeling Results," in press, *Journal of Contaminant Hydrology*.

Mattson, E. D., E. R. Lindgren, and R.S. Bowman, "Electrically Induced Movement of Ions in Unsaturated Soil: 1. Model Development Assuming Constant Electrical Conductivity," in press *Journal of Contaminant Hydrology*.

### **Presentations**

Mattson, E. D., J. M. Hubbell, J. B. Sisson, and D. E. McElroy, "The Value of Continuous Long-Term Monitoring of Vadose Zone State Variables," *American Geophysical Union, Annual Fall Meeting, December 2000*.

Hubbell, J. M., "Advanced Tensiometer and Type B Probe Deployment at the RWMC" *Ad Hoc Review Committee (AHRC) on Waste Area Group (WAG) 7, Idaho Falls, ID, May, 2001*.

Hubbell, J. M., "Advanced Tensiometer Deployment at the RWMC" *Environmental Management Advisory Board 's (EMAB) Technology Deployment and Transfer (TD&T) Committee, Idaho Falls, ID, March 13-14, 2001*.

Hubbell, J. M., "Design and Use of Drive Point Instruments for Monitoring in Waste at the Radioactive Waste Management Complex," *Unsaturated Zone Interest Group, Presentation, Scoville, ID, August 2, 2001*.

Hubbell, J. M., "Geology, Hydrology, Waste Characteristics Relating to the Instrumented Probing Project at the RWMC, WAG-7," *BEMET*

(Bechtel Environmental Management Exchange Team), Scoville, ID, May 2001.

Hubbell, J. M., "Vadose Zone Monitoring Using the Advanced Tensiometer," *Unsaturated Zone Interest Group, Poster Session, Idaho Falls, ID, July 31, 2001*.

Hubbell, J. M., "Water Potential in Fractured Basalt from Infiltration Events," *Evaluation and Remediation for Low permeability and Dual Porosity Environments, ASTM (American Society for Testing and Materials) Reno, NV, January 24, 2001*.

Sisson, J. B., "Analysis of Exfiltrometer Data for Estimation of Unsaturated Hydraulic Properties of Soils," *Western Regional Meeting of Soil Physicists, (W-188 regional meetings) Las Vegas, NV, January 2000*.

Sisson, J. B., A. L. Schafer, and E. D. Mattson, Unsaturated Hydraulic Properties With the

Exfiltrometer," *2000 Annual Meetings of the Soil Science Society of America, Minneapolis, Minn., November 5–9, 2000*.

Sisson, J. B., E. D. Mattson, and A. Wylie, "Long-Term Soil Water Monitoring Data at Arid and Semiarid Sites," *Eighth Biannual Unsaturated Zone Interest Group Meeting, Idaho Falls, ID, July 30- August 2, 2001*.

Sisson, J. B., G. Gee, J. M. Hubbell, and W. L. Bratton, "Advanced Tensiometer Results in Sands and Gravels," *2000 Annual Meetings of the Soil Science Society of America, Minneapolis, Minn., November 5–9, 2000*.

Sisson, J. B., Guest Lecturer, Vadose Zone 2001: Hydrogeophysical Characterization and Modeling Short Course, University of Arizona Campus, Tuscon, AZ, March 12–15, 2001.

## REFERENCES

1. R. Falta, B. Looney, and T. French, *Vadose Zone Science and Technology Solutions, Future Science and Technology Focus*, edited by B. B. Looney and R. W. Falta, Battelle Press, Columbus, OH, 2000.
2. Nuclear Regulatory Commission, *Research Needs in Subsurface Science, U.S. Department of Energy's Environmental Management Science Program*, National Research Council, National Academy of Science, 2000.
3. Nuclear Regulator Commission, *Seeing into the Earth*, National Research Council, National Academy of Science, 2000.
4. U.S. Department of Energy Idaho Operations Office, *National Roadmap for Vadose Zone Science and Technology; Understanding, Monitoring, and Predicting Contaminant Fate and Transport in the Unsaturated Zone*, DOE/ID-10871, August 2001, <http://www.inel.gov/vadosezone/documents/roadmap.pdf>.
5. J. M. Hubbell and J. B. Sisson, "Advanced Tensiometer for Shallow or Deep Soil-Water Potential Measurements," *Soil Science*, Vol. 163, No. 4, 1998, pp. 271–277.
6. M. Beckman, 1999, "Journey to the Center of the....Vadose Zone," July/August, *Radwaste Magazine*, Vol. 6, No. 4, 1999, pp. 55–57.
7. D. D. Evans and T. J. Nicholson, "Flow and Transport Through Unsaturated Fractured Rock: An Overview," *Flow and Transport Through Unsaturated Fractured Rock*, Eds. D.D. Evans and

- T.H. Nicholson, Geophysical Monograph 42, American Geophysical Union, Washington, D.C, USA, 1987, pp. 1–10.
8. P. Montazer, “Monitoring Hydrologic Conditions in the Vadose Zone in Fractured Rock, Yucca Mountain, Nevada,” in *Flow and Transport Through Unsaturated Fractured Rock*, Eds. D. D. Evans and T. H. Nicholson, *Geophysical Monograph Vol. 42*, American Geophysical Union, Washington, D.C. USA, 1987, pp. 31–42.
  9. J. C. Walton, R. G. Baca, and T. L. Rasmussen, 1989, “Flow and Transport of Radionuclides in Unsaturated Fractured Basalt,” Presented at Waste Management 89, University of Arizona, March.
  10. R. Nativ, E. Adar, O. Dahan, and M. Geyh, “Water Recharge and Solute Transport Through the Vadose Zone of Fractured Chalk Under Desert Conditions,” *Water Resources Research*, Vol. 31, No. 2, 1995, pp. 253–261.
  11. F. M. Durnivant, M. E. Newman, C. W. Bishop, D. Burgess, J. R. Giles, B. D. Higgs, J. M. Hubbell, E. Neher, G. T. Norrell, M. C. Pfeifer, I. Porro, R. S. Starr, and A. H. Wylie, “Water and Radioactive Tracer Flow in a Heterogeneous Field-scale System,” *Ground Water*, Vol. 36, No. 6, 1998, pp. 949–958
  12. G. W. Gee and D. Hillel, Groundwater Recharge in Arid Regions: Review and Critique of Estimation Methods, *Hydrological Processes*; Vol. 2, No. 3, 1988, pp. 255-266.
  13. S. M. Magnuson, *Inverse Modeling for Field-Scale Hydrologic and Transport Parameters of Fractured Basalt*, INEEL-95/0637, Idaho Falls, Idaho, U.S. Department of Energy, Idaho Operations Office, 1995, p. 41.

# Investigation of Interfacial Chemistry of Microorganisms

J. C. Ingram and D. E. Cummings (INEEL), H. Y. Holman (Lawrence Berkeley National Laboratory)  
F. Caccavo, Jr. (Whitworth College), and M. Downing (Shawnee High School, NJ)

## SUMMARY

Remediation of DOE sites contaminated with toxic metals and radionuclides is a complex and costly problem. Several bioremediation strategies currently being explored exploit the metabolism of naturally-occurring, dissimilatory, metal-reducing bacteria (DMRB). The versatile metabolism of DMRB may provide an effective mechanism for remediating contaminated subsurface environments.<sup>1</sup> A fundamental understanding of the molecular-level interactions between DMRB and contaminant metals and DMRB and mineral surfaces is requisite to the effective application of this metabolism in bioremediation, but interfacial processes are difficult to probe. Most microbiological characterization techniques require the extraction of cells or cell components from the surface of the solid sample.<sup>2</sup> Such approaches potentially lose all information regarding the nature of the interfacial processes when the cell was active. The goal of this proposed work is to use surface analysis techniques to directly probe the interfacial surface chemistries of DMRB cells and the underlying surface. This approach provides an in situ molecular picture of this interfacial chemistry because it does not require that the microorganisms be extracted from the mineral surface.

## PROJECT DESCRIPTION

### Background

The bioremediation of metals and radionuclides is highly dependent on the electron transfer processes that control the transport and speciation of metals and radionuclides in the subsurface. The mechanisms by which microorganisms accomplish electron transfer in the subsurface are influenced by their interfacial interactions with contaminant metals and minerals. These interfacial processes are critically important to developing

bioremediation strategies because understanding the intimate microbe/mineral relationship is the first step in identifying the desired biological process. Data from studies of these processes will yield information about temporal changes to the cell's physiology during its habitation on the mineral and the mineral modification following colonization and cell activity.

DMRB microorganisms are significantly relevant to the bioremediation of metals and radionuclides. These ubiquitous microorganisms respire oxidized metals and radionuclides as terminal electron acceptors under anaerobic conditions.<sup>3</sup> DMRB have tremendous potential to immobilize and detoxify contaminant metals via bioreduction reactions.<sup>4,5</sup> A growing body of knowledge surrounds the mechanisms of microbial metal sequestration and the likelihood of successful application and control of such bacteria to remediate contaminated aquifer sediments and groundwaters.<sup>1,6</sup> However, by the very nature of the technology, indigenous or introduced microorganisms are directly exposed to toxic inorganic compounds that may inhibit metal-reducing activity, and even cause cell death. Therefore, the application of this technology will depend on stable microbial populations capable of tolerating the substrates they are intended to remediate in addition to co-contaminating metals found at all DOE sites. Unfortunately, little information is currently available regarding the effects of metals and radionuclides on metal-reducing bacteria's ability to transform target contaminants. This project addresses these issues.

### Project Plan

This project focuses on investigating the following hypotheses:

- Dissimilatory metal-reducing bacteria (DMRB) exhibit biomolecular changes

associated with their interactions with reducible mineral surfaces, which subsequently alter the surface chemistry of the cell wall.

- These biomolecularly induced changes in the surface chemistry of the cell wall can be spectroscopically detected from intact DMRB.
- Direct determination of these signatures and alteration of the mineral surface chemistry will provide insights into mechanisms associated with microbial metal reduction processes.

To test these hypotheses, we are directly probing interfacial surface chemistries of DMRB cells and the underlying mineral, which eliminates the need to extract the microorganisms from the mineral's surface, thus providing an in situ molecular picture of this interfacial chemistry. The tools applied to these investigations include static secondary ion-mass spectrometry (SIMS) to directly probe top layers of the interfacial surface chemistry, microbial biochemistry and physiology techniques to characterize the microbiology, infrared (IR) spectroscopy, and other surface analysis tools.

We chose the *Shewanella putrefaciens* DMRB for these investigations because it is a facultative anaerobe, meaning that it can be grown under aerobic or anaerobic conditions. This well characterized DMRB has been the recent subject of many studies aimed at gaining mechanistic information concerning metal reduction in environmental systems.<sup>7,8</sup>

The initial project objectives were to collect spectral libraries (SIMS and IR) of various relevant components of the cell membrane for reference, and to investigate the cell surface chemistry of DMRB strains which have differing adhesion capabilities. Early in the project<sup>9</sup> we added an objective to continue the evaluation of SIMS for interrogation of intact microbial cells. Although this work was initiated through an earlier project, a few issues had not been addressed, and we specifically wanted to determine the extent of alteration caused to the intact microbial cells by the SIMS. This determination is important to understanding the SIMS data, as we have assumed

that we are interrogating the top layers of the microbial cells. If these cells were significantly disrupted, then our interpretation would be suspect. A second modification to the original project plan was to replace the investigation of adhesive capabilities of DMRB with an investigation of the effects of contaminant metals on the cell surface chemistry of DMRB. This change came after writing a proposal for DOE's Natural and Accelerated Bioremediation Research Program in which we found few toxicological studies of the effects of metals on bacteria of interest to bioremediation efforts, and yet, this is an important issue. In contrast, the adhesion capability of DMRB, which is also an important subject in bioremediation, is an area of research being studied by a number of groups. Thus, we decided to modify the original objective from investigating adhesion capabilities to investigating the effects of contaminant metals on DMRB.

## Results

The results of this research are divided in terms of our project objectives: (a) determine the alteration of intact microbial cells using SIMS analysis, (b) build spectral libraries (SIMS and IR) of various relevant components of the cell membrane for use as reference spectra, and (c) investigate the cell surface chemistry of DMRB strains with exposure to contaminant metals (toxicological study).

### **Objective A: Determine the Alteration of Intact Microbial Cells Using SIMS Analysis**

To accomplish this objective we used scanning probe microscopy to investigate alterations in the microorganisms that may be induced by the SIMS analysis, and an in-house designed and constructed SIMS instrument that uses a triple quadrupole (Extrel) and is equipped with a  $\text{ReO}_4^-$  primary ion gun.<sup>10</sup> A TopoMetrix scanning probe microscope was used in the noncontact, atomic force, microscopic mode. Images were collected from bacteria that had been filtered through 25-mm polycarbonate filters with a pore size of 0.2  $\mu\text{m}$  (Osmonics, Inc.). In these experiments, we collected images of *Shewanella putrefaciens* cells from samples that had been:

1. Filtered onto a polycarbonate filter, then air dried overnight.
2. Prepared like item 1 above, then placed in the instrument, and evacuated to  $10^{-7}$  torr for 15 minutes.
3. Prepared like item 2 above, with the addition of bombarding the sample with  $4.6 \times 10^{12}$   $\text{ReO}_4^-$  impacts per  $\text{cm}^2$ , which is slightly less than the static SIMS limit ( $10^{13}$  impacts per  $\text{cm}^2$ ).

We then compared the images of those *Shewanella putrefaciens* cells and observed very little difference in the cell structures (see Figure 1). These results suggest that under the conditions used to collect SIMS data, the *Shewanella putrefaciens* cells are not adversely affected by the instrumental conditions used for SIMS analyses. The second subtask in this objective was to determine if changes in the cell surface chemistry could be monitored by SIMS during different growth stages of the DMRB. The approach we took in these experiments relates to the work done in Objective C (Effect of Exposure of Contaminant Metals on DMRB) in which *Shewanella putrefaciens* was exposed to varying concentrations and species of arsenic. Because this subtask is tied to Objective C, the results are discussed in that section.

### Objective B: Building Spectral Libraries for Use As Reference Spectra

We used three different approaches to accomplish this task. First, we used the existing

spectral libraries of biochemical and cell components. There are large spectral libraries that contain a number of biologically-related compounds for infrared spectroscopy, but for SIMS, very few that have many spectra of compounds of interest to this project; thus, a greater need to create our own library for SIMS. Second, we acquired off-the-shelf biochemicals for use as reference material. This approach is good for providing specific information useful for chemical interpretation of complex systems such as microbial cells. Third, we acquired cell components, and collected their spectra. The spectra of cell components are much more complex than the specific biochemicals, but provide a good reference for the spectral signatures of specific components of the cells. To accomplish this approach, we collaborated with Professor Frank Caccavo, Jr. of Whitworth College, who is a microbiologist with expertise in fractionating microbial cells. Professor Caccavo and senior undergraduate student Scott Sulpizio fractionated cells of *Shewanella putrefaciens* sent to him from our laboratory, as well as *Shewanella alga* strains BrY and Rad 20 into surface fraction, outer membrane fraction, cytoplasmic membrane fraction, and the soluble fraction (cytoplasm and periplasm). A comparative analysis of intact cells and subcellular fractions by SIMS, IR, and SDS-PAGE will be used to aid in the interpretation of the spectral response of intact cells. Since data collection and interpretation are currently in process, the results of this work could not be reported here.

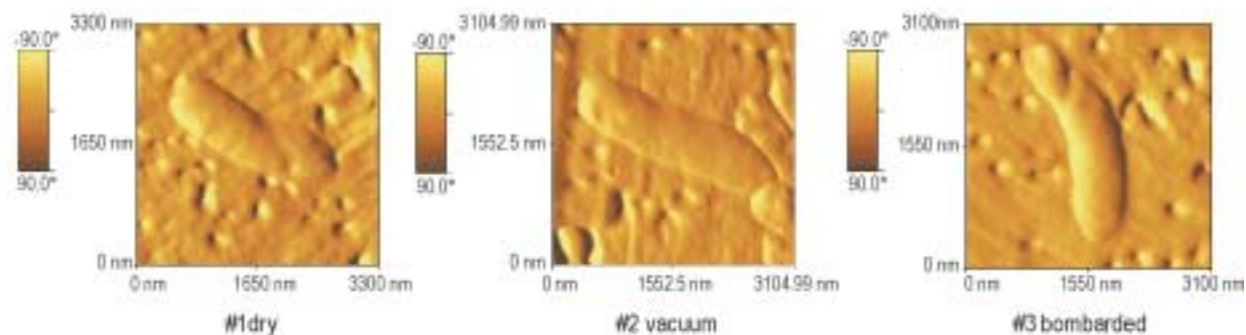


Figure 1. Comparison of *Shewanella putrefaciens* cells under different conditions.

### **Objective C: investigate the Effect of Contaminant Metals Exposure on DMRB Cell Surface Chemistry**

In this study, we investigated the biomolecular changes of DMRB caused by interactions with contaminant metals, which can alter the surface chemistry of the cell wall and subsequently mineral formation. The goal of our present work is to assess the damage caused by DOE-relevant metals to the common DMRB *Shewanella putrefaciens*.

*Shewanella putrefaciens* (ATCC 8051) was grown in a defined medium (M1)<sup>11</sup> under batch aerobic conditions. All experiments were performed with *Shewanella putrefaciens* grown under aerobic conditions because these initial experiments were used to establish protocols as well as investigate the physiological and biochemical effects of metal exposure. Culture growth was monitored by the absorbance of light at a wavelength of 600 nm, or by total protein in the culture flask using the Lowry method.<sup>12</sup> A key to consistent results in this study has been in the methodical preparation of inoculum with which to initiate the experiments: a chip of frozen *Shewanella putrefaciens* was added to 50 mL M1 medium and shaken at 150 rpm at room temperature. When the culture absorbance was between 0.600 and 0.800 Abs units at 600 nm, 1% (0.5 mL) was transferred to 50 mL medium and again shaken at room temperature until culture density reached 0.600 to 0.800 Abs units. This culture was then used to inoculate the experimental treatments.

All chemicals were reagent grade or higher. Stocks of sodium arsenate ( $\text{Na}_2\text{HAsO}_4$ ) and sodium arsenite ( $\text{NaHAsO}_2$ ), the oxidized (+5 valence) and reduced (+3 valence) forms of inorganic arsenic, were prepared in nanopure water and sterilized by autoclaving. The arsenite stock was prepared in anoxic ( $\text{N}_2$ -purged) nanopure water. Various concentrations of arsenate and arsenite were added to sterile growth medium from stock solutions to test the effects of arsenic on the growth kinetics of *Shewanella*

*putrefaciens*. Amorphous hydrous ferric oxide (HFO) was prepared according to published methods<sup>13</sup> by neutralizing a solution of  $\text{FeCl}_3$ , followed by multiple washes with nanopure water. All glassware were acid-washed and rinsed in nanopure water prior to initiating experiments.

### **Effects of Arsenic on Growth Kinetics**

The concentration of As(III) that inhibited growth of *Shewanella putrefaciens* cells was determined in M1 medium amended with sodium arsenite. As seen in Figure 2, between 2.5 and 5 mM As(III) completely inhibited the growth of *Shewanella putrefaciens* in M1 medium. Effects could be seen by as little as 500  $\mu\text{M}$  As(III), which caused a slightly increased lag phase, slower exponential phase growth rate, and lower final density (data not shown). Growth in 1 mM As(III) was biphasic (Figure 2). This concentration caused not only an extended lag, diminished growth rate, and lower final density, but also a second lag at 48 h, suggesting a secondary physiological response of the cells to accumulating insult.

Sodium arsenate was approximately 1,000-fold less growth inhibiting to *Shewanella putrefaciens* than the reduced form. Figure 3 shows that 100 mM As(V) has only a minimal effect on growth kinetics (no suppression). This effect may even be due to the effect of osmolarity (ionic strength of the medium) rather than toxicity. This dramatic distinction between the toxicity of the two oxidation states bears great environmental relevance. Aerobic environments rich in arsenic are likely to be of no concern for the introduction and/or manipulation of *Shewanella putrefaciens*. However, any action that leads to reducing conditions, such as the nutrient amendments central to biostimulation reclamation, will lead to toxic conditions to *Shewanella* if the As concentrations are 500  $\mu\text{M}$  (37.5 ppm) or greater. An interesting observation was that *Shewanella putrefaciens* cells grown in the presence of As(III or V) maintained higher absorbance values in stationary phase than did unexposed cells (see Figures 2 and 3). This observation is addressed again later in this report.

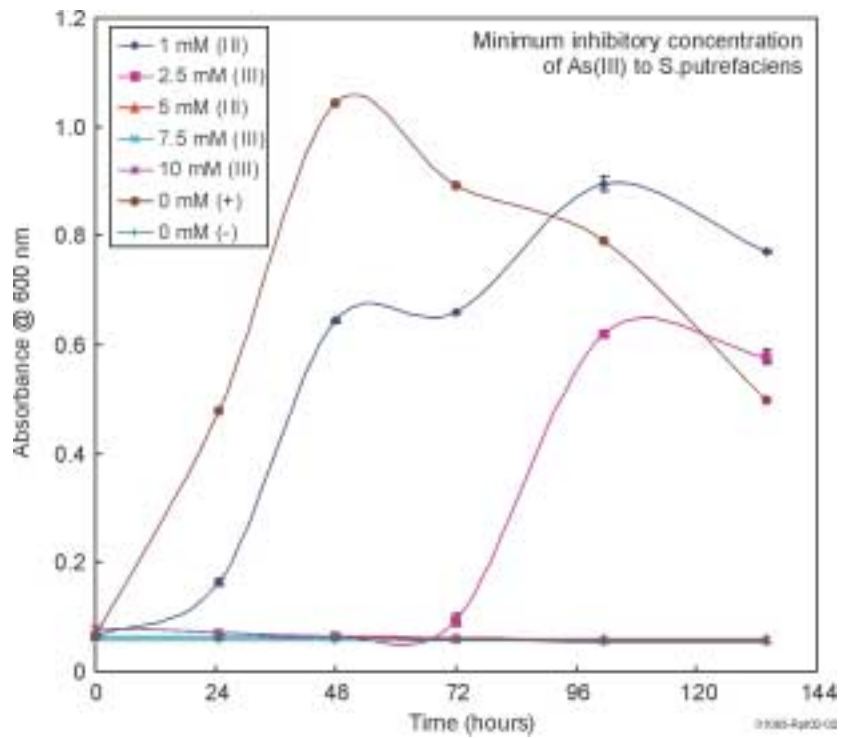


Figure 2. Minimum inhibitory concentration of As(III) to *Shewanella putrefaciens*.

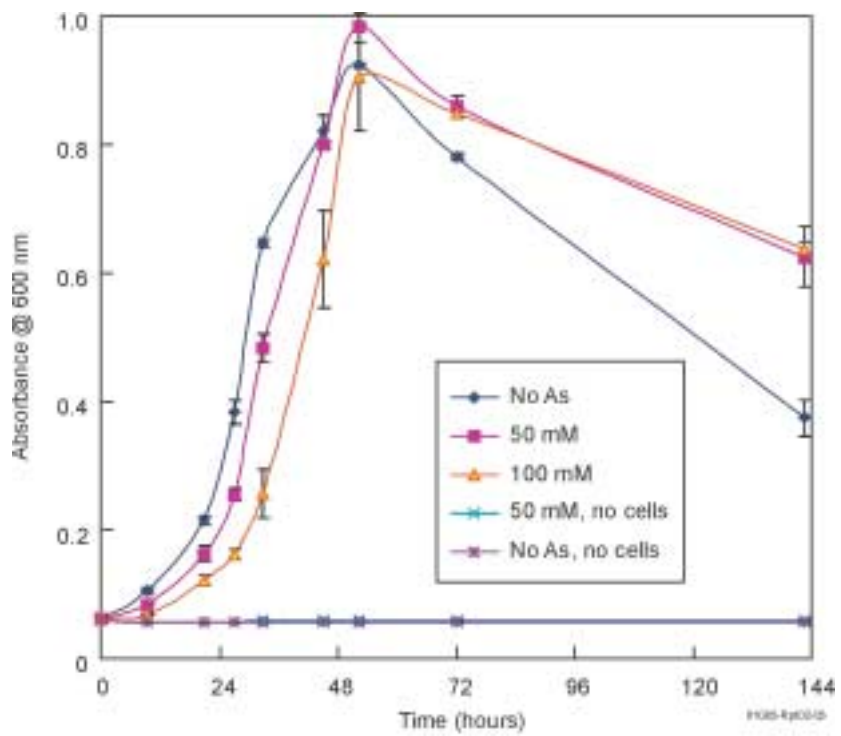


Figure 3. Minimal effect of 100 mM As(V) on growth kinetics.

### Effects of As on Protein Production

The general phases of growth could be clearly identified by total protein concentrations. However, when the protein content of cells exposed to different arsenic species and concentrations were directly compared, it was apparent that the different treatments elicited different responses in protein production (Figure 4). The greatest amount of protein was produced by cells exposed to 50 mM As(V), while the least was produced by cells not exposed to arsenic. When we tried to normalize these concentrations to cell numbers (to determine specific protein content) the error generated by direct cell counts was too high to detect any differences between treatments. Because specific protein content may be an informative indicator of cellular stress, we will continue work on this method to minimize the experimental error.

### Accumulation of As Toxicity

When late exponential phase cells (0.600–0.800 Abs at 600 nm) grown in the presence of 100 mM As(V) are transferred into new media also with 100 mM As(V), the final density is

inhibited even further. This observation suggests that the damage caused by As(V) accumulates over successive generations or over even longer periods of time. It appears, though, that the cells may be better adapted to handle the As(V) in the short term, as the lag decreased and the growth rate increased when cells were previously exposed to As(V), prior to reinoculation. In order to better understand these effects, similar experiments need to be performed under continuous culture conditions rather than in batch culture.

### Reversibility of As Toxicity

When cells grown in the presence of 100 mM As(V), 500 uM As(III), or no arsenic were inoculated into fresh media with no arsenic, there was no discernible difference in growth kinetics (Figure 5). This strongly suggests that the inhibition caused by As(V or III) to cell growth is reversible, at least after the short exposure time (temporal and generational) in this batch experiment. Inhibition that can be reversed by decreasing or removing arsenic is an important capability as this suggested a robustness of these microbes to adapt.

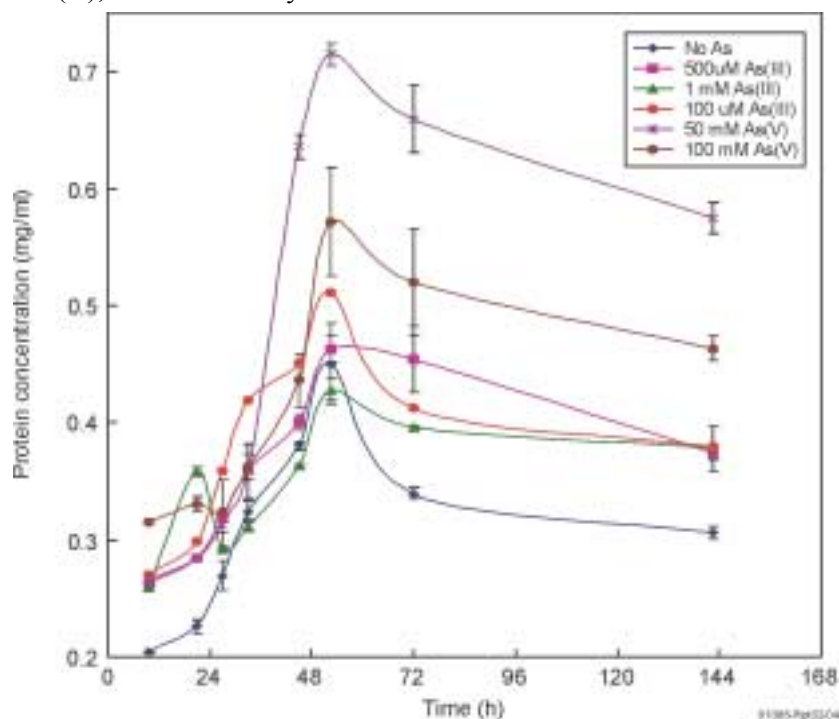


Figure 4. Responses in protein production elicited by different treatments.

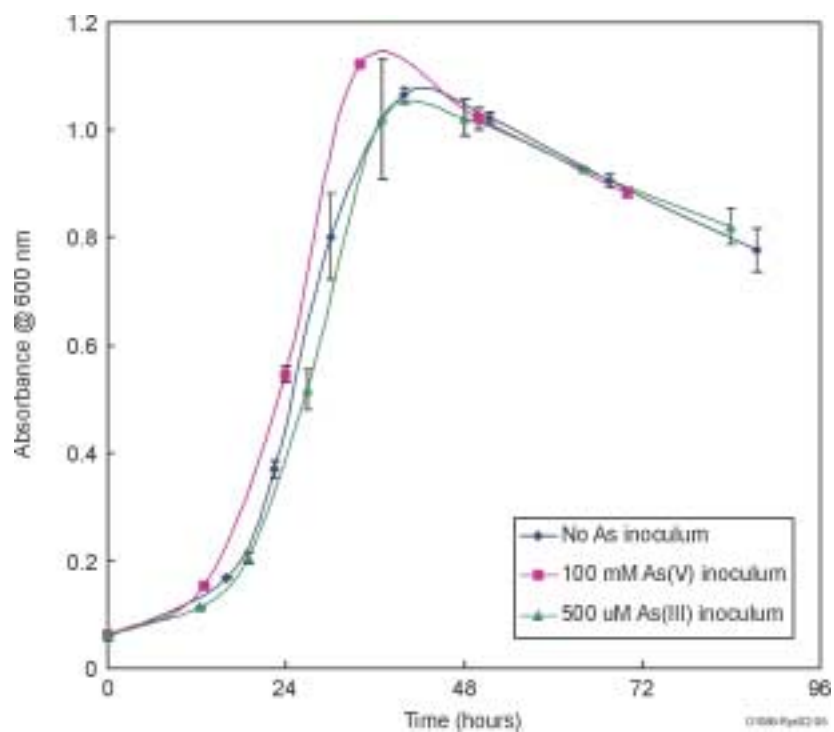


Figure 5. Comparison in growth kinetics between the cells grown in the presence of 100 mM As(V), 500 uM As(III), or no arsenic and those inoculated into fresh media with no arsenic.

### **Suppression of As Toxicity by Hydrous Ferric Oxide**

Iron oxides are a prevalent coating on many subsurface soils and a well-known electron source for DMRB. In this work, we wanted to determine what affect iron oxides would have on the As toxicity of *Shewanella putrefaciens*. When hydrous ferric oxide (HFO) contained within dialysis tubing (MWCO 10,000) was added to growth media amended with arsenate or arsenite the inhibition imposed by arsenic appeared to be relieved. The great capacity of HFO to adsorb As(V or III), removing much of it from solution, may account for this relief. This experiment needs to be performed again using total protein or direct cell counts or both as an indicator of growth rather than light absorbance. Additionally, detailed geochemical analyses would provide insight into the bioavailability of the adsorbed arsenic—information sorely missing from the literature.

### **Attachment of Cells to As-bound Hydrous Ferric Oxide**

One of the primary objectives of this work is

to understand the impacts of arsenic contamination on the ability of *Shewanella putrefaciens* to perform metal-reduction, an activity that can be attachment-dependent, such as in the case of HFO reduction. To this end, we examined the ability of *Shewanella putrefaciens* cells to attach to HFO in the presence and absence of adsorbed As(V or III). The attachment assay of Caccavo<sup>14</sup> was used in this study. Briefly, *Shewanella putrefaciens* grown aerobically in M1 was suspended in anoxic (boiled and N<sub>2</sub>-purged), sterile 10 mM PIPES buffer with 0.1 mL HFO suspension (approximately 60 mg Fe). Prior to inoculation, suspensions were modified with 1 mM arsenite or arsenate and allowed to adsorb for 24 h. M1-grown cells were washed in anoxic, sterile PIPES buffer and 0.1 mL was added to the HFO-As suspensions. Cells were allowed to attach to HFO by 1 h incubation with gentle shaking. Planktonic, nonattached cells were counted directly in the microscope with the DNA stain DAPI. To count total cells, an aliquot of the HFO suspension was incubated in hydroxylamine-HCl to dissolve the HFO; cells were protected with glutaraldehyde, and stained with DAPI for direct counts.

Microscopic examination revealed that As(V) adsorbed to the surface of HFO completely inhibited attachment of cells, while equimolar As(III) had no effect, relative to As-free HFO. This finding has important implications for the ability of *Shewanella putrefaciens* to colonize As contaminated environments, particularly if Fe(III)-reducing conditions are to be sustained. More work is needed to elucidate the exact mechanism of attachment inhibition. We have three hypotheses: (a) high As(V) concentrations inhibit exopolysaccharide production, which may be important for attachment to HFO; (b) As(V) entrained onto HFO surfaces may represent vastly higher local concentrations than when diffused in the medium, possibly killing the cells; and (c) the free oxygen of HFO-bound  $\text{AsO}_4^{3-}$ , which is not present when  $\text{AsO}_2^-$  binds HFO, creates a net negative charge on the HFO surface, prohibiting the negatively charged cell surface from coming into close contact.

### **Cell Surface Chemistry of Exposed Cells**

As stated in Objective A, SIMS was used to monitor the surface chemistry of the *Shewanella putrefaciens* exposed to 2 mM As (III), 100 mM As(V), and no As (control). The SIMS instrument used in these studies is described in detail in the literature<sup>15</sup>; a brief description is provided here. The instrument uses  $\text{ReO}_4^-$  at 5.25 keV as the primary bombarding particle, which is produced by heating an  $\text{Eu}_2\text{O}_3/\text{Ba}(\text{ReO}_4)_2$  ceramic in a vacuum.<sup>10</sup> We synthesized the ceramic in our laboratories and processed it in a form that could be used as an ion source; the ion gun was typically operated at 250 pA. Acquisitions required less than 100 s, and a typical sample had an area of about  $0.06 \text{ cm}^2$ ; thus, primary ion doses were less than  $2.6 \times 10^{12}$  ions/ $\text{cm}^2$ , which is below the commonly accepted static SIMS limit.<sup>16</sup> We have developed patented methods to overcome surface charging in which the extraction of positive and negative charge is balanced so that the sample, on average, gains no net charge.<sup>17,18</sup> This technique, when used with the  $\text{ReO}_4^-$  primary ion gun, mitigates charge buildup on the surface of the sample and thus permits facile analysis of electrically insulating samples such as minerals and leaves. We used a triple quadrupole system (2 to 600 amu) manufactured by Extrel

(Pittsburgh, Pennsylvania) and modified in our laboratory. The base pressure in the instrument was typically  $3 \times 10^{-7}$  torr.

In these experiments, we were interested in changes in the fatty acid profiles of the lipid composition of *Shewanella putrefaciens* during various stages of its growth. In past work, SIMS has been useful for detecting the fatty acid profiles of intact bacteria.<sup>19</sup> The experiment was performed by growing the *Shewanella putrefaciens* in M1 media in a manner similar to that described above. The *Shewanella putrefaciens* were exposed to 2 mM As (III), 100 mM As(V), and no As (control); samples were taken at four different times during growth. The sampling times were determined from the growth curves shown in Figures 2 and 3. The first samples were taken during the early stages of microbial growth, the second and third samples were taken at stages of high microbial growth, and the fourth samples were taken at late, stationary growth stages. Samples were prepared by washing cells in nanopure water and concentrating them 20 $\times$ . Ten  $\mu\text{L}$  of this washed 20 $\times$  suspension was then applied to a planchet and allowed to dry for 24 hours. In Figure 6, the normalized abundances of various fatty acid anion fragments are plotted as a function of time.

The results show that for the three different growth environments the fatty acids present in the *Shewanella putrefaciens* are similar. However, there are distinct differences observed in the relative abundances of these fatty acids at the various growth stages. For example, comparing the *Shewanella putrefaciens* for the no As and 100 mM As(V) environments, the trend in the data shows the no As case to have a decrease in overall abundance of the fatty acids as the *Shewanella putrefaciens* began to move into high microbial growth, then quickly increase in abundance. In contrast, the *Shewanella putrefaciens* in the 100 mM As(V) case show the opposite trend—high increase early in high microbial growth, followed by a quick decrease. The fatty acid abundances for the *Shewanella putrefaciens* grown in 2 mM As(III) show similar growth changes to those seen for the *Shewanella putrefaciens* grown in 100 mM As(III), in that the fatty acid abundances increase at high microbial growth,

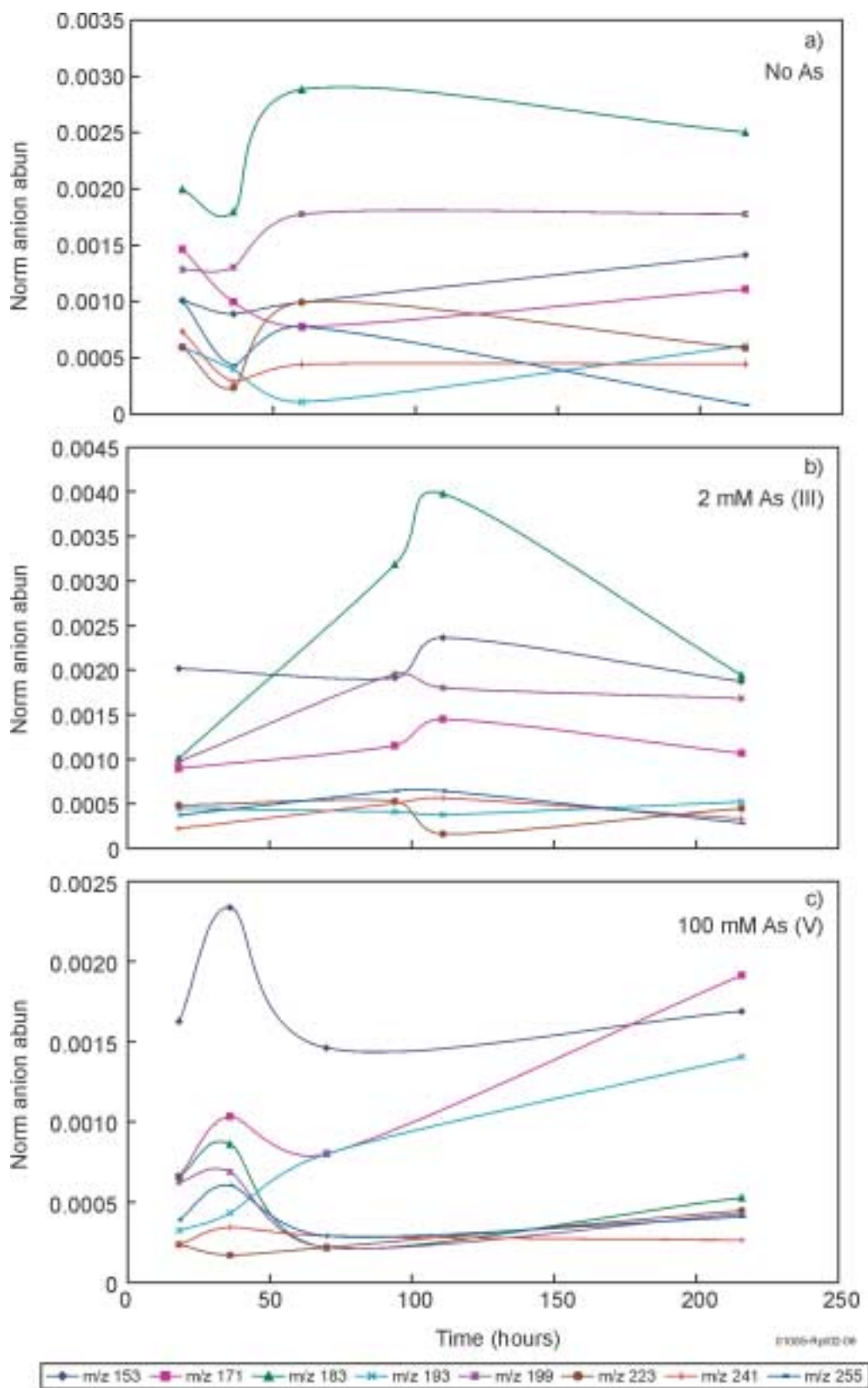


Figure 6. Normalized abundances of various fatty acid anion fragments plotted as a function of time.

then decrease as they move into stationary phase. Follow-on work using the Microbial Identification System (MIS: a gas-chromatography technique to detect fatty acids) needs to be done to confirm these results.

Overall, the use of SIMS appears to be useful for monitoring changes in the fatty acid composition of *Shewanella putrefaciens* as a result of exposure to As. Future work will expand on the use of this technique to probe interfacial chemical changes to microbial cells induced by changes in their environment.

Additionally, synchrotron radiation Fourier transform infrared spectroscopy (SR-FTIR) was performed at the Lawrence Berkeley National Laboratory (LBNL) in collaboration with Dr. Hoi-Ying Holman. Beamline 1.4.3 at the Advanced Light Source (LBNL) is directed into a Nicolet magna 760 FTIR bench, then passed through a Nic-Plan IR microscope. The samples were analyzed by applying up to 10  $\mu$ L on a gold-coated microscope slide, and analyzed directly from the slide.

SR-FTIR was used to analyze *Shewanella putrefaciens* cells with and without exposure to 100 mM As(V). The main difference between the spectra of stationary phase cells was the clear lack of a broad peak associated with carbohydrates in the As-exposed cells that was present in the unexposed cells (Figure 7). In its place were two distinct peaks indicative of phosphodiester bonds. Phosphodiester bonds are abundant in cell membranes, forming the junction between glycerol and fatty acids. Cell surface carbohydrates likely indicate either a capsule (exopolysaccharides), or common membrane lipids called lipopolysaccharides (LPS). The role of the capsule is especially important in nature, where it can aid the cell in its defense against viruses, hydrophobic toxins such as detergents, and desiccation. In addition, it has been implicated in the attachment of some microorganisms to solid substrates. An impaired ability to form exopolysaccharides would likely limit the cells competitive fitness in nature. The LPS may be largely responsible for the net negative charge on the cell surface, implicated in attachment, metal binding, and nutrient transport across the outer membrane. Additionally, the LPS

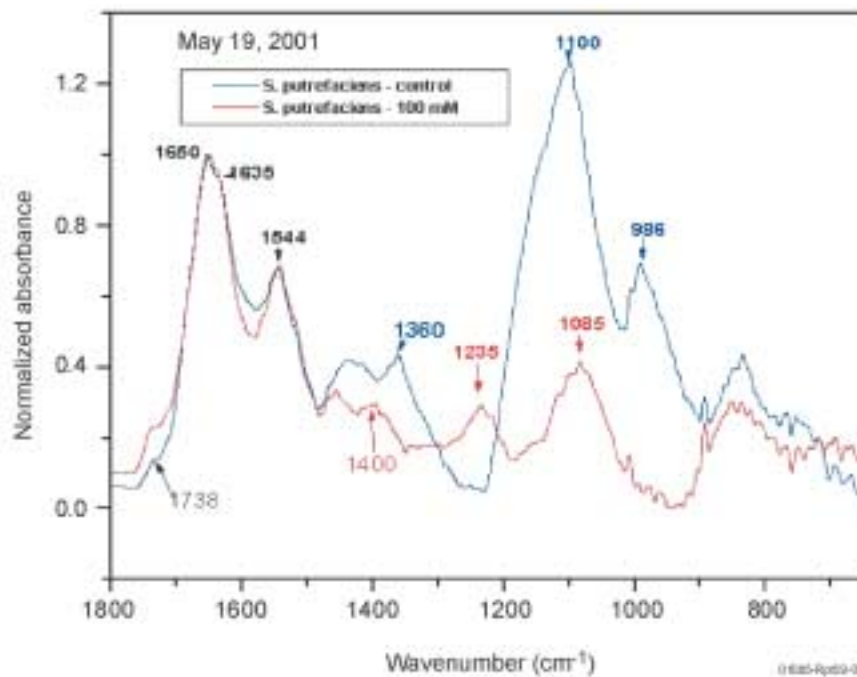


Figure 7. SR-FTIR analysis of *Shewanella putrefaciens* cells with and without exposure to 100 mM As(V) showing the clear lack of a broad peak associated with carbohydrates in the As-exposed cells and the two distinct peaks indicative of phosphodiester bonds.

may stabilize the membrane's physical shape and structure. An impaired LPS would also put the cells at a disadvantage in the environment.

## Future Work

Based on the research results from FY 2001, we plan to split follow-on work into two efforts: (a) continue to develop SIMS as a tool for interfacial microbial/mineral studies, and (b) extend the research focused on toxicological effects of contaminant metals on DMRB. Continuing to develop SIMS is also follow-on work for a related Environmental Systems Research Candidates project, "Secondary Ion Mass Spectrometry Characterization of Environmental Microbial Processes" To further develop SIMS as a bioanalytical tool we will need to address both quantitative and qualitative issues. Currently, the number of microbial cells required on a sample for detection by SIMS is not well-defined, although preliminary results indicate that very sensitive measurements can be made using the fatty acids components of the cells ( $<10^7$  cells per sample). Work is still needed to better define the lower limit of detection as well as to determine if the detection limit is dependent on the specific microorganism or underlying substrate or both. Several qualitative questions still need to be addressed. What biomarkers in addition to the fatty acids are useful for characterizing the microbes? Can mixed cultures be characterized by SIMS? What are the limits on how complex the mixtures can be?

Determining the toxicological effects of contaminant metals on DMRB is an out-growth effort of the first project that will have both important technical and relevant contributions to bioremediation. Some of the key areas of research for this effort include working with anaerobically grown cells, as these are of great interest to subsurface environments, expanding the types of DMRB to include *Geobacter* spp., identifying other indicators of toxic stress to resting cells such as ATP content or fatty acid usage (cell growth may be an unrealistic indicator of toxic stress in the natural environment), and better defining the biochemical effects of contaminant metal toxicity. We will continue to use SIMS, IR, and other surface analytical tools as a means for

understanding biomolecular changes in the DMRB as a result of stress.

## ACCOMPLISHMENTS

This project show that the SIMS is capable of probing the interfacial surface chemistry of *Shewanella putrefaciens* that have been exposed to various arsenic species. Further, the teaming of microbiological methods with SIMS and IR analyses provides detailed information about the physiological and biochemical changes in stressed microbial species. These results suggest that subtle changes in the cell surface chemistry can be monitored quickly using SIMS offering a means for obtaining molecular-level information without the need for complex sample preparation.

Additionally, new work was spawned by this project to investigate toxicological effects of contaminant metals on DMRB. The results presented in this report show that the combination of microbiological and surface analytical techniques provides an advantageous approach to studying biomolecular changes associated with the interactions of DMRB with contaminant metals. It is from these types of studies that a comprehensive understanding of the use of DMRB for bioremediation of metals can be realized. Applying this strategy will depend on stable microbial populations capable of tolerating the contaminant metals they are intended to remediate in addition to any co-contaminating metals present at the various DOE sites. Continued toxicological studies of metals on DMRB will provide the insights needed to yield stable microbial populations for use in bioremediation of metals.

## Publications

### In Preparation or Submitted

Cummings, D. E., J. C. Ingram, and M. Downing, "Toxicity of Arsenic to the Dissimilatory Metal-reducing Bacteria *Shewanella putrefaciens* and Suppression of Toxicity by Iron Oxides," in preparation for *Applied and Environmental Microbiology*.

## Presentations

*American Society for Mass Spectrometry Meeting  
in Chicago, IL, May 2001.*

Ingram, J. C., D. E. Cummings, and R. M. Lehman, Poster Presentation, "Evaluation of Static SIMS to Characterize Intact Bacterial Cells," *48th*

## REFERENCES

1. D. R. Lovley, "Bioremediation of Organic and Metal Contaminants with Dissimilatory Metal Reduction," *J. Ind. Microbiol.*, 14, 1995, pp. 85–93.
2. P. L. Siering, "The Double Helix Meets the Crystal Lattice: The Power and Pitfalls of Nucleic Acid Approaches for Biomineralogical Investigations," *Amer. Mineralog.*, Vol. 83, 1998, pp. 1593–1607.
3. D. R. Lovley, "Dissimilatory Metal Reduction," *Annu. Rev. Microbiol.*, Vol. 47, 1993, pp. 263–290.
4. J. K. Fredrickson, H. M. Kostandarithes, S. W. Li, A. E. Plymale, and M. J. Daly, "Reduction of Fe(III), Cr(VI), U(VI), and Tc(VII) by *Deinococcus radiodurans* R1," *Appl. Environ. Microbiol.*, Vol. 66, 2000, pp. 2006–2011.
5. D. R. Lovley and E. J. P. Phillips, "Bioremediation of Uranium Contamination with Enzymatic Uranium Reduction," *Environ. Sci. Technol.*, Vol. 26, 1992, pp. 2228–2234.
6. G. L. Harding, "Bioremediation and the Dissimilatory Reduction of Metals," *Manual of Environmental Microbiology*, ASM Press, Washington, D.C., 1998, pp. 806–810.
7. J. K. Fredrickson, J. M. Zachara, R. K. Kukkadapu, Y. A. Gory, S. C. Smith, and C. F. Brown, "Biotransformation of Ni-Substituted Hydrous Ferric Oxide By an Fe(III)-Reducing Bacterium," *Environ. Sci. Technol.*, Vol. 35, 2001, pp. 703–712.
8. D. C. Cooper, F. Picardal, J. Rivera, C. Talbot, "Zinc Immobilization and Magnetite Formation via Ferric Oxide Reduction by *Shewanella putrefaciens*," *Environ. Sci. Technol.*, Vol. 34, 2000, pp. 100–106.
9. J. C. Ingram, R. M. Lehman, W. F. Bauer, F. S. Colwell, A. D. Shaw, "SIMS Characterization of Environmental Microbial Processes", Environmental Systems Research Candidates Program, FY2000-FY2001.
10. J. E. Delmore, A. D. Appelhans, E. S. Peterson, "A Rare Earth Oxide Matrix for Emitting Perrhenate Anions," *Int. J. Mass Spectrom. Ion Proc.*, Vols. 146/147, 1995, pp. 15–20.
11. C. Myers and K. H. Neelson, "Microbial Reduction of Manganese Oxides: Interactions with Iron and Sulfur," *Geochim. Cosmochim. Acta*, Vol. 52, 1988, pp. 751–756.
12. O. H. Lowry, N. J. Rosebrough, A. L. Farr, and R. J. Randall, "Protein Measurement with the Folin Phenol Reagent," *J. Biol. Chem.*, Vol. 193, 1951, pp. 265–275.
13. U. Schwertmann and R. M. Cornell, *Iron Oxides in the Laboratory: Preparation and Characterization*, 2<sup>nd</sup> Ed., Wiley-VCH Publishing, Weinheim, 2000.

14. F. Caccavo, Jr., P. C. Schamberger, K. Keiding, P. H. Nielsen, "Role of Hydrophobicity in Adhesion of the Dissimilatory Fe(III)-reducing Bacterium *Shewanella alga* to Amorphous Fe(III) Oxide," *Appl. Environ. Microbiol.*, Vol. 63, 1997, pp. 3837–3843.
15. A. D. Appelhans, D. A. Dahl, J. E. Delmore, "Neutralization of Sample Charging in Secondary Ion Mass Spectrometry Via a Pulsed Extraction Field," *Anal. Chem.*, Vol. 62, 1990, pp. 1679–1686.
16. J. C. Vickerman, "Introducing Secondary Ion Mass Spectrometry," In: Vickerman, J. C., Brown, A., Reed, N. M. (Eds.), *Secondary Ion Mass Spectrometry Principles and Applications*, Oxford Science Publications, New York, 1989, p.1.
17. A. D. Appelhans, D. A. Dahl, J. E. Delmore, "Neutralization of Sample Charging in Secondary Ion Mass Spectrometry Via a Pulsed Extraction Field," *Anal. Chem.*, Vol. 62, 1990, pp. 1679–1686.
18. D. A. Dahl and A. D. Appelhans, "Sample Charge Compensation Via Self-Charge-Stabilizing Ion Optics," *Int. J. Mass Spectrom. Ion Proc.*, Vol. 178, 1998, pp. 187–204.
19. J. C. Ingram, R. M. Lehman, W. F. Bauer, S. P. O'Connell, F. S. Colwell, A. D. Shaw, "Detection of Phospholipid Fatty Acids from Intact Microorganisms by Static Secondary Ion Mass Spectrometry Utilizing a Molecular Beam", *J. Microbiol. Methods*, in preparation.



# Geomicrobiology of Subsurface Environments

F. Colwell, R. M. Lehman, and G. Bala; INEEL Research Contributors: J. Ingram, M. Kauffman, D. Newby, S. O'Connell, K.T. Raterman, D. Reed, F.F. Roberto, E.P. Robertson

## SUMMARY

The goal of this project is to enhance our understanding of subsurface biological properties such that we can develop predictive knowledge of contaminant fate and transport. To accomplish this we targeted two knowledge gaps related to DOE's subsurface contamination problems<sup>1</sup>: (a) our current inability to characterize physical, chemical, and biological properties of the subsurface, including approaches to understanding the properties of the geologic system, and relate them to contaminant fate and transport, and (b) our current inability to characterize highly heterogeneous systems. We then addressed the need arising from these knowledge gaps, which is the need to improve the capabilities for characterizing the biological properties of the subsurface, including biological heterogeneity, on a scale that controls contaminant fate and transport.

Microorganisms are the primary agents of geochemical change in the subsurface and thus important in the mediation of contaminant transport and degradation phenomena. The following research tasks reported for this project are driven by critical deficiencies in the existing microbiological knowledge base that limit in situ remedial applications:

- Molecular assessment of partitioning of microorganisms and their activities in saturated geologic media
- Evaluation of imbibition and wettability parameters mediated by microbial perturbations
- Linking structure and function in environmental microorganisms.

These tasks target real site problems within the DOE complex, including site problems relevant to the INEEL. End-point applications of the work include remediation of contaminated

geologic media at DOE sites and facilities nationwide and industrial sites throughout the world, as well as agriculture, mining, resource recovery (energy), aquifer contamination, and waste disposal.

## PROJECT DESCRIPTION

### Molecular Assessment of Partitioning of Microorganisms and Their Activities in Saturated Geologic Media=

R. M. Lehman (Task PI)

This task consists of experimental work that effectively describes the distribution and spatial scales of biogeochemical processes in the subsurface. Microorganisms are known to inhabit the subsurface and influence fate and transport of subsurface contaminants. However, little emphasis has been placed on distinguishing organisms (and their functions) in the saturated subsurface that are associated with the geologic media from those suspended in the groundwater. Emerging evidence<sup>2,3</sup> demonstrates that both microbial functional traits and the rates of biogeochemical transformation are unevenly distributed between these two habitats. There is extensive literature that documents radical changes in the physiology (enzyme expression) when single organisms become attached to or detached from substrata during laboratory experimentation.<sup>4</sup> The dichotomy between attached and unattached microbe-mediated transformations in aquifers represents an additional facet of heterogeneity in the subsurface.

A long-term goal of subsurface microbiological investigations is to develop a predictive knowledge base concerning the distribution of microorganisms and their activities in subsurface environments so that activities such as remediation can be accomplished efficiently

with a minimum of costly site characterization studies at each location (see Reference 1). Many of these locations that are amenable to remediation are saturated. To achieve degradation (or other desirable interaction), it is necessary to place the substrate, transforming population, and stimulus at the same location simultaneously. Predictive knowledge relative to microbe distribution and activities drives the design of relevant laboratory biodegradation and numerical models, allowing site characterization efforts to focus on either core or groundwater, and which should be subsequently monitored.

Specific task objectives involve quantifying the impact of microbial partitioning between the geologic media and groundwater on biogeochemical transformations—both metabolic capabilities and rates of biotransformations. Compositional and functional attributes of attached and unattached communities have been examined in controlled laboratory experiments using both porous- and fracture-flow columns, and in paired field samples of the core and groundwater. Strategies for appropriate sampling and analysis of attached and unattached aquifer microorganisms are being considered. Several experimental subtasks were developed to empirically address these questions and progress during FY 2001 as reported below.

### **Subtask 1**

This subtask centers around the use of laboratory columns constructed with either basalt or quartz sand and perfused with Snake River Plain Aquifer (SRPA) groundwater to simulate an aquifer and provide materials that were subjected to microbiological analyses. It also covers the development of appropriate methods for analyzing microorganisms indigenous to groundwater and geologic media.

In FY 2001, data analysis and reduction were performed on the results of basalt core flood experiments conducted in FY 2000. These laboratory core flood experiments were conducted to examine the partitioning of indigenous groundwater bacteria between the basalt and groundwater. Replicated experiments with fracture-flow and porous flow core flood units

were performed to determine if there were differences in microbial partitioning between these two flow hydrological regimes. We concluded that (a) attached and unattached communities were compositionally and functionally different, (b) a combination of culture-dependent and independent approaches are complimentary and useful for depicting differences between communities, and (c) units of biomass comparison such as mass, volume, or surface area are important for comparison of attached and unattached microorganisms.<sup>5</sup>

To allow the use of bulk nucleic methods for analyses of attached and free-living organisms inhabiting natural and simulated subsurface environments, we developed methods for extracting bulk DNA suitable for polymerase chain reaction (PCR)-amplification from low biomass sediments and rocks. These newly developed extraction methods were applied to two experimental systems that examined the effect of trichloroethylene (TCE) on microbial diversity: batch microcosms containing only groundwater, and packed columns containing quartz sand. In both experimental systems, we found that TCE (up to 10 ppm) had only a modest effect on a species richness indicator using three different methods of assessment: traditional culturing, PCR—denaturing gradient gel electrophoresis (DGGE) banding patterns, and dilution-extinction of community level physiological profiles (CLPP). At higher concentrations (>10 ppm) TCE had a significant effect on species richness. However, at concentrations of 10 ppm and less, species evenness (relative distribution of population abundances) was affected. The examination of this aspect (evenness) of microbial diversity represents a novel and perhaps sensitive method of using indigenous communities as environmental indicators. During the investigation of the ambient diversity in the oxic groundwater of the SRPA, it was found that significant numbers of Archaea are present in this community (Table 1). Until recently, the Archaea were believed to represent mostly by microorganisms from extreme environments such as high temperature and saline (see Reference 5). Our evidence points to an additional habitat, namely an oxic freshwater aquifer, wherein these cells are an important component of the microbial community. Specific

Table 1. BLAST and RDP II sequence identification matches for 600 bp archaeal PCR products from SRPA groundwater DNA extracted from wells TAN36 and USGS103, and using primers 340F and 915R.

Clone	Database Match	Similarity	Phylogeny	Environment Sampled
SRPA-A (1) <sup>a</sup>	ABS12	82, 96%*	Euryarchaeota	Methanogenic rice soil
SRPA-B (3) <sup>c</sup>	Car106b	86–89%	Euryarchaeota	Cariaco Basin (anoxic)
SRPA-C (1) <sup>a</sup>	Car127c	93, 91%	Euryarchaeota	Cariaco Basin (anoxic)
SRPA-D (1) <sup>a</sup>	Car42fc	84%	Euryarchaeota	Cariaco Basin (anoxic)
SRPA-E (2) <sup>c</sup>	pMC2A35	86–89%	Euryarchaeota	Deep sea hydrothermal vent
SRPA-F (5) <sup>a</sup>	DOURO2	99%	Crenarchaeota	Estuary sediment
SRPA-G (7) <sup>a</sup>	LMA229	98–99%	Crenarchaeota	Lake Michigan sediment
SRPA-H (1) <sup>b</sup>	VC2.1 Arc31	93, 89%	Crenarchaeota	Deep sea hydrothermal vent
SRPA-I (1) <sup>b</sup>	CIARC-3	84%	Euryarchaeota	Sulfurous lake

(#) Indicates the number of clones recovered for a related sequence.

a Indicates sequences found in TAN36 groundwater.

b Indicates sequences found in USGS103 groundwater.

c Indicates sequences found in both groundwater sources.

\*Indicates that two portions of the 16S rDNA gene fragment, rather than the whole sequence, matched to differing degrees.

to DOE's cleanup issues, Archaea are believed to play an important role in the community of cells that were stimulated by the injection of lactate to the SRPA at Test Area North (TAN).<sup>6</sup>

In the quartz sand packed columns, attached and unattached communities were assayed for total cell numbers,  $\beta$ -glucosidase and aminopeptidase exoenzyme activities, and banding patterns and sequence identity by PCR-amplification of 16S rDNA fragments and subsequent separation by DGGE. We found that 95% of the cells (expressed per volume of porous media) were attached; however 16S rDNA analyses indicated a wider diversity of phlotypes existing suspended in the groundwater versus attached to the quartz sand (see Figure 1). Attached communities had significantly greater  $\beta$ -glucosidase (see Figure 2) and aminopeptidase (see Figure 3) exoenzyme activities than unattached communities when the activities were expressed on a per-mass or per-volume basis. However, unattached cells had a significantly higher cell specific activity for  $\beta$ -glucosidase than attached cells, while the converse was true for aminopeptidase specific activity. This observation provides corroborative evidence for previous observations made in our laboratory using different techniques regarding the relative predilection of attached and unattached communities for carbohydrate and amino-acid

substrates. This observation may have important implications for the fundamental roles of attached and unattached microorganisms in biogeochemical cycling in the subsurface.

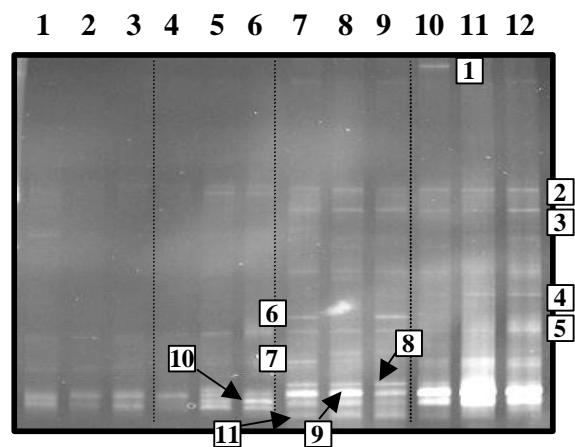


Figure 1. Digital image of DGGE gel showing 16S rDNA fragment migration patterns for sand samples with no TCE treatment (lanes 1–3); sand samples receiving TCE treatment (lanes 4–6); groundwater samples with no TCE treatment (lanes 7–9) and groundwater samples receiving TCE treatment (lanes 10–12). Bands that were successfully excised from the gel and sequenced are numbered.

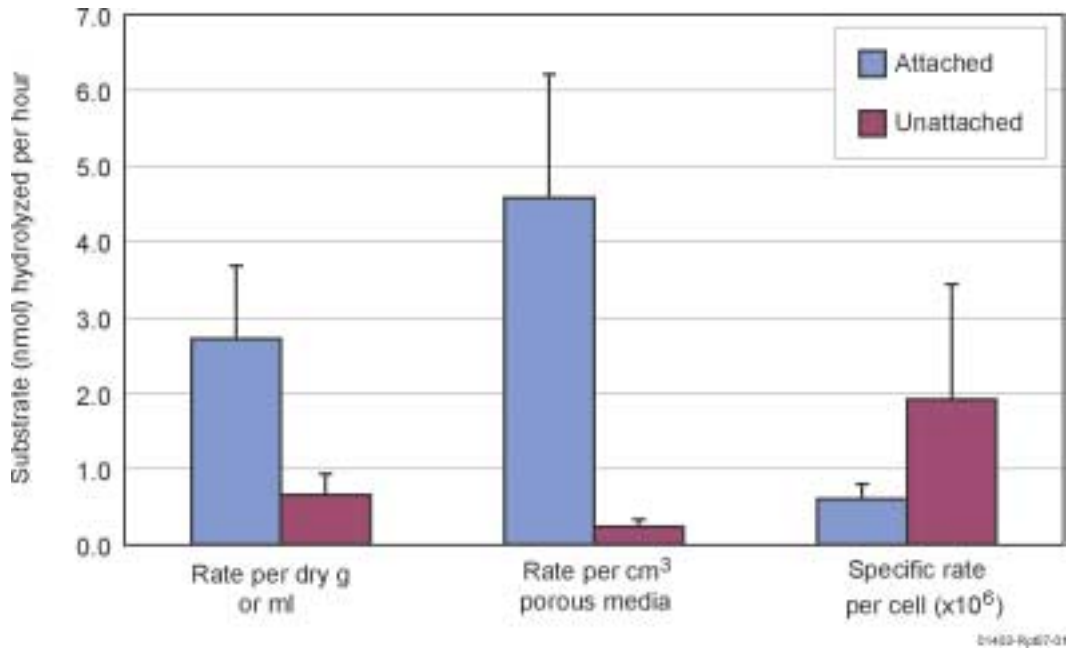


Figure 2.  $\beta$ -glucosidase exoenzyme activities in attached and unattached aquifer microorganisms.

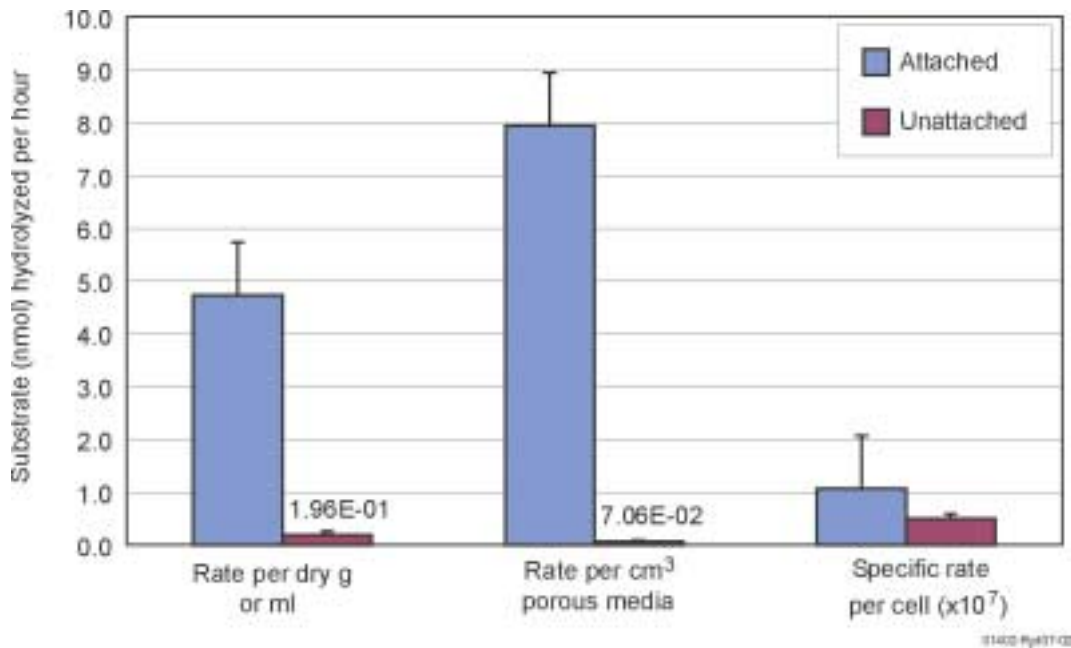


Figure 3. Aminopeptidase exoenzyme activities in attached and unattached aquifer microorganisms.

### Subtask 2

This subtask involves noninvasive assessment of in situ microbial activities using low-energy infrared radiation in a collaborative study with

H. -Y. Holman (LBNL). It includes a study of the surface associations of organisms, degradative substrate, and mineral type on basalt by applying synchrotron radiation-based Fourier transform spectromicroscopy (SR-FTIR) using the 1.4.3

Beam line experimental end station of a particle accelerator, the advanced light source (ALS) at LBNL. Advantages of this nondestructive method are the resolution conferred by a 10-micron spot size and the high intensity infrared radiation source. This technique is being used to study the degradation kinetics of aromatic and chlorinated hydrocarbons by attached and unattached organisms. *Burkholderia cepacia* G4 is being used as a test organism, basalt as the mixed-mineral substratum, and TCE as the organic substrate. The induction of the enzymes (toluene mono-oxygenase, [TMO]) which co-metabolically degrade TCE, are being studied with toluene and phenol as an inducer, and 3-hydroxyphenyl-acetylene as an analogue substrate and activity indicator. The major accomplishment associated with several periods of beam time at the ALS at LBNL and the use of light (epifluorescent and diffracted light illumination) microscopy at the INEEL include the following:

- The Kramers-Kronig correction factor was applied to all spectral data previously collected at the ALS, which significantly improved the signal to noise ratio for all spectral data
- Experiments were performed that confirmed TMO activity in *Burkholderia (B.) cepacia* G4 by assaying for conversion conversion of

naphthalene to naphthol and experiments employing competitive inhibition of probe transformation by alternative enzyme substrates

- Several experiments were performed that verified the use of the TMO probe (3-HPA) on environmental samples (pristine and TCE-contaminated groundwater)
- Experiments were performed that verified the IR spectra of transformed probe and allowed visualization of cells attached to basalt that retain the transformed probe
- SR-FTIR was collected on *B. cepacia* G4 attached to the four major minerals in basalt (olivine, plagioclase, ilmenite, and augite) and on the mixed-mineral (basalt).

The minerals were presented separately and together. This series of experiments demonstrated that attachment of *B. cepacia* G4 was influenced by mineral type and the availability of alternate minerals and that the biochemistry of *B. cepacia* G4 was mediated by attachment to the different mineral phases (Figure 4).

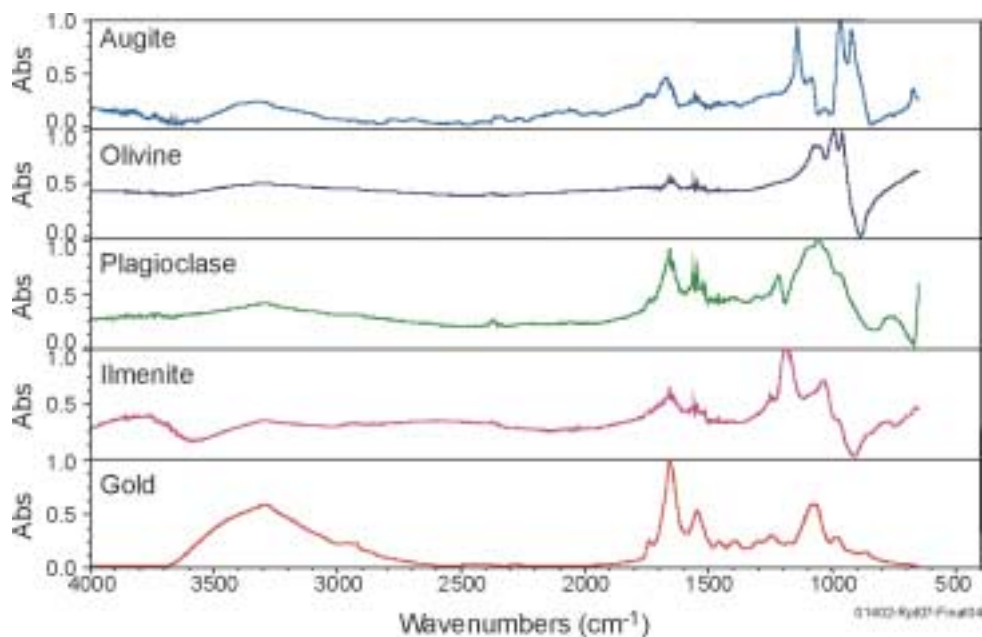


Figure 4. SR-FTIR spectra of *B. cepacia* G4 in contact with the four major minerals found in basalt.

### Subtask 3

This subtask involves development of experimental approaches and the spectral database to use secondary ion mass spectrometry (SIMS) instrumentation to detect populations of organisms as they occur in situ. This task is a collaborative effort with J. Ingram at the INEEL. The spectra are related to cell surface lipids by parallel characterization of organisms by fatty acid methyl ester analysis. Research was initiated to obtain spectral signatures for three classes of potential TCE metabolizers: sulfate-reducing bacteria (SRB), methanogenic bacteria, and methanotrophic bacteria. Representative organisms of three genera of SRB, three genera of methanogens, and two genera of methanotrophs were obtained from American Type Culture Collection and growth initiated in appropriate media. However, progress on this subtask has been delayed due to the failure of scale-up culturing approaches with the methanogens, interference with cell pellet harvesting by metal-sulfides with the SRB, and contamination of the methanotroph cultures. To date, a SIMS spectra has been obtained for one methanogen, *Methanococcus maripaludis*, but the FAME characterization failed due to insufficient biomass. In a related collaborative experiment, *Arthrobacter globiformis* was used as a test organism to estimate the limit of detection of the SIMS instrument for bacteria. Following SIMS analysis of varying quantities of biomass, the biomass on the planchet was solubilized with sodium hydroxide and the protein quantified using a modified Lowry assay. The amount of protein was related to the number of cells by the construction of standard curves. Using this approach, we found that the detection limit for SIMS was less than  $10^8$  cells/cm<sup>2</sup>; however, more sensitive biomass measures will have to be used to more accurately estimate the detection limit. Performance of rough calculations of cell concentrations in soils and extrapolation of SIMS spectral abundances at the  $10^8$  cells/cm<sup>2</sup> concentration indicated that the method is approaching an environmentally-relevant detection limit.

### Subtask 4

This subtask involves microbiological analyses of field samples of geologic media and groundwater

taken across temporal and spatial scales with respect to contaminant introduction and elimination. This subtask involves a collaboration with M. Barcelona (University of Michigan), who is the Director of the National Center for Integrated Bioremediation Research and Development (NCIBRD), and with D.C. White (University of Tennessee) in a field experiment at the Michigan Integrated Remediation Technology Laboratory (MIRTL) at Wurtsmith Air Force Base, Oscoda, MI (MIRTL2: A Natural Gradient Reactive Fate and Transport). For this experiment we intentionally injected labeled contaminants (benzene, toluene, ethylene, xylene, and methyl-tert-butylether) into the aquifer so we knew the exact quantity, type, and time of contaminant introduction; the site had been previously characterized for contaminant dispersion parameters. We have followed the dissolved plume through periodic sampling of established transects of multilevel well installations along the flow axis in this relatively shallow, sandy aquifer. Our role in this experiment is to examine the response of the indigenous microbial communities in both the groundwater and the associated sediment during introduction of and subsequent elimination of hydrocarbon contaminants. In the last 2 years we have analyzed over 500 groundwater samples and over 300 sediment samples using community-level physiological profiles (CLPP), which fingerprint the community according to its ability to degrade selected organic compounds. Preliminary data analyses demonstrate a large difference in the attached and unattached community profiles and a divergence in their response to introduction of the contaminants. White's research parallels ours by measuring structural attributes of the microbial community at this site. He has just finished analyzing sediment samples for phospholipid fatty acid community profiles, which fingerprint the community according to structural (cell wall) components and for PCR-DGGE analyses of 16S rDNA fragments. As of this writing, an approach for correlating the three biological and one chemical datasets, which span spatial and temporal scales, and a manuscript outline have been exchanged with A. Peacock in White's laboratory.

## Evaluation of Imbibition and Wettability Parameters Mediated by Microbial Perturbations

G. A. Bala (Task PI)

The fate and transport of organic contaminants (nonaqueous phase liquids [NAPLs]) in the subsurface depend on complex interactions between several system components such as fluid chemistries, geochemistry, microbiology, geology, and physical (gravitational and capillary force) parameters. Past literature suggests that the flow of NAPLs in saturated media is ostensibly predicated on the spatial arrangement of contrasting textures.<sup>7-10</sup> However, the cited literature wholly assumes that all of the solid surfaces are preferentially water-wet (water, but not organics, will spread across the surface).

A more detailed investigation of NAPL flow acknowledges several effects that range from macro- to micro-scale phenomena. Examples of these phenomena include the effect of pore-scale processes such as “snap off” (the physical release of contaminants from a solid surface) on NAPL entrapment<sup>11</sup> as well as larger-scale processes such as “fingering”(see Reference 7). Microscale processes such as wettability (the tendency of a fluid to spread along a solid surface in the presence of another immiscible fluid) have profound impacts on capillary pressure<sup>12</sup> and relative permeability<sup>13</sup> relationships. Changes in wettability have been documented to effect the fate and transport of organic materials.<sup>14</sup> Numerous factors have been described that mediate wettability changes such as contaminant aging,<sup>15</sup> contaminant adsorption,<sup>16</sup> addition of surface active constituents,<sup>17</sup> mineralogy,<sup>18</sup> distribution of organic complexes,<sup>19</sup> and pore surface topology.<sup>20</sup> Wettability effects with respect to the relations of hydraulic properties are a matter of debate and have been reported to be both dependent<sup>21-23</sup> and independent<sup>24,25</sup> of saturation.

Allowing for interaction of all recognized components, flow and transport of NAPLs in high permeability (fracture) subsurface environments are dominated by viscosity and gravity, while flow and transport of NAPLs in low permeability

(matrix) systems are dominated by capillary forces. In fracture-matrix systems, fluid distribution in the matrix is dictated by capillarity—which is in turn influenced by wettability. Wettability is one of the system properties that influences capillary processes during multiphase flow. In general terms, imbibition describes how fast capillarity takes place—the rate kinetic of capillarity is imbibition. Hence, wettability of subsurface rocks and soils and the effect of wetting on imbibition processes significantly influence contaminant distribution and the rate at which bulk contaminant saturations can be reduced by displacement processes. The imbibition or mass transfer of contaminant liquids between fractures and matrix blocks is an important phenomena in establishing the distribution and flow of contaminants in the subsurface. It is equally important in determining the rate and degree to which contaminants can be recovered from matrix blocks in a fractured porous medium.

Highly irregular distribution and flow patterns of NAPLs have been observed (see References 7 and 9) in heterogeneous subsurface systems. It is therefore logical to extrapolate that discrepancies are driven by a combination of physical and chemical heterogeneities in the environment. With the advent of aggressive remediation technologies, it is important to understand the effect of technology strategy on the ultimate fate and transport of the contaminant. Although this will be very complex, changes in wettability will be a key factor. With respect to biologically mediated remediation strategies, the potential effect of biologically mediated changes to wettability have not knowingly been reported. Although complex, the biological component can be viewed simplistically as the discrete presence of cells or biofilms, nutrient packages that may be introduced to support or suppress these organisms and the end products resulting from metabolism and growth. Microbial activities capable of affecting surface or aqueous chemistries that mediate change in the wettability index include the introduction of nutrients; attachment, detachment, and film formation; transformation of contaminants; production of metabolites; and cell death.

The effect of wettability alterations driven by microbiological perturbations may be both positive and negative. If the system is driven to a less water-wet condition, the organic contaminants will have a tendency to spread across the surface of the solid media resulting in a larger bulk volume of contaminated solids. This could be a negative outcome, but it could also be a positive outcome if the intention of the remediation technology is to improve the bioavailability of the contaminant and the appropriate organisms are present to transform or degrade the contamination.

This work describes imbibition studies to assess the incipient interaction between dodecane and pertinent mineral surfaces as a function of aqueous chemistry and microbiological perturbation. These studies were aimed at quantifying the areal extent of altered wetting and the nature of the surfaces produced. This information is necessary towards understanding how contaminant distribution and recovery may be influenced. This research supports the Subsurface Science Initiative by promoting more effective fate and transport modeling for risk analysis and remediation. An understanding of wetting in the systems of interest will lead to better strategies for remediation. The technology has broad application to the INEEL and other DOE sites. The rate of fluid imbibition can be scaled, and, this scaled rate can be used in simulators to correctly predict contaminant movement from fractures to matrix as the contaminant percolates through the vadose and saturated zones. Similar scaled rates can be determined for contaminant recovery.

## Measurement Techniques

Several methods have been proposed and used to evaluate wettability. Techniques derived from field data vary from “rules of thumb” driven by the shape of relative permeability curves,<sup>26</sup> to the shape of water flood recovery curves, NMR relaxation, dye adsorption, x-ray photoelectron spectroscopy, and well logs.<sup>27</sup> Laboratory methods based on the principles of capillarity and spontaneous imbibition have also been developed. The most popular laboratory methods are the Amott-Harvey method,<sup>28</sup> USBM method,<sup>29</sup> relative permeability method,<sup>30</sup> and imbibition method.<sup>31</sup> The most attractive methods for this study were

the Amott-Harvey test, USBM method, and imbibition method. With respect to the Amott-Harvey technique, the metric depends on final recovery of displaced fluids from porous media, but not rate. The USBM method defines wettability of a sample by comparing the work required for one fluid to displace the other. Comparison of the Amott-Harvey and USBM methods by Buckley<sup>32</sup> did not give consistent results. Imbibition is a complex phenomena that interrelates numerous variables that cannot always be controlled or matched between experiments such as permeability, organic and aqueous viscosity, porosity, interfacial tensions between aqueous and organic components, and wettability. Although seemingly intractable, the difficulties encountered with the imbibition method were addressed by Ma et al.<sup>33</sup>

The imbibition measurement technique selected for use in this study is one of the simplest and quickest methods for measuring wettability.

## Component Selection

Selected system components were Berea Sandstone, synthetic SRPA water, microbiological growth media R2A, Berea sandstone cores (1 × 3 in.), field cores (1 × 3 in.) from TAN well at TAN-33 on the INEEL, and dodecane. The microbiological component selected for study was comprised of six isolates that originated from the same well as the core samples. Detailed information is given in Tables 2–6 and Figure 5. Cultures were grown from over-night freezer stocks (–80°C) in fresh R2A media. A 1% inoculum was placed into 50 ml of media in a 125 ml Erlenmeyer flask. Cells were grown aerobically at 30°C for at least 12 hours at a shaking speed of 150 rpm.

Cores were drilled from the same block of Berea sandstone and Hysol epoxy 1-C was used to seal the length of the cores, leaving one or two ends of the cores open. The epoxied cores were placed in a pressurized sleeve (200+ psi), and carbon dioxide was passed through the cores to measure gas permeability using Darcy’s law. The dry weights of the cores were measured and the cores were saturated with degassed DI water by vacuum. Water permeability was measured by

Table 2. Characterization of Berea Sandstone cores used for experimentation.

Core	Length (cm)	Diameter (cm)	Porosity	Permeability Water, (mD)	Organic Sat. Initial (mL)	Water Sat. Initial (mL)
Z10	7.611	2.529	0.219	272	5.35	0.361
Z11	7.570	2.527	0.220	249	5.15	0.384
Z13	7.559	2.527	0.212	383	5.15	0.359
Z14	7.635	2.529	0.216	384	5.26	0.366
Z15	7.624	2.518	0.220	384	5.35	0.359
Z17	7.607	2.526	0.215	570	5.43	0.339
Z18	7.621	2.538	0.220	597	5.58	0.342
Z22	7.649	2.535	0.207	603	5.45	0.317
Z23	7.673	5.534	0.201	477	5.03	0.353
Z24	7.672	2.529	0.219	556	5.22	0.381

Table 3. Characterization of TAN-33 cores prepared for experimentation.

Core	Length (cm)	Diameter (cm)	Porosity	Permeability Gas, (mD)
281-1	7.535	2.538	0.145	0.775
281-2	7.279	2.540	0.117	0.357
281-3	7.394	2.539	0.110	0.564
281-4	7.198	2.535	0.110	1.978
340-4	7.573	2.534	0.083	7.756
340-5	7.414	2.535	0.083	3.649
340-6	7.147	2.534	0.961	4.630

Table 4. Formulation of synthetic SRPA water.

Component	g/L H <sub>2</sub> O
KNO <sub>3</sub>	0.004
CaCl <sub>2</sub>	0.192
NaHCO <sub>3</sub>	0.092
MgSO <sub>4</sub>	0.11
NaNO <sub>3</sub>	0.003
KHCO <sub>3</sub>	0.006

Table 5. Formulation of microbiological media R2A.

Component	g/L H <sub>2</sub> O
Yeast Extract	0.5
Protease Peptone (#3)	0.5
Casamino Acids	0.5
Dextrose	0.5
Sodium Pyruvate	0.3
K <sub>3</sub> PO <sub>4</sub>	0.3
MgSO <sub>4</sub>	0.05
Soluble Starch	0.5

Table 6. Microbial isolates selected for wettability/imbibition experiments.

Isolate	Gram Reaction	Spore Formation	Growth Temp
<i>Acintobacter genospecies</i>	-	No	20-30°C
<i>Rhodococcus luteus</i>	+	No	26-30°C
<i>Hydrogenophaga pseudoflava</i>	-	Yes	20-45°C
<i>Arthrobacter ramosus</i>	+	No	25-30°C
<i>Arthrobacter globiformis</i>	+	No	25-30°C
<i>Bacillus atrophaeus</i>	+	Yes	20-30°C

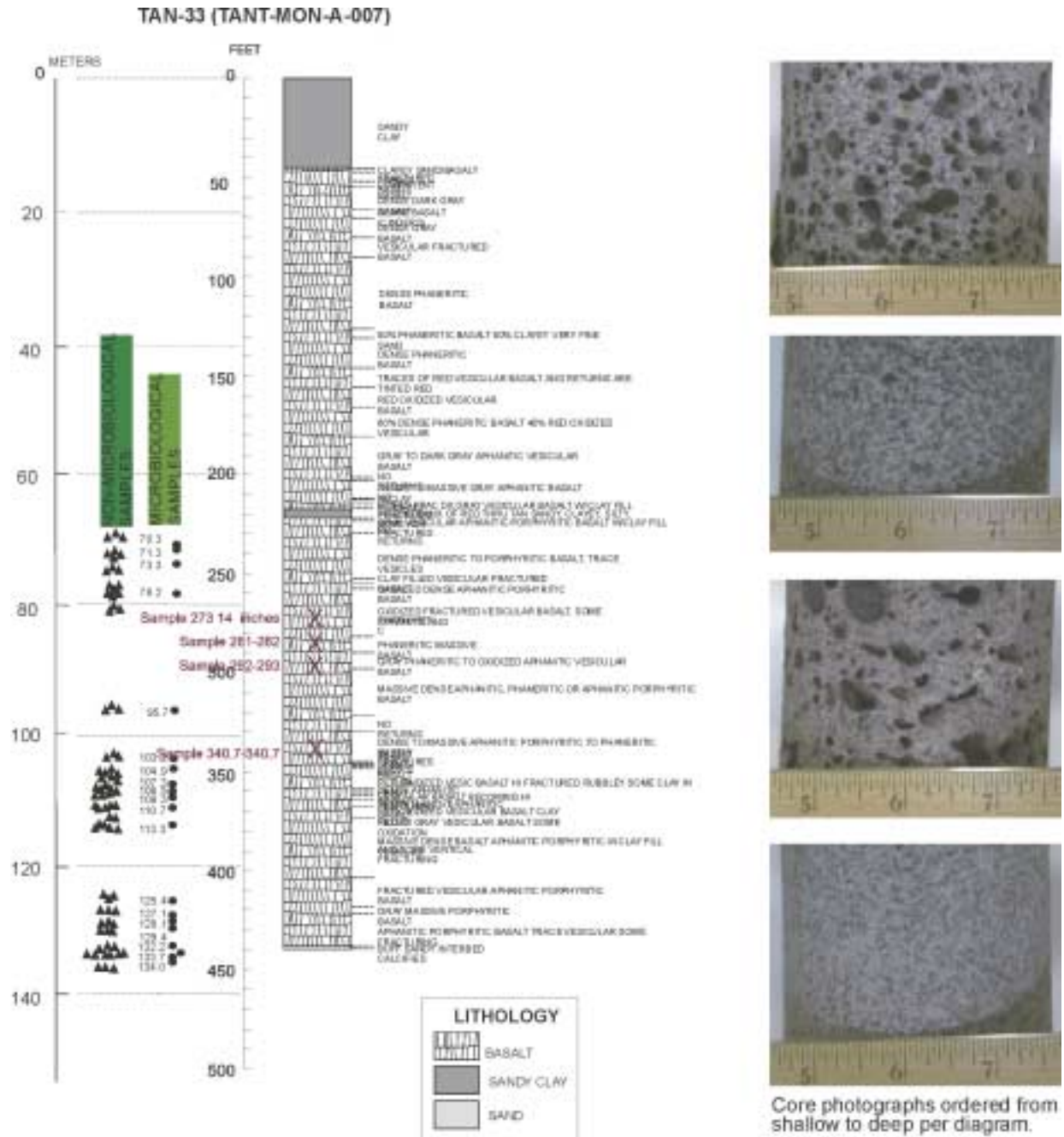


Figure 5. Lithology diagram for collected core material from TAN-33.

placing the cores in the pressurized core holder and DI water was injected through the cores while measuring flow rate and pressure drop across the cores. Again, Darcy's law was used to calculate the water-saturated permeability. After permeability measurements were taken, the cores were weighed again to obtain the weight of the cores when saturated with water. Core porosity was calculated based on the mass differences of the saturated and dry states and the density of the water. Five pore volumes of dodecane were then injected through each core at an upstream pressure of 50 psig. The water produced from the core during the dodecane injection was collected and quantified. The volume of dodecane inside the core after the dodecane flood was set equal to the produced water volume and the remaining water saturation was calculated. After the dodecane flood, the cores were stored submerged in dodecane until used in imbibition experiments.

Following core preparation, the cores were hung from a weigh-below port on an analytical balance and suspended in a beaker containing the aqueous component to be tested (synthetic SRPA water, microbiological growth media, or spent growth media with metabolic end products). The weight of the core was recorded in real time increments of 30 seconds to 5 minutes by connecting the balances directly to a PC through a RS232 multiport board. As the cores imbibe water, they gain weight (the lighter organic fluid is drained as the heavier aqueous fluid is imbibed) proportionally. The data were recorded and transferred automatically into an Excel spreadsheet for reduction.

## Data Treatment

Changes in core weight was reduced to incremental recovery of organic as a fraction of original organic in place (OOIP) and ultimately graphed as a function of maximum recovery attained for that core ( $\text{Recovery}/\text{Recovery}_{\text{max}}$ ). The time component was transformed into dimensionless time according to Ma et al. (see Reference 33) through the use of the correlation coefficient:

$$td = \sqrt{\frac{k}{\phi}} \frac{\sigma}{\sqrt{\mu_w \mu_o}} \frac{t}{L^2 c} \quad (1)$$

where:

- $td$  = dimensionless time
- $k$  = permeability
- $\phi$  = porosity
- $\mu_o$  = organic Viscosity
- $\mu_w$  = aqueous viscosity
- $\sigma$  = interfacial Tension between the organic and aqueous phase
- $L_c$  = characteristic Length
- $t$  = time.

Interfacial tensions were measured by video image analysis of inverted pendant drops as previously published.<sup>34</sup>

The characteristic length is defined mathematically by a relationship that takes boundary conditions into account. For all experiments reported here, the core configuration was either "two ends open" ( $L_c = \text{Length}/2$ ) or "All Faces Open" ( $L_c = L_d/2(d+2L)0.5$ ).

The true utility of dimensionless time correlation is the isolation of intractable variables such as permeability, organic and aqueous viscosity, porosity, and interfacial tensions between aqueous and organic components.

Graphed data ( $R/R_{\text{max}}$  vs.  $td$ ) were fit with the single parameter mass transfer function described by Aronofsky et al.<sup>35</sup> in the following equation to aid in distinguishing differences between control and test experiments:

$$R / R_{\text{max}} = 1 - e^{-\alpha td} \quad (2)$$

where

- $R$  = organic recovered by imbibition
- $R_{\text{max}}$  = ultimate organic recovered by imbibition
- $\alpha$  = organic production decline curve

$t_D$  = dimensionless time.

Experiments designed to evaluate the accuracy of the analytical system were performed with Berea Sandstone cores. Cores were hung in the vertical as well as horizontal position, with either one or two ends open. Original experiments using all faces open cores resulted in erroneous data due to the relatively fast time frame of imbibition coupled with the adhesion of dodecane to the exposed rock surface. These difficulties were mitigated by applying a system using a two-faces-open architecture to minimize exposed rock surface and slow the water imbibition. These changes resulted in an experimental system with good repeatability.

## Results/Discussion

Data sets from Berea Sandstone cores (ostensibly a very strongly water-wet system) and synthetic SRPA water were compared to literature data for accuracy and system performance. Data were compared to strongly water-wet systems originally using alundum and sandstone cores,<sup>36</sup> aluminum silicate systems,<sup>37</sup> and Berea sandstone systems.<sup>38</sup> All literature systems evaluated resulted in a mass transfer function ( $\alpha$ ) of  $-0.03$  to  $-0.07$

for strongly water-wet systems. Data collected for this work fell well within this bracket irrespective

of the configuration (one end open vs. two ends open or vertical or horizontal position).

Careful examination of the data presented in Figure 6 results in a slight discrepancy with respect to those data points collected during the early time frame and the mass transfer function. Although this discrepancy does not influence the overall interpretation, it is important to understand the origin of the difference. During early time points, a very slight retardation in the release of organic from the face of the core can drive very large apparent delays in dimensionless time. It is hypothesized that manual cleaning of the core face before a weight was taken would remedy the problem.

Additional experimentation to evaluate the effect of imbibition of microbiological growth media (R2A) in cores originally saturated with synthetic SRPA water resulted in a tangible shift to a less water-wet state (see Figure 7). Imbibition data from these experiments have a mass transfer function of  $-0.005$  to  $-0.003$ , or one log cycle difference. This difference was demonstrated to be repeatable.

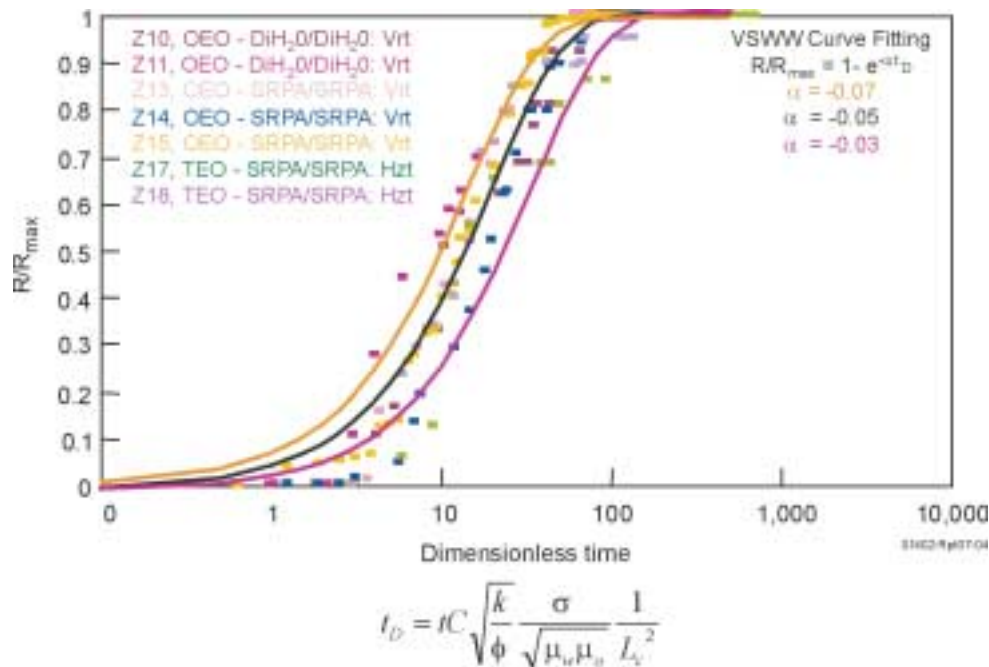


Figure 6. Imbibition of synthetic SRPA water into dodecane saturated cores.

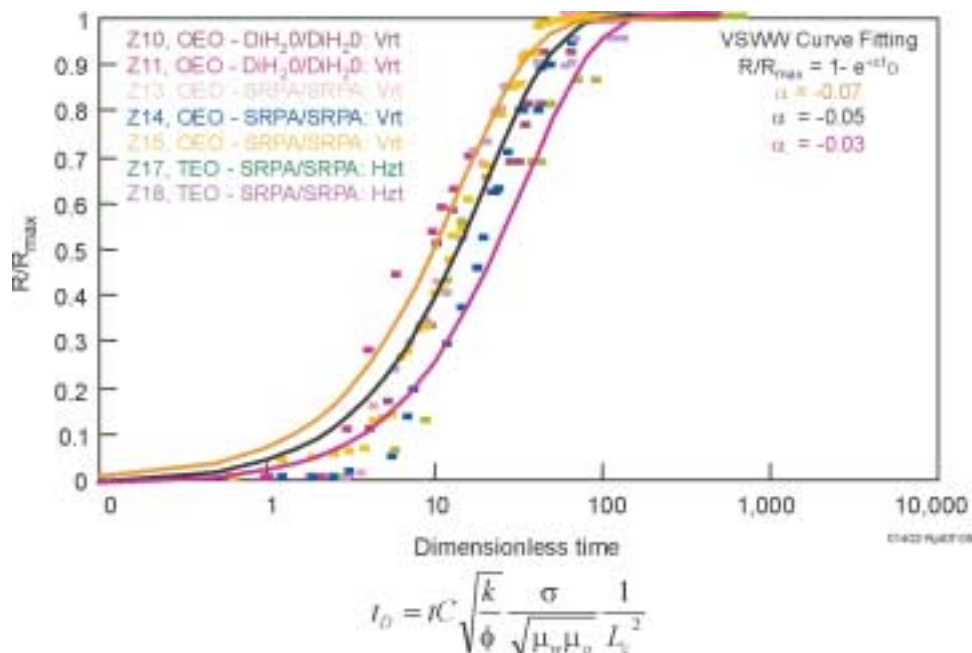


Figure 7. Imbibition of R2A microbiological media into dodecane saturated Berea sandstone cores.

## Linking Structure and Function in Environmental Microorganisms

F. S. Colwell (Task PI)

TCE contamination of groundwater is a widespread problem at many locations, including DOE sites. The SRPA near the TAN facility at the INEEL (see Figure 8) is of particular interest due to apparent natural attenuation of a large TCE plume (see Reference 6). Ubiquitous aerobic gram-negative methanotrophic bacteria (methanotrophs) are believed to be one of the microbial physiologies responsible for attenuation of the TCE plume. Type I (RuMP assimilation pathway,  $\alpha$ -proteobacteria) and Type II (serine assimilation pathway,  $\alpha$ -proteobacteria) methanotrophs have been shown to be capable of degradation of chlorinated compounds, including TCE.<sup>39</sup> The methanotrophic enzyme, methane mono-oxygenase (MMO), which oxidizes methane to methanol, can also cometabolize TCE.<sup>40</sup> This enzyme exists as a soluble (sMMO) form or a membrane associated particulate (pMMO) form. Even though both forms of the enzyme are capable of degradative process, presumably the soluble

form of this enzyme is environmentally important since it demonstrates substantially higher rates of cometabolism of halogenated solvents than does pMMO. Type I methanotrophs generally have only the pMMO while Type II methanotrophs typically have both the soluble and particulate forms of MMO. There are some exceptions to this; for example, some *Methylomonas* strains (Type I) contain only the sMMO. Such findings may be important since Type I methanotrophs have higher carbon conversion efficiencies than Type II methanotrophs, and thus may be more active in the environment. We studied microorganisms from the pristine basalt aquifer surrounding TAN to gain insight into the observed natural attenuation of TCE. We investigated the role that methanotrophs may play in this process, and the effect that dissolved methane concentrations may have on methanotroph populations and distribution. Initial groundwater analyses determined water pH, temperature, dissolved oxygen and methane concentrations, and total cell numbers. Groundwater pH, temperature, and dissolved oxygen were determined using the Scout 2 Hydrolab (Hydrolab Corp. Austin, Texas). Results show water from each well to be near neutral pH and oxic (see Table 7). Total counts of microbial cells, determined by acridine orange direct count,

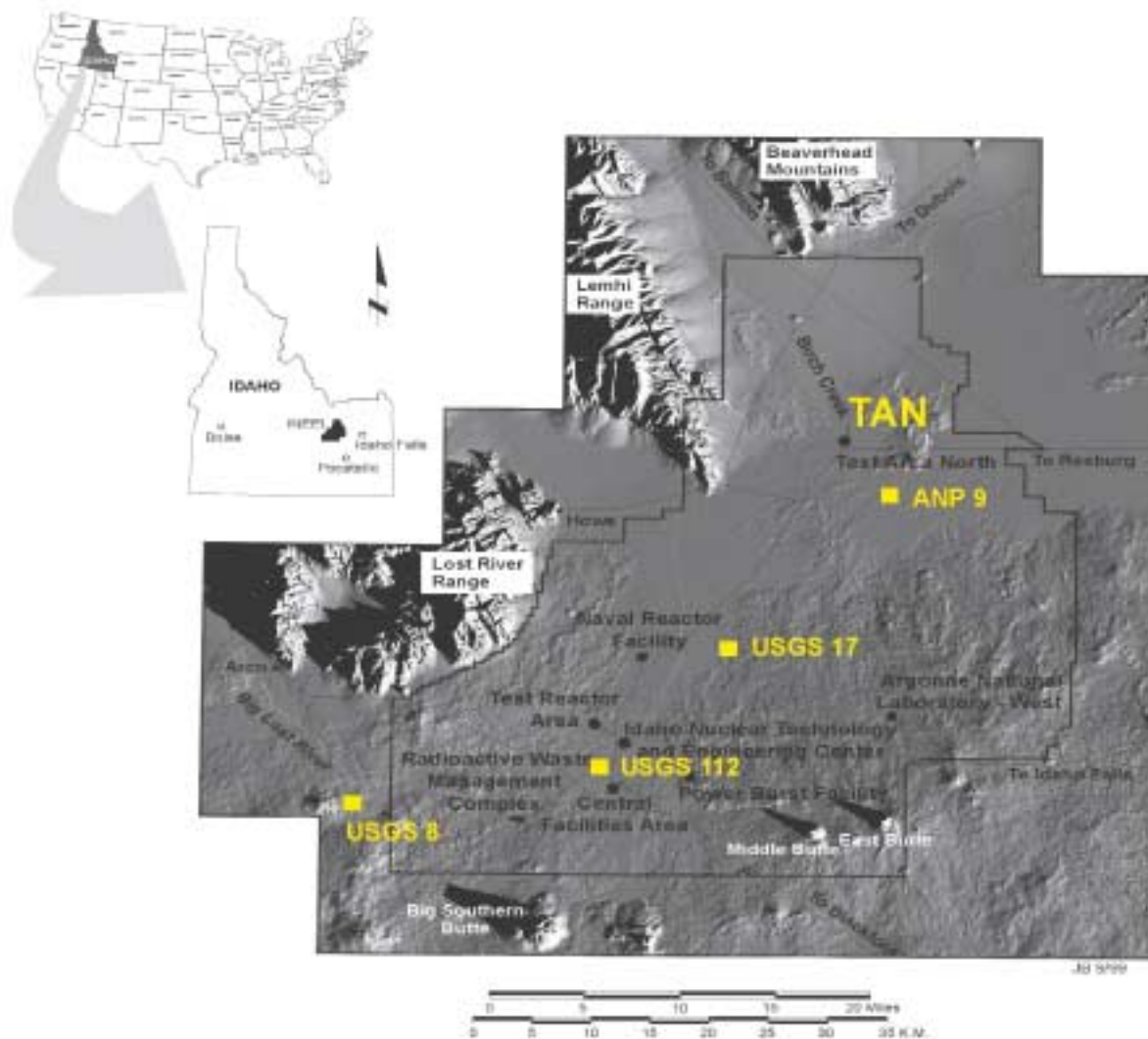


Figure 8. Location of wells from which groundwater was collected for methanotroph studies.

Table 7. Geochemical and microbial properties in groundwater sampled from selected wells in the SRPA.

Condition	Well			
	ANP9	USGS 8	USGS 17	USGS 112
pH	7.86	7.7	7.89	7.62
Temp (C )	14.10	11.37	12.78	13.06
Dissolved Oxygen (mg/L)	8.43	8.18	9.65	8.63
Cell Mass (cells/ml)	$3.9 \times 10^3$	$1.7 \times 10^3$	$3.3 \times 10^3$	$3.7 \times 10^3$
Methane (nM) <sup>a</sup>	40	70–1,050	50–90	1–6

a. Atm methane in water is about 3 Nm

were between  $10^3$  and  $10^4$  cells per mL. Dissolved methane gas measured using a Reduction Gas Analyzer (Trace Analytical, Inc. Menlo Park, California) varied from near local atmospheric methane levels (3 nM) to significantly greater (see Figure 9). Dissolved methane concentration variations provided the framework for determining a methane-using microbial community distribution and analysis.

Samples were screened for the presence of both Type I and Type II methanotrophs since both types have co-metabolic capabilities and diverse populations have been detected in freshwater environments. Microorganisms from groundwater were filtered and analyzed directly for the presence of methanotrophs or were used as inocula for enrichment of methanotrophs. For the culture-independent direct analysis of natural

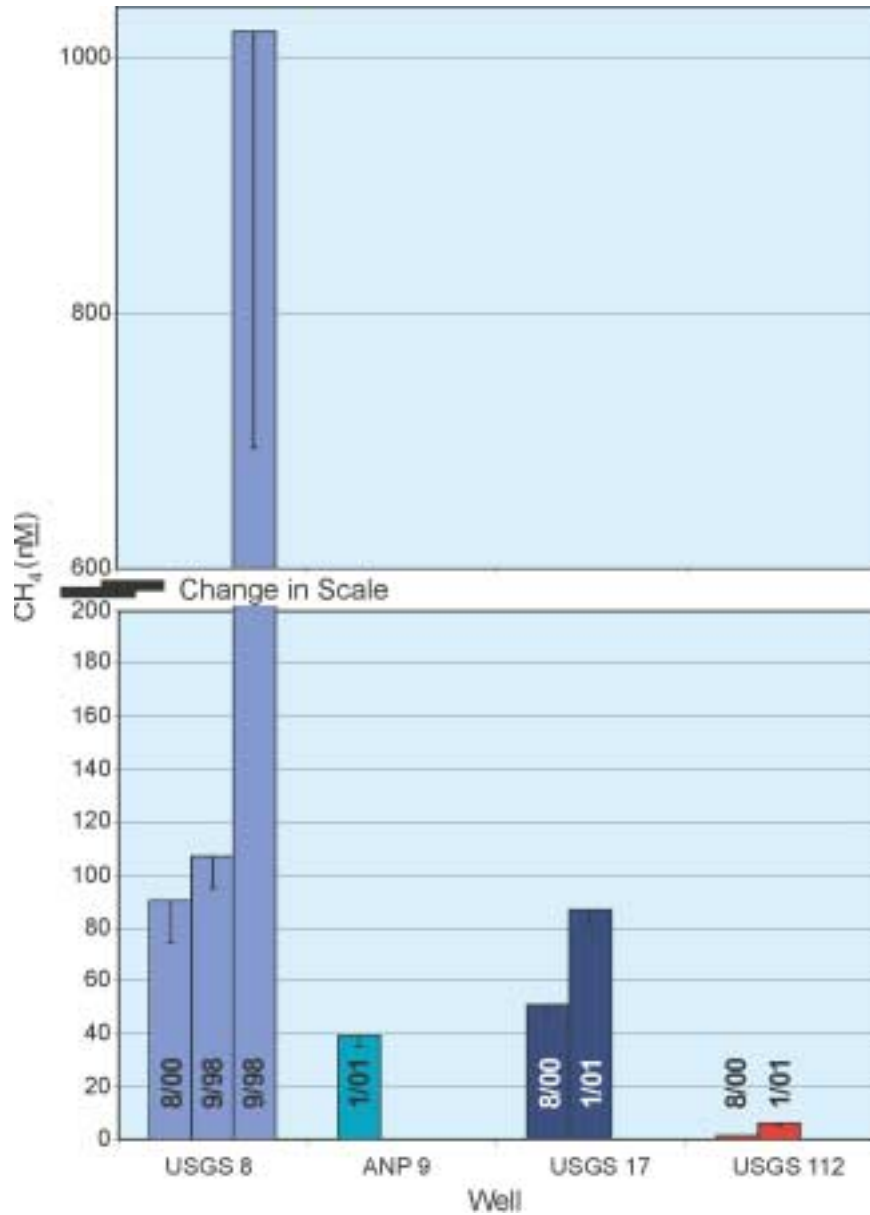


Figure 9. Historic variation in groundwater methane concentration between sampled wells. Error bars represent standard deviation in measurements. If error bars are absent then only one dissolved methane sample has been collected from that well.

methanotrophs, 100 L of groundwater was filtered onto a 142 mm Supor membrane disc (see Figure 10). DNA was subsequently extracted from the filters using a scaled up version of the MoBio Water DNA kit. For culture-dependent analysis of methanotrophs, 1 L of groundwater was filtered onto a 47 mm Supor filter and the filter was subsequently used as the inocula for growth in nitrate minimal salts (NMS) broth in serum bottles. We used 1X NMS or 0.2X NMS concentrations to enrich for Type I and Type II methanotrophs, respectively. The headspace

atmosphere was 90:9:1 (air:methane:CO<sub>2</sub>) or 99:1 (air:CO<sub>2</sub>) for control vials without methane. The methane atmosphere was maintained by periodic flushing of the headspace. One set of vials (see Figure 11) was analyzed for each well at each NMS concentration.

DNA primers that specifically target the 16S rRNA gene(s) in methanotrophs or genes that code for subunits of soluble (mmoX) or particulate (pmoA) methane monooxygenase were used to characterize the diversity of microbial populations



Figure 10. Sampling groundwater from well on the Eastern Snake River Plain.



Figure 11. Methanotroph enrichment cultures depicting typical growth or absence of growth for different treatments. Vials 1 and 2 contain methanotroph cultures with methane added; vial 3 is a control that contains methanotrophs, but no methane; and vial 4 is a control with no methanotrophs, but methane has been added.

via PCR, cloning, and sequencing (see Table 8 and Figure 12). The 16S rDNA primers MethT1bR with MethT1dF were specific for Type I methanotrophs and MethT2R with bacterial-specific 8F targeted Type II methanotrophs. Each primer pair amplified approximately a 1 Kb DNA fragment (see Figure 13). Diversity of pMMO was assessed using primers specific for pmoA, which codes for subunit A, a protein, of the pMMO enzyme. The primer pair pmof1 and pmor

amplifies about half (330 base pairs) of the pmoA DNA and is the only set of primers that do not also amplify the ammonia monooxygenase gene (amoA) from ammonia oxidizers. Primer pair mmoXA and mmoXB, which amplify most (1,230 base pairs) of the mmoX gene, which codes for the alpha subunit of the hydroxylase component of sMMO, were used to assess the diversity of the soluble form of this enzyme.

Table 8. Summary of PCR amplification results that discriminate SRPA wells with respect to methanotroph communities. Three means of detecting methanotrophs was possible: DNA extracted from filtered groundwater, enrichments inoculated with groundwater, and isolates obtained from enrichments.

Well	Template	Target			
		SMMO (mmoX)	PMMO (pmoA)	Type I (16S rDNA)	Type II (16S rDNA)
ANP 9	Groundwater	ND	Detected	ND	ND
	Enrichment	Detected	—	Detected	Detected
	Isolates	—	#8 & #9	#8 & #9	—
USGS 17	Groundwater	Detected	Detected	ND	ND
	Enrichment	Detected	—	Detected	Detected
	Isolates	—	—	—	—
USGS 112	Groundwater	ND	Detected	ND	ND
	Enrichment	Detected	—	Detected	Detected
	Isolates	#5	#5	—	—
USGS 8	Groundwater	ND	ND	Detected	Detected
	Enrichment	Detected	—	Detected	Detected
	Isolates	—	—	—	—

\* ND, indicates PCR was conducted, but target non-detected

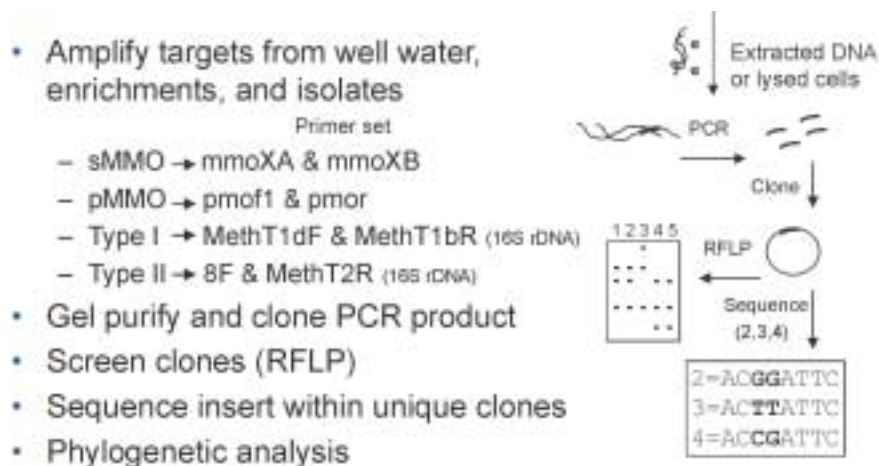


Figure 12. Approach for molecular characterization of microorganisms obtained via filtration from groundwater, in enrichments, or as potential methanotroph isolates.

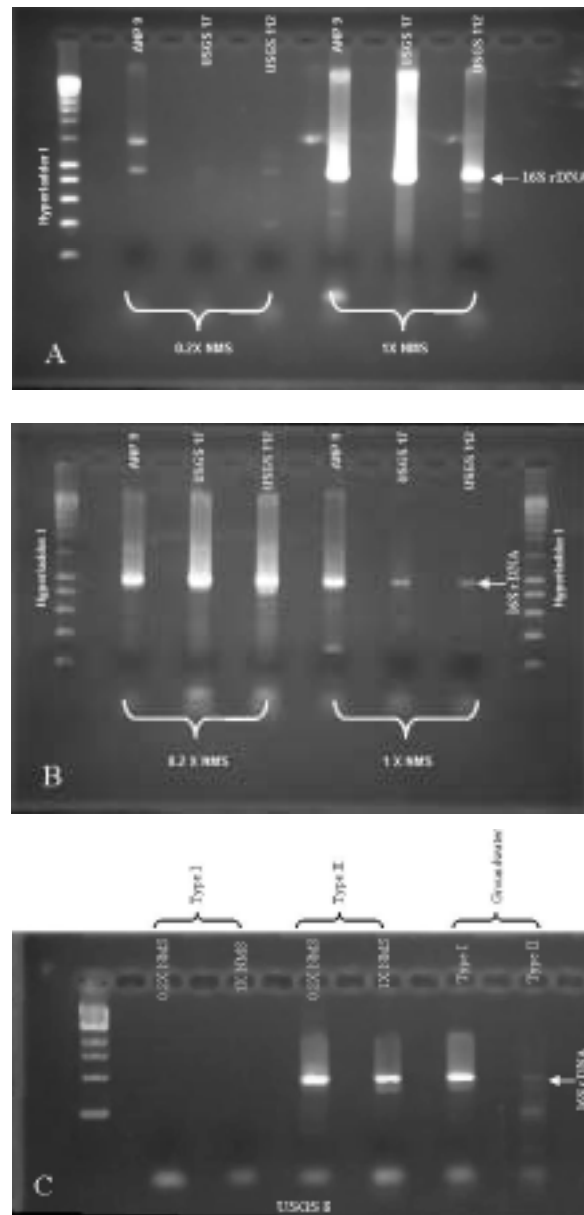


Figure 13. Amplified 16S rDNA using: (A) Type I primers with DNA from enrichments; (B) Type II primers with DNA from enrichments; and (C) Type I and Type II primers with DNA from USGS 8 enrichments and groundwater. For enrichments, Nitrate Mineral Salts (NMS) medium were provided at full strength (1x) or diluted (0.2x).

These primers were selected because they targeted amplification of most of the *mmoX* gene, which will presumably allow better sequence discrimination. However, due to analytical difficulties, it will be necessary to modify this approach. Potential use of a primer pair (*mmoX* f882 with *mmoX* r1403) that amplifies a shorter gene region will have less nonspecific product amplified. To identify unique amplified

16S rDNA or pMMO gene clones, we screened approximately 50 clones from each well by restriction fragment length polymorphism (RFLP) analysis. We then analyzed clones from each library using tetrameric restriction enzymes *HinP1* and *Msp1* (see Figure 14), grouped them according to unique RFLP patterns, and the sequenced and analyzed genes on plasmids from representative clones (Tables 9 and 10).



Figure 14. Representative restriction fragment length polymorphism (RFLP) patterns showing variation in cloned pmoA fragments from PCR using pmof1 and pmor primers. Amplified DNA was extracted from cells filtered from groundwater.

Table 9. Numbers of clones exhibiting unique RFLP patterns for the pmoA gene and closest apparent relationship to known microorganisms. The source of the DNA from which the clones were created was filtered groundwater from selected wells in the SRPA.

PmoA (RFLP- pattern)	Well (number of clones)				Related organisms or group (UC=uncultured organism)	Related Methanotroph group	Percent Sequence identity
	ANP9 (46)	USGS8 (37)	USGS17 (48)	USGS112 (46)			
A	27	—	—	30	<i>Methylocystaceae</i> (AML-A6)	Type II	98
B	11	—	—	3	<i>Methylocystaceae</i> (AML-A6)	Type II	98
C	—	15	29	—	UC <i>Methylobacter</i> sp. (PF42)	Type I	91
D	—	—	8	—	UC RC4/ <i>Methylococcus</i> <i>capsulatus</i>	Type I	92/87
E	—	—	6	13	UC <i>Methylocystis</i> sp.	Type II	96
F	2	—	—	—	<i>Methylocystaceae</i> (AML-A6) <i>Methylobacter</i> (LW12)	Type II Type I	97 95
G	6	—	—	—	<i>Methylocystaceae</i> (AML-A6)	Type II	98
H	—	—	5	—	UC RC4/ <i>Methylococcus</i> <i>capsulatus</i>	Type I	93/87
I	—	20	—	—	—	—	—
J	—	2	—	—	—	—	—

Table 10. Numbers of clones exhibiting a unique RFLP pattern from DNA of methanotrophs enriched from each well. For enrichments, Nitrate Mineral Salts (NMS) medium was provided at full strength (1x) or diluted (0.2x).

Type I (RFLP- pattern)	Well (number of clones)								Related organisms or group (UC=uncultured organism)	Related Methanotroph group	Percent Sequence identity
	ANP9		USGS 8		USGS17		USGS112				
	0.2X (23)	1X (22)	0.2X (0)	1X (16)	0.2X (6)	1X (5)	0.2X (18)	1X (36)			
A	—	—	—	—	—	—	1	1	<i>Methylocystaceae</i> (AML-A6)	Type II	99
B	—	—	—	—	1	—	—	—	<i>Methylosinus trichosporium</i>	Type II	99
F	8	2	—	—	—	—	7	—	<i>Pseudomonas saccharophila</i>	—	97
G	1	—	—	—	—	—	—	—	<i>Ultramicrobacterium</i> (ND5)	—	97
H	—	13	—	—	—	1	—	8	<i>Methylomonas methanica</i>	Type I	98
I	—	7	—	—	—	3	1	16	<i>Methylomonas methanica</i>	Type I	97
J	—	—	—	—	—	—	1	—	<i>Acidovorax temperans</i>	—	99
K	—	—	—	—	—	—	2	3	<i>Pseudomonas saccharophila</i>	—	99
L	—	—	—	—	—	—	1	7	<i>Methylomonas methanica</i>	Type I	99
M	—	—	—	—	—	—	—	1	<i>Methylomonas methanica</i>	Type I	98
N	—	—	—	—	—	—	—	1	<i>Methylomonas methanica</i>	Type I	98
O	—	—	—	—	5	—	—	—	<i>Escherichia coli K12</i>	—	99
P	—	—	—	—	—	1	—	—	<i>Methylobacter psychrophilus</i>	Type I	98
Q	10	—	—	—	—	—	—	—	<i>Pseudomonas saccharophila</i>	—	99
S	4	—	—	—	—	—	—	—	<i>Methylocystaceae</i> (AML-A6)	Type II	98
W	—	—	—	5	—	—	—	—	—	—	—
X	—	—	—	7	—	—	—	—	—	—	—
Y	—	—	—	2	—	—	—	—	—	—	—
Z	—	—	—	1	—	—	—	—	—	—	—
AA	—	—	—	1	—	—	—	—	—	—	—

Table 10. (Continued).

Type II (RFLP- pattern)	Well (number of clones)								Related organisms or group (UC=uncultured organism)	Related Methanotroph group	Percent Sequence identity
	ANP9		USGS 8		USGS17		USGS112				
	0.2X (49)	1X (49)	0.2X (52)	1X (52)	0.2X (50)	1X (49)	0.2X (49)	1X (46)			
A	16	21	47	46	50	41	48	39	<i>Methylocystaceae</i> (AML-A6)	Type II	99
B	1	22	—	—	—	1	—	2	<i>Methylosinus trichosporium</i>	Type II	99
C	2	—	—	—	—	—	—	—	<i>Methylosinus trichosporium</i>	Type II	96
D	—	—	—	—	—	—	—	1	<i>Methylocystaceae</i> (T2-02)	Type II	—
E	1	—	—	—	—	—	—	1	<i>Methylocystaceae</i> (AML-A6)	Type II	99
P	—	2	—	—	—	—	—	—	UC/ <i>Methylobacter psychrophilus</i>	Type I	99/98
R	—	—	1	1	—	3	—	4	<i>Methylocystaceae</i> (AML-A6)	Type II	97
S	29	3	6	5	—	2	—	—	<i>Methylocystaceae</i> (AML-A6)	Type II	98
T	—	—	—	—	—	1	—	—	<i>Neisseria Meningitidis</i>	—	81
U	—	—	—	—	—	1	—	—	<i>Rhizobiaceae</i>	—	97
V	—	—	—	—	—	—	1	1	<i>Methylocystaceae</i> (AML-A6)	Type II	96

Based on research conducted during the first year of this task, RFLP and sequence analyses suggest that methanotroph populations vary between wells and potentially according to methane concentration. For example, USGS 8 had the highest dissolved methane concentration of the wells and the lowest RFLP 16S rDNA Type II diversity from enrichments (Table 11), whereas USGS 112 had the lowest methane concentration and the highest RFLP 16S rDNA Type II diversity from enrichments. Although AODC counts indicated a very low biomass in the groundwater, bacterial 16S rDNA from the filtered groundwater was detected from each well. However, only DNA from USGS 8 groundwater (unenriched) could be used to directly detect Type I and Type II methanotroph specific 16S rDNA via PCR, suggesting a more abundant methanotroph population (particularly Type I) in groundwater with higher dissolved methane levels (refer to Table 8).

Both Type I and Type II methanotrophs were enriched from all wells (refer to Table 8), although enrichment tended to favor growth of Type II methanotrophs. In general, depending upon NMS concentration, differential enrichment was consistent with an earlier report, which indicated that 1X NMS enriched for microorganisms can be amplified using Type I methanotroph specific primers and that 0.2X NMS preferentially enriched for microorganisms can be amplified using Type II primers. An analysis of sequence data indicated that Type I specific primers amplified 16S rDNA from enrichments for Type I methanotrophs related to *Methylomonas methanica* (97–99% identity) and *Methylobacter psychrophilus* (98% identity) (refer to Table 10). Most of the 16S rDNA amplified from enrichments using Type II specific primers were most closely related to the Type II Methylocystaceae group (96–99% identity) (refer to Table 10). In fact, RFLP pattern A (Methylocystaceae) was the predominant Type II 16S rDNA in all the wells. Particulate methane monooxygenase genes amplified from filtered groundwater were closely related to the Type I *Methylobacter* (91% identity) and *Methylococcus* (87% identity) genus, and the Type II Methylocystaceae group (97–98% identity) (Refer to Table 9). One isolate (#5) enriched from USGS 112 has genes for both sMMO and pMMO, and

thus, is presumably Type II, although neither Type I nor Type II methanotroph 16S rDNA specific primers amplified the DNA from this isolate. This suggests there is a methanotrophic population present in the SRPA that is as yet undetectable using the conventional phylogenetic primers for this group of microorganisms. Isolates #8 and #9 from ANP9 were pink (a characteristic of methanotrophs) and had a pMMO gene most closely related to the Type I *Methylomonas* genus.

These steps towards understanding the diversity of methanotrophs and their distribution with respect to dissolved concentrations of methane in the SRPA are important because they help complete the picture of how natural attenuation of TCE in the aquifer may be occurring. This basic knowledge of the microorganisms that appear to be responsible for diminished levels of TCE surrounding the dissolved plume at TAN will be applied towards developing methods that allow explicit in situ TCE degradation rates to be inferred. Quantification of the rate of contaminant degradation and verification of an ongoing process that must be depended upon for the long-term management of a waste plume are essential aspects of what stakeholders require in order to adopt a particular remediation approach. This effort will clarify the route by which other biological processes can be used to ensure natural attenuation as a viable treatment technology. Specifically, the research addresses Site Technology Coordination Group stated needs (see, for example, Science and Technology Needs ID-6.1.04 In-situ Treatment of VOC Contaminated Groundwater in Saturated and Unsaturated Deep Fractured Rock; <http://www.inel.gov/st-needs/need-detail.asp?id=ID-6.1.04>).

## ACCOMPLISHMENTS=

In several studies, we found corroborating evidence that attached and free-living aquifer microbial communities were compositionally different and possess unique functional attributes.

We found that a combination of molecular (culture-independent) and culture-dependent approaches best described the composition of aquifer microbial communities.

In a simulated aquifer, we found that cell-specific  $\beta$ -glucosidase activities were higher for attached bacterial cells than free-living cells while the converse was true of aminopeptidase activities.

We developed methods for extracting high quality (minimally sheared, PCR-amplifiable) DNA from low biomass groundwater, sediment and rock samples.

We documented the presence of Archaea in the oxic, temperate groundwaters of the eastern Snake River Plain Aquifer by analysis of 16S rDNA sequences in bulk DNA extracts.

We found that TCE contamination (10 ppm) had little effect on groundwater bacterial communities.

We found that attachment of a model bacterium, *B. cepacia* G4, to basalt was influenced by the specific mineral phases contained in basalt and that the biochemical expression of this organism was mediated by the specific mineral substrata.

We demonstrated that our newly developed probe for TMO activity, 3-HPA, can be successfully applied to groundwater samples collected from the eastern Snake River Plain Aquifer.

In a collaborative study, we demonstrated that the detection limit for SIMS characterization of intact cells approaches environmentally-relevant densities of microorganisms.

We were able to measure wettability and imbibition, which provided insight for the determination of flow, transport, distribution, and recovery of contaminants.

We conducted imbibition experiments that controlled for numerous variables, which revealed important differences in wettability.

We determined that aqueous and organic composition and concentration effect the flow, distribution, and recovery of contaminants. It is expected that manipulation of subsurface microbial communities will result in changes to the aqueous and organic constituents, which will potentially result in changes to wettability and imbibition.

Our imbibition experiments indicate that systems prepared with synthetic aquifer water and challenged with R2A media are less water-wet than the same systems challenged with synthetic aquifer water.

We acquired new capabilities and equipment for wettability and imbibition measurements. This capability enhances the competitive position of the INEEL and complements the existing analytical tools to provide research services for the INEEL, industry, and government sponsors as they respond to regulatory and compliance drivers. The acquisition of this capability allows a broad base of researchers at the INEEL to access techniques that were not previously available.

We developed molecular approaches to determine the diversity of methanotrophic microorganisms capable of natural attenuation of chlorinated solvents.

We were able to discern high methanotroph diversity in the SRPA as demonstrated by 16S rDNA analysis of both filtered groundwater and methanotroph enrichments of groundwater.

We found that one Type II methanotroph related to the Methylocystaceae was predominate in all wells as evidenced by extracted DNA from filtered well water and enrichments.

We found an apparent relationship between the variability of methanotroph communities to differences in dissolved methane concentrations in the wells. Type II methanotroph 16S rDNA diversity appears to be inversely correlated to dissolved methane concentration.

We found both Type I and Type II methanotrophs present in all of the SRPA wells studied.

## **Publications**

### **In Preparation or Submitted**

Lehman, R. M. and S. P. O'Connell, " $\beta$ -Glucosidase and Aminopeptidase Exoenzyme Activities and Community Structure by Denaturing Gel Electrophoresis of rDNA Amplification Products of Attached and Unattached Bacterial Communities in Porous

Media,” in preparation for submittal to *Applied and Environmental Microbiology*.

O’Connell, S. P., D. E. Cummings, R. M. Lehman, O. Snoeyenbos-West, M. E. Watwood, and F. S. Colwell, “Detection of Archaeal DNA Sequences in an Oxic, Fractured Rock Aquifer,” In preparation for submittal to *Applied and Environmental Microbiology*.

### Accepted or Published

Lehman, R. M. F. S. Colwell, and G. A. Bala, “Attached and Unattached Microbial Communities In a Simulated Basalt Aquifer Under Fracture- and Porous-flow Conditions,” *Applied Environmental Microbiology*, Vol. 67, No. 1, 2001, pp. 2799–2809.

Lehman, R. M., F. F. Roberto, D. Earley, D. F. Bruhn, S. F. Brink, S. P. O’Connell, M. E. Delwiche, and F. S. Colwell, “Attached and Unattached Microbial Communities In Closely-Paired Groundwater and Core Samples from an Acidic, Crystalline Rock Aquifer,” *Applied Environmental Microbiology*, Vol. 67, No. 5, 2001, pp. 2095–2106.

O’Connell, S. P., and J. L. Garland, “Dissimilar Response of Microbial Communities in Biological GN and GN2 Plates,” *Soil Biology and Biochemistry* (in press), 2001.

### Presentations

Ingram, J. C., D. E. Cummings, and R. M. Lehman, “Evaluation of Static SIMS to Characterize Intact Bacterial Cells,” Extended Abstract, *49th Annual Conference on Mass Spectrometry and Allied Topics sponsored by the American Society of Mass Spectrometry in Chicago, IL* May 28–31, 2001.

Kauffman M. E., H-Y. Holman, R. M. Lehman, M. C. Martin, and W. R. McKinney, “Mineralogical Constraints on the Spatial Distribution and Biochemistry of Bacteria Attached to Basalt,” Abstract, *Fall Meeting of the American Geophysical Union, SF, CA, Dec. 2000*.

Kauffman, M. E., H-Y. Holman, R. M. Lehman, M. C. Martin, and W. R. McKinney, “Investigation Into the Biochemistry of Bacterial Attachment to Various Mineral Phases Using Synchrotron Radiation-Based Fourier Transform Infrared Microspectroscopy (SR-FTIR),” Abstract, *Advanced Light Source Users Conference, Berkeley, CA, Oct. 2000*.

Kauffman, M. E., W. K. Keener, R. M. Lehman, M. E. Watwood, H-Y. Holman, and M. C. Martin, “Effects of Bacterial Attachment on the Production of Toluene 2-monoxygenase,” Abstract, *Battelle In Situ and On-Site Bioremediation Meeting, San Diego, CA, June 2001*.

Lehman, R. M. “Attached and Unattached Bacteria in Saturated Subsurface Environments,” Abstract, *Ninth International Symposium on Microbial Ecology, Amsterdam, The Netherlands, August 2001*.

McKinley, J. P., and F. S. Colwell, “Co-conveners of a Session Entitled: Assessing Bioremediation at the Fall Meeting of the American Geophysical Union,” December 2001.

Newby, D. T., D. W. Reed, M. E. Delwiche, J. P. McKinley, F. F. Roberto, and F. S. Colwell, “Molecular Characterization of Methanotrophic Communities from an Aerobic, Fractured Basalt Aquifer,” Abstract, *100th General Meeting of the American Society for Microbiology, Orlando, FL, May 2001*.

Newby, D. T., D. W. Reed, M. E. Delwiche, J. P. McKinley, F. F. Roberto, and F. S. Colwell, “Methanotroph Diversity as it Correlates to Methane Concentrations Within Pristine Groundwater,” Abstract, *Ninth International Symposium on Microbial Ecology, Amsterdam, The Netherlands, August 2001*.

O’Connell, S. P., D. E. Cummings, R. M. Lehman, M. E. Watwood, and F. S. Colwell, “Detection of Archaeal DNA Sequences In an Oxic, Fractured Rock Aquifer,” Abstract, *100th General Meeting of the American Society for Microbiology, Orlando, FL, May 2001*.

O'Connell, S. P., M. E. Watwood, R. M. Lehman, and F. S. Colwell, "Molecular and Culture-Based Techniques for Monitoring Trichloroethylene-Exposed Microbial Communities," Abstract, *Battelle In Situ and On-Site Bioremediation Meeting, San Diego, CA, June 2001*.

O'Connell, S. P., M. E. Watwood, R. M. Lehman, and F. S. Colwell, Estimation of Groundwater Microbial Species Diversity Using Denaturing Gradient Gel Electrophoresis and Plate Count Methods," Abstract, *Intermountain Branch of the American Society for Microbiology Annual Meeting, Pocatello, ID, April 2001*.

O'Connell, S. P., R. M. Lehman, and J. L. Garland, "Biolog Media Formulation (GN2 vs. GN) Affects Community-Level Physiological Profiles," Abstract, *International Symposium on Microbial Ecology, Amsterdam, The Netherlands, August 2001*.

Reed, D. W., D. T. Newby, M. E. Delwiche, A. Igoe, J. P. McKinley, F. F. Roberto, and F. S. Colwell, "Diversity of Methanotrophic Communities in a Pristine Basalt Aquifer: Implications for Natural Attenuation of TCE," Abstract, *submitted to the Fall Meeting of the American Geophysical Union, December 2001*

## REFERENCES

1. National Research Council, *Research Needs in Subsurface Science – U.S. Department of Energy's Environmental Management Science Program*, National Academy Press, Washington, D.C. 2000.
2. Lehman, R. M., F. S. Colwell, and G. A. Bala, "Attached and Unattached Microbial Communities in a Simulated Basalt Aquifer Under Fracture- and Porous-flow Conditions," *Appl. Environ. Microbiol.*, Vol. 67, 2001, pp. 2799–2809.
3. Lehman, R. M., F. F. Roberto, D. Earley, D. F. Bruhn, S. E. Brink, S. P. O'Connell, M. E. Delwiche, and F. S. Colwell, "Attached and Unattached Bacterial Communities in a 120-Meter Corehole in an Acidic, Crystalline Rock Aquifer," *Appl. Environ. Microbiol.* Vol. 67, 2001, pp. 2095–2106.
4. Van Loosdrecht, M. C. M., J. Lyklema, W. Norde, and A. J. B. Zehnder, "Influence of Interfaces on Microbial Activity," *Microbiological Reviews*, Vol. 54, 1990, pp. 75–87
5. E. DeLong, "Archaeal Means and Extremes," *Science*, Vol. 280, 24 April 1998, pp. 542–543.
6. K. S. Sorenson, L. N. Peterson, R. E. Hinchee, and R. L. Ely, "An Evaluation of Aerobic Trichloroethene Attenuation Using First-Order Rate Estimation," *Bioremed. J.* Vol. 4, 2000, pp. 337–357.
7. H. I. Essaid, W. N. Herkelrath, and K. M. Hess, "Simulation of Fluid Distributions Observed at a Crude Oil Spill Site Incorporating Hysteresis, Oil Entrapment, and Spatial Variability of Hydraulic Properties," *Water Resour. Res.* Vol. 29, 1993, pp. 1753–1770.
8. B. H. Kueper and E. O. Frind, "Two-Phase Flow in Heterogeneous Porous Media 2. Model Application," *Water Resour. Res.* Vol. 27, 1991, pp. 1059–1070.
9. M. Poulsen and B. H. Kueper, "A Field Experiment to Study the Behavior of Tetrachloroethylene in Unsaturated Porous Media," *Environ. Sci. Technol.*, Vol. 26, 1992, pp. 889–895.
10. J. L. Wilson, S. H. Conrad, W. R. Mason, W. Peplinski, and E. Hagan, "Laboratory Investigation of Residual Liquid Organics from Spills, Leaks and the Disposal of Hazardous Wastes in Groundwater, EPA/600/6-90/004, Environmental Protection Agency, 1990.

11. I. Chatzis, N. R. Morrow, and H. T. Lim, Magnitude and Detailed Structure of Residual Oil Saturation, *Soc. Petrol. Eng. J.* Vol. 23, 1983, pp. 311–326.
12. W. G. Anderson, “Wettability Literature Survey – Part 4: Effects of Wettability On Capillary Pressure,” *J. Petrol. Technol.*, Vol. 39, 1987, pp. 1283–1300.
13. E. C. Donaldson and R. D. Thomas, Presentation at the SPE Annual Technical Meeting, 1971.
14. N. R. Morrow, “Wettability and Its Effect On Oil Recovery,” *J. Petrol. Technol.*, Vol. 42, 1990, pp. 1476–1484.
15. S. E. Powers and M. E. Tamblin, “Wettability of Porous Media After Exposure to Synthetic Gasolines,” *J. Contam. Hyudrol.*, Vol. 19, 1995, pp. 105–125.
16. J. H. Jan Plancher and N. R. Morrow, “Wettability Changes Induced by Adsorption of Asphaltenes,” *SPE Prod. & Facil.*, Nov 1997, pp. 259–266.
17. A. H. Demond, F. N. Desai, and K. F. Hayes, “Effect of Cationic Surfactants On Organic Liquid-Water Capillary Pressure-Saturation Relationships,” *Water Resour. Res.* Vol. 30, 1994, pp. 333-342.
18. W. G. Anderson, “Wettability Literature Survey – Part 1: Rock/Oil/Brine Interactions and the Effects of Core Handling On Wettability,” *J. Petrol. Technol.*, Vol. 38, 1986, pp. 1125–1144.
19. L. W. Dekker and C. J. Ritsema, “How Water Moves In a Water Repellent Sandy Soil, 1, Potential and Actual Water Repellency. *Water Res. Res.* 30, 1994.2507–2519.
20. N. R. Morrow, “The Effects of Surface Roughness On Contact Angle with Special Reference to Petroleum Recovery,” *J. Can. Petrol. Technol.*, Vol. 14, 1975, pp. 42–53.
21. S. A. Bradford, and F. J. Leij, “Fractional Wettability Effects On Two- and Three-Fluid Capillary Pressure-Saturation Relations,” *J. Contam. Hydrol.*, Vol. 20, 1995, pp. 89–109.
22. R. J. S. Brown, and I. Fatt, “Measurements of Fractional Wettability of Oilfield Rocks by the Nuclear Magnetic Relaxation Method,” *Trans. Am. Inst. Min. Metall. Pet. Eng.*, Vol. 207, 1956, pp. 262–264.
23. R. A. Salatheil, “Oil Recovery by Surface Film Drainage In Mixed-Wettability Rocks,” *J. Petrol. Technol.*” Vol. 255, 1973, pp. 1212–1224.
24. A. H. Demond and P. V. Roberts, “Effect of Interfacial Forces On Two-Phase Capillary Pressure-Saturation Relationships,” *Water Resour. Res.*, Vol. 27, 1991, pp. 423–437.
25. N. R. Morrow, “Capillary Pressure Correlations for Uniformly Wetted Porous Media,” *J. Can. Petrol. Technol.*, Vol. 15, 1976, pp. 49–69.
26. F. F. Craig, “The Reservoir Engineering Aspects of Waterflooding,” *Spe Monograph Series 3*, Richardson, Texas, 1971.
27. L. E. Cuiec, “Evaluation of Reservoir Wettability and Its Effects On Oil Recovery,” (pp. 319–375) in N. R. Morrow (Ed. ), *Surfactant Science Series, Interfacial Phenomena In Petroleum Recovery*, Marcel Dekker, Inc., 1990.

28. E. Amott, "Observations Relating to the Wettability of Porous Rock," *Trans Aime.*, Vol. 216, 1959, pp. 156–162.
29. E. C. Donaldson, *Presented at the Proc. American Chemical Soc. Div. of Petroleum Chemistry, 1981.*
30. W. W. Owens and D. L. Archer, "The Effect of Rock Wettability On Oil-Water Relative Permeability Relationships," *Trans Aime.*, Vol. 251, 1971, pp. 873–878.
31. P. P. Jadhunandan and N. R. Morrow, "Spontaneous Imbibition of Water by Crude Oil/Brine/Rock Systems, In Situ, Vol. 15, 1991, pp. 319–345.
32. J. S. Buckley, Ph.D., Heriot-Watt University, Edinburgh, Scotland, 1996.
33. S. Ma, N. R. Morrow, and X. Zhang, "Generalized Scaling of Spontaneous Imbibition Data for Strongly Water-Wet Systems," *J. Pet. Sci. & Eng.*, Vol. 18, 1997, pp. 165–178.
34. M. D. Herd, G. D. Lassahn, C. P. Thomas, G. A. Bala, and S. L. Eastman, *Presented at the Doe/Spe Eighth Symposium On Enhanced Oil Recovery, Tulsa, Oklahoma, 1992.*
35. J. S. Aronofsky, L. Masse, and S. G. Natanson, "A Model for the Mechanism of Oil Recovery From the Porous Matrix Due to Water Invasion In Fractured Reservoirs, *Trans. Aime.*, Vol. 213, 1958, pp. 17–19.
36. C. C. Mattax and J. R. Kyte, "Imbibition of Oil Recovery from Fractured, Water Drive Reservoir. *Soc. Pet. Eng. J.*, June 1962, pp. 177–184.
37. G. Hamon and L. V. Vidal, *Presented at the Euro. Pet. Conf. London, England, 1986.*
38. X. Zhang, N. R. Morrow, and S. Ma, *Presented at the SPE Annual Technical Conference, 1996.*
39. R. S. Hanson and T. E. Hanson, "Methanotrophic Bacteria," *Microbiol.*, Rev. 60, 1996, pp. 439–471.
40. A. A. Dispirito, J. Gullede, J. C. Murrell, A. K. Shiemke, M. E. Lidstrom, and C. L. Krema. Trichloroethylene Oxidation by the Membrane Associated Methane Monooxygenase In Type I, Type II, and Type X Methanotrophs, *Biodegradation*. Vol. 2, 1992, pp. 151–164.



# Upscaling, Averaging, and Modeling of Coupled Subsurface Processes

Randall LaViolette, Annette Schafer, Clinton van Siclen, Ray Berry, and Richard Martineau (INEEL); Tom Beck (University of Cincinnati)

## SUMMARY

The ability to predict the response of contaminants in the subsurface in the presence or absence of various treatments is essential in making decisions concerning the implementation of any remediation or restoration plan for the subsurface. For example: What will be the impact of various natural or imposed degradation processes on how much contaminant will be left, where the remaining contaminant is going, and how long it will take to get there? The answer to this question requires a prediction of the transport of reacting contaminants, nutrients, etc., because fluid transport is the primary means by which these are distributed in the subsurface. Although the study of transport is a mature field in physics and engineering, there remain significant (and not merely quantitative) unsolved problems for subsurface transport in environmental applications that require prediction of the transport for very long times and minute contaminant concentrations. The most important of these problems originate in the fact that one must here consider transport on a wide variety of temporal and spatial scales, even where the flow itself may not be turbulent. For example, the transport of dissolved phase constituents is strongly influenced by microscale phenomena such as reactions occurring on mineral surfaces and fluid migration through individual pores and fractures; meso- and field-scale transport through geologically heterogeneous media occurs on spatial scales smaller than the discretization level practical in numerical simulators.

Our objective is to integrate multiscale phenomena into a predictive framework based on theory, calculation, and experiment for reactive transport in the subsurface for environmental applications.

## PROJECT DESCRIPTION

The above objective demands the use of upscaled processes and parameters to capture the effects of smaller scale heterogeneity at each discretization level. Analyzing transport phenomena at the microscale is important from the perspective of defining the fundamental relationships that must be incorporated to describe field-scale chemisorptive processes and associated hydrogeochemical parameters. Predicting field-scale vadose zone transport requires understanding the combined influence of hydrogeochemical heterogeneity and external driving forces. This research therefore examined the following tasks:

- Influence of geochemical heterogeneity in transient vadose zone systems (Annette Schafer)
- Transport in heterogeneous media-scaling relationships to define effective permeability in fractured systems, and the effects of this heterogeneous property on fluid transport (Clinton van Siclen, Muhamed Sahimi)
- Kinetics and effects of heterogeneous chemisorption on solute transport (Randall LaViolette, Tom Beck)

Complex dynamics of fluids and solids (Ray Berry, Richard Martineau). These four tasks are described in detail below.

## Influence of Geochemical Heterogeneity in Transient Vadose Zone Systems

Even though evaluations of field-scale transport have widely recognized the importance of hydraulic heterogeneity in controlling fluid migration, they have not acknowledged its influence. This project focuses on (a) determining the relationships between geochemical and hydraulic heterogeneity for a representative site,

(b) developing a numerical simulator to include the effects of transient and hysteretic flows through variably saturated media, and  
(c) conducting flow and transport experiments in a Monte-Carlo mode through stochastically generated, random fields representative of the field data.

The first objective in this task was to analyze data taken at the DOE Oyster VA Bacterial Transport Site for cross-correlation between geochemical properties and air permeability, and the spatial distributions of these properties. This work formed the bulk of this years activities. Previous studies have shown that uranium adsorption and air permeability are correlated through the surface area—hydraulic radius concepts for data collected at the DOE Oyster Bacterial Transport site. This data was assumed to be appropriate and sufficient to form the basis of this study. However, analysis of the spatial relationships of this data were required in order to first derive the stochastic parameters for both surface area and air permeability. In support of this, the spatial structure of air permeability was analyzed. The preliminary analysis of this data suggested that the permeability was strongly biased by measurement and data errors, leading to poor resolution of the stochastic description of permeability. Furthermore, the data appeared to be strongly dependant on the lithologic unit from which the data was derived. As a result, a nonparametric or indicator analysis approach was warranted. The questions became (a) how to use biased permeability information to derive the nonparametric relationships, (b) whether or not the parametric description of permeability would correlate to the lithology, and (c) whether or not flow simulations through these parameters would result in adequate characterization of transport.

The other objective in this process was to elucidate the role of geochemical heterogeneity in controlling transport through variably saturated porous media. We therefore took the resultant spatially variable reactive and transport properties to simulate flow-through variably-saturated porous media. Monte-Carlo simulations were conducted in two- and three-dimensional (3-D), steady-state and transient-flow, and transient-solute transport in hydrologically and geochemically

heterogeneous media. In these simulations the saturated hydraulic conductivity and characteristic parameters were spatial stochastic variables correlated to grain size and reactive surface area. Simulations were conducted over a range of correlation scales, variance, and moisture contents. Performance measures for these simulations include first arrival, in addition to the moments of the mean plume for use in comparison to those obtained for flows through the equivalent homogeneous media. The results of these numerical experiments and simulations support the concept of anisotropic effective reactive surface area as indicated by directionally dependent retardation. For unsaturated porous media, geochemical (or biogeochemical) heterogeneity is a function of moisture content in addition to being a function of the hydrologic variability. Additionally, transient infiltration leads to effective geochemical (or biogeochemical) properties that are functions of the wetting and drying history of the porous media.

## **Transport In Heterogeneous Media-scaling Relationships to Define Effective Permeability In Fractured Systems, and the Effects of This Heterogeneous Property on Fluid Transport**

Subsurface heterogeneity has profound effects on transport properties such as fluid permeability and electrical conductivity, and on the evolution of contaminant plumes. For example, a connected network of fractures may provide preferential fluid flow paths that effectively increase the subsurface permeability by orders of magnitude above that of the rock matrix. A contaminant plume migrating through such a network will exhibit a chemical concentration distribution that is highly skewed towards the injection point rather than the symmetric Gaussian distribution characteristic of transport through a homogeneous medium.

Clearly, the influence of heterogeneity on transport properties must be understood to predict contaminant behavior in the subsurface. Field studies are of limited use, as the subsurface cannot be sufficiently well characterized; laboratory

studies are of limited applicability, since the scale of heterogeneity is bounded by the size of the sample. Thus, theoretical research is indicated both to characterize the heterogeneity and to relate the heterogeneity to the effective transport properties.

This task takes a fundamental approach to these issues using concepts and techniques from statistical physics. Several research activities were conducted. (1) Experimental observations of a power law relationship between the permeability and the electrical conductivity of saturated, fractured rock motivated the development of a conceptual model for fracture networks that reproduces this relationship and provides an interpretation for the observed values of the power law exponent. (2) The stochastic “walker diffusion method,” previously introduced by the author, was further developed to enable calculation of local as well as effective transport properties, and to accommodate material systems represented by regular and irregular resistor networks; thereby permitting properties of two-dimensional fracture networks to be calculated, for example. (3) New renormalization schemes were developed for obtaining “upscaled” transport properties from high-resolution subsurface realizations. (4) Tracer advection through a well characterized heterogeneous medium was studied in order to relate the moments of the tracer distribution to the various correlation lengths and fractal dimensions characterizing the heterogeneity. (5) Electric and hydraulic properties of self-affine, two-dimensional, saturated fractures were calculated to determine the relationship between these transport properties and geomorphological properties, such as fracture surface roughness and average fracture aperture; this work was done in collaboration with Professor Muhammad Sahimi of the University of Southern California.

These activities are briefly discussed in the following subsections. Research activities one and two are presented in much greater detail in papers cleared (and submitted) for publication. Research activities three, four, and five are currently underway and may eventually appear in papers intended for publication; therefore, we did not include their details in this report. A last subsection describes research undertaken at the

University of Southern California in connection with this project.

### Equivalent Channel Network Model for Permeability and Electrical Conductivity of Fracture Networks

It is remarkable that the permeability ( $k$ ) and electrical conductivity ( $\sigma$ ) of saturated, fractured rock exhibits a power law relationship with exponent  $r$  ( $1.5 \leq r \leq 3$ ) as pressure is applied to the rock. To understand this behavior, the fracture network is viewed as a collection of connected, planar fractures. This allows the construction of algebraic expressions for the transport properties of the fracture network, in which the local effective properties, namely the hydraulic aperture  $d_h$  and the electric aperture  $d_e$  of the representative planar fracture (the equivalent channel), are distinguished from the network properties (e.g., fracture connectivity) parameterized by the tortuosity factors  $\tau_h$  and  $\tau_e$ .

This conception of a fracture network leads to the following equations for the network permeability and electrical conductivity:

$$k = N_A \frac{d_h^3 w}{12 \tau_h} \quad \text{and} \quad \sigma = N_A \sigma_0 \frac{d_e w}{\tau_e} \quad (1)$$

where the quantity  $N_A$  is the areal number density of fractures intersecting a cross section of the material perpendicular to the fluid pressure or electrical potential gradient,  $w$  is the typical width of a planar fracture, and  $\sigma_0$  is the electrical conductivity of the saturating fluid.

Combining these equations gives the identity:

$$k \propto \sigma^r \frac{d_h^3 \tau_e^r}{d_e^r \tau_h} \quad (2)$$

where the proportionality constant is unaffected by applied mechanical pressure. Thus the power law relationship  $k \propto \sigma^r$  is recovered when the ratios  $d_h^3/d_e^r$  and  $\tau_e^r/\tau_h$  are slowly varying over the range of applied pressures.

To verify that the first condition holds generally, the transport properties of single, planar fractures (e.g., Figure 1) are obtained from the two-dimensional Reynolds equations for fluid and electrical current flow. In particular, the hydraulic aperture  $d_h$  is given by  $d_h^3 = \langle d(\mathbf{r})^3 \rangle D_h$ , and the electric aperture  $d_e = \langle d(\mathbf{r}) \rangle D_e$ , where  $d(\mathbf{r})$  is the fracture aperture at the position  $\mathbf{r}$  in the fracture plane. The quantities  $d_h^3$  and  $d_e$  are the effective values of the fields comprised of the local values  $d(\mathbf{r})^3$  and  $d(\mathbf{r})$ , respectively. The scale-invariant quantities  $D_h$  and  $D_e$  account for the spatial correlation of these aperture fields. The view shown in Figure 1 is normal to the fracture plane, with the black regions indicating where the two surfaces touch and the contours of increasingly lighter shading signifying increasingly greater aperture. The connected regions of relatively large aperture constitute flow channels through the fracture.

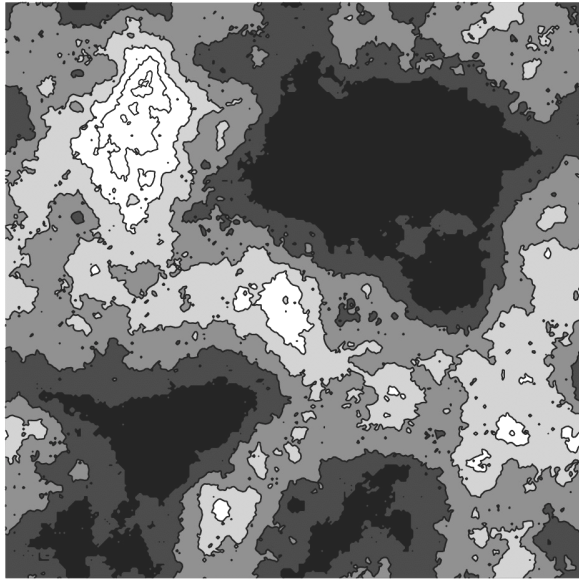


Figure 1. Example of a rough, planar fracture created from two self-affine surfaces having roughness exponent  $\zeta = 0.8$ .

The effective apertures for several simulated fractures are plotted in Figure 2 where each symbol type identifies a set of fractures where successive members of a set are obtained by further reducing the aperture of an initial fracture. Thus the data points of a set, going from right to left, correspond to a planar fracture under

increasing pressure, and the slope of a curve drawn through those data points gives the value of the power law exponent  $r$  for that fracture. The squares and triangles (circles) are data points for fractures with fracture surface roughness exponent  $\zeta = 0.8$  (0). The filled (open) symbols indicate fractures created with a small (large) fracture surface height variance. The crosses are data points for fractures created from surfaces that are uncorrelated—surface heights are assigned randomly from a Gaussian distribution—and have a small height variance.

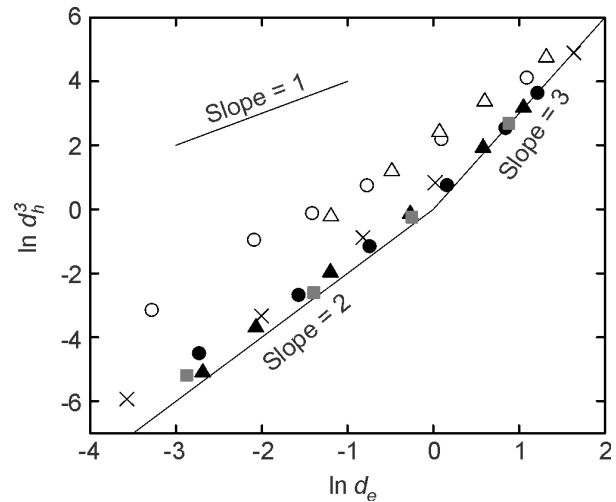


Figure 2. Computational results obtained for a variety of simulated, planar fractures.

The most striking feature of the log–log plot in Figure 2 is the alignment of data points with Slope (or power law exponent) 2. The significance of Slope 2 becomes apparent when the partially closed fracture is regarded as a 3-D porous material—a collection of connected pores all lying in the fracture plane. (Figure 1 can certainly be viewed in this way.) An equivalent channel network model for porous media produces  $k \propto \sigma^s$  with  $1 \leq s \leq 2$ ; furthermore, experiments with porous media typically find  $s = 2$ . Evidently  $r$  values between 3 and 2 are simply crossover values that indicate a fracture undergoing the pressure-induced structural transition to a porous medium. This transition is complete when the fracture is 2–5% closed.

## Walker Diffusion Method for Calculation of Transport Properties of Finite Composite Systems

The electrical properties of a conducting medium are governed by the set of transport equations,  $\nabla \times \mathbf{E}(\mathbf{r}) = 0$ ,  $\nabla \cdot \mathbf{J}(\mathbf{r}) = 0$ ,  $\mathbf{J}(\mathbf{r}) = \sigma(\mathbf{r}) \mathbf{E}(\mathbf{r})$ ,  $\mathbf{E}(\mathbf{r}) = -\nabla\phi(\mathbf{r})$ , that relate the electric field  $\mathbf{E}$  and the current density  $\mathbf{J}$  at the point  $\mathbf{r}$ . The heterogeneity of the medium is expressed through the local conductivity  $\sigma(\mathbf{r})$ . This same set of equations, with appropriate vector and scalar fields, enables calculation of the thermal, dielectric, and diffusivity properties as well. Again, the local transport coefficients in each case reflect the heterogeneity of the medium. The electrical analog is often extended to fluid permeability. A local version of Darcy's law for fluid flow is:

$$\mathbf{Q}(\mathbf{r}) = - (k(\mathbf{r})/\mu) \nabla P(\mathbf{r}) \quad (3)$$

where  $\mathbf{Q}(\mathbf{r})$  is the volumetric flow rate,  $P(\mathbf{r})$  is the fluid pressure,  $k(\mathbf{r})$  is the permeability of the saturated medium, and  $\mu$  is the viscosity of the fluid. The incompressibility of the fluid produces the additional equation:

$$\nabla \cdot \mathbf{Q}(\mathbf{r}) = 0. \quad (4)$$

Solving these equations for given boundary conditions is typically accomplished by the finite difference method (FDM). This approach is equivalent to solving Kirchhoff's laws for a resistor network, and indeed porous and fractured media are often explicitly modeled as resistor networks. More generally, a heterogeneous medium is represented by a scalar field comprised of the  $\sigma(\mathbf{r})$  or  $k(\mathbf{r})$ , for example, which is effectively converted to a regular resistor network to permit FDM calculations.

This author recently introduced the walker diffusion method (WDM) for calculating the effective transport properties of scalar fields.<sup>1,2</sup> In contrast to the FDM, the WDM works directly with the scalar field, and does not require boundary conditions to determine the effective properties of the medium. The WDM also obtains the transport property correlation length  $\xi$  (the length scale above which the medium is

effectively homogeneous with respect to the transport property of interest, and below which the medium is heterogeneous) and the transport property scaling law, which is relevant when the system size is less than  $\xi$ .

To broaden its utility, the WDM was further developed to treat finite scalar fields (those having nonperiodic boundary conditions), and finite and infinite resistor networks. Thus the WDM enables studies of the effects of imposed boundary conditions on transport properties of heterogeneous media, and allows direct comparison of calculated properties for media represented by scalar fields and by regular resistor networks, respectively.

The WDM exploits the isomorphism between the transport equations and the diffusion equation for a collection of noninteracting random walkers in the presence of a driving force. The phase domains in a composite microstructure correspond to distinct populations of walkers, where the equilibrium walker density  $\rho^0(\mathbf{r})$  of a population is given by the value of the transport coefficient  $\sigma(\mathbf{r})$  of the corresponding phase domain. The principle of detailed balance ensures that the population densities are maintained, and provides the rules for walker diffusion over a scalar field (or digitized microstructure). The path of a walker thus reflects the phase composition (population density) and morphology of the domains that are encountered, and may be described by a diffusion coefficient  $D_w$ , that is related to the effective (macroscopic) transport coefficient  $\sigma$  by:

$$\sigma = \langle \sigma(\mathbf{r}) \rangle D_w \quad (5)$$

where  $\langle \sigma(\mathbf{r}) \rangle$  is the volume average of the constituent transport coefficients. The diffusion coefficient  $D_w$  is calculated from the equation:

$$D_w = \langle R^2 \rangle / (2 d t) \quad (6)$$

where the set  $\{R\}$  of walker displacements, each occurring over the time interval  $t$ , comprises a Gaussian distribution that must necessarily be centered well beyond  $\xi$  (the walker diffusion is otherwise anomalous). Remarkably, the effective transport coefficient  $\sigma$  is obtained without solving

the set of transport equations or imposing boundary conditions on the system.

The WDM can additionally be used to solve the set of transport equations; that is, to calculate the vector fields and the potential field  $\phi(\mathbf{r})$  for given boundary conditions. The concept of walker populations (representing phase domains in a composite) together with the walker diffusion rules is sufficient to *derive* the flux equation:

$$\mathbf{J}(\mathbf{r}) = -\sigma(\mathbf{r}) \nabla\phi(\mathbf{r}) \quad (7)$$

where the  $\phi(\mathbf{r})$  are found to be simple functions of the walker densities.

At equilibrium (the absence of a driving force), a single diffusing walker will populate (or occupy) the sites of a composite in proportion to the corresponding transport coefficients  $\sigma(\mathbf{r})$ ; thus, in the limit of infinite time, the equilibrium walker density  $\rho_i^0$  at site  $i$  is proportional to the fraction of time spent by the walker at that site. However, these walker densities are altered when a chemical potential gradient is created by injecting walkers into the system at one boundary or point and removing them at another. The resulting steady-state walker density  $\rho_i$  at site  $i$  is again proportional to the fraction of time spent at that site, but this value is of course different from  $\rho_i^0$ . The densities  $\rho_i^0$  and  $\rho_i$  and the chemical potential  $\mu_i$  are related by the principle of detailed balance, from which the identification  $\phi_i = \rho_i / \rho_i^0$  can be made.

As an example, the electrical properties were calculated for the two-dimensional, multiphase system shown in Figure 3A. This figure was obtained by superposing a circle of radius 24 on a  $64 \times 64$  square region, then setting the conductivity of each site  $i$  to the areal average value  $\sigma_i = f + 0.1(1-f)$ , where  $f$  is the fraction of the site contained within the circle. Equipotential surfaces at the left and right edges were established by releasing walkers at one edge and absorbing them at the other. Figure 3B shows calculated equipotential surfaces (lines, in this case), the density of lines reflecting the magnitude of the local potential gradient.

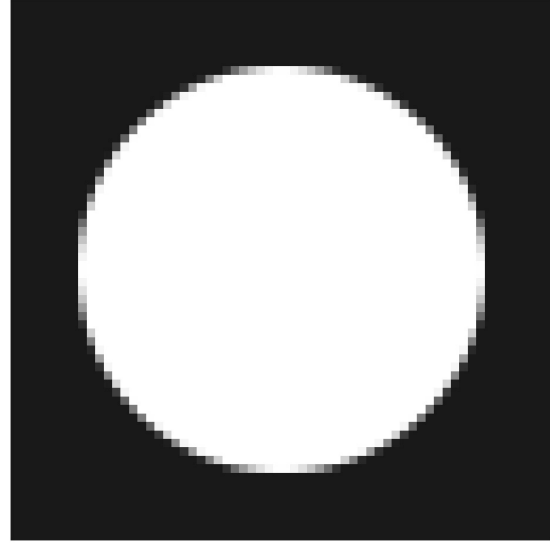


Figure 3A. Two-dimensional, multiphase composite approximating a continuous system comprised of a circular region of conductivity 1.0 (white) centered in a square of conductivity 0.1 (black). The interfacial phases have intermediate conductivity values indicated by the shade of gray.

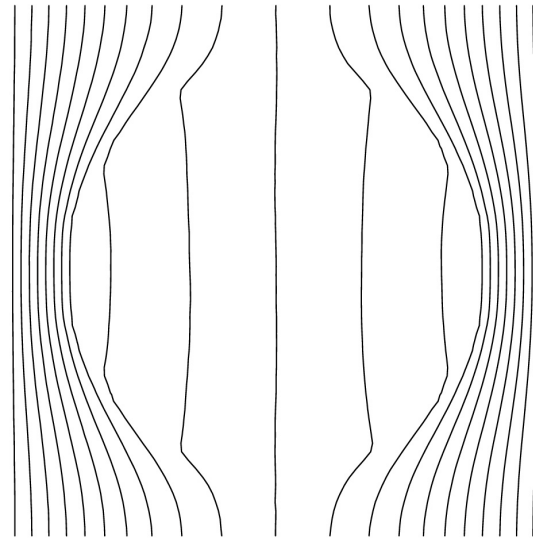


Figure 3B. Equipotential lines.

The isomorphism between sets of transport equations referred to above may again be invoked to develop the WDM for resistor (or conductor) networks. In this case, the equilibrium walker density  $\rho_i^0 = 1$  at all nodes  $i$  in the network, and the effective (macroscopic) transport coefficient for the regular network is  $\sigma = D_w$ . The principle of

detailed balance again gives the walker diffusion rules. To eliminate unsuccessful move attempts, thereby reducing the computer time required for a calculation, a variable residence time algorithm was derived by statistically weighing the behavior of the walker such that every attempt is successful but the move is accomplished over a variable time interval. Interestingly, this algorithm enables calculations to be made for irregular (nodes not equally spaced) as well as regular networks. The algorithm was verified analytically (by use of Markov chain theory) for one-dimensional conductor networks, and numerically for two-dimensional conductor networks whose properties are already known from percolation theory.

The local properties of finite (bounded) networks are found in a manner similar to that described above for finite scalar fields. In this case, the steady-state walker density  $\rho_i$  at node  $i$  equals the fraction of time spent by the walker at that site (in the limit of infinite time), so that the potential  $\phi_i = \rho_i$ .

Thus the WDM can be used to calculate the effective (macroscopic) and local (microscopic) transport properties of a heterogeneous medium represented by a scalar field of local transport coefficients (e.g., conductivity) or by a resistor network derived from that scalar field. As a calculation can be accomplished by monitoring the position of a single walker, the method requires very little computer memory and so is especially suitable for highly complex material systems such as geomedia. Because the walkers solve the transport equations “on the fly” the WDM may also be useful in studies of dynamic phenomena such as miscible fluid invasion in permeable media.

### New Renormalization Schemes for Upscaling Transport Properties

It is now routine to generate subsurface realizations with millions of volume elements. Unfortunately, current computational resources will not accommodate such detail, as one or more transport equations are associated with each element; these equations are coupled and so must be solved simultaneously. Thus, the system size must be reduced to a manageable number of

elements—the realization must be upscaled. This is typically accomplished by a renormalization procedure that generates a new, coarser realization comprised of elements created by grouping adjacent elements in the original realization. Calculation of group properties, such as fluid permeability, must not only be computationally fast, but must account for existing spatial correlations between property values of the original elements. As these are incompatible requirements, much research has gone into finding an optimal balance between them. Different renormalization schemes are generally evaluated by comparing the property values of the single element remaining at the end of a sequence of renormalizations to the corresponding effective values for the original realization.

The renormalization method most commonly used is that attributed to P. R. King.<sup>3</sup> In the case of a two-dimensional realization, the group consists of four elements in a square configuration; thus, each renormalization maintains the square grid structure but reduces the number of elements by a factor of four. King obtains an analytic expression for the conductivity  $\sigma_g$  of the group by converting it into a resistor network with a potential difference between two opposite sides of the square configuration and no current flow permitted across the other two sides. Surprisingly good results may be obtained by this scheme, despite the conversion of the scalar field to a resistor network and the introduction of anisotropic boundary conditions in the calculation of the group properties. These problematic aspects remain in similar methods proposed by other researchers, but they are avoided by considering the group of elements as a homogeneous “effective medium.” This stochastic approach gives the analytic result:

$$\sigma_g = \left\langle \frac{2\sigma_i\sigma_j}{\sigma_i + \sigma_j} \right\rangle_{i \in g} \quad (8)$$

where  $\sigma_i$  and  $\sigma_j$  are the conductivities of adjacent elements  $i$  and  $j$ , and the angle brackets signify that an average is to be taken over all elements  $i$  belonging to the group. Here the group is not limited to four elements in a square configuration, rather, the chosen configuration simply has to tile

(fill) the space of the realization. For example, some calculations were performed in which the groups consisted of five adjacent elements forming a cross, to see whether that configuration better maintained the spatial correlations, in local conductivity values, present in the original two-dimensional realization. Note that the element  $j$  in the expression above may or may not be required to belong to the group, giving different results in each case. Coupling between adjacent groups occurs in the latter case, which may help preserve spatial correlations during renormalization. Anisotropic group conductivities are obtained by including only adjacent elements  $i$  and  $j$  oriented in the direction of interest.

Calculations using King's method and various implementations of this "effective medium" renormalization scheme give comparable results for two-dimensional realizations of high contrast, two-phase random systems, where the high conductivity phase is at the percolation threshold. Additional calculations are needed for well characterized realizations that more closely resemble the highly correlated, multiphase, heterogeneous subsurface; these can be created by fractional Brownian motion, for example. Because in practice the sequence of renormalizations is terminated when a manageable (but still large) number of elements is reached, local (field) as well as effective properties of the terminal realizations obtained by these different methods should be compared as well.

### Flow Properties of Heterogeneous Media

Recent laboratory experiments and sophisticated analyses of field data have shown that the spatial distribution of a contaminant "pulse" (plume) moving through a heterogeneous medium is not Gaussian. Rather, the distribution of chemical concentration is skewed towards the contaminant source. Evidently the heterogeneity retards the migration of the bulk of the plume, while providing a few "preferential" flow paths that enable relatively fast transport.

Various researchers have reproduced these skewed concentration profiles in computer simulations of tracer advection, in which a tracer is moved a unit distance in the flow direction over a

time  $t$  chosen randomly from the power law distribution  $\psi(t) \sim t^{-1-\beta}$  with  $0 < \beta < 1$ . The shape of the plume comprised of a very large number of such tracers may be related to the value of the exponent  $\beta$ . However, it is not clear that subsurface heterogeneity should give rise to such a power law residence time distribution. Thus the connection between the heterogeneity and the plume evolution remains to be made.

An initial step in that direction is to verify the existence of a tracer path correlation length  $\xi_\tau$  and relate it to the permeability correlation length  $\xi_k$ . The latter quantity is that length scale above which the measured fluid permeability  $k$  has a uniform value, that is, the length scale above which the medium is effectively homogeneous with respect to permeability measurements. In contrast,  $\xi_\tau$  is that length scale above which the tortuosity  $\tau$  of a tracer streamline or path has a uniform value. (Note that  $\xi_\tau$  is independent of the fluid pressure drop across the system, the local porosities, the local residence times, etc., and so is determined entirely by the permeability heterogeneity.) An argument relating the correlation lengths to the anomalous diffusion of biased and unbiased random walkers leads to the general result  $\xi_\tau < \xi_k$  for well-connected systems, although  $\xi_\tau$  will approach  $\xi_k$  for systems near their percolation thresholds. This result was verified (in fact  $\xi_\tau \ll \xi_k$ ) for the two-dimensional, two-phase system shown in Figure 4A. The fluid pressure field for this system is indicated in Figure 4B; the tracer paths are perpendicular to the lines of equal pressure shown in the figure. Similar calculations should be done for correlated, multiphase (more than two) systems that more closely resemble subsurface volumes such as systems created by fractional Brownian motion, where the degree of correlation can be varied independently of other system parameters.

The distribution of tracer path lengths becomes Gaussian when the average tracer displacement reaches several times  $\xi_\tau$ . The distribution of tracer path lengths for systems sizes much larger than  $\xi_\tau$ , while broadened due to the system heterogeneity, cannot account for the skewed tracer concentration distribution.

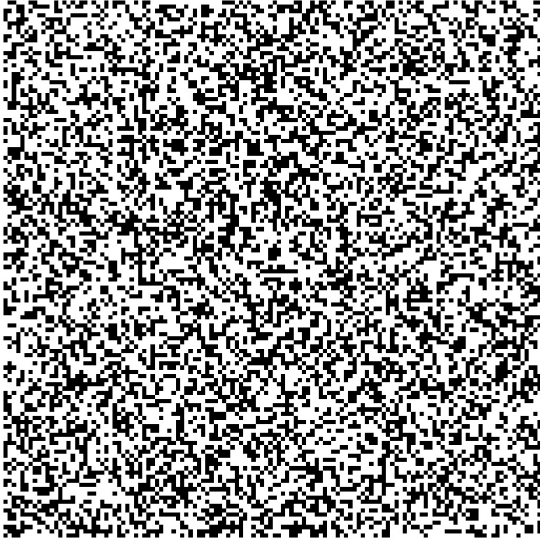


Figure 4A. Two-dimensional, two phase disordered composite for which the ratio of the two conductivities is 100:1.

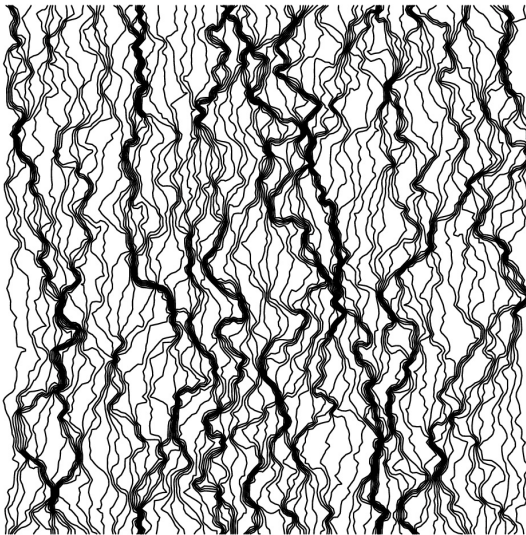


Figure 4B. Equipotential lines calculated for a potential difference applied across the composite.

A next step is to determine the distribution of fluid volumetric flow rates for various correlated, multiphase systems and for a number of tracer streamlines present in those systems. The local flow rates may be related to the local tracer velocities in a variety of ways; the resulting velocity distributions can be inverted to give the corresponding tracer residence time distributions  $\psi(t)$ . Perhaps these will turn out to be power law

distributions, with an upper cutoff due to the finite resolution of the simulated medium. (The finite spatial resolution implies that there is a minimum, nonzero, local pressure gradient in the system, which implies there is a minimum fluid velocity, which implies there is a maximum local residence time.)

### Transport Properties of Saturated, Planar Fractures

The basic component of a fracture network (real or model) is the planar fracture. Typically it is assumed to have smooth, parallel faces, so that its transport properties are completely determined by its aperture. That is a useful assumption for simple network models where flow properties are calculated for various aperture distributions, which is in fact state of the art. However, real fracture surfaces are not flat but self-affine (the spatial distribution of surface heights is correlated in a particular way) over lengths on the order of centimeters. It is thus of interest to understand how the surface roughness affects the electrical and hydraulic properties of saturated fractures.

This is most easily achieved by studying simulated fractures. The fracture surfaces are characterized by the variance  $\sigma_h(L)^2$  of the distribution of surface heights, where  $L^2$  is the planar area of the fracture, and the self-affine roughness exponent  $\zeta$ , which equals 0.8 for most real fractures. A few researchers have in fact calculated the electrical conductivity or fluid permeability of 3-D planar fractures for the purpose, incidentally, of comparing these values to those obtained by use of the Reynolds approximation. However, these computations are so extremely time (computer) consuming that too few fractures have been considered to draw any conclusions. Other researchers have attempted to find relationships between the fracture geometry and the transport properties calculated by the Reynolds approximation, but with uncertain success.

To get at these relationships, the transport properties were calculated for two-dimensional fractures having  $\zeta = 0.25, 0.5, \text{ and } 0.8$ , for a range of separations of the two fracture surfaces in each case. The two-dimensional fractures were studied

not only to establish a protocol for the more interesting study of 3-D fractures, but to contribute to current fracture network models, nearly all of which are two-dimensional. The electrical properties were calculated at the INEEL using the walker diffusion method, while the hydraulic properties were calculated by Prof. Muhammad Sahimi at the University of Southern California using a lattice Boltzmann technique. Relationships between electrical conductivity, fluid permeability, and fracture geometry may be ascertained for each fracture by comparing the average aperture  $d$ , the electric aperture  $d_e$ , and the hydraulic aperture  $d_h$ . The effective aperture  $d_e$  is the aperture of a parallel plate fracture that produces the same electric current as the planar fracture for a given potential difference applied across the length of the fracture, while  $d_h$  is the aperture of a parallel plate fracture that produces the same volume flow as the planar fracture for a given fluid pressure difference applied across the length of the fracture.

The additional dimension available to current and fluid flow in 3-D fractures may significantly alter those relationships between the average and effective apertures. The simulation results may be tested experimentally at the INEEL using fabricated fractures.

### **Research at the University of Southern California**

Additional research was supported at the University of Southern California under the direction of Prof. Muhammad Sahimi. The following problems were studied:

- A novel method, based on the application of wavelet transformations, was developed for upscaling complex subsurface realizations. The great virtue of this approach, which is a competitor to the renormalization methods mentioned above, is that it detects those regions where detailed information must be retained and so suggests a spatially variable coarsening of the original realization that substantially preserves the local flow properties.
- Solute transport through a disordered medium near the percolation threshold was studied. In particular, the longitudinal dispersion

coefficient, which is related to the second moment of the chemical plume mentioned above, was shown, both by scaling arguments and by simulations, to monotonically increase with travel distance in agreement with numerous experiments. This work is also relevant to well connected systems when most of the flow is contained in only a few streamlines such as most fracture networks.

- A comprehensive, 3-D model of gas generation and transport in landfills was developed. This model, which can be rigorously tested against experimental data from well instrumented landfills, may form the basis for a simulator for the soil vapor extraction remediation process.

### **Kinetics and the Effects of Heterogeneous Chemisorption On Solute Transport**

This task is devoted to predicting the impact of chemisorption upon solute transport in the subsurface. This task is also concerned with developing and exploiting methods to model chemisorption of aqueous organic and organo-metallic compounds (corresponding to wastes in water) onto mineral surfaces. Although simple models of chemisorption have been employed for nearly a century, these have been developed explicitly only for laboratory-scale experiments. For this project, we require models that can be integrated and upscaled into fluid flow models, and therefore employ different parameters than those models that have been developed only for laboratory-scale experiments.

One upscaling problem that we addressed concerns the extraction of thermodynamic properties from first-principles electronic structure calculations of clusters of atoms or molecules. In collaboration with scientists at Los Alamos National Laboratory and Vassar College we extended the quasi-chemical approximation<sup>4</sup> (which we had developed on this program in previous years) in order to obtain an accurate theory for the equation of state of a simple atomic fluid. The extension to associated liquids (water, etc.) is part of future work.

Stochastic dynamics and Monte-Carlo simulations are carried out to determine the steady-state kinetics of chemisorption of multidentate ligands. The results are correlated with the results of experiments planned under other subsurface science projects. The goal here is to develop microscopic models that are free from the restrictive assumptions required in standard, but simplistic and scale-dependent, one-parameter, adsorption isotherms. In so doing, the relevant parameters are identified and correlated with the results of experiments planned under other subsurface science projects.

Spatially heterogeneous chemisorption has already been shown to be capable of inducing kinetic and transport anomalies in low Peclet number flow.<sup>5</sup> The goal in this task is to see if and how these anomalies develop in systems studied experimentally under other tasks. In this task, chemisorption kinetics occurring at random sites will be coupled with mesoscopic-scale, advective-diffusive dynamics to predict the transport of desorbed solutes in the flow. Monte-Carlo techniques are employed throughout this work.

The aim of the collaboration between the PI and Prof. Tom Beck and his students in the Chemistry Department of the University of Cincinnati is to model molecular adsorption in soil organic matter by analogy with reversed phase liquid chromatography. Several laboratory techniques have been used to estimate the organic-carbon partition coefficient.<sup>6</sup> One result is the ability to rapidly screen a wide range of chemicals. The methods include water solubility measurements, n-octanol/water partition coefficients, reversed phase liquid chromatography (RPLC), and estimation of molecular parameters using linear solvation energy relationships. The RPLC system is well established for the separation of chemicals in solution. It has also been proposed as a useful tool for estimating thermodynamic quantities for solute partitioning between phases. The retention factor  $k'$  (related to the time spent in the column relative to a standard) is the product of an equilibrium partition coefficient  $K$  and the ratio of the mobile and stationary phase volumes  $\Phi$ . The partition coefficient  $K$  is determined by the excess chemical potential profile for a solute as it passes from the mobile phase (typically water:methanol

or water:acetonitrile) into the stationary phase (tethered alkane chains of length  $N = 3-18$ ). There is a close analogy between chromatographic retention and chemical partitioning into soils. In this first phase, we intend to initiate molecular dynamics simulations of the chromatographic system and to use the simulation data to compute accurate excess chemical potential profiles for solute passage from the aqueous to tethered alkane organic phases.<sup>7,8</sup> We will be performing these simulations on our local Beowulf parallel computer using the CHARMM molecular modeling package obtained from the Karplus group at Harvard.

## Complex Dynamics of Fluids and Solids

The physical description of the disparate length and time scales inherent with the hierarchical systems of geological, multiphase, fluid transport is accomplished using continuum theory. This theory views the fluids and solids as interpenetrating mixtures, each being governed by conservation laws either postulated or derived from the methods of ensemble or volume averaging. This Eulerian continuum approach results in field equations for the flow properties of all phases in the multiphase mixture system. As currently practiced, there are two major drawbacks with using this approach—both can be traced to the loss of information resulting from the averaging process. First, when manipulating the averaged equations, covariance terms are typically neglected because pore- or crack-scale models are needed for their construction. Second, because the pore- and crack-scaled information is filtered in the averaging process, the resulting equation system is not complete and constitutive relations must be developed to obtain closure. In other words, the averaging leads to unknown terms representing the interactions between the phases. These terms must be modeled to close the description of the system. The nature of the detailed interactions between the solid and the fluid phases cannot be understood from the application of mixture theory alone. It is the pore- and crack-scale physics that determine the nature of these constitutive relations, though such information is seldom used. However once these

interaction terms are determined, the Eulerian continuum approach is most efficient and has been widely used in multiphase flow simulations. Our work with CFDLIB, for example,<sup>9</sup> is aimed at providing the most general multiphase flow platform at the macro- or field-scale into which the various microscopically derived constitutive relations can be inserted to yields solutions in the large.

Increased understanding of the pore- and crack-level physics should be used to construct the covariance and constitutive closure relations. A proposed approach to gaining this closure is obtained by performing detailed pore- and crack-level modeling on a broad range of representative porous and/or crack configurations with various physical and chemical effects occurring. This approach, termed direct numerical simulation (DNS), is possibly the only theoretical tool capable of studying the nonlinear and geometrically complicated phenomena of multiphase inter pore flow. The DNS approach has been followed in single-phase fluid dynamics and directly computes the detailed hydrodynamic forces, motions, and phasic interactions. The results from these microscopic flow analyses could then be used directly to facilitate the development of constitutive relations, correlate covariance terms, improve overly simplistic models, and provide more accurate closure to the macroscopic, continuum-level equations used for the large scale simulation of subsurface flows. The longer-term benefit of this approach would be a significantly improved understanding and the development potential for more complete and physically accurate microscopic and macroscopic models for complex subsurface flows. However, because of the complicated geometrical configurations and the nonlinearity of the pertinent physics and chemistry, numerical simulation methods must be used, but these problems present severe challenges for traditional numerical approaches: finite difference, finite volume, and finite element. With DNS, it is possible to simplify the flow description considerably by ignoring the viscous effects completely (inviscid potential flow), or by ignoring the fluid inertia completely (Stokes flow, which upon averaging yields the popular Darcy porous flow model). In recent years, a number of numerical methods have been attempted for

simulations of fluid-solid systems at finite Reynolds numbers, such as arbitrary Lagrangian-Eulerian (ALE) moving, unstructured, finite-element-mesh techniques, front-tracking finite-difference methods, space-time finite elements, and the lattice Boltzmann method (LBM).<sup>10</sup> All of these methods are computationally intensive and very difficult to add additional physics to capture increasing more complex real-behavior.

We have been developing novel approaches that address these needs in the form of meshless or grid-free, Lagrangian, numerical methods to simulate the microscopic flow of multiple fluid phases, chemical constituents with volumetric and surface reactions and pore-surface adsorption and transport, suspended particulate transport and deposition, etc., for cases in which the flows are slow. With these grid-free approaches no permanent connectivity occurs between computational nodes so they can be applied to problems where traditional Eulerian and Lagrangian techniques fail, such as those involving large deformation, fluid–fluid or fluid–solid interactions, and contorted geometries—precisely the situation present in detailed pore-scale modeling. In some of the meshless methods the computational nodes are referred to as particles because of the context in which they are derived; therefore, such computational methods are often called particle methods. Intuitively, a continuum is modeled as a system of particles where, in the limit, the particles’ sizes vanish and the distances between adjacent particles approach zero. In this limit, the system of particles approaches a deformable continuum. In other words, an integral over a continuous body may be considered as the limiting extension of a summation over a corresponding system of particles. Weighting or interpolation functions are applied in the summation, as are various manipulations, to smooth the particle representation and produce more of a continuum effect. Initial attempts at developing constitutive models for porous flows using a particle method for direct numerical simulation were reported for a multiphase (gas/liquid) flow with no porosity.<sup>11,12,13</sup> We have developed particle neighbor tracking, edge detection algorithms, and code structures for these methods.<sup>14</sup> While these particle methods are also

computationally intensive, it is relatively easy to add increasing more complex physical behaviors.

For this reporting period we have developed and evaluated several gridless methods for computing spatial derivatives including several variants of smoothed particle hydrodynamics (SPH), moving point semi-implicit (MPS), and moving least squares (MLS); detailed documentation of these results are in preparation. Steep linear and paraboloid, two-dimensional spatial profiles were initially assigned to a dependent variable on a nonuniform particle configuration. Various first and second spatial derivatives/ operators were computed with these methods and compared to the known analytical results. Figure 5 shows typical results for the x-directional derivative for a first order least squares method. Generally, the methods could be ranked from worst to best as SPH, MPS, corrected SPH, first order MLS, and second order MLS, respectively.

We have also developed a basic model for unsaturated liquid flow through a very open porous media with a small particle, contaminant transport and deposition method for subsurface flows. Detailed documentation of this model is in preparation. The method is a hybrid of a basic SPH approach with the incorporation of a basic Riemann analytic solution (for condensed phase hydrodynamics) method, similar to an approach recently developed for high velocity impact of solid bodies.<sup>15</sup> For this hydrodynamic simulation we are using explicit time integrations and compressible equations of state for our simulations, necessitating the use of a very small integration time step size. Low speed, approximately incompressible flows are approximated through the use of a modified barotropic equation of state, which employs a modified sound speed that is reduced such that the flow Mach number is on the order of 0.1 and density variations are around 0.01. This results in a respectable, stable material Courant number of about 0.1. While this produces a valid approximation for incompressible flow, we still believe, however, that a unified, pressure-implicit numerical treatment should be developed for this particle method (Reference 13). This model should

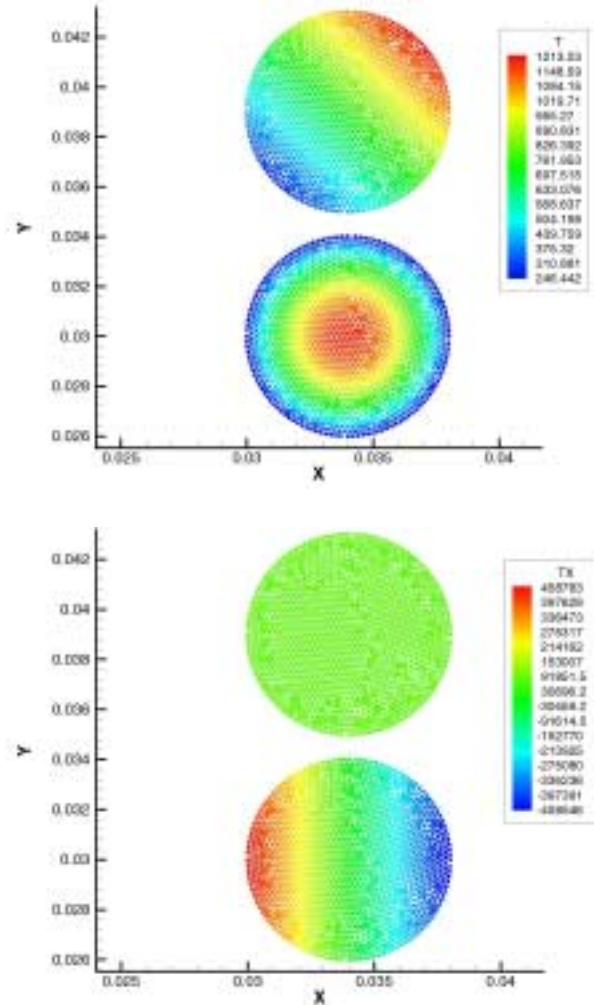


Figure 5. Typical results for the x-directional derivative for a first order least squares method.

be viewed as a first attempt a direct numerical simulation of porous flows with suspended contaminants, using a particle method. This first effort has no surface tension and only one fluid phase, but is designed to clearly illustrate the potential of this approach. In the future the complexities for multiphase flow, surface tension, chemical diffusion and reactions, solid matrix compressibility/deformation, etc., will be considered. This simulation models a column of water, initially 1.2 mm deep with the appropriate hydrostatic head and fully contaminated with a normalized value (dependent variable) of 1.0, placed on top of a column of representative porous material also 1.2 mm high and totally uncontaminated with a normalized value of 0.0. The water is allowed to flow down through the

porous material under the influence of gravity, and out the bottom where it falls into a catch-pan and accumulates. The degree of flow saturation is not only time dependent, but is spatially varying as well. Figure 6 shows a time snapshot of the spatial variation of velocity magnitude and Figure 7 is a snapshot of the contaminant distribution at the same time. Figure 8 shows the distribution of contaminant much later in time where it can be readily seen that a significant portion of the contaminant has been absorbed onto the porous solid particles, thereby reducing its presence in the water. It should be noted that in Figures 7 and 8 the color scale of the contaminant level ranges only between normalized values of 0.0 and 1.0, but that the contaminant level on some of the porous solid particles approaches normalized values of 150, which are also displayed as white along with any contaminant level greater than the full-scale value of 1.0. A simulation of this type would be very difficult or impossible with traditional numerical methods, but makes the potential benefits of pursuing the DNS approach with grid-free Lagrangian methods that we have proposed clear.

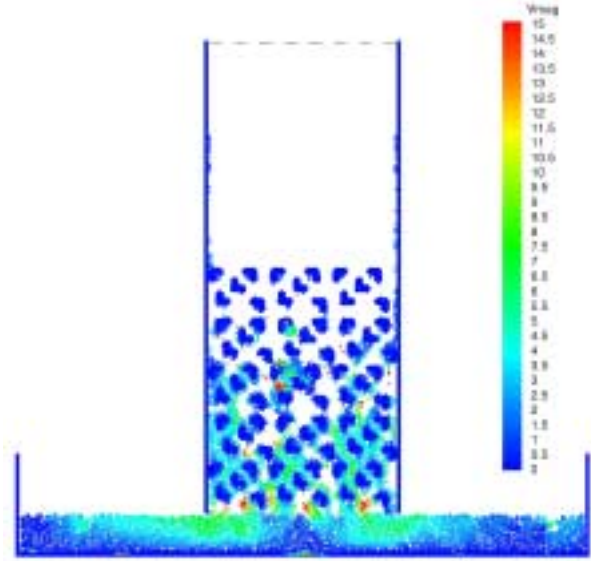


Figure 6. A snapshot of the spatial variation of velocity magnitude.

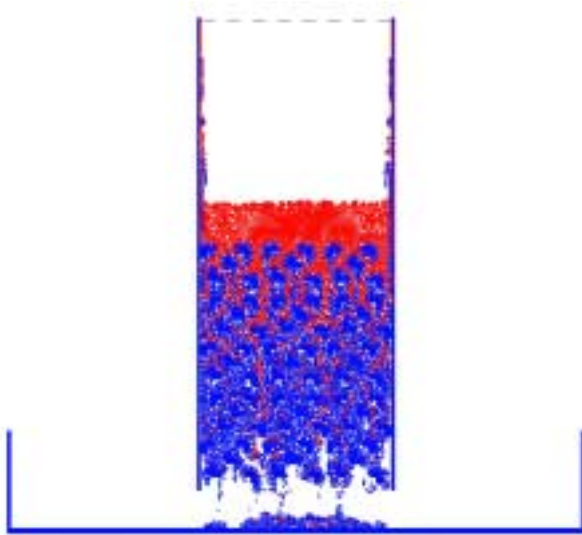


Figure 7. A snapshot of the contaminant distribution taken at the same time as Figure 6.

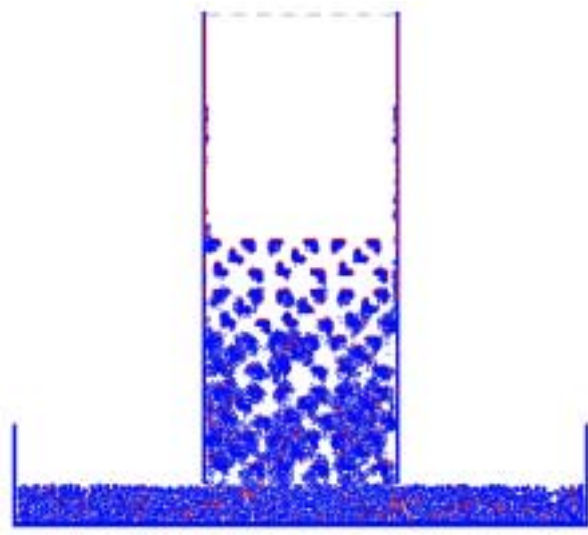


Figure 8. A snapshot showing the distribution of contaminant much later in time from that in Figure 7.

## ACCOMPLISHMENTS

### **Influence of Geochemical Heterogeneity in Transient Vadose Zone Systems**

Our investigation of flow and transport through “known” fields (a) generated random fields of saturated permeability and Gardner’s alpha (used to parameterize the constitutive equations relating saturated permeability capillary pressure and capillary pressure to water saturation), (b) sampled the random fields (as if sampling a field site), (c) perturbed the sample data by the expected (based on the instrument used) bias, (d) computed the corresponding indicator variograms of the biased hydraulic properties, and (e) compared the variogram parameters for the initial fields to those of the indicator fields in a Monte-Carlo mode. Based on this analysis, it was possible to reconstruct the correlation length scale of the original random fields from the indicators derived from biased data. Monte-Carlo simulations were carried out through the indicator-derived spatial distributions of air permeability and Gardner’s alpha (assuming all other parameters are constant) to answer the question of how much information is lost through the indicator approach and whether that loss impacts the ability to predict transport. Prior to these simulations, a finite element code was modified to allow simulation of variably saturated transport through this particular representation of unsaturated flow domains. The code modified was based on the van Genuchten-Brooks Corey characteristic relationships, which were replaced by the Russo-Gardener relationships. The simulations were extremely nonrobust, and in a Monte-Carlo mode presented convergence problems over the range of indicator cutoffs used, correlation length scales of the original random field data, and over all of the underlying variances. However, these issues were recently resolved.

### **Transport In Heterogeneous Media-scaling Relationships to Define Effective Permeability In Fractured Systems, and the**

### **Effects of This Heterogeneous Property on Fluid Transport**

The task established a theoretical capability in subsurface science at the INEEL. Eventually it will impact the experimental and computer modeling components of the Subsurface Science Initiative, but in the meantime it distinguishes the Subsurface Science Initiative from otherwise similar programs elsewhere.

The project research addressed the fundamental problem of relating the subsurface heterogeneity to the transport properties of the medium. In particular: a conceptual model of fracture networks was created that reproduces and explains various experimental results; a new stochastic method for calculating transport properties of complex media was further developed; new renormalization schemes for upscaling high-resolution subsurface realizations were developed; contaminant plume evolution in heterogeneous media was studied; and transport properties of self-affine fractures were related to the fracture geometry.

### **Kinetics and the Effects of Heterogeneous Chemisorption On Solute Transport**

The collaboration between the PI and scientists at LANL and Vassar College resulted in a new formulation of quasicheical theory for dense liquids, and a first-principles trial calculation of the hard sphere equation of state. This work has been documented in a manuscript that was invited to and has been accepted for the Howard Reiss Festschrift to appear in the Journal of Physical Chemistry.

A new analysis of our theory for the transient trapping of flows in the presence of spatial disorder revealed substantial concentration anomalies near the origin of the contaminant plume. In particular, the exponent  $p$  in the time tail  $1/t^p$  becomes less than unity in the presence of disordered traps, in contrast to the well known result for ordered traps, (or no traps)  $p = 3/2$  in three dimensions. The simulation results for multidentate ligand adsorption equilibria, carried

out in collaboration with a summer student intern, destroys published speculation that the exponent in the concentration of free sites on the surface should be unity or less.<sup>16</sup> Instead we find, on both computational and theoretical grounds, that the exponent not only exceeds unity, but also must approach the degree of binding by the ligand (e.g., three for trimers). Finally, the collaboration with Prof. Beck and his students in the Chemistry Department at the University of Cincinnati have yielded the following results:

- We developed methods to thermally equilibrate the systems using repeated heating/cooling cycles.
- We performed a series of test calculations on bulk water to look at the impact of the treatment of the Coulomb interactions on the excess chemical potentials of simple solutes (hard sphere and methane). We found little change in the chemical potentials with or without Ewald's summation for these nonpolar solutes, which is not surprising. Two models for water were simulated: TIP3P and TIP4P.
- We have written our own particle insertion code and have now successfully tested this code on the methane in water system. We have generalized the code to handle multiple interactions in the chromatographic system and are just starting our calculations of the free-energy profile using our own code.
- We have successfully prepared the liquid chromatographic model, run annealing cycles and a 250 ps equilibration trajectory, and are finishing a 250 ps trajectory for subsequent data analysis with our code for the chemical potential profile.

## Complex Dynamics of Fluids and Solids

The Principal Investigator for this task implemented several recent variants of SPH, MPS, and moving weighted least squares grid-free methods into a program in which various spatial derivatives needed to solve partial differential equations of interest (gradient, divergence, and Laplacian) were computed for known functions

and compared with their analytical values. The investigators developed and demonstrated a Lagrangian hybrid SPH-Riemann model for the direct numerical simulation of a transient unsaturated flow of water through a representative porous subsurface medium with small contaminant transport and deposition.

## Publications

Ebrahimi, F., and M. Sahimi, "Multiresolution Wavelet Coarsening and Analysis of Transport In Heterogeneous Media." Accepted for publication in *Physical Review E*.

Hashemi, M., H. I. Kavak, T. T. Tsotsis, and M. Sahimi, "Computer Simulation of Gas Generation and Transport In Landfills. I: Quasi-Steady-State Condition," Accepted for publication in *Chemical Engineering Science*.

Pratt, L. R., R. A. LaViolette, M. A. Gomez, and M. E. Gentile, "Quasi-Chemical Theory for the Statistical Thermodynamics of the Hard-Sphere Fluid," *J. Phys. Chem.*, July 24, 2001. (Accepted for publication in the special issue: "Howard Reiss Festschrift.")

Rivard, C., O. Banton, F. Delay, and M. Sahimi, "Simulations of Solute Transport In Fractured Porous Media Using Percolation Networks," submitted to *Water Resources Research*.

Van Sicle, C. DeW., "Equivalent Channel Network Model for Permeability and Electrical Conductivity of Fracture Networks." accepted for publication in the *Journal of Geophysical Research*.

Van Sicle, C. DeW., "Walker Diffusion Method for Calculation of Transport Properties of Finite Composite Systems." accepted for publication in the *Physical Review E*.

## Presentations

Holt, R. M. and A. L. Schafer, "Indicator Variograms Estimated From Spatially-Biased Field Data," *Annual Meeting of the Geological Society of America, Boston MA, November 1-10, 2001* (contributed presentation).

LaViolette, R. A., "Obstacles to Realistic Models of Contaminant Fate in the Subsurface," *Theoretical and Simulational Chemistry Symposium, Joint Northwest-Rocky Mountain Meeting of the American Chemical Society, Seattle, WA, June 14–17, 2001* (invited presentation).

Schafer, L., "Modeling Unsaturated Flow and Transport using Zones: Aliasing Errors," *Fall Meeting of the American Geophysical Union, San Francisco, CA, December 10–14, 2001* (contributed presentation).

## REFERENCES

1. C. DeW. Van Sielen, "Walker Diffusion Method for Calculation of Transport Properties of Composite Materials," *Physical Review E*, Vol. 59, No. 3, 1999, pp. 2804–2807.
2. C. DeW. Van Sielen, "Anomalous Walker Diffusion through Composite Systems," *Journal of Physics A: Mathematical and General*, Vol. 32, 1999, pp. 5763–5771.
3. P. R. King, "The Use of Renormalization for Calculating Effective Permeability," *Transport in Porous Media*, Vol. 4, 1989, pp. 37–58.
4. L. R. Pratt and R. A. LaViolette, "Quasi-Chemical Theories of Associated Liquids," *Mol. Phys.* 94 909 (1998).
5. D. H. Dunlap, R. A. LaViolette and P. E. Parris, "The Spatial Evolution of Particles Diffusing in the Presence of Randomly Placed Traps," *J. Chem. Phys.* 100 8293 (1994).
6. B. M. Gawlik, N. Sotiriou, E. A. Feicht, S. Shulte-Hostede, and A. Kettrup, *Chemosphere* **12**, 2525 (1997)
7. T. L. Beck and S. J. Klatte, in *Unified Chromatography*, ACS Symposium Series, edited by T. Chester and J. Parcher, (American Chemical Society, New York, 2000).
8. S. J. Klatte and T. L. Beck, *J. Phys. Chem.* 100, 5931 (1996).
9. Ray A. Berry, "Modeling of Complex Fluid and Solid Dynamics," p. 195-202 of *Environmental Systems Research, FY-99 Annual Report* (D. L. Miller, Program Manager), INEEL/EXT-99-01008, January 2000.
10. Robert S. Maier, Daniel M. Kroll, Robert S. Bernard, Stacy E. Howington, John F. Peters, and H. Ted Davis, "Pore-scale Simulation of Dispersion," *Physics of Fluids* **12** 2065 (2000).
11. Mark L. Sawley, Paul W. Cleary, and Joseph Ha, "Modeling of Flow in Porous Media and Resin Transfer Moulding Using Smoothed Particle Hydrodynamics," Second International Conference on CFD in the Mineral and Process Industries, Melbourne, Australia, 6–8 December 1999.
12. W. Alda, W. Dzwinel, J. Kitowski, J. Moscinski, J. Rybicki, and K. Boryczko, "Simulation of Flow Through Porous Media Using Particle Models," *Computer Physics Communications*, 121 and 122 594 (1999).

13. Noriyuki Shirakawa, Hideki Horie, and Yuichi Yamamoto, "A Study on the Evaluation Method of Flow Regimes with the Particle Interaction Method," 7<sup>th</sup> *International Conference on Nuclear Engineering, Tokyo, Japan, 19–23 April 1999*.
14. Ray A. Berry, "Macroscopic Dynamics of Complex Fluids and Solids (FD)," pp. 218–223 of *Environmental Systems Research, FY-2000 Annual Report*, (D. L. Miller, Program Manager), INEEL/EXT-01-01085, January 2001.
15. Anatoly N. Parshikov, Stanislav A. Medin, Igor I. Loukashenko, and Valery A. Milekhin, "Improvements in SPH Method by Means of Interparticle Contact Algorithm and Analysis of Perforation Tests at Moderate Projectile Velocities," *International Journal of Impact Engineering*, 24, p. 779 (2000).
16. F. M. M. Morel and J. G. Hering, *Principles and Applications of Aquatic Chemistry*, John Wiley & Sons, Inc., New York, 1993, p. 588.

## **Waste Management Science**



# Nondestructive Assay

Y. D. Harker (PI), J. D. Cole, M. W. Drigert, J. K. Hartwell,  
J. W. Mandler, C. A. Mcgrath, R. P. Keegan, E. W. Killian

## SUMMARY

The overall objective of this project is to advance the state-of-the-art in nondestructive assay (NDA). The thrust of our research focuses on developing new signatures that will provide more detail concerning isotopics and improve the overall accuracy of the data. To meet our objective, we divided this project into four research and development (R&D) tasks: Fission Physics Research, Down-Hole Probe Development, High Count-Rate Systems Development, and Radiation Transport Analysis. Through these tasks we expect to address the present and future NDA needs of spent nuclear fuel (SNF), contact-handled transuranic (CH-TRU) waste, remote-handled transuranic (RH-TRU) waste programs, and environmental monitoring and remediation programs.

The objectives in the area of fission physics for FY 2001 were to continue the current measurement and data analysis efforts, to establish a second experiment at the Oak Ridge Electron Linear Accelerator (ORELA), and to begin measurements with a new  $^{237}\text{Np}$  target. With the exception of the new  $^{237}\text{Np}$  measurements, we met all these objectives. The  $^{237}\text{Np}$  measurement awaits receipt of the target from the supplier. In the borehole probe development project, the goals were to develop and construct two borehole probes, to complete a test facility at TRA, and to perform initial field tests at the INEEL Radioactive Waste Management Complex Subsurface Disposal Area Pit 9 and at an INEEL monitor well. For the most part, we accomplished all these goals. The Gamma-Ray Transport Analysis project reached its objective of having the absolute gamma assay coded adopted by the 3,100-Cubic Meter Program at RWMC. In the area of high-count-rate systems development, the focus shifted to studying hole-trapping effects in cadmium-zinc-telluride detectors.

## PROJECT DESCRIPTION

### Down-Hole Probe Development for Subsurface Characterization

In FY 2000 a need was identified to address the safety issues of possible criticality concerns and volatile organic chemicals (VOCs) in buried waste at the Subsurface Disposal Area (SDA) on the INEEL. To address these issues we needed the ability to measure fissionable material down to 10 nCi/g in soil and chlorine to the level of 5,000 ppm in the interstitial soil.

This task focuses on meeting this need by developing a pair of borehole probes—the pulsed fission neutron (PFN) probe and neutron gamma (NG) probe—designed for use in both monitoring wells and buried waste pits at the INEEL and across the DOE complex.

The PFN probe is designed to locate and quantify fissionable material. This is done using the differential die-away method wherein neutrons are emitted by a Zetatron-design neutron generator and measured by a suite of neutron detectors within the probe. The decay time of the higher-energy neutron signal is related to the amount of fissionable material present in the surrounding environment. Roughly, more fissionable material leads to more neutron multiplication, which leads to a longer decay time for higher energy neutrons. In addition to detecting fissionable material, the PFN probe can also measure hydrogenous, liquid-saturated porosity independently of the concentration of neutron absorbing materials (Pu and Cl) present. This “porosity/capture cross section” mode uses an array of gamma-ray detectors in place of the fast neutron detectors. The gamma detection method increases the depth into the formation at which the saturated porosity and absorption effects are gauged. More information about the design of this probe can be found in the FY 2000 ESR Annual Report.<sup>1</sup>

The NG probe is designed, in part, to detect VOCs. It does this by using the Prompt Gamma Neutron Activation Analysis (PGNAA) technique. A neutron generator provides neutrons that “activate” various elements in the environment surrounding the probe. When these elements decay or de-excite, the emitted gamma rays are detected using a high-purity germanium (HPGe) detector. These gamma rays are characteristic of certain elements and are detected in quantities roughly proportional to the amount of these elements present. Using various activation and detection modes, the NG probe can be used to measure many elements including: uranium, plutonium, carbon, oxygen, silicon, iron, calcium, sulfur, chlorine, titanium, boron, gadolinium, hydrogen, chromium, nickel, copper, aluminum, manganese, vanadium, magnesium, gold, and sodium. As with the PFN probe, more information about the design of the NG probe can be found in the FY 2000 ESR Annual Report.<sup>1</sup>

### **FY 2001 Activities**

The first activity to be completed on this task in FY 2001 was the construction of a facility and lab in a decommissioned critical facility (ETRC) at the Test Reactor Area (TRA). This facility contains a steel-lined pit approximately 20 ft deep wherein a structure is installed consisting of three separate test holes having diameters of 60, 30, and 4.5 in. The pit was backfilled with approximately 17 ft of gravel. Surrogates will be constructed that can fit into the 30 in. test hole to simulate various environmental media. The other test holes have been installed to supply future flexibility.

The largest single activity of FY 2001 was designing and constructing the probes themselves. The design was largely completed in FY 2000, but there were some changes made and some serious issues that needed to be addressed; for example, delivery of the A320 neutron generator, scheduled for September 2000, is still pending.

### **NG Probe Construction and Assembly**

Construction of the NG probe was beset with various problems and design changes. At one point during the year, it became clear that budgetary and scheduling considerations would not allow for the installation of the down-hole digital spectrometer

so we decided to use a standalone, tabletop version of the spectrometer for the initial demonstration.

The A320 neutron generator, intended for use in the NG probe, arrived in June, approximately 9 months past the scheduled delivery date. During acceptance testing, we found that it produced far fewer neutrons than called for in the specification. In fact, eventually it completely failed and was returned to the manufacturer (MF Physics) for repair who found a major design flaw, so the unit was not returned to us in FY 2001.

Combining the neutron generator with the standalone spectrometer constituted the most innovative feature of the NG probe. The failure of the neutron generator meant that the probe could not be tested in an active mode—only passive gamma-ray measurements would be possible. It would however be possible to test the detector and the various power supplies, but the detector failed and required repair by the manufacturer. We therefore substituted a similar detector, owned by the Environmental Remediation program, which was the detector deployed in the field tests at the end of September.

### **PFN Probe Construction and Assembly**

Construction of the PFN probe went somewhat more smoothly than that of the NG probe. Except for delays in deploying the sodium iodide detectors, the PFN probe was fully operable at the end of FY 2001.

The A211 Zetatron neutron generator arrived in July 2001, having been delayed approximately 5 months by design and construction problems. When it arrived we gave it a series of acceptance tests wherein it initially performed quite well. The probe was slowly assembled with individual components being tested as they were installed. When we started to integrate the control electronics with the accelerator head, we found that they were pretty much incompatible. Some quick electronics work resulted in a solution, but along the way, the A211 was damaged and returned to the factory for repair. Fortunately, each time the unit failed, identifying the reason and instituting controls to prevent future occurrences were straightforward. For example, a signal conditioner card was installed with a default condition that, in a partial power failure, might

lead to a blown fuse within the accelerator head. A small circuit was installed to change the default condition and prevent this in the future.

Perhaps the most frustrating problem encountered in the assembly of the PFN probe was the length of the pressure housing. The originally proposed PFN probe was to be under 10 ft long, the one delivered was just under 15 ft long. As it turned out, even this was not sufficient. It is unclear at what point in the design process the mistake was made, but the pressure housing was delivered approximately 5 inches too short. This necessitated welding an additional 7 in. to the bottom of the pressure housing, making the final length of the PFN probe about 15 ft-6 in.

### **Probe Software**

The probe software had to be easy for operations personnel to use, as comprehensive as possible, and include all the necessary data acquisition and analysis functions, along with the required monitoring and control functions for the neutron generators.

We chose the LABVIEW platform to integrate the various software and hardware functions. We developed a code package that would have a uniform interface for the two tools and provide streamlined data acquisition and analysis for monitoring of various tool parameters and for control of the neutron generators. The code is modular in nature and can be expanded in the future with little difficulty. We will likely add other features such as hoist control, radiation dose monitoring, and file management and control.

### **Probe Demonstrations**

The NG and PFN probes were demonstrated near the end of FY 2001 to meet a performance milestone. These demonstrations involved measurements at a monitoring well and at Pit 9 in the SDA. But before the demonstrations could be held, we had to secure approval from the various facilities involved. This approval process was made especially difficult by the inclusion of the neutron generators. A conservative estimate of the time spent on this process would be at least one man year. Fortunately, much of the work will carry over into FY 2002. We expect future procedural and compliance costs to much less.

The first demonstration was conducted at a monitoring well near RWMC. This well, named OW1, is a steel-cased well that penetrates the aquifer. Prior to this measurement the 800-ft cable on the logging truck had been replaced with a 100-ft cable. This was done in an attempt to correct shorting problems within the cable. Unfortunately, this did not correct the problem, which meant that the measurement could be conducted at a maximum depth of only 60 ft. In the end, this was not a particularly onerous limitation because the lack of a neutron generator in the NG probe led to a lack of interesting data anyway. This particular test well was known to have no contamination, so the PFN probe was not exercised in the least and the NG probe only provided a passive measurement of the background radiation.

Despite the lack of interesting results, the monitor well demonstration was important because it introduced involved personnel to the difficulty of work in the field and provided an important test of the various systems that must be coordinated. Though only a few data points were collected, the test was considered successful. Figure 1 shows the spectrum accumulated using the NG tool at a depth of 37 ft and Figure 2 shows the spectrum from the PFN probe at the same depth. Figures 3 and 4 are photographs of the demonstration at the monitoring well.

The second demonstration was conducted at Pit 9 within the SDA at RWMC. The test was conducted using a Type A” probehole—a fully enclosed hole cased with one-half-inch steel. These probes are driven sonically to resistance in the waste pits. The logging truck was still equipped with the 100-ft cable, but with a hole depth of just 13 ft, this was not important. The particular hole used, named P9-15, was selected for ease of access and not for the activity it might contain. Therefore it was unlikely that the second measurement would yield much more than the first. The passive NG measurement ran exactly as expected, with the resulting data resembling a background spectrum. Unfortunately, the PFN probe suffered an electronic failure after being placed in the hole. No spectra were recorded. Figures 5 and 6 show the probes deployed at pit 9.

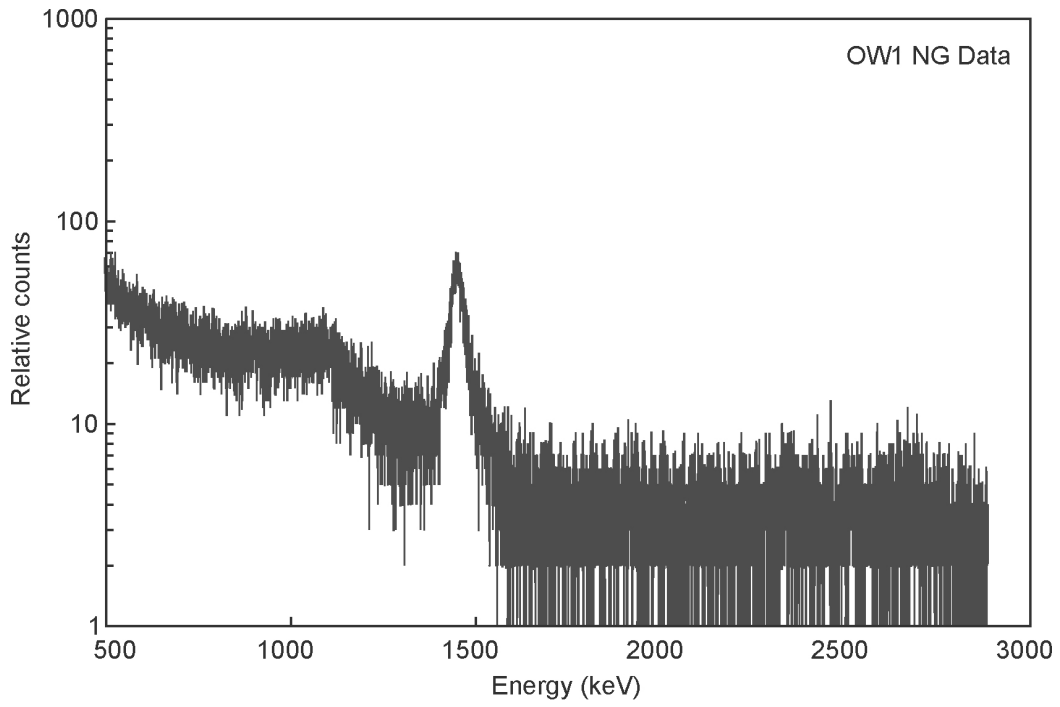


Figure 1. Representative spectrum acquired using the NG probe in passive mode in OW1 monitor well.

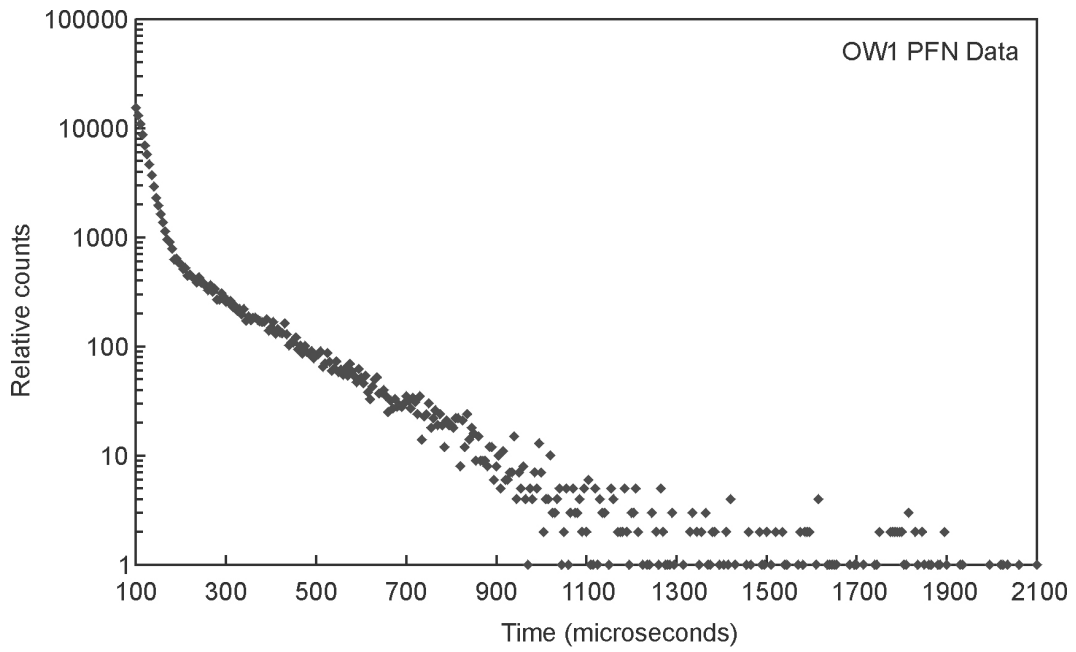


Figure 2. Representative spectrum acquired using the PFN probe in the OW1 monitor well.



Figure 3. Logging truck, logging personnel, and NG probe at the monitor well OW1.



Figure 4. PFN probe in monitor well OW1. The chains make up the wellhead interlock system.



Figure 5. Photograph of the NG probe being guided into probe-hole P9-15 at Pit 9.



Figure 6. Photograph of the PFN probe and logging truck deployed at Pit 9.

## Future Directions

In FY 2002, there will be important tasks necessary to prepare the program for transfer to operations. The surrogates for the lab in ETRC will be built, the probes will be calibrated and characterized, and some of the electronics will be upgraded to improve both performance and reliability. All this would not have been possible without the successful work done in FY 2001.

## Fission Physics Research

### Fission Yields and the Structure of Fission Fragments

Since the early 1990s, significant new fission studies using arrays of detectors that look directly at the prompt fission process have been completed or are still ongoing. As a result, we now have

specific information available that correlates various radiation emissions with fragment emission before beta-decay occurs, and new information on the excitation modes of the fragments when gamma rays and neutrons are emitted and not emitted. These data are specific to this prompt-time region following fission and before the first beta-decay occurs.

Prior to the 1990s, most fission studies measured average quantities or totals of parameters such as total energy release or mass yields. Most models of fission were based on a liquid drop model of the nucleus with some parametric correction for shell model effects in both the isotopes undergoing fission and the fission fragments produced. Most experimental low-energy nuclear structure physicists were focused on nuclear models that involved both collective and single particle motions of the nucleons in a meson type potential. The study of nuclear deformation and rotational motion, as observed in bands or cascades of gamma rays, required the study of nuclei series over as long a region of mass, neutron number, or proton number as possible to establish trends or changes in the nuclear states. The nuclei produced in fission comprise a rich set of isotopes for such studies, but producing these isotopes for study by traditional methods or using them for reaction studies are

impossible at this time. Our primary goal in beginning the fission studies was to study the structure of the prompt fission products.

The new models advanced to describe nuclei and nuclear structure physics primarily looked at level schemes. The liquid-drop model was generally replaced in these studies, but this was not true in describing fission. The basic reason being that most fission studies either measured average values or studied the fragments by beta-decay. Experiments with fission chambers and various gamma-ray calorimetric methods did not reveal specifics on the prompt states occurring immediately following the fragment separation. This situation changed however, with the development of arrays of detectors operating in coincidence, with extremely fast timing electronics that use list-mode data storage and post-acquisition sorting based analysis. What was once considered a dead subject for experimental measurement and theoretical interest is revived to provide new information for the nuclear many-bodied problem.

Figure 7 illustrates the prompt-time region that these new studies are revealing. Considerable energy is available from isotopes in spontaneous fission, or that are fissile (fission that can be induced by thermal neutrons). Most of this energy appears as kinetic energy of the two fragments, but tens of MeV are available for particle emission or

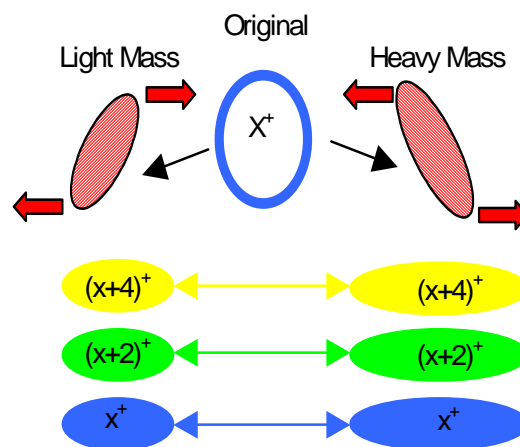


Figure 7. Graphical presentation of high spin and parity population and rotational excitation.

gamma-ray emission. Exactly what occurs depends on the conservation of three quantities: angular momentum, spin, and parity. These parameters were such that the liquid-drop model was not correct and some of the basic average values assigned to fission, would not explain the experimental results.

Our first important observation was that the rotational motion of the fragments can carry significantly more energy than allowed by traditional views. Level energies of states depopulated by gamma-ray emission exist well above the energy needed to evaporate a neutron. The fragments display the typical rotational bands seen in in-beam studies. This should not have been a surprise because high-spin bands allow the nucleus to have high-excitation energy that cannot be dissipated by the emission of a particle. The rotational states block the emission of particles and gamma-ray emission occurs until a state is reached where this is allowed. In general, the first such states for the fragments may be energetically too low for particle emission. The angular momentum of the two fragments must conserve the initial angular of the fissile isotope; therefore, if one fragment has high angular momentum, so must the other. The spin and parity of the fragments must also conserve the initial numbers of the fissile isotope; Figure 7 represents this result. The two fragments will have very similar angular momentum states, but there is sufficient energy being distributed to drive this, and the initial states of the of the two fragments will be that which is allowed by the parent. This becomes a considerably more complex problem for ternary or higher fragmentation, but is not important for this discussion.

We were able to observe these experimental results because of a theoretical basis developed in just the past few years. In our studies, the high-energy part of the gamma-ray energy spectra show a rich population of transitions that the coincidence methods enhance, just as these methods suppress the backgrounds from the fission source. For the case of  $^{252}\text{Cf}$ , these results have been presented in various papers that cover the new high energy gamma rays observed, and the new yield data from approximately 120 fragment pairs. There is no reason to think that the structure

information developed for the fragments from the  $^{252}\text{Cf}$  data will not be the same for uranium and plutonium. It may well be, that even more fragments would be produced in high-spin states for the uranium and plutonium fission because the competing neutron emission (average neutron multiplicity) is lower in these isotopes than in the case of  $^{252}\text{Cf}$ .

## Experimental Program of FY 2001

The induced fission work at IPNS and that attempted work at ORELA are the very first studies of induced fission using techniques that illuminate the prompt fission time period.

Our work on the fission studies for FY 2001 was expanded to attempt to have running setups at both ANL/IPNS and ORNL/ORELA. The move to have a second setup at ORELA was driven by the experimental goal of collecting induced fission with a nonthermal neutron beam, such as that available at IPNS. We know that the fission fragment yields change at higher neutron energy, but our goal was to collect gamma-gamma coincidence data tagged on the incident neutron energy. In the fall of 2000, we set up an experiment on beam-line 6 at ORELA that was identical to the one located at IPNS. For this setup a duplicate of the IPNS support structure was fabricated at the Vanderbilt University machine shop and transported to ORNL. During the course of the setup at ORELA we found several improvements in the setup of the signal processing electronics that significantly enhance the performance of the detection system, which we plan to incorporate into the IPNS setup.

The experimental program at IPNS during FY 2001 continued the series of induced fission measurements on various fissile isotopes. In the fall of 2000 a  $^{233}\text{U}$  target was installed in the IPNS target position and several months of data were collected. We carried out the initial analysis of the  $^{233}\text{U}$  data to obtain the calibration and stability information needed to setup the gamma-gamma coincidence matrix sorts. In the spring of 2001 the  $^{233}\text{U}$  was removed in favor of a mixed target containing a number of  $^{235}\text{U}$  foils and a number of  $^{239}\text{Pu}$  foils. The goal of the measurement was to collect some benchmarking data on what kind of

coincidence spectra could be observed by a system attempting to characterize a mixed sample such as would be prevalent in SNF and RH-TRU samples. Data was collected with the combined sample for a couple of months, and is waiting to be analyzed.

Initial in-beam runs at ORELA with a set of  $^{235}\text{U}$  foils as the target produced unsatisfactory results. The coincidence count rates observed were on the order of two orders of magnitude below what a similar set of foils produced in the IPNS setup. We currently think the reason for this result is a much lower neutron beam intensity than expected, or else a very small component of the neutron beam is in the lower energies where the induced fission cross-sections are significantly higher. From available experimental results, we have decided that the plan to carry out the neutron energy tagged coincidence experiments at ORELA is not feasible, and have therefore broken down the fission setup there for shipment to IPNS. The current setup at IPNS will be taken down and the old electronics used in the system will be replaced by the newer components purchased for the ORELA setup. At this time the system improvements implemented in the ORELA fission setup will be incorporated. Based on our experience at ORELA, this will significantly improve the quality of the induced fission data collected at IPNS. Our goal is to get the new updated measurement system up and running at IPNS by the early part of January 2002. Moving the ORELA setup to IPNS will result in 12 instead of 8 detectors in the array with newer electronics.

Efforts have been underway during FY 2001 to obtain a  $^{237}\text{Np}$  target from the Russians for use in the next set of induced fission measurements. We expect that the  $^{237}\text{Np}$  target will be shipped to IPNS at the end of December in time for use during the spring IPNS run schedule. The target is manufactured and the Russians are awaiting the approval of the export license. There has also been some discussion about the availability of some of the longer-lived curium isotopes.

The next stage of data analysis is to complete the calibration and setup work needed to build the  $^{233}\text{U}$  gamma-gamma coincidence matrices. There are also plans to refine the sorting process for the  $^{235}\text{U}$  and  $^{239}\text{Pu}$  coincidence data already in hand.

The initial coincidence matrices were constructed without using the prompt and random coincidence timing information available in the data stream. This means that the random backgrounds present in the gated coincidence spectra are higher than they need to be.

## High Count Rate Systems Development

### NDA Systems (High Count Rate systems Development)

Following publication early in FY 2001 of our prior work on evaluation of commercial digital signal processing electronics at ultra-high counting rates,<sup>2</sup> this task has focused on rapid and improved techniques for trapping corrections in room temperature, cadmium zinc telluride (CZT), gamma-ray detectors. Our research method used digital signal processing (DSP) techniques to acquire spectral and preamplifier waveform data from a selection of CZT detectors to allow direct inspection of preamplifier wave forms affected and unaffected by hole trapping. These waveforms are then available for developing classification and correction algorithms to improve the performance of these detectors.

Hole trapping is a solid-state, charge transfer problem that plagues room temperature solid-state detectors. Ionization events in the detector produce electron-hole pairs that must be fully collected to yield good spectrometric performance. In materials like CZT, hole transport is poor and the positive ( $^+$ ) holes created within the detector volume are often trapped before collection. A number of analog and design features have been advanced to ameliorate the effects of hole trapping. Our approach in this research is to develop fast digital processing techniques to correct for the effects of hole trapping.

The DSP being used is an XIA DGF-4C that incorporates four DSP input channels capable of acquiring and storing digitized preamplifier wave forms and reconstituting a normal gamma-ray spectrum from the acquired pulses. To selectively produce trapped versus untrapped preamp wave forms, a precision scanning system was built that incorporates a  $0.4 \times 10$  mm slit collimator in a  $5 \times$

5-cm-tungsten block mounted on a micrometer-adjusted linear scanning bed. Since ionization events occurring near the detector cathode are relatively free of hole trapping effects and those occurring near the anode are highly trapped, scanning with a radioactive source from cathode to anode allows acquisition of pulses dominated by trapping and pulses free from trapping.

A modification to the detector electronics was required to allow acquisition of the required waveform and spectral data from one detector type of interest. A co-planar grid (CPG) detector design acquires pulse data on two separate anode grids, one of which has a small differential bias with two separate preamplifiers using a subtraction circuit to produce an output signal. The subtraction output of a CPG detector is relatively free of hole trapping effects. Our CPG detector was modified to provide separate preamplifier output channels in addition to the subtraction output channel. Preamplifier waveform data and spectra were acquired on this modified detector, monitoring both preamplifier and subtraction circuit outputs. Figures 8A and B present the spectra acquired from the CPG subtraction output with a  $^{22}\text{Na}$  source irradiating near the cathode and the anode respectively. Figures 9A and B present similar results taken from the preamplifier attached to the unbiased (collecting) anode. The effect of hole trapping on the spectra taken near the detector anode is obvious. It is also clear that although the subtraction output of the CPG detector provides substantial correction for the effects of hole trapping, there is much room for improvement.

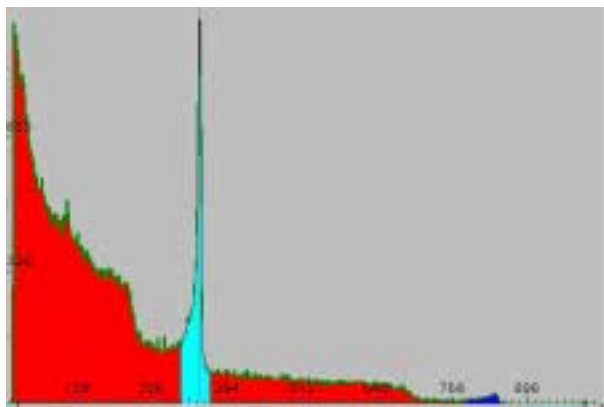


Figure 8A. Na-22 spectrum CPG detector near cathode subtraction circuit out.

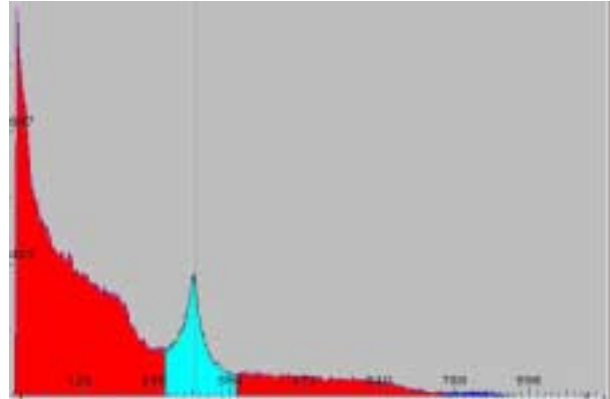


Figure 8B. Na-22 spectrum CPG detector near anode subtraction circuit out.

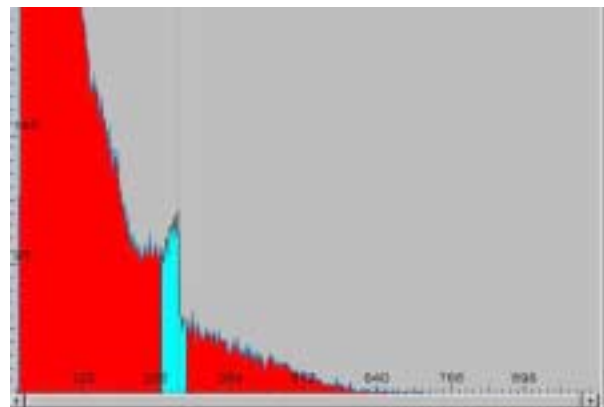


Figure 9A. Na-22 spectrum CPG detector near cathode collecting electrode preamplifier output.

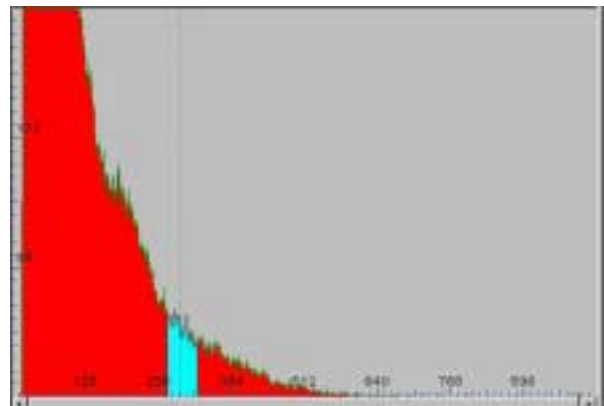


Figure 9B. Na-22 spectrum CPG detector near anode collecting electrode preamplifier output.

Figure 10 presents an example of the waveform data acquired by the DSP on all the waveform channels. The top (CH0) is subtraction

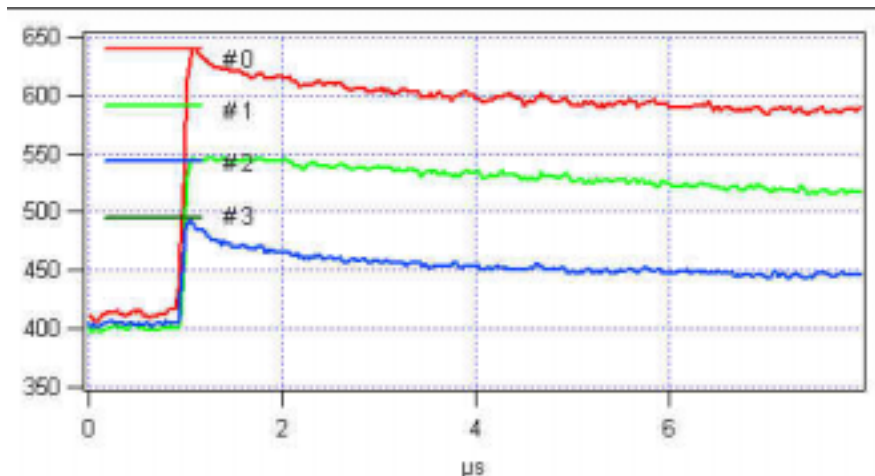


Figure 10. Example wave forms for a pulse detected by the CPG detector.

circuit out, the middle (CH1) is collecting electrode Preamp out, and the bottom trace (CH2) is the output of the non-collecting (biased) electrode. The CH2 trace has been inverted for display purposes; it is a negative-going pulse. These data have been acquired on the CPG detector and initial work was beginning on a planar CZT detector system. Little work on pulse classification was completed.

## Radiation Transport Analysis

### Passive Gamma Spectrometry Based Assay

A small task has been on-going over the last 3 years to determine the capabilities of a strictly passive gamma spectrometer as a standalone system for assaying 208-liter drums of transuranic waste. Strictly passive gamma spectrometry refers to a system that relies solely on the gamma radiation signature emanating from the source material. Such a system does not use transmission sources or other interrogation methods to aid in the assay. In waste characterization, strictly passive gamma spectrometer systems are used primarily to determine relative isotopic mass ratios. However, as was determined from this program, they can play a more expanded role and with the proper analysis can be used as standalone assay systems. During FY 2001, an assay analysis computer program called RESPMATs was developed and used to analyze over 100 gamma spectra from the SWEPP gamma-ray spectrometer (SGRS). The

results of that study were presented at the 7th NDA Transuranic Waste Characterization Conference held in Salt Lake City, UT in May 2000. During the first quarter of FY 2001, the absolute assay code (RESPMATs) was combined with the gamma spectrum analysis code (PCGAP) to produce a production assay code called SWEPP RESPMATs Absolute Assay Code (SRAAC). The INEEL 3100 Cubic Meter Program has now adopted this code and under their sponsorship, SRAAC is being implemented for use in assaying drums using the SGRS as a standalone assay system.

As part of the 3100 Cubic Meter Program implementation plan, a total measurement uncertainty analysis was completed for SRAAC/SGRS. In this analysis, gamma-ray spectra from approximately 800 assays involving all types of waste were analyzed to arrive at the measured Pu-239 mass. The assay set analyzed in this manner included only those waste codes for which the INEEL Passive Active Neutron (PAN) system had been previously qualified by the Carlsbad Field Office (CBFO) for characterizing waste for shipment to the Waste Isolation Pilot Plant (WIPP). The results of this analysis are given in Figure 11, where the Pu mass determined using SGRS/SRAAC is compared with the corresponding Pu mass determined using PAN. A linear regression of these data show that the SGRS/SRAAC Pu mass is biased 11% below the PAN Pu mass and that the total measurement uncertainty for the SGRS/SRAAC results is

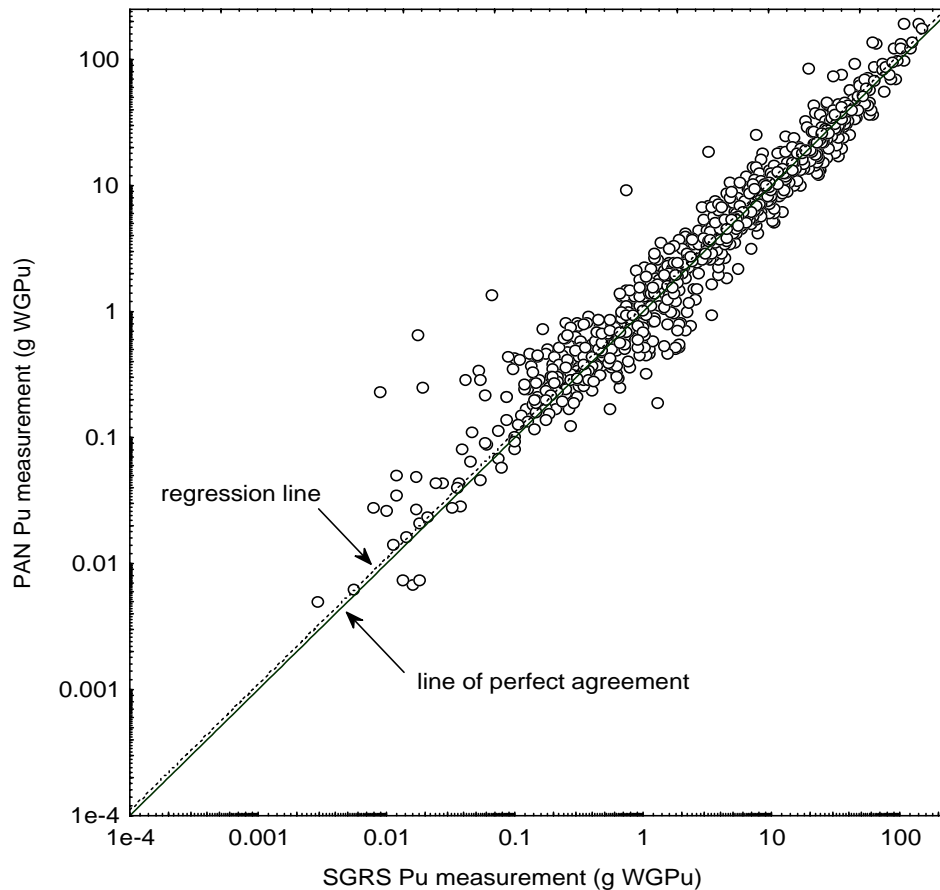


Figure 11. PAN Pu mass vs. SGRS Pu mass.

approximately 20%. It is also interesting to note that the SGRS/SRAAC was able to assay waste where as little as 10 mg of weapons-grade plutonium was present. These results will certainly satisfy the NDA requirements as specified in the CBFO Waste Acceptance Criteria for shipment of transuranic waste to WIPP.

In summary, this is an example where a small task in the NDA Science and System project has produced a direct benefit to the INEEL 3100 Cubic Meter Program. Other programs throughout the DOE complex with similar objectives could benefit from this development as well.

## ACCOMPLISHMENTS

In the area of fission physics, we collected  $^{233}\text{U}$  data at the IPNS facility and started a

measurement combining  $^{235}\text{U}$  and  $^{239}\text{Pu}$  targets for future use as a benchmark for possible spent fuel or RH-TRU measurements. These measurements were carried out at the ORELA. However, the results were unsatisfactory so we disassembled the equipment and shipped it back to IPNS and INEEL.

During FY 2001 the borehole project took significant steps forward, the PFN was assembled in nearly its final form, the NG probe was assembled without the neutron generator and used in only passive mode, and the needed software and much of the tedious compliance work was completed. We also converted the ETRC facility at TRA into an experimental facility for probe work, and, even though the PFN probe was plagued by an easily correctable cable malfunction, successfully completed three of the four possible

field tests at the Pit 9 monitoring well in the SDA at the RWMC.

In the area of high-count-rate systems development, the focus shifted to studying hole-trapping effects in cadmium-zinc-telluride detectors. Many spectra were acquired to be used in FY 2002 activities. These data have been acquired on the CPG detector and initial work was beginning on a planar CZT detector system. Little work on pulse classification was completed.

In the area of gamma-ray transport analysis, the absolute gamma assay code RESPMATS that was developed in FY 2000 was converted to a production assay system called SRAAC, and adopted by the 3100 Cubic Meter Program at RWMC.

## Publications

Hamilton, J. H., Y. X. Luo, J. K. Hwang, E. F. Jones, A. V. Ramayya, S. H. Zhu, P. M. Gore, C. J. Beyer, J. Kormicki, X. Q. Zhang, T. N. Ginter, M. G. Wang, J. D. Cole, M. W. Drigert, W. C. Ma, P. G. Varmette, G. M. Ter-Akopian, Y. T. Oganessian, A. V. Daniel, J. Kliman, J. O. Rasmussen, I. Y. Lee, R. Donangelo, A. P. de Lima, "Octupole Correlations and Deformation In Ba, La and Pr," *Acta Physica Polonica B*, Vol. 32, Issue 3, March 2001, pp. 957–969.

Hartwell, J. K., and G. D. McLaughlin, "A Comparison of the High Count-Rate Performance of Two Commercially Available Digital Gamma-Ray Spectrometers," *Radioactivity & Radiochemistry*, Volume 11, Issue 4, December 2000.

Hwang, J. K., A. V. Ramayya, J. H. Hamilton, E. F. Jones, P. M. Gore, S. J. Zhu, C. J. Beyer, J. Kormicki, X. Q. Zhang, L. K. Peker, B. R. S. Babu, T. N. Ginter, G. M. Ter-Akopian, Y. T. Oganessian, A. V. Daniel, W. C. Ma, P. G. Varmette, J. O. Rasmussen, I. Y. Lee, J. D. Cole, R. Aryaeinejad, M. W. Drigert, M. A. Stoyer, S. G. Prussin, R. Donangelo, H. C. Griffin, "Possible Octupole Correlation In Pr-147 and  $\pi h(11/2)$  bands in Pr-149, Pr-151," *Physical Review C*, Volume 6204, Issue 4, p. 4303.

Jones, E. F., P. M. Gore, J. H. Hamilton, A. V. Ramayya, A. P. deLima, R. S. Dodder, J. Kormicki, J. K. Hwang, C. J. Beyer, X. Q. Zhang, S. J. Zhu, G. M. Ter-Akopian, Y. T. Oganessian, A. V. Daniel, J. O. Rasmussen, I. Y. Lee, J. D. Cole, M. W. Drigert, W. C. Ma, "A New Phenomenon: Shifted Identical Yrast Bands In Neighboring Even-even Nuclei," *Nuclear Physics A*, Volume 682, pp. 79c–87c.

Jones, E. F., P. M. Gore, J. H. Hamilton, A. V. Ramayya, A. P. de Lima, R. S. Dodder, J. Kormicki, J. K. Hwang, C. J. Beyer, X. Q. Zhang, S. J. Zhu, G. M. Ter-Akopian, Y. T. Oganessian, A. V. Daniel, J. O. Rasmussen, I. Y. Lee, J. D. Cole, M. W. Drigert, W. C. Ma, "Shifted Identical Bands: A New Phenomenon," *Physics of Atomic Nuclei*, Vol. 64, Issue 7, July 2001, pp.1157–1164.

Sakhaee, M., S. J. Zhu, C. Y. Gan, L. Y. Zhu, L. M. Yan, R. Q. Xu, M. G. Jon, Z. Jiang, Z. Zhang, J. H. Hamilton, A. V. Ramayya, B. R. S. Babu, J. K. Hwang, W. C. Ma, J. Komicki, J. D. Cole, R. Aryaeinejad, M. W. Drigert, J. O. Rasmussen, M. A. Stoyer, S. Y. Chu, K. E. Gregorich, M. F. Mohar, S. G. Prussin, I. Y. Lee, Y. T. Oganessian, G. M. Ter-Akopian, A. V. Daniel, "Collective Band Structures In Neutron-rich Odd-A Ce-145, Ce-147 Nuclei," *High Energy Physics and Nuclear Physics – Chinese Edition*, Volume 24, Issue 11, pp.1018–1023.

Yang, L. M., S. J. Zhu, K. Li, J. H. Hamilton, A. V. Ramayya, J. K. Hwang, X. Q. Zhang, L. Y. Zhu, C. Y. Gan, M. Sakhaee, G. L. Long, R. Q. Xu, Z. Zhang, Z. Jiang, M. G. Jon, W. C. Ma, B. R. S. Babu, J. Komicki, E. F. Jones, J. D. Cole, R. Aryaeinejad, M. W. Drigert, I. Y. Lee, J. O. Rasmussen, M. A. Stoyer, G. M. Ter-Akopian, A. V. Daniel, "Collective Bands in Neutron-rich Mo-104 Nucleus," *Chinese Physics Letters*, Volume 18, Issue 1, pp. 24–26.

Zhang, X. Q., J. H. Hamilton, A. V. Ramayya, S. J. Zhu, J. K. Hwang, C. J. Beyer, J. Kormicki, E. F. Jones, P. M. Gore, B. R. S. Babu, T. N. Ginter, R. Aryaeinejad, K. Butler-Moore, J. D. Cole, M. W. Drigert, J. K. Jewell, E. L. Reber, I. Y. J. Gilat, Lee, J. O. Rasmussen, A. V. Daniel, Y. T. Oganessian, G. M. Ter-Akopian, W. C. Ma,

P. G. Varmette, L. A. Bernstein, R. W. Loughed, In Neutron-rich Pd-118,” *Physical Review C*,  
K. J. Moody, M. A. Stoyer, R. Donangelo, J. Y. Volume 6302, Issue 2, p. 7302.  
Zhang, “Observation of a  $\nu h(11/2)$  Pair Alignment

## REFERENCES

1. David L. Miller, Program Manager, *Environmental Systems Research, FY 2000 Annual Report*, INEEL/EXT-2000-02085, January 2001.
2. J. K. Hartwell and G. D. McLaughlin, “A Comparison of the High Count-Rate Performance of Two Commercially Available Digital Gamma-Ray Spectrometers,” *Radioactivity & Radiochemistry*, Volume 11, No. 4, December 2000. 273.



# Nuclear Structure Data Relevant to the INEEL Mission

J. W. Mandler,<sup>a</sup> R. J. Gehrke,<sup>a</sup> R. G. Helmer,<sup>b</sup> C. A. McGrath,<sup>a</sup> R. P. Keegan,<sup>a</sup> J. D. Baker,<sup>a</sup> C. L. Riddle,<sup>a</sup> M.H. Putnam,<sup>c</sup> H. C. Griffin,<sup>d</sup> R. P. Gardner,<sup>e</sup> and E. B. Nieschmidt<sup>e</sup>

## SUMMARY

Nuclear structure data provides the foundation for understanding the atomic nucleus and the operation and calibration of ionizing radiation detectors used in radioanalysis and nondestructive elemental analysis. Our first project objective is to identify and measure the nuclear structure data needed to test nuclear models and perform radioanalyses and elemental analyses for programs important to DOE. These measurements must be highly accurate, and often use complex, innovative methods. Our second objective is to put this nuclear data in a format that renders it immediately useful to all members of the nuclear science and technology community.

In some cases we have applied our results to solve real problems at the INEEL, in others we have not. But we have added to the body of knowledge in nuclear science and technology, which we believe will prove valuable in the future as demonstrated in the past, where reports written years ago have found new relevance and application today.

As a result of our accomplishments from this and previous years' efforts, methods have been developed and implemented at the Stored Waste Experimental Pilot Plant (SWEPP) facility on the INEEL for the robust assay of <sup>233</sup>U and <sup>237</sup>Np in transuranic (TRU) waste.

Improved methods for the radioassay of TRU waste from discoveries made during FY 2001 hold promise for the radioassay of fissile materials directly from their short half-life fission products

(e.g., 0.16  $\mu$ s <sup>134m</sup>Te). A second new method for the assay of fissile material is useful when strong  $\alpha$  emitters dominate the waste matrix. This assay is performed from total neutron counter measurements (fissile neutrons and neutrons from  $[\alpha, n\gamma]$  reactions), and Ge  $\gamma$ -ray spectrometer measurements of the prompt reaction  $\gamma$ -rays from  $(\alpha, n\gamma)$  reactions to measure the associated neutrons. The neutrons from  $(\alpha, n\gamma)$  reactions are subtracted from the gross neutron counts that include all neutrons to yield the fissile neutrons and thus the amount of fissile material.

The INEEL received time on the Los Alamos LANSCE accelerator to measure  $(n, n'\gamma)$   $\gamma$ -ray production rates for NaI and Ge, two detector materials of importance in Monte Carlo modeling of prompt  $\gamma$ -ray neutron activation analysis experiments.

Methods have also been developed during FY 2001 for achieving extremely accurate Ge detector efficiencies that offer the opportunity to make a number of high-accuracy (<0.5%) measurements of nuclear parameters (e.g., log ft values, internal conversion coefficients). These measurements are necessary for quantification of radioisotopes in interrogated samples.

## PROJECT DESCRIPTION

During FY 2001, we worked on four subtasks: actinide studies, prompt  $\gamma$ -rays from alpha-induced reactions, nuclear data measurements for prompt  $(n, n'\gamma)$ , and methods development. These subtasks are described individually in this section.

---

a. Idaho National Engineering and Environmental Laboratory, P.O. Box 1625, Idaho Falls, ID 83415.

b. Idaho Accelerator Center, Idaho State University, Pocatello, Idaho.

c. 2055 N 26 West, Idaho Falls, Idaho.

d. Department of Chemistry, University of Michigan, 4403 Chem 1055, Ann Arbor, Michigan.

e. Nuclear Engineering Department, North Carolina State University, Raleigh, North Carolina.

## Actinide Studies

The purpose of this subtask is to improve our understanding of the nuclear decay chains and schemes of individual actinides, and learn how this information can be used to enhance present radioanalyses, especially of TRU waste and spent fuel. This is accomplished using calibrated Ge spectrometers to methodically study actinide and other radionuclides.

Initially, high-quality  $\gamma$ -ray spectra of the radionuclides are acquired with well-characterized Ge spectrometer systems. The detectors are located inside graded shields of lead, cadmium or tin, and copper with a layer of aluminum covering the copper for the low-energy Ge detector (LEGE). For the majority of the actinides a LEGE detector is set up to provide an 8,192-channel spectrum, that extends from  $\sim 5$  keV to  $\sim 1,500$  keV. For those actinides with  $\gamma$ -rays extending above 1,500 keV, a large 110% efficient Ge detector is used, whose energy scale extends from  $\sim 30$  keV to  $\sim 3,000$  keV. Both Ge spectrometer systems are equipped with an INEEL developed dual-energy pulser to ensure that no gain or zero shifts are present in the collected data. The gain of each detector is often measured before use, but this practice is not required since the pulser peaks, which are digitally offset to buffers above the  $\gamma$ -ray spectrum, have energy equivalence and are automatically used to calculate the energy scale.

A significant number of radioisotopes were studied over this past year and compared to the most recent evaluated nuclear structure data file (ENSDF) maintained by the National Nuclear Data Center (NNDC) at Brookhaven National Laboratory. The actinides studied include:  $^{226}\text{Ra}$ ,  $^{227}\text{Ac}$ ,  $^{232}\text{Th}$ ,  $^{231}\text{Pa}$ ,  $^{233}\text{Pa}$ ,  $^{232}\text{U}$ ,  $^{234}\text{U}$ ,  $^{236}\text{U}$ ,  $^{244}\text{Pu}$ ,  $^{243}\text{Cm}$ ,  $^{244}\text{Cm}$ ,  $^{245}\text{Cm}$ ,  $^{249}\text{Cf}$ ,  $^{251}\text{Cf}$ ,  $^{252}\text{Cf}$ , and  $^{253}\text{Es}$ . We tried to obtain the purest material, but at times the best available was contaminated with neighboring isotopes and even radionuclides of other elements. In some cases, actinides were obtained on loan from the transplutonium element production and isotope distribution facilities at Oak Ridge National Laboratory (ORNL). We are indebted for their use to the Office of Science and the Office of Nuclear Energy, DOE who fund the

facilities at ORNL. Whenever necessary and possible, the radionuclide of interest was chemically purified, but no provision was made to remove contaminating isotopes when present in the best material available. In one case, the  $^{251}\text{Cf}$  was contaminated with the isotopes  $^{91}\text{Y}$  and  $^{257}\text{Fm}$ .

The radionuclide,  $^{91}\text{Y}$ , decays by pure  $\beta^-$  and was chemically separated from the  $^{251}\text{Cf}$  and counted separately. The K x-rays of Zr are visible in the spectrum and are from shakeoff electrons. This is a very weak ( $\sim 1-5$ ) $\times 10^{-4}$  x-rays per decay) nuclear phenomenon in which atomic electrons are ejected during nuclear  $\beta^-$  decay and is attributed to the sudden change of the nuclear Coulomb field.<sup>1-3</sup> We also observed this effect in the decay of  $^{210}\text{Bi}$ , a daughter of  $^{210}\text{Pb}$ . Possible use of x-rays from shakeoff as an analytical tool is being contemplated. These spectra also provide an excellent example in teaching students in nuclear physics, since very few examples of this phenomenon are in the literature and those are of marginal quality.

Several peaks in the spectrum of  $^{238}\text{U}$  could not be identified, even after extensive efforts. After studying each of the progeny of  $^{238}\text{U}$ , it is believed that the decay schemes of  $^{234\text{m}}\text{Pa}$ ,  $^{234}\text{Pa}$  and  $^{234}\text{Th}$ <sup>3,4</sup> are at best incomplete and possibly some transitions are misidentified. A recent literature search indicates that the decay schemes of  $^{234\text{m}}\text{Pa}$  and  $^{234}\text{Pa}$  have not been recently studied. Realizing the importance of  $^{238}\text{U}$  we believe that a comprehensive study of the decay of these isotopes of Pa should be carried out.

In studying  $^{236}\text{U}$  we were able to detect a 171.1-keV  $\gamma$ -ray that we determined was depopulating the  $6^+$   $^{232}\text{Th}$  level.<sup>5</sup> While inelastic scatter has previously identified the 332-keV  $6^+$  level in  $^{232}\text{Th}$ , it has not been previously observed as populated in the decay of  $^{236}\text{U}$ .

Observation of the feeding of the  $6^+$  level in  $^{232}\text{Th}$  from the decay of  $^{236}\text{U}$  led us to investigate whether the  $6^+$  level in  $^{230}\text{Th}$  is populated from the decay of  $^{234}\text{U}$ . Initial measurements indicated that this was a distinct possibility, but the associated 184-keV transition depopulating this level could not easily be separated from the 185-keV contaminant from the major  $\gamma$  ray from  $^{235}\text{U}$  in the

time we allotted to this effort. The population of the  $6^+$  levels from the  $\alpha$ -decay of even-even actinides and the relative intensities of these  $\alpha$ -decay branches are important for the verification and improvement of nuclear models. The  $^{236}\text{U}$  measurements are important because there are still many even-even actinides for which these relative  $\alpha$ -branch intensities have not been measured due to the weakness of these transitions.

Although we have studied actinide  $^{227}\text{Ac}$  during FY 2001, difficulties in identifying whether all of the peaks in the spectrum belong to the parent, a daughter, or are contaminants leave this isotope needing further study in FY 2002. This isotope is of most concern from a cleanup standpoint for several locations at the DOE Mound Laboratory, since it is one of several radioactive contaminants found in their soils.

In consultation with R. Aryaeinejad, measurements were initiated to search for the presence of a 1,279-keV  $\gamma$ -ray associated with the fission product 0.16 microsecond  $^{134\text{m}}\text{Te}$ . In 1994 this  $\gamma$ -ray was reported in TRU waste by the authors,<sup>6</sup> but its potential importance was not recognized at that time. It was also reported in the proceedings of an international conference in 1999.<sup>7</sup> During FY 2001, we observed this  $\gamma$ -ray in the spontaneous fission decay of  $^{244}\text{Cm}$ , and  $^{252}\text{Cf}$ . The use of this and other fission product  $\gamma$ -rays for the direct radioassay of fissile material looks encouraging because this  $\gamma$ -ray was also identified during FY 2000 in a TRU waste drum containing ~15 grams of plutonium, which corresponds to ~1 g of the spontaneously fission  $^{240}\text{Pu}$  isotope. This finding needs to be pursued in follow-on work.

A collaboration initiated several years ago with Washington State University has resulted in an important publication on the decay of  $^{226}\text{Ra}$ .<sup>8</sup> There has been a significant discrepancy in the reported values for the emission probability,  $P_\gamma(186)$ , of the 186-keV  $\gamma$ -ray resulting from the  $\alpha$ -decay of  $^{226}\text{Ra}$  to the 186-keV  $2^+$  excited state of  $^{222}\text{Rn}$ . By the 1970s, nuclear data evaluators realized that this discrepancy was between the  $P_\gamma(186) = (3.59 \pm 0.06)\%$  (Reference 9) measured using mass standards and the  $P_\gamma(186) =$

$(3.29 \pm 0.03)\%$  (Reference 10) deduced from the  $\alpha$ -branch intensity to the  $^{222}\text{Rn } 2^+$  first excited state and the E2 theoretical internal conversion coefficient. This discrepancy could be the result of inaccurate measurements, but it could also be due to the mass standard being incorrect, the  $^{226}\text{Ra}$  half-life being wrong, the measured  $\alpha$ -branch intensity being incorrect or even the E2 theoretical internal conversion coefficient being in error. For these reasons, it was important to resolve this discrepancy, especially for a radionuclide that is so ubiquitous in the environment.

The alpha branching to the ground and first excited states of  $^{222}\text{Rn}$  was carefully measured by alpha spectrometry at Washington State University. The percent alpha branching to the second excited state of  $^{222}\text{Rn}$  ( $2^+$  level) divided by the quantity one plus the theoretical conversion coefficient of the pure E2 186 keV transition to the ground state ( $0^+$  level) yields the 186-keV  $\gamma$ -ray emission probability. Our value was measured to be  $(3.64 \pm 0.05)$   $\gamma$ -rays per 100 decays (Reference 8) and demonstrates that there is no conflict (within our measured uncertainties) between the mass-based standards and the activity-based standards, at least for this important radionuclide.

In addition to the above studies, we investigated radionuclides  $^{126}\text{Sn}$ ,  $^{126\text{m}}\text{Sb}$ , and  $^{126}\text{Sb}$ . Radionuclide  $^{126}\text{Sn}$  is a very long half-life fission product ( $2.5 \times 10^5$  yr) and  $^{126\text{m}}\text{Sb}$  and  $^{126}\text{Sb}$  are its daughters. After 10,000 years the fission products in spent fuel have essentially decayed leaving a few very long half-life fission products including  $^{93}\text{Zr}$  ( $1.5 \times 10^6$  yr),  $^{99}\text{Tc}$  ( $2.13 \times 10^5$  yr),  $^{107}\text{Pd}$  ( $6.5 \times 10^6$  yr),  $^{126}\text{Sn}$  ( $2.5 \times 10^6$  yr) and daughters  $^{126\text{m}}\text{Sb}$  and  $^{126}\text{Sb}$ ,  $^{129}\text{I}$  ( $1.5 \times 10^7$  y), and  $^{135}\text{Cs}$  ( $2.3 \times 10^6$  y). Of these radionuclides, all but  $^{126}\text{Sn}$  and its daughters and  $^{129}\text{I}$  are pure  $\beta^-$  emitters. With  $\gamma$ -rays having energies extending above 1 MeV. The daughter radionuclides of  $^{126}\text{Sn}$  ( $^{126\text{m}}\text{Sb}$  and  $^{126}\text{Sb}$ ) are important in determining the long-term radiation dose exposures of these fission products.

Finally, Prof. Henry Griffin and his students at the University of Michigan completed work that resulted in nuclear data for  $^{24}\text{Na}$ ,  $^{49}\text{Ca}$ , and  $^{88}\text{Rb}$ .

The studies consisted of acquiring a quality spectrum of each of these radionuclides, identifying each peak in the spectrum, and fully annotating the spectrum. A paper reporting a new transition in the decay of  $^{49}\text{Ca}$  was submitted for publication.<sup>11</sup> These radionuclides, along with their decay chains, decay schemes, lists of  $\gamma$ -ray energies, and emission probabilities have been placed on the INEEL Gamma-Ray Spectrometry Center website with acknowledgement for use by academia, government laboratories, and industry.

### Prompt $\gamma$ -rays from Alpha-induced Reactions

During the study of  $^{241}\text{Am}$  spectra and the spectra of 55-gal-TRU waste drums at the SWEPP facility, we observed several peaks that are not from the decay scheme of the parent or any of the progeny. These peaks were identified as alpha-induced reactions (e.g.,  $^{19}\text{F}[\alpha, n]^{22}\text{Na}$ ) from the alpha particles emitted in the decaying actinide, which interact with low atomic number elements present in the waste matrix, with the emission of prompt reaction  $\gamma$ -rays. These  $\gamma$ -ray peaks have been observed in the past but no serious effort appears to have been made to exploit their use in the radioassay of actinides by using the neutron-to- $\gamma$ -ray ratio ( $n/\gamma$ ) to measure the fraction of neutrons emitted due to  $\alpha$ -induced reactions.<sup>12-14</sup> Last year, spectra from a set of 27 drums of TRU wastes were analyzed using a  $n/\gamma$  intensity ratio deduced from literature values of reactions/alpha,  $\gamma$ -rays/alpha, and neutrons/reaction. Among the 27 drums examined, 33% were within 30% of the known value of neutrons emitted from ( $\alpha, n\gamma$ ) reactions. The results of these analyses showed some improvement when an improved efficiency calculation was used to re-analyze the 27 drums. This year's scope of work was a follow on to last year's in that it focused on obtaining accurate measurements of the  $n/\gamma$  ratios for several low atomic number elements.

A doubly encapsulated stainless steel sealed source of an alpha-emitting radionuclide intimately mixed with an element of low atomic number was prepared for the  $^{19}\text{F}(\alpha, n\gamma)^{22}\text{Na}$  reaction using  $\text{CaF}_2$ . It was prepared in a glove box used for alpha-emitting radionuclides by

dissolving the  $^{244}\text{Cm}$  material in nitric acid. Then, a known aliquot of the dissolved  $^{244}\text{Cm}$  was deposited onto the  $\text{CaF}_2$  matrix located in the cavity of the inner capsule. A calcium fluoride source was prepared because it is the most common chemical form of plutonium from the processing activities at the Rocky Flats Plant, and the dominant  $\alpha$ -induced reaction in the INEEL TRU waste in 55-gal drums. A second doubly contained sealed source was prepared at the same time using fine nickel powder as the matrix to provide a background source (no [ $\alpha, n\gamma$ ] reactions are expected from a nickel matrix). The inner capsules of the two sources were thoroughly decontaminated after sealing the radioactive material inside the inner capsules and prior to removing them from the glove box.

In addition to the doubly encapsulated  $^{244}\text{Cm}/\text{CaF}_2$  and  $^{244}\text{Cm}/\text{Ni}$  sources prepared at the INEEL, many years ago we purchased a  $^{13}\text{C}(\alpha, n)^{16}\text{O}$  reaction  $\gamma$ -ray source from Chalk River National Laboratory or one of its subsidiaries. In spite of the fact that this source has gone through one half-life of  $^{244}\text{Cm}$ , the source of  $\alpha$  particles, it is still a viable reaction  $\gamma$ -ray source emitting 6.129-MeV  $\gamma$ -rays. We have also collected  $\gamma$ -ray and neutron data on this source and are in the process of analyzing it for the  $n/\gamma$  ratio for the  $^{13}\text{C}(\alpha, n)^{16}\text{O}$  reaction for the 6,129-keV  $\gamma$ -ray. This ratio may be useful in the analysis of TRU waste containing graphite crucibles.

A large coaxial HPGe detector was used to perform the  $\gamma$ -ray measurements. The efficiency of the detector was measured from 122 to 1,500 keV with a standard source of  $^{152}\text{Eu}$  from PTB, the German national standards laboratory. The efficiency was measured above 1,500 keV up to  $\sim 6$  MeV with a  $^{232}\text{Th}$  source and by producing the chlorine capture  $\gamma$ -rays with a small 0.15  $\mu\text{g}$  source of  $^{252}\text{Cf}$  (source Y-288) by ( $n, \gamma$ ) reactions on samples of NaCl and on polyvinyl chloride resin. The low-energy relative peak efficiencies from the chlorine prompt reaction  $\gamma$ -rays (at 778, 1,164, 1,950, 1,959 and 2,864 keV) were normalized to the existing efficiency curve, and the normalized values of the high-energy (at 5,715, 6,619, and 6,627 keV) Cl efficiencies were added to the efficiency curve. This efficiency curve is essential

to determining the 582-, 890-, and 6129-keV  $\gamma$ -ray emission rates associated with the  $^{19}\text{F}(\alpha, n\gamma) ^{22}\text{Na}$  and  $^{13}\text{C}(\alpha, n) ^{16}\text{O}$  reactions.

An active well coincidence neutron counter (AWCC) was used to quantify the neutron emission rate. Gamma-ray attenuation in the doubly encapsulated sources was calculated for a range of  $\gamma$ -ray energies and also experimentally measured from the  $^{244}\text{Cm}$   $\gamma$ -rays. In addition, neutron moderation and attenuation due to the capsules and their contents were calculated. The  $n/\gamma$  ratios for the 582-keV  $\gamma$  ray is  $2.7 \pm 0.4$ ; for the 890-keV  $\gamma$ -ray it is  $7.3 \pm 1.2$  neutrons per  $\gamma$ -ray.

An experiment performed by a student on a fellowship during the summer of 2000, demonstrated the ability to use cosmic-ray produced neutrons to perform prompt  $\gamma$ -ray neutron activation analysis (PGNAA) on 2–3 gal samples of sodium chloride solution with a 7.6-cm diameter  $\times$  7.6-cm high NaI(Tl) spectrometer even in small Rocky Mountain colleges lacking a radioactivity license.<sup>15</sup> The significance of this experiment is two-fold: it demonstrates the pervasiveness of neutron radiation that is produced from cosmic rays in our environment, and provides a prompt capture neutron activation analysis experiment for colleges and universities in the Rocky Mountain and other high-elevation regions that do not possess a license from the Nuclear Regulatory Commission to handle radioactive material.

### **Nuclear Data Measurements for Prompt ( $n, n'\gamma$ )**

To conduct quantitative PGNAA on complex matrixes such as hazardous, mixed, and radioactive waste, it is necessary to use modeling codes to guide and assist in the calibration and analysis of the acquired spectral data due to the inherent nonlinearity of the interactions. For these reasons, accurate neutron capture and inelastic cross sections and  $\gamma$ -ray production rates, as a function of neutron energy, are needed by the Monte Carlo neutron modeling codes because the scattering and absorption cross sections vary as a function of neutron energy. The neutron energies of particular interest and for which there is a paucity of data are for neutron energies above

thermal and extending to approximately 14 MeV. Neutron data for many of the elements of interest and the  $\gamma$ -ray production rates of importance in modeling PGNAA experiments have been acquired but not necessarily analyzed by the LANL staff. Ron Nelson of LANL provided the INEEL with this data for the elemental targets boron, magnesium, titanium, sulfur, and manganese. These data were collected at LANSCE by an HPGe detector system at the Weapons Neutron Research (WNR) facility from which neutron inelastic scatter  $\gamma$ -ray production rates can be extracted. But these data were not analyzed due to the different interests and priorities of the Los Alamos staff. The above analyses of these data over the energy range of interest to the INEEL were completed in FY 2001. A recent subcontract was let to LANL to provide the remaining data they have on inelastic neutron scatter of 1 to 14 MeV neutrons of interest to the INEEL. We anticipate receiving this data in early FY 2002. When complete, the analyzed data will be placed in a tabular form suitable for use by the calculational codes to better predict the interactions of the interrogating neutrons, emitted photons, and the effects of the waste matrix.

Because the data collected by Los Alamos staff does not include all of the elements of interest (especially detector materials Ge and NaI) to the INEEL, a proposal was written during FY 2001 and a more detailed presentation was made to the LANSCE User Program Advisory committee (PAC) to request beam time on the LANSCE facility. This was only the second time that our organization developed an accepted proposal to use the LANSCE facility with the first being in the mid 1980's to assist Los Alamos personnel in developing a helium-jet transport system on the beam line in Area B for the study of short half-life neutron deficient radionuclides near the proton drip line. Our present proposal was approved and beam time scheduled for summer 2001 and again for November 2001. Preparation for these measurements was carried out with the understanding that Los Alamos could provide some of the detectors and instrumentation. Initial experience from the beam time received this summer indicated that we are best to take our own instrumentation that we have previously tested at the INEEL.

Thermal neutron capture production cross sections for materials comprising NaI(Tl) scintillation detectors and HPGe detectors were initiated at the North Carolina State University (NCSU) Pulsar reactor. Both singles and coincidence data were collected using the reactor's external thermal neutron beam. The purpose of the coincidence data was to obtain additional information on the weak gamma-ray transitions that are lost in the singles spectra continua, but hopefully observed in the coincidence data so that they can be accounted for in the depopulation of the excited levels of the capture isotope. Data on several elements including NaI, S, Fe, Cu, Ge and In were successfully collected. Data on Ge and NaI(Tl) is still needed and especially important since it includes the material of which the detectors are comprised. This data will be used to more accurately model PGNAA experiments and their analyses. Unfortunately, these measurements were not completed and their analysis has been delayed due to the unexpected retirement of the principal Investigator, the failure of one of the HPGe detectors, and failure during the experiment of the NCSU reactor.

Preliminary analysis of the sulfur spectra has been accomplished with the assignment of six  $\gamma$ -ray transitions from the capture state. The coincidence spectra are required for the identification and assignment of additional previously unreported transitions from the capture state. Analyses of single spectra of the other targets is continuing. Software is presently unavailable for the analysis of the coincidence spectra.

Prior to completing a collaboration agreement with Anton Tonchev at Idaho State University at the end of the last fiscal year to study the high-spin states created by the excitation of the radionuclide  $^{108m}\text{Ag}$ , Dr. Tonchev left Idaho State University. He accepted a research scientist position at the Triangle Universities Nuclear Laboratory (TUNL) at Duke University. Physics staff at ISU, interested in studying the high-spin states that may be excited from a target of  $^{108m}\text{Ag}$ , have submitted a proposal to the National Science Foundation with several INEEL staff listed as collaborators. This work offers interesting research in nuclear structure physics and would be desirable to pursue.

We are in the fortunate position of possessing about 20  $\mu\text{Ci}$  of high-purity  $^{108m}\text{Ag}$  that initially was considered a contaminant and now remains after the decay of millicurie amounts of shorter-lived  $^{110m}\text{Ag}$ .

We have received tentative approval for our proposed measurements of the radiations from  $\alpha$ -induced ( $\alpha, n$ ) and ( $\alpha, p$ ) reactions for low  $Z$  elements at the University of Kentucky this fall. These measurements will supplement those made at the INEEL with  $\text{CaF}_2$  using the  $\alpha$  decay of  $^{244}\text{Cm}$  as the source of excitation. These experiments will permit the measurement of  $\alpha$ -induced reactions and the associated  $n/\gamma$  intensity ratios resulting from these reactions on elements for which we lack data and for which this data is needed if a radioanalytical method to measure neutrons due exclusively to the  $\alpha$ -induced reactions is to be developed.

## Methods Development

This subtask is designed to provide a mechanism by which more accurate and dependable measurements can be made as a result of improved counting and analysis methods development. It also provides a mechanism to better understand the idiosyncrasies encountered throughout the entire  $\gamma$ -ray spectrometry process from detection through to analysis such as detector response as a function of crystal location at which  $\gamma$ -ray interactions occur. The following are the method development studies performed in FY 2001.

**High Accuracy Efficiency Measurements.** During FY 2001, further progress was made in the development of measurement methods and in the use of Monte Carlo electron and photon transport codes to more accurately determine the efficiency of Ge semiconductor  $\gamma$ -ray detectors. In the past, the most precise measurements of relative  $\gamma$ -ray emission rates from a radioactive source with a Ge semiconductor detector were limited to the accuracy of the detector efficiency curve. This limit was about 0.5% from 100 to 2,000 keV and 1.0% below 100 keV. In 1997 a paper from the University of Michigan by A. I. Hawari<sup>16</sup> described a measurement method to develop an efficiency curve with a precision of about 0.1%

over a limited energy range, 660–1,330 keV in this case. Our involvement in this development began in 2000 when R. G. Helmer and M. Ludington<sup>17</sup> (Albion College; Albion, Michigan) published a paper that extended the work of Hawari in two ways. First, it extended the energy range to 433 to 2,754 keV without any loss in precision. Second, it showed that Monte Carlo electron and photon transport codes could, under suitable conditions, compute the relative detector efficiencies with similar accuracy. Our interest in this work is in making a significant improvement in the capabilities of  $\gamma$ -ray spectrometry for basic nuclear structure research and for applied use. The ability to accurately calculate detector efficiencies will dramatically improve our confidence to calculate efficiencies for large sample geometries that are important in radioanalyses for cleanup operations.

During FY 2001, we joined with Professor John Hardy at Texas A&M University in an effort to develop a precise efficiency curve for his Ge detector and to extend this technique to below 70 keV. Prof. Hardy needs this capability to carry out measurements that are important in the testing of the theory of beta decay. In this work, Prof. Hardy and his students have carried out the measurements and R. G. Helmer has carried out Monte Carlo calculations. The concept is to carry out measurements with radioactive sources that have well known ratios of the emission probabilities of a few  $\gamma$ -rays, and thereby, obtain a very accurate measurement of the relative detector efficiencies at these energies. Then the absolute efficiencies computed by the Monte Carlo method can be used as an aid to normalize all of the measured efficiency ratios to the same scale. In the work completed so far, seven radioactive nuclides have been used. Once a sufficiently accurate set of detector parameters have been determined, the utility of this method is that the Monte Carlo calculated results can be used as an interpolation method to give the shape of the efficiency curve in any energy region. The Monte Carlo results can also provide for accurate corrections for the experimental geometry when small changes are made in the geometry.

At our request, the German radiation standards group at the Physikalisch-Technische Bundesanstalt (PTB), Braunschweig, Germany

produced two sources of  $^{60}\text{Co}$  for which they were able to determine the activities and  $\gamma$ -ray emission rates with an accuracy of 0.06%. Only a source measured to an accuracy of <0.1% can test the ability to calculate efficiencies to an accuracy of <0.2%. These sources, which would be very expensive on the commercial market, were provided free of charge as a contribution to our research effort. The results from the measurements with these two sources were used to normalize the relative shape of the efficiency curve to absolute efficiencies (counts per net peak area).

To carry out accurate Monte Carlo calculations, one needs to know the specifications for the Ge detector. Although the manufacturer provides these with the detector, they are nominal values lacking precision (see also study reported below on detector specifications). Collimated beams of  $\gamma$ -rays of 81 and 1,250 keV were used to scan the detector and determine its position within its housing as well as the actual length of the sensitive volume of the detector. This length is about 2 mm shorter than the manufacturer's specifications (an effect of 2.5% at 1,000 keV); this shortening is probably related to processing of the back end. Measurements of the counting rates of 32- and 36-keV x-rays compared to the associated 661-keV  $\gamma$ -rays from  $^{137}\text{Cs}$  were used to determine the first estimate of the actual thickness of the dead layer of Ge on the front of the detector. Many comparisons have been made between the Monte Carlo calculated and measured efficiencies to adjust other detector specifications and improve the agreement. It was also necessary to hold several conversations with the detector manufacturer to determine if our adjustments of the specifications are realistic in terms of their knowledge of their detector manufacturing process. The magnitude of these deviations in the Ge crystal dimensions and position within the cryostat from company specifications can cause a significant error in calculated efficiencies, and hence, measured  $\gamma$ -ray emission rates. The adjustments of the detector parameters resulted in changes in the calculated efficiencies of ~14% at 32 keV, ~4% at 200 keV, and ~9% at 1,836 keV compared to these with original specifications. These changes are very significant compared to our goal of ~0.1% accuracy.

The results of our first complete comparison of a set of measured efficiency data and a set of Monte Carlo calculations for a source-detector distance of 15 cm was presented at the biennial symposium of the International Committee on Radionuclide Metrology.<sup>18</sup> This meeting was held at PTB in Germany, and will be published in *Nuclear Instruments and Methods*. The conclusion in this paper is that, between 200 and 1,836 keV, the deduced relative efficiency curve is accurate to 0.2%, and between 50 and 200 keV it is accurate to 0.4% and the absolute efficiency curve has a comparable uncertainty. These results demonstrate that nuclear structure problems requiring measured accuracies of 0.2% can be addressed, and that the Monte Carlo code describes the physics accurately over this energy range (50 to 1,836 keV).

At the same time this level of precision was obtained for the measurements at 15 cm, it was determined that the measured efficiencies at 100 cm differed from the calculated values by 1%. The interesting fact in this case was that this difference was independent of the  $\gamma$ -ray energy. Hence, a total understanding of the physics of interactions or of the true dimensions of the detector and its mount have not yet been achieved.

**Detector specifications.** With the increasing use of Monte Carlo electron/photon transport codes to calculate detector efficiencies, especially for extended sources (an extended source is one whose dimensions extend beyond that of a source that can simulate a “point” source and have more than a negligible solid angle with respect to the detector) a study was undertaken to determine whether the manufacturer’s quoted detector specifications are sufficient and known to the accuracy required to calculate the detector efficiency. Since these calculations apply to ideal detectors, less than optimal crystals and poor or uneven charge collection are undesirable. The calculation of peak efficiencies, especially above 1 MeV, requires that the dimensions of the active volume of the detector crystal and all of the materials surrounding the crystal be known. We unless specifically requested. While peak shapes of FWTM/FWHM = 1.9 and FWFm/FWHM = 2.7 for a peak at 1,332 keV are commonly achieved in large manufactured detectors, which compare favorably with the true

have observed differences of ~20% at 1 MeV between the physical and the active dimensions for detectors of essentially the same physical size (diameter and thickness) as deduced from the difference in the measured and calculated peak efficiencies. It is therefore prudent for the user to request the manufacturer to provide physical and active detector dimensions or, alternately, at least the detector relative efficiency at 1,332 keV, if efficiencies are to be accurately calculated.

To determine the reason(s) for this difference the detector crystals were scanned across the diameter and along the side with collimated sources of <sup>145</sup>Pm and <sup>232</sup>U (and progeny) to map the active volumes of crystals of the same quoted dimensions. Differences in the active volumes were found at the back end of the crystal that we attribute to poor charge collection or modifications to the crystal during its manufacture. Efforts by the manufacturer to improve charge collection by the use of machined grooves or rounded edges helped the charge collection but modified the detector crystal dimensions and hence, the efficiency, especially at the higher energies. The loss of detector efficiency across the center coaxial hole was also observed.

Finally, it was noted that detectors of the same size did not necessarily have the same recommended bias voltage. In one test of one detector we found that the efficiency at the higher energies was increased about 4% when the bias voltage was raised from -2,000 to -2,800 V.

In a companion study, we investigated the peak shape for large coaxial detectors beyond 1,332 keV. The peak shape is usually characterized by the full width at half maximum (FWHM), full width at tenth maximum (FWTM), and full width at fiftieth maximum (FWFM). The manufacturer normally does not quote the energy resolution, peak shape (i.e., FWFm/FWHM), or the peak efficiency above 1,332 keV [e.g., at 2,614 keV (<sup>208</sup>Tl)] for large coaxial Ge detectors

Gaussian values, FWTM/FWHM = 2.1 and FWFm/FWHM = 3.6 for a peak at 2,614 keV are marginally acceptable but not preferred. One reason for this change in peak shape at higher energies above ~1,332 keV is believed to be due to

the coaxial hole drilled in the center of the coaxial crystal. Whether it is possible to provide good peak shape without impacting the peak energy resolution is a challenge for the manufacturer. These results were reported at the 2001 Annual Meeting of the American Nuclear Society (ANS) held in Milwaukee, WI.<sup>19</sup>

### **Modeling Detectors for High-energy $\gamma$ -Ray Response**

This study entailed an investigation into the ability of version 4XU of the Monte Carlo N-Particle (MCNP) transport code, and Version 3 of the CYLTRAN Integrated Tiger Series transport code to accurately calculate gamma-ray spectra resulting from high-energy  $\gamma$ -rays (1.5 to 9 MeV) interacting in HPGe detectors. Some differences were found between the results generated by MCNP and by CYLTRAN. In particular, although both codes give comparable total efficiencies, the peak efficiencies differed. Further, unexpected differences in escape peak and in the annihilation radiation peak at 511-keV were found. Investigations of the cross sections used by the two codes could not resolve these differences. For the bare detector (no collimator or shielding present), the total efficiencies calculated by the two codes agreed to within 1% for all cases (0.5 to 9 MeV). However, the areas of the full-energy peak (FEP) calculated by CYLTRAN were consistently higher than those calculated by MCNP, which difference increased with  $\gamma$ -ray energy (varying from ~6% at 0.5 MeV to ~25% at 9 MeV). The ratio of the single escape peak (SEP) to the area of the FEP and the ratio of the area of the double escape peak (DEP) to the area of the FEP also differed. At 2.223 MeV, both CYLTRAN and MCNP gave comparable SEP/FEP and DEP/FEP ratios. However, for 6- to 9-MeV  $\gamma$ -rays, the ratios predicted by MCNP were 10% or more higher than those predicted by CYLTRAN. This difference appears to increase with  $\gamma$ -ray energy. In addition, near the pair production threshold (1.173 MeV), CYLTRAN predicted definite single and double escape peaks, while MCNP predicted a possible very weak SEP and no DEP. A measured spectrum of  $^{60}\text{Co}$  (1.173-MeV  $\gamma$ -ray peak) from the detector modeled showed a very small SEP but no definite DEP. These results were presented at the ANS Annual Meeting held last June in Milwaukee, WI.<sup>20</sup>

## **ACCOMPLISHMENTS**

We observed the 1,280-keV  $\gamma$ -ray from the decay of 0.16 microsecond  $^{134\text{m}}\text{Te}$  from the spontaneous fission of  $^{240}\text{Pu}$ ,  $^{244}\text{Cm}$  and  $^{252}\text{Cf}$ . This peak can be used to directly identify the amount of  $^{240}\text{Pu}$  present in TRU waste and deduce the total amount of Pu from the Pu isotopic abundances. When the TRU waste is dominated by plutonium, this method of TRU assay may be a more direct and simple measurement than present passive/active neutron methods.

We measured the  $n/\gamma$  intensity ratio for the monoisotopic element fluorine resulting from the  $^{19}\text{F}(\alpha, n)^{22}\text{Na}$  reaction; the  $\alpha$ -induced reactions occur in a TRU waste matrix with elements of low atomic number. The gross neutron counting rate minus the neutron counting rate from  $(\alpha, n)$  reactions yields the neutron counting rate from spontaneous fission and the amount of fissile material. This is a valuable tool for assaying TRU waste dominated by  $^{241}\text{Am}$  and for assaying TRU waste from one side.

We used the NCSU pulsar reactor and the LANSCE accelerator to collect data on targets of NaI and Ge (detector materials) and a number of other elements. These measurements were made to obtain improved inelastic and capture production cross sections and to improve the cross section database used by Monte Carlo modeling for quantitative analysis via prompt  $\gamma$ -ray neutron activation analysis.

We significantly improved the accuracy of Ge detector efficiency measurements to 0.1 to 0.2% through very careful Monte Carlo modeling and measurement of accurately known cascade  $\gamma$ -rays and highly accurate standards (<0.1% uncertainty). This improvement permits the measurement of nuclear data to accuracies previously unachievable.

The nuclear structure information provided through the INEEL Gamma-ray Spectrometry Center Web site has been extensively used at the INEEL and throughout the DOE complex. It has been a resource to many involved in waste characterization, decontamination, and decommissioning of DOE facilities and sites, and environmental remediation.

## Publications

### Accepted or Published

Gehrke, R. J., J. D. Baker, and C. L.O. Riddle, "Feeding of the  $^{232}\text{Th}$  Levels from the Decay of  $^{236}\text{U}$ ," accepted for publication in *Intern. J. Appl. Radiat. Isot.*

Gehrke, R. J., J. R. Davidson, P. J. Taylor, R. G. Helmer, and J. W. Mandler, "Radioactinide Additions to the Electronic Gamma-ray Spectrum Catalogue," *Journal of Radioanalytical and Nuclear Chemistry*, Vol. 248, 2001, p. 417.

Gehrke, R. J., M. C. Chisolm, and E. B. Nieschmidt, "Prompt Gamma-Ray Neutron Activation Analysis Without the Neutron Source: Experiments for Small Colleges," *Transactions of the American Nuclear Society*, Vol. 81, 2000, p. 488.

Gehrke, R. J., R. P. Keegan, and P. J. Taylor, "Specifications for Today's Coaxial HPGe Detectors," *Transactions of the American Nuclear Society*, Vol. 82, 2001, p. 329.

Lamont, S. P., R. J. Gehrke, S. E. Glover, and R. H. Filby, "Precise Determination of the Intensity of  $^{226}\text{Ra}$  Alpha Decay to the 186-keV Excited State," *Journal of Radioanalytical and Nuclear Chemistry*, Vol. 248, 2001, p. 247.

Ludington, M. A., and R. G. Helmer, "High-Accuracy Measurements and Monte Carlo Calculations of the Relative Efficiency Curve for an HPGe Detector from 433 to 2,754 keV," *Nucl. Instrum. Methods Phys. Res., Section A*, Vol. 466, 2000, p. 446.

Mandler, J. W., and R. G. Helmer, "Modeling Detectors for High-Energy Gamma-Ray Response," *Transactions of the American Nuclear Society*, Vol. 82, 2001, p. 330.

### Presentations

Davidson, J. R., and R. J. Gehrke, "Developing a Web Site of the Gamma-Ray Spectrometry Data for Actinide Nuclei," *25th Actinide Separations Conference, May 2001 in Boise, Idaho.*

Davidson, J. R., et al., *Presentation made in Boise in April at the Actinides Separation Conference.*

Gehrke, R. J., "The INEEL Gamma-ray Spectrometry Center Web Site with Actinide Spectra," *25th Actinide Separations Conference, May 2001 in Boise, Idaho.*

Gehrke, R. J., et al., *Presentation made in Boise in April at the Actinides Separation Conference.*

Gehrke, R. J., J. W. Mandler, R. G. Helmer, and J. R. Davidson, "Extension of the Electronic Gamma-Ray Spectrum Catalogue Web Site," *Proceedings of the 16th International Conference on the Application of Accelerators in Research and Industry (CAARI 2000), Nov. 1-4, 2000 at North Texas State University in Denton, TX.*

Hardy, J. C., et al., "Precise Efficiency Calibration of an HPGe Detector: Source Measurements and Monte Carlo Calibration with Subpercent Precision," *Proceedings of the ICRM 2001 Symposium, Braunschweig, Germany, May 2001.*

## REFERENCES

1. F. Boehm and C. S. Wu, "Internal Bremsstrahlung and Ionization Accompanying Beta Decay," *Phys. Rev.*, Vol. 93, No. 3, 1954, p. 518.
2. J. Law and A. Suzuki, "Orbital K-electron Shakeoff in  $\beta$  Decay," *Phys. Rev. C*, Vol. 25, No. 1, 1982, p. 514.
3. C. Ardisson, J. Dalmaso, and G. Ardisson, " $^{234}\text{U}$  excited states fed in the  $\beta$  decay of  $^{234}\text{Pa}$ ," *Phys. Rev. C*, Vol. 33, No. 6, 1986, p. 2,132.

4. I. Adsley, J. S. Backhouse, A. L. Nichols, and J. Toole, "U-238 Decay Chain: Resolution of Observed Anomalies in the Measured Secular Equilibrium Between Th-234 and Daughter Pa-234m," *Jour. of Appl. Radiat. Isot.*, Vol. 49, Nos. 9–11, 1998, p. 1337.
5. R. J. Gehrke, J. D. Baker, and C. L. Riddle, "Feeding of the  $^{232}\text{Th}$  Levels from the Decay of  $^{236}\text{U}$ ," accepted for publication in *Intern J. Appl. Radiat. Isot.*
6. R. J. Gehrke, R. Aryaeinejad, K. D. Watts, D. R. Staples, and D. W. Akers, Application of PINS and GNAT to the Assay of 55-gal Containers of Radioactive Waste, EGG-NRE-11236, March 1994.
7. J. D. Cole et al., "Using New Fission Data with the Multi-Detector Analysis System for Spent Nuclear Fuel," Proceedings of the International Conference, Perspectives in Nuclear Physics, J. H. Hamilton, H. K. Carter and R. B. Piercey, editors, World Scientific Publishers, Singapore, New Jersey, London, Hong Kong, 1999, pp. 35–46.
8. S. LaMont, R. J. Gehrke, S. E. Glover, and R. H. Filby, "Precise Determination of the Intensity of  $^{226}\text{Ra}$  Alpha Decay to the 186 keV Excited State," *J. Radioanal. Nucl. Chem.*, Vol. 248, No. 1, 2001, p. 247.
9. W. J. Lin and G. Harbottle, "Gamma-Ray Emission Intensities of  $^{226}\text{Ra}$  In Equilibrium with its Daughter Products," *J. Radioanal. Nucl. Chem.*, Vol. 153, 1991, p. 137.
10. N. Coursol and F. Lagoutine, "Evaluation of Non-neutron Nuclear Data for the  $^{226}\text{Ra}$  Decay Chain," *Intern. J. Appl. Radiation Isotopes*, Vol. 34, 1983, p. 1,269.
11. H. Griffin, "Decay of  $^{49}\text{Ca}$ ," submitted for publication.
12. E. W. Lees and D. Lindley, "Neutron Production from ( $\alpha$ , n) Reactions in  $^{241}\text{AmO}_2$ ," *Annals of Nuclear Energy*, Vol. 5, 1978, p. 133.
13. C. E. Moss and J. T. Caldwell, "Assay of TRU Wastes Containing ( $\alpha$ , n) Sources," Proceedings of the 27th Annual Meeting of the Institute of Nuclear Materials Management, New Orleans, Louisiana, June 22–25, 1986, pp. 427–432.
14. S. Croft, "The Use of Neutron Intensity Calibrated  $^9\text{Be}$  ( $\alpha$ , n) Sources as 4,438 keV Gamma-Ray Reference Standards," *Nuclear Instruction and Methods in Physical Research*, A281, 1989, p.103.
15. R. J. Gehrke, M. C. Chisolm, and E. B. Nieschmidt, "Prompt Gamma-Ray Neutron Activation Analysis Without the Neutron Source: Experiments for Small Colleges," *Transactions of the American Nuclear Society*, Vol. 81, 2000, p. 488.
16. A. I. Hawari, R. F. Fleming, M. A. Ludington, "High-Accuracy Determination of the Relative Full-Energy Peak Efficiency Curve of a Coaxial HPGe Detector in the Energy Region 700–1,300 keV," *Nuclear Instruction and Methods in Physical Research*, A398, 1997, p. 276.
17. M. A. Ludington and R. G. Helmer, "High-Accuracy Measurements and Monte Carlo Calculations of the Relative Efficiency Curve for an HPGe Detector from 433 to 2,754 keV," *Nucl. Instrum. Methods Phys. Res.*, A466, 2000, p. 506.

18. J. C. Hardy, et al., "Precise Efficiency Calibration of An HPGe Detector: Source Measurements and Monte Carlo Calibration with Subpercent Precision, Proceedings of the ICRM 2001 Symposium, Braunschweig, Germany, May 2001.
19. R. J. Gehrke, R. P. Keegan, and P. J. Taylor, "Specifications for Today's Coaxial HPGe Detectors," Transactions of the American Nuclear Society, Vol. 82, 2001, p. 329.
20. J. W. Mandler and R. G. Helmer, "Modeling Detectors for High-Energy Gamma-Ray Response," Transactions of the American *Nuclear Society*, Vol. 82, 2001, p. 330.

# Biocorrosion

Patrick J. Pinhero and Richard N. Wright

## SUMMARY

Microbially-influenced corrosion (MIC) as it relates to the storage of spent nuclear fuel (SNF) is a potential problem of profound significance at the INEEL, and other sites across the DOE complex. Detection and mitigation of MIC in SNF storage, both wet and dry, is the ultimate goal of this task. Supporting goals are to (a) verify that MIC is active and indeed a problem in SNF storage facilities, (b) identify and understand the fundamental corrosion mechanisms inherent to MIC, and (c) design and construct a deployable device that can be used to measure MIC activity in SNF storage environments. These goals are congruent with those of the DOE Office of Environmental Management (DOE-EM) to invest in research and development (R&D) that can provide long-term, cost-effective solutions for dealing with an increasing inventory of nuclear waste. One of the fundamental needs in the MIC field is definitive evidence correlating bacterial activity with corrosion. During FY 2001, our efforts focused on (a) developing spatially-resolved redox-sensitive probes for quantifying electrochemical activity on alloy surfaces at local sites, (b) investigating species specific fluorescent probes that can be used to correlate individual bacteria with corrosion activity, and (c) fabricating robust devices for measuring MIC activity pertinent to long-term storage. A new capability, scanning electrochemical microscopy (SECM), was developed for characterizing localized corrosion processes. Two fundamental studies were completed with the SECM to prove its utility in studying the dynamics of corrosion. Additionally, expertise developed through this ESR program is being applied to the National Spent Nuclear Fuel Program (NSNFP), the Tanks Focus Area (TFA), and a DOE-BES sponsored Synthesis and Processing Center (S&P Center) on "The Science of Localized Corrosion".

## PROJECT DESCRIPTION

DOE is the custodian of several thousand metric tons of SNF, primarily as a result of experimental nuclear reactor development and Naval Reactor activities during the Cold War. This stockpile also includes fuel from energy research and naval reactors. The long-term containment performance of the fuel under storage and disposal conditions is uncertain. These uncertainties have a direct bearing on DOE's ability to license disposal methods. The DOE-EM emphasizes the fundamental need to identify mechanisms that may adversely affect the performance of the fuel package during storage. Deleterious effects recognized as being incompletely characterized include corrosion and degradation rates for the fuel matrices; mechanisms that may lead to accelerated degradation of containers; and the effects of microbes on fuel packages.

MIC is a known problem in various industries; for example, severe biofouling occurs in transport piping used in the petroleum industry. Sulfate-reducing bacteria (SRB) are particularly important because they are responsible for souring of oil and for MIC. Water content of just 1% is adequate to support substantial development of SRBs within a few weeks. The INEEL uses large "swimming pools" of water to temporarily store and cool SNF before it is processed and transported to final storage. Before being transported to a repository for final disposition, the SNF is dried and placed in appropriate transport containers. Prior research examined the viability of bacteria and their ability to form biofilms in radiation-rich environments. As is demonstrated in the following sections, our FY 2001 research focused on developing tools to interrogate potential links between microbial activity and their associated chemical redox mechanisms with areas of localized (pitting) corrosion. Pitting is the most aggressive but least understood type of corrosion. It is believed to be the process by which bacteria degrade materials.

During FY 2001, we studied two very different types of spatial probes and their potential for being coupled to each other—electrochemical probes that use scanning electrochemical microscopy (SECM), and bacteria-embedded fluorescent probes. In brief, SECM is a scanning probe technique that allows one to quantitatively measure local redox activity at distinct sites on a specimen surface, and fluorescence-based techniques, such as fluorescent in situ hybridization (FISH) and green fluorescent protein (GFP), potentially allow for the association of unique bacterial species with an observed corrosion site or redox activity. FISH is the more selective technique of the two, since the fluorophore is bound to a species unique segment of bacterial DNA. The disadvantage of FISH is that it requires the immobilization or fixation of bacteria, which means they are not in situ. GFP techniques hold greater promise because they do not require immobilization and it is believed that a given fluorophore can be passed intergenerationally (up to 4 generations). The drawback for GFPs is that there are only around five unique probes available, and their species selectivity is not as pronounced as FISH.

An additional facet of this report is the consideration of research aimed at developing a deployable remote sensor designed to examine corrosion processes inside SNF packages—two studies are discussed. The first focuses on using an SECM like dynamic measurement to monitor electrochemical activity on a specimen's surface, the second focuses on developing low-cost electrode materials for use in monitoring activity over extremely long periods.

## **Localized Electrochemical Probes for Biocorrosion**

Much of our effort during FY 2001 was devoted to developing two-dimensional (2-D) imaging techniques for measuring localized redox variations associated with MIC. Research in this area is by no means exclusive to the INEEL, though very few groups apply these techniques to corrosion, and virtually no group has applied them to biocorrosion. Currently, there are two methods for imaging local activity at an electroactive site

on a working electrode. The Scanning Reference Electrode Technique (SRET) is a four electrode technique consisting of a working electrode (specimen of interest), a counter electrode, and two reference electrodes. One of the reference electrodes defines the potential of the electrochemical cell, the other is a 30  $\mu\text{m}$  diameter platinum (Pt) microelectrode that is vibrated normal to the surface with an amplitude of approximately 30  $\mu\text{m}$  and a frequency on the order of kilohertz (kHz). In addition to vibrating normal to the surface, it translates through a mean ( $\pm 15 \mu\text{m}$ ) x-y plane parallel to the working electrode. The SRET technique is based on the gradient nature of an electric field associated with current flow (the infamous "IR drop"). At electroactive sites, the flow of charged species is defined by a set of isopotentials extending into the solution (electrolyte). Theoretically, these isopotentials are a fundamental function of both the magnitude of flow from the electroactive site (point source) and its geometric shape. The problem with SRET is the difficulty calibrating a measured current density.

The SECM method was developed about a decade ago. A handful of papers, including two submitted by our group, detailed the use of SECM in characterizing localized corrosion processes. SECM, like SRET, is a four electrode electrochemical technique. The primary difference is that instead of employing a second reference electrode for determining isopotentials emanating from a corrosion site, SECM uses a second working electrode (ultramicroelectrode [UME] tip) that can be polarized independent of the specimen. In our configuration, we use an 8  $\mu\text{m}$  carbon fiber electrically insulated in heat cured epoxy resin as our UME tip. Prior to measurement, the insulated fiber is cleaved to expose an 8  $\mu\text{m}$  disc at its extreme tip. The disc is translated in a plane displaced less than one diffusion length (defined by the diameter of the tip electrode) from the specimen, and oriented parallel to the surface of interest. In our experiments, the SECM is operated in a potentiometric substrate generation/tip collection (SG/TC) mode, where the tip acts as a current collector and travels within a thick diffusion layer generated by specimen electrode.

The next section describes the two studies completed in FY 2001 by the biocorrosion program to determine the utility of SECM in studying biocorrosion processes. Baseline studies were performed with Type 304 stainless steel because of a larger amount of peer reviewed literature devoted to stainless steels than the other two alloys on which we have focused in prior years, namely Aluminum Alloy 6061-T6 and Zircaloy 4.

## Scanning Electrochemical Microscopy (SECM)

Once the scanning electrochemical microscopy (SECM) was constructed (February 2001) we chose to evaluate our system using a recently published study by Paik et al.<sup>1</sup> This seemed a good place to start since the study focused on the dissolution of manganese sulfide (MnS) inclusions in Type 304 stainless steel. From the perspective of biocorrosion, it is even more relevant due to the connection between sulfate reducing bacteria (SRB) and MIC processes.<sup>2</sup> Using SECM, the detection of localized dissolved sulfide could be correlated with SRB activity, thus providing a tool for the study of what is considered the most common type of steel biocorrosion. Two probes considered for the detection of sulfide are an iodide/triiodide ( $I^-/I_3^-$ ) mediated detection scheme developed by Paik et al. (Reference 1) and commercially available hydrogen sulfide ( $H_2S$ ) amperometric microelectrode sensors.

Experimentally,  $I_3^-$  is used as a mediator species, generated by oxidation of  $I^-$  at the microelectrode. In the presence of sulfide ( $S^{2-}$ ) or thiosulfate ( $S_2O_3^{2-}$ ) ions,  $I_3^-$  is oxidized back to  $I^-$ , resulting in an amplification of the background current at the microelectrode for  $I^-$  oxidation. As mentioned previously, the corrosion of stainless steel is proposed to occur at dissolving MnS inclusions which produces an undetermined sulfur species, likely  $HS^-$  or  $S_2O_3^{2-}$ . Our initial investigations were able to reproduce the results illustrated in Figure 1. This site of localized sulfur (S) concentration was observed while polarizing the sample galvanostatically at  $100 \mu A/cm^2$  which correlated with a potential of approximately 250 mV vs. Ag/AgCl (after initially rising into the

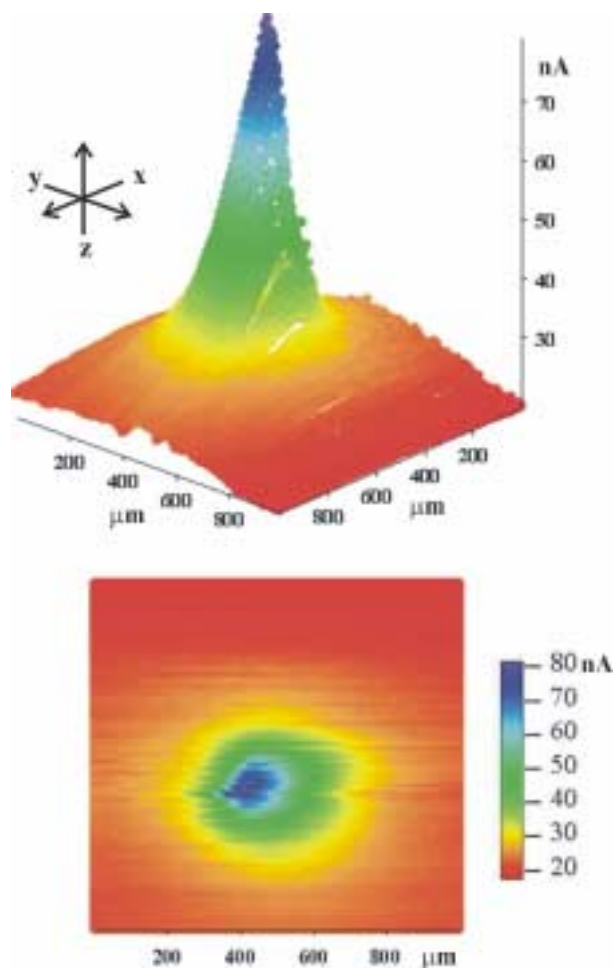


Figure 1. SECM images of dissolved sulfur above a 304 SS surface. The microelectrode was held at 600 mV and the sample current was  $100 \mu A$ . The top panel is a 3-D perspective image displaying the shape of the current response registered at the SECM tip; the lower panel is a birds-eye view of the distribution of current across the surface and active site, from  $y = 0$  (bottom of image) to  $y = 1,000 \mu m$  (top of image).

pitting region at about 400 mV for a short time period). At these low current densities, we were able to image sites which varied from less than 2 nA to over 80 nA above the background  $I^-$  oxidation. The philosophy of using galvanostatic polarization instead of potentiostatic polarization was that the total corrosion rate could be forced to remain constant during the course of a SECM scan, and distribution of this current through individual active sites could be spatially resolved

and quantified. Additionally, we found potentiostatic methods more experimentally complicated in this system due to pitting and increased current generation through the active pits with time. Paik et al. (Reference 1) performed the experiment potentiostatically by polarizing near the breakdown potential, then backing the potential to lower values during measurement, which is comparable to a galvanostatic potential versus time trace. In Figure 2A a potential versus time measurement of type 304 SS is made while stepping to progressively higher currents. While

the initial potential excursions are more positive for higher currents, the potential tends to a similar equilibrium value for the currents tested. For comparison, a sample was polarized in a similar fashion in 0.1 M NaCl without KI present. With only NaCl present (Figure 2B) a less positive potential was required to sustain the current passed, thus displaying the passivating effect of KI. At 1  $\mu\text{A}$  current, KI prevented the noise attributed to pitting corrosion, thus higher current was required to achieve breakdown in the samples.

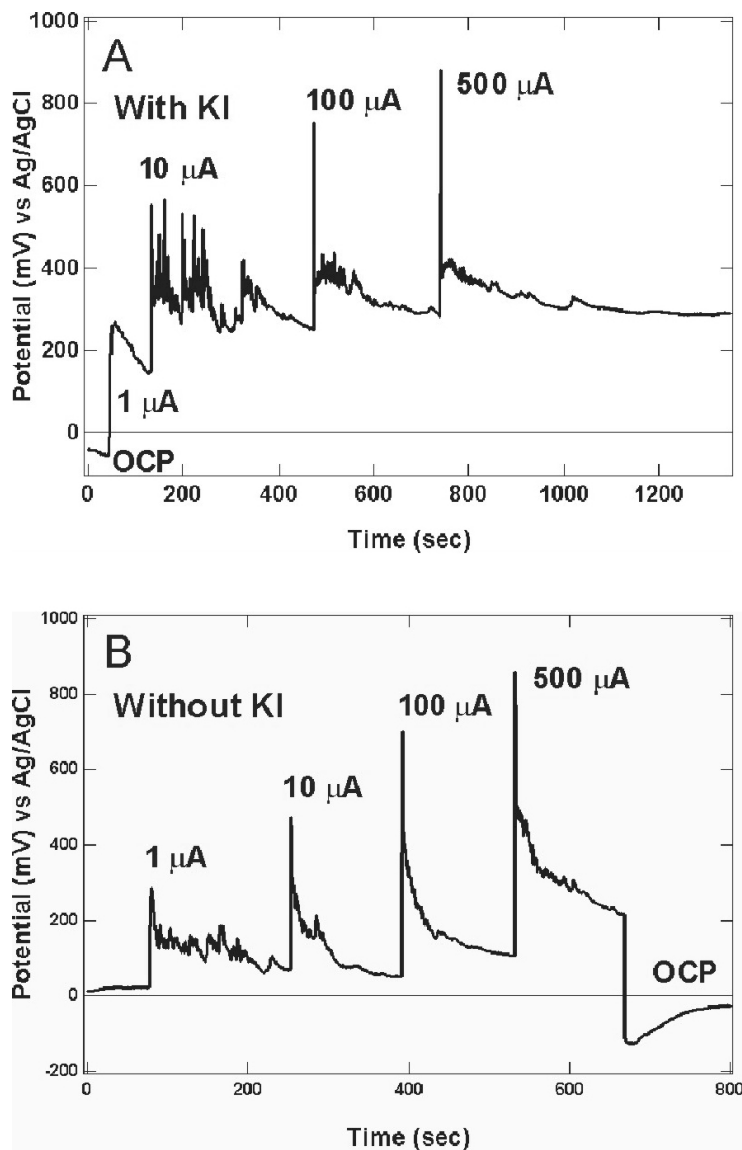


Figure 2. Potential versus time traces of two type 304 SS samples polarized galvanostatically from initial OCP to successively higher currents. Plot A has 10 mM KI added to 0.1 M NaCl electrolyte, Plot B has no KI present.

The SECM study demonstrates its potential utility in examining corrosion processes on exposed surfaces. This is not a phenomena limited to biocorrosion, but extends to all localized corrosion processes such as pitting corrosion, crevice corrosion, stress corrosion cracking (SCC), etc. SECM can be applied to map pH variations across an area as well as map both physical (Figure 3a–d) and chemical (Figure 3e–f) heterogeneities. As is the case with any analytical technique, it does not provide a whole picture, but if coupled (in situ) with the biofluorescence probes being developed in the other part of our project, we may have a complete biocorrosion probe.

### Dynamical SECM

The investigation of corrosion reactions on metal surfaces is a topic of great fundamental interest and helps aid potential applications that may lead to its prevention. Traditionally, corrosion is studied by performing accelerated testing using an external electric field, possibly followed by post-mortem analysis of the surface to determine material loss and morphology. These tests provide knowledge about corrosion rates and

morphological changes in a specimen of interest, but not about the localized dynamics of the corrosion process being studied. This type of information may aid in developing a better fundamental understanding of corrosion processes. Most recently, in situ scanning probe microscopy probes (STM, AFM, SECM) have been developed to allow real-time study of surface reactions at interfaces. In terms of studying pitting corrosion, the SECM appears most suitable to these studies due to its ability to analyze larger areas of a specimen in realistic time intervals. Another advantage of SECM is that it potentially provides chemically specific information about a process. To date, most studies have focused on the localized electrochemical behavior of redox probe molecules for elucidating the role that an oxide layer plays in determining the reactivity of the surface. In a recent study of type 304 SS, we performed SECM imaging measurements over a large area of a specimen surface during the course of several hours. These images show that the surface is not static in its reactivity, but evolves over time. To our knowledge, this behavior, although suggested in some reports, has not been demonstrated in detail, despite its significance.

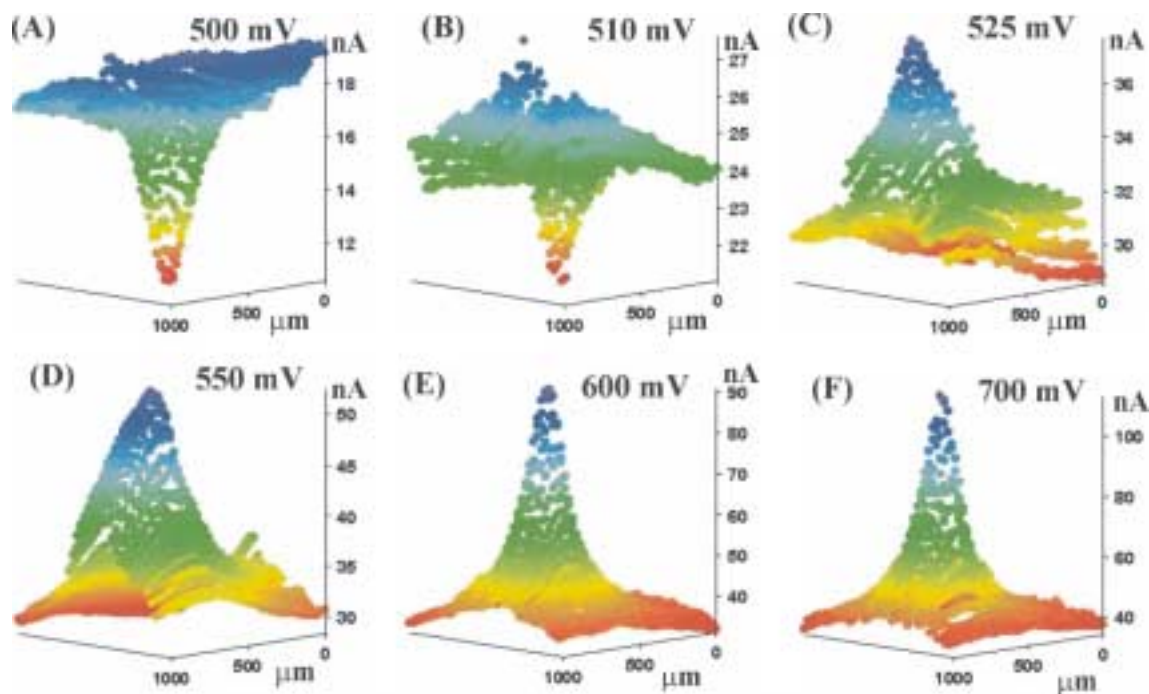


Figure 3. SECM images of active site on 304 SS with 100  $\mu\text{A}$  of applied current at different tip collection potentials: (A) 500 mV, (B) 510 mV, (C) 525 mV, (D) 550 mV, (E) 600 mV, and (F) 700 mV.

During the polarization experiment, we imaged samples repetitively using the SECM probe over a  $3.0\text{ mm} \times 3.0\text{ mm}$  encompassing an area approximately one-third of the total exposed surface area. We took the sequence of 25 images (Figure 4) with a previously unbiased sample following a step from 0 mV to 600 mV, where it was held for the duration of the imaging. In all cases, the active areas (oxidation of I<sup>-</sup>) were spread across the surface, with some areas showing higher activity than others. However, in subsequent images, this activity became localized to a couple of sites with those remaining sites showing increased current densities over those observed in the first scan. We observed this behavior in all samples, with most sites having a temporary nature. We observed that the areas of activity shifted from image-to-image in similar measurements. In some cases, a site that passivated would reactivate at a later time. Eventually, as shown in the final image, the surface passivates completely as evidenced by the absence of surface activity and the total sample current was less than 1  $\mu\text{A}$  in magnitude. This

agrees with the current-time plot in Figure 4 and was observed repeatedly with all samples poised in the 500–600 mV range. We can reactivate the surface by biasing the potential to 100 mV or more positive, resulting in increases in the total sample current and in localized I<sup>-</sup> oxidation activity.

In the above studies, the use of I<sup>-</sup> allowed the surface to remain passive in a potential range where I<sup>-</sup> oxidation could be accessed. To further explore the effect of inhibitors, we added sulfate ions to our solution of 10 mM KI and observed the surface with the microelectrode again tuned to I<sub>3</sub><sup>-</sup> reduction. The addition of sulfate had the expected passivating effect illustrated in Figure 5 where the onset of current is displaced to 800 mV. With the sample held at 900 mV, the sample was imaged five times in sequence as illustrated in Figure 6. At this sample potential, there is some localization of the production of I<sub>3</sub><sup>-</sup> produced. However, the peaks are more like ridges that extend along the fast scan axis in the image (see arrow), very different than the symmetric peaks observed in Figure 4. The symmetric peaks suggest that the I<sub>3</sub><sup>-</sup> is produced at

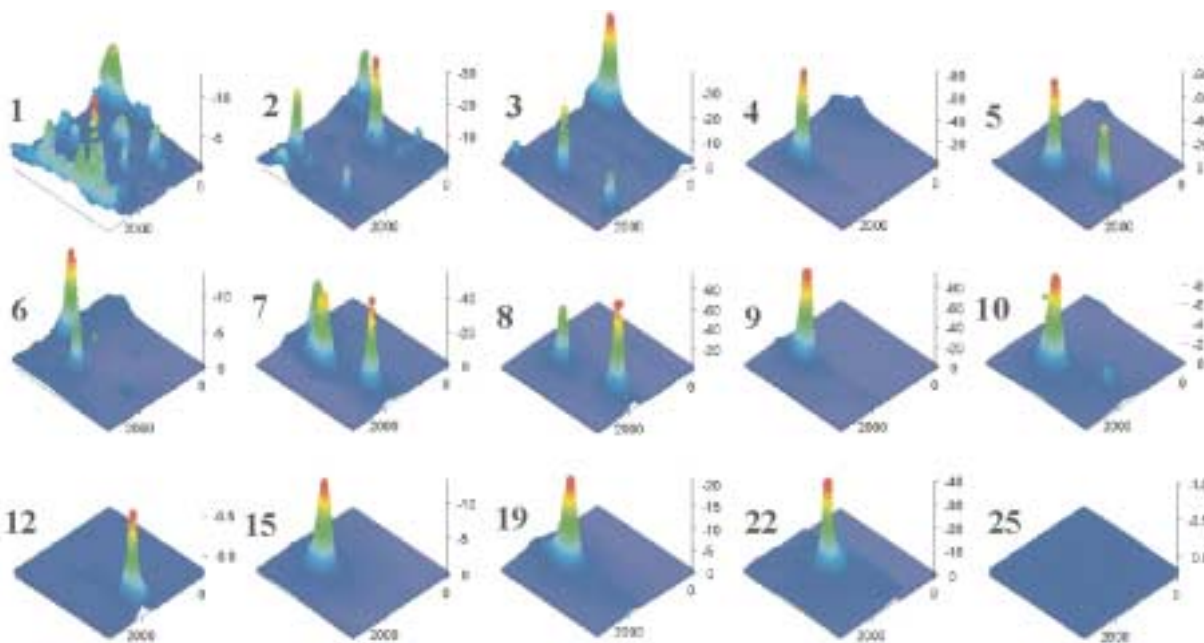


Figure 4. Sequence of SECM images of  $3.0\text{ mm}^2$  area of a fresh type 304 SS sample initiated immediately after jumping potential to 500 mV from 0 mV (near OCP). The current axis (z-axis) is in nanoamps and the x-y axes is in micrometers. A total of 25 images were taken; the first 10 along with selected images of the remainder (number next to plot corresponds to the scan number) are displayed. Each image took 49.8 minutes to acquire; approximately 10 seconds was needed to reset the tip to begin the next image.

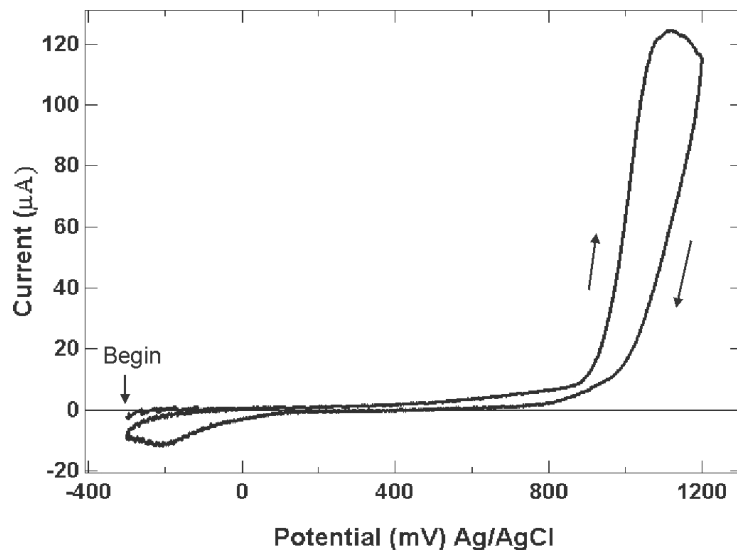


Figure 5. Cyclic Voltammogram of Type 304 SS in 10 mM KI + 0.1 M Na<sub>2</sub>SO<sub>4</sub>. Scan Rate: 5 mV/sec.

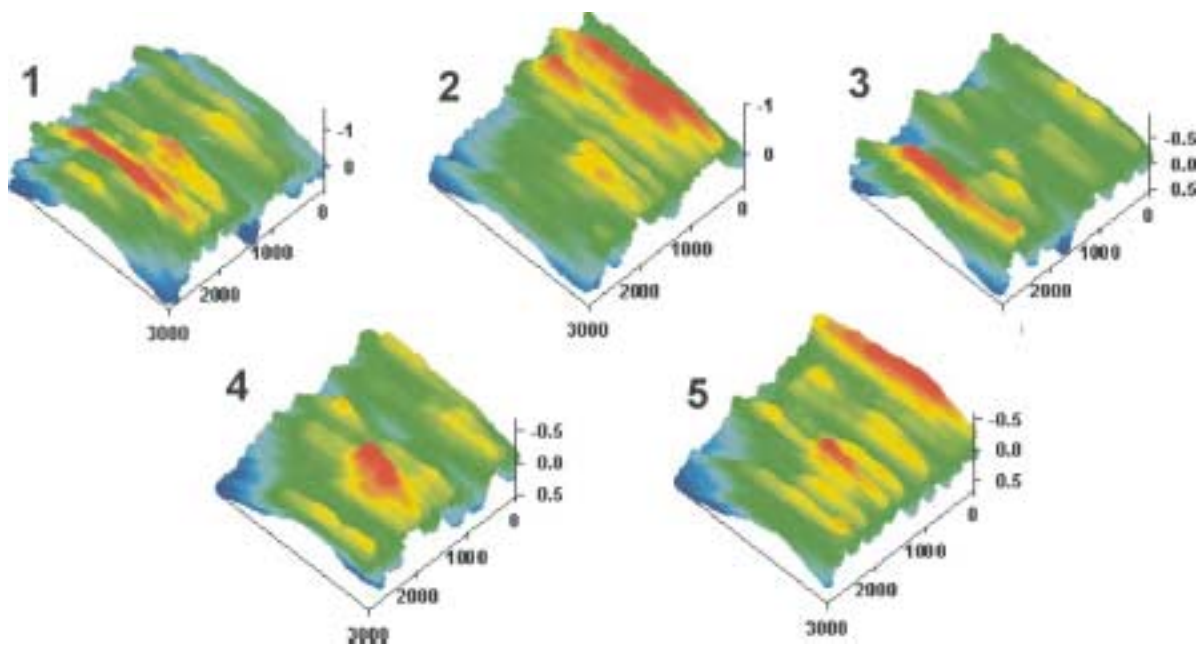


Figure 6. Sequence of SECM images taken in 10 mM KI + 0.1 M Na<sub>2</sub>SO<sub>4</sub> at 800 mV.

one point on the sample and spherical diffusion creates a circular bloom of I<sub>3</sub><sup>-</sup>. The ridges of intensity on the surface suggest that the electrochemical activity on the surface is localized in a much different manner that cannot be captured by our relatively slow probe. Holding the probe in one position over a ridge and measuring the current response (Figure 6) shows that the current fluctuation is quite rapid and may account for the

streaky images observed. Considering that sulfate reduces the pitting of 304 SS, the quick movement of electrochemical activity across the surface might explain the effect sulfate has on the passivation layer.

This study demonstrates the utility of time-dependent SECM and its potential for long-term stewardship applications. The localized effect of

sulfate inhibitors has direct application to biocorrosion where sulfate reducing bacteria (SRBs) are believed to play a prominent role.

## Visual Correlation of Bacteria with Corrosion

Biocorrosion is often characterized indirectly through measurement of accelerated corrosion rates, and direct observation of bacteria in vicinity of a corrosion area. Irrefutable links have not been shown directly. Our program seeks to fill this void through developing species specific biofluorescent probes, and by using triangulation methods for pinpointing local degradation and linking it with a specific bacterial population. The SECM provides us with the necessary probe for observing and measuring localized corrosion. Developing the fluorescent probes will provide the means for observing bacteria. In addition to fluorescent probes, we are continuing to work with electron microscopy and atomic force microscopy in linking bacteria with local degradation sites.

Figure 7 displays *Desulfovibrio desulfuricans* growing on metal coupon stained with DAPI (binds to DNA). Currently, we are developing techniques that will allow us to use selective biofluorescence to identify one species of bacteria in a consortium of many bacteria. The realization of this technique will not only permit us to identify biocorrosion active bacteria, but eventually allow us to identify their presence in SNF storage facilities. If we are able to locate problem bacteria, it will be more cost-effective to treat (mitigate biocorrosion) it remotely in select locations where problems exist, than to treat an entire facility, and possibly introduce other detrimental effects to any corrosion inhibition supplied by biofilms.

We are continuing to make great strides in correlating images obtained from Environmental Scanning Electron Microscopy (ESEM) with local corrosion areas. Figures 8A and B show bacteria located at areas where local corrosion was observed in a new single corrosion cell system. Figure 8A clearly shows some helical SRB microbes, while Figure 8B shows rod shaped *Pseudomonads*.

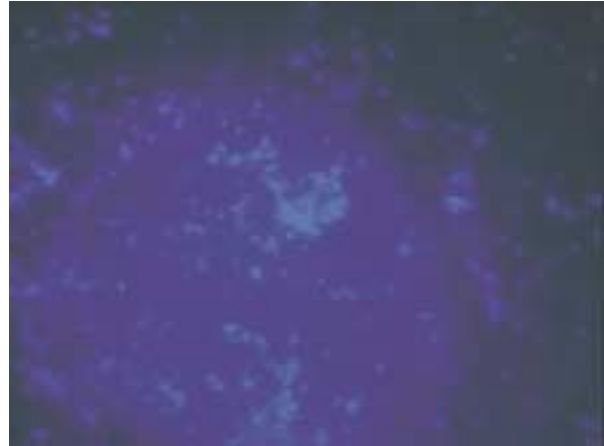


Figure 7. Fluorescent In Situ Hybridization (FISH) of *Desulfovibrio desulfuricans* growing on metal coupon stained with DAPI (binds to DNA).



Figure 8. Environmental SEM (ESEM) micrograph of (A) SRB in region of a local corrosion site, and (B) *Pseudomonas aeruginosa* in vicinity of corrosion site.

## R&D Of Low-Cost Field Deployable Corrosion Sensors

### Low-Cost Stable Microelectrodes (Au Electrodeposited on HOPG)

Our objectives are to (a) fabricate a device that can be introduced into a SNF environment, allowing us to determine if biocorrosion exists and its location, and (b) develop a means for selective mitigation through eradication of problem bacteria from areas where the potential for biocorrosion exists without disrupting stable regions of the storage facility. We are therefore examining stable cost-effective microelectrodes that can be used in SNF storage facilities. Without fail, there are two materials that every electrochemist and/or corrosion scientist considers with respect to stability, gold (Au) and platinum (Pt).

Over the last 20 years a push to miniaturize features for circuit printing, battery technology, chemical sensors, etc., has resulted in nanometer-size features. Many investigations have focused on nanostructures of metals to understand and exploit the differences between these nanostructures and the properties of bulk metals. A variety of methods have been developed to deposit metal structures onto surfaces including thermal vacuum evaporation<sup>3-9</sup> using scanning probe tips for site-specific deposition,<sup>10-13</sup> lithography methods,<sup>14,15</sup> and potential pulse or sweep electrochemical techniques.<sup>16-23</sup>

There are reports on electrochemistry of Au in solution with complex forming anions, such as  $\text{Cl}^-$ ,  $\text{Br}^-$ , and  $\text{CN}^-$  due to Au importance in electrorefining, gold plating, and circuit printing. These reports use a variety of substrates such as Pt,<sup>18</sup> HOPG,<sup>21,22</sup> n-Si, and Au.<sup>24,25</sup> With the exception of Arvia *et al.*<sup>25</sup> where the authors used Au substrates, very little is mentioned in any of these studies about the electrochemical oxidation of Au(0) particles from a native or foreign substrate. Therefore, examination of the fundamental properties governing the surface dynamics, including the forward and reverse processes, could be important in the electronics industry and for the development of new electrochemical sensing devices, such as those we are attempting to

develop for SNF storage, and high-level waste (HLW) tank farms.

In this subsection, we discuss our studies that examine the electrochemical deposition and stripping of Au micro and nanoparticles at a HOPG substrate. For the purpose of this report, we will focus on discussing observations made with respect to freshly cleaved and thermally etched graphite surfaces. It is important to recognize that thermal etching, which induces pitting in the graphite material, is most probably an important state for the graphite SNF in storage. It is also important in examining our UME fibers in SNF storage environments. Additionally, basing multielement UME arrays on HOPG base substrates where we can engineer site defects seems like an ideal way to fabricate corrosion detectors for characterizing SNF packages.

The freshly cleaved surface shown in Figure 9 curve A, had a stripping efficiency of 52.9%, determined by subtracting the charge removed during the oxidation step from the total charge deposited in the initial reduction step. Under these conditions an average stripping efficiency on 10 different fresh HOPG surfaces was found to be  $50.8\% \pm 8.3\%$  (Table 1). This result suggests that a considerable amount of Au(0) remains adsorbed at the HOPG substrate.

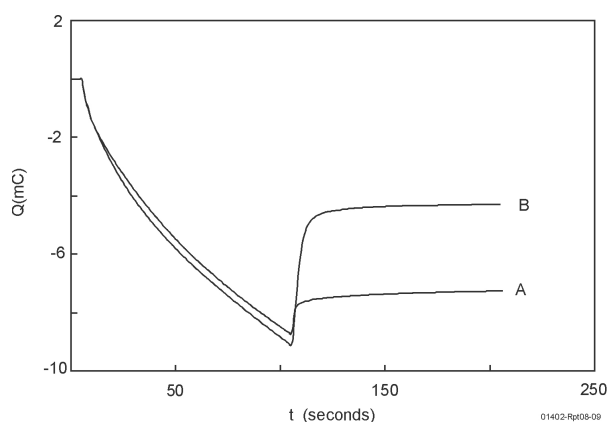


Figure 9. Background subtracted double-step coulometry plots of charge versus time for (A) freshly cleaved HOPG, and (B) thermally etched HOPG. Initially,  $E_i = .700 \text{ V}$  ( $\tau = 0$ ) and the first potential step is to  $E_1 = .250 \text{ V}$  for  $\tau = 100$  seconds. The second potential step is from  $E_1 = .250 \text{ V}$  to  $E_2 = .900 \text{ V}$  for  $t = 100$  seconds.

Table 1. Percentage of electrodeposited Au particles oxidized at HOPG and thermally etched HOPG.

	Percent Oxidized at 0.90 V	Percent Oxidized at 1.00 V	Percent Oxidized at 1.20 V
HOPG	50.8 ± 8.3	72.8 ± 4.1	82.9 ± 4.9
Thermally etched HOPG	25.8 ± 11.8	42.0 ± 14.0	50.2 ± 10.3

Thermally etching the HOPG surface has been shown to create monolayer deep pits with a surface density of 1 to 25  $\mu\text{m}^2$ , which significantly increases the amount of exposed edges and kink sites on the surface. It has been shown that electron-transfer reactions are facile at exposed edge steps and kink sites of the HOPG surface, relative to the basal plane itself. The difference in activity has been established by kinetic studies for soluble redox species, and shown in the morphology of electrochemically deposited metals, and organic polymers. Electron transfer rates are more facile at edges because of increased thermal conductivity for the in-plane axis; while the out-of-plane axis (perpendicular to the basal plane) has a much slower rate of electron transfer ( $\sim 2$  orders of magnitude). In the case of the thermally etched HOPG in Figure 9, the stripping efficiency was dramatically different. Table 1 shows the stripping efficiency for thermally etched HOPG surfaces to be 25.8% ± 11.8%. It also gives the values tabulated for  $E_2 = 1.00$  V and  $E_2 = 1.20$  V for both types of surfaces. Regardless of stripping potential, thermally etched surfaces always retained a greater percentage of the Au(0) initially deposited. This result is surprising due to the known increase in the electron transfer kinetics at step edges discussed earlier. As will be discussed later, microscopy reveals the retention of more Au(0) is the direct result of stabilized nanometer sized particles on the HOPG substrate.

Through the course of this work, SEM micrographs and AFM images were recorded for both deposition and stripping processes as a function of time and surface preparation (freshly cleaved versus thermally oxidized). Figure 10 shows AFM images for the oxidation of Au(0) adsorbed to a freshly cleaved HOPG substrate, (Figures 10A–C), and for a thermally etched HOPG substrate, (Figures 10D–F). For both

sample sets in Figure 10,  $\tau = 100$  seconds at  $E_1 = 0.25$  V, and  $t = 100$  seconds at  $E_2 = 0.90$  V. As evidenced from the SEM micrographs, some large micron size particles remain on the HOPG surface, and these particles are found periodically when using the AFM and large scan areas (20  $\mu\text{m} \times 20 \mu\text{m}$ ). For the higher resolution images shown in Figure 10, the nanometer size particles are predominant. Line scans of the nanometer size particles for the fresh HOPG surface show they have an average height of  $2.2 \pm 0.8$  nm, and are  $\sim 10$  nm in width. The same argument for tip deconvolution can be used here to estimate the width of these nanoparticles. The density of the remaining nanometer size particles was found to be  $3 \pm 1 \times 10^9$  particles/cm<sup>2</sup>. Similarly, the nanometer size particles for the thermally etched surface are  $3.1 \pm 0.8$  nm in height and  $\sim 10$  nm in width. However the density of these particles was found to be  $8 \pm 1 \times 10^9$  particles/cm<sup>2</sup>. The difference in the densities between the two types of substrates was expected based upon the conclusions drawn from the double-step chronocoulometry data discussed earlier. Comparing the basal plane surface density of Figure 10B and the edges and steps of Figure 10E, it can be clearly seen that a greater number of particles still exist on the thermally etched surface of Figure 10E. This difference is consistently seen in numerous samples, and therefore cannot be attributed to variations in sample nucleation density.

The location of the un-oxidized gold particles is also very interesting. In every AFM image recorded, the particles appear to be on top of the step edges and kink sites, rather than on the lower plane and up against the edge itself. This observation contradicts the predictions from the early work of Kossel and Stranski<sup>26</sup> whose “textbook model” suggest that particles

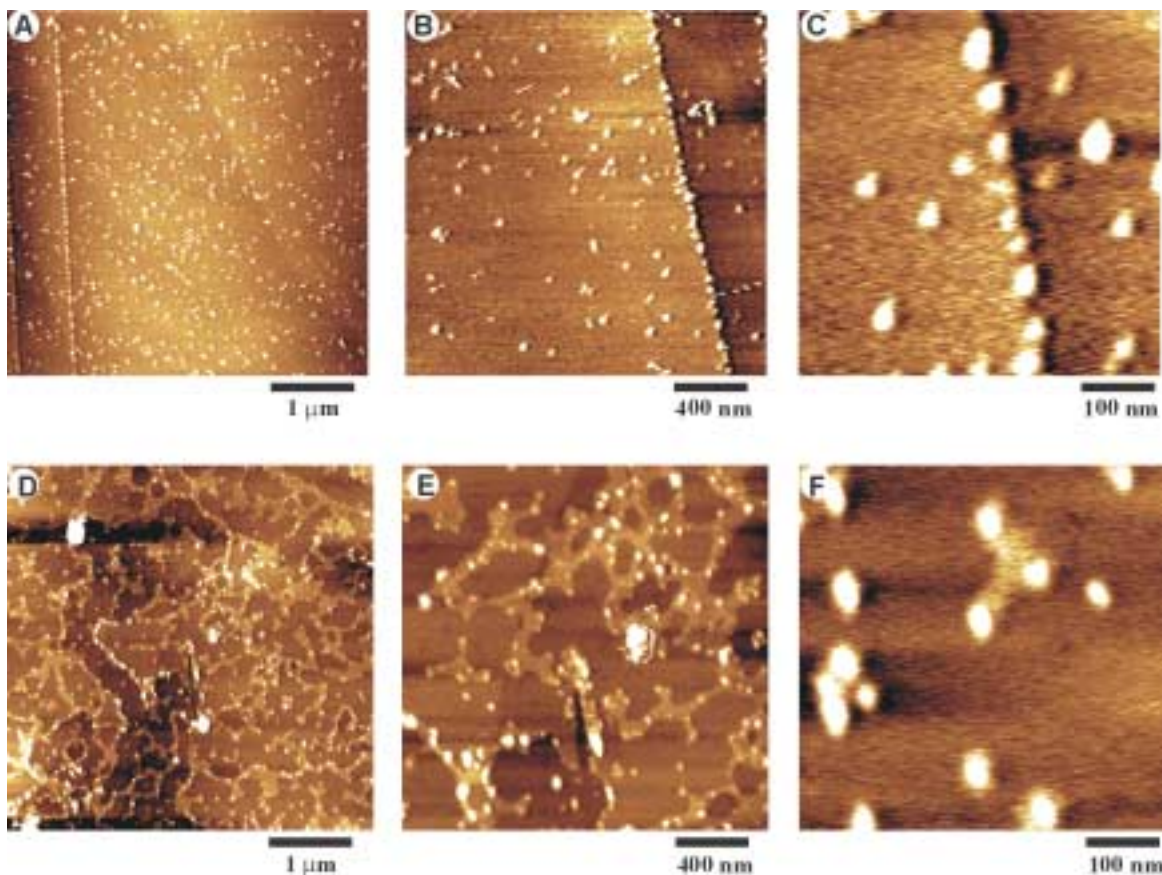


Figure 10. AFM images of Au(0) oxidation using two different HOPG substrates. Au(0) was initially deposited onto both HOPG surfaces by stepping the potential to  $E_1 = .250$  V for  $\tau = 100$  seconds.

preferentially nucleate on the lower surface plane of surface defect sites, such as steps and kink sites. This model is completely analogous to the step-decoration method, used quite frequently for edge decoration transmission electron microscopy experiments (TEM), or edge decoration SEM. A review of the literature showing metal deposition onto foreign and native metal substrates has numerous examples that support the validity of the prediction that metal deposits nucleate on the lower plane of the metal surface. Some examples include Pb deposition on Ag surfaces, Cu deposition onto Au, Ag deposits on Au, and many others. This “textbook model,” also known as the terrace-ledge-kink model (TLK), predicts that deposition should occur first at kink sites, then edge sites, and finally at terraces. This is because on an atomistic level kink sites essentially provide three nearest neighbors in which a nucleated particle of critical size could be coordinated. In

step edges there are two nearest neighbors for the particle to be coordinated to, and a terrace provides only one nearest neighbor in which to bind. Having a higher number of nearest neighbor atoms to bind, translates into a higher coordination for the particle and lowers the thermodynamic free energy of the particle making it more stable on the surface. In electrochemistry an increase in stabilization implies that the potential applied to the substrate to initiate nucleation requires less driving force—terraces require the most negative potential for nucleation of particles to proceed and kink sites require a less negative potential. Conversely, in the oxidation or stripping process, those particles with higher coordination are removed from the surface last, and require a larger positive potential to induce oxidation. This prediction again can be attributed to the increased stability of the particles on the surface due to the higher number of nearest neighbors to coordinate.

It should also be recalled that for HOPG substrates the rate of electron transfer for various redox reactions was faster at edge sites than the basal plane, because of increased thermal conductivity for the in-plane axis. This means that for HOPG, not only should the particles be on the lower plane because of a lower free energy, but also because electrochemical reduction/oxidation would occur much faster at sites which were on the in-plane axis. Immediately following deposition the potential was stepped to  $E_2 = .900$  V for oxidation. Images A–C are for a  $t = 100$  second oxidation time using a freshly cleaved HOPG surface, and images D–F are for a  $t = 100$  second oxidation time, using a thermally etched HOPG substrate.

Despite the numerous articles supporting the predictions of the TLK model, it does not correctly predict the behavior seen when using HOPG samples. In the literature many authors show images (AFM, STM, SEM) of metal deposits on HOPG in both locations—on the upper plane of an edge or on the lower plane of an edge. If the metal of interest has been vacuum deposited and annealed on HOPG, then the metal particles follow the TLK model and nucleate on the lower plane of an edge or kink site. However, when metals are electrochemically deposited on the HOPG surface, they almost always appear on the upper edge of a step or kink site. The most notable exception to this was the electrodeposition of  $\text{MoO}_x$  onto the lower plane of step edges by the edge decoration method. To our knowledge, nobody has ever discussed these differences between the predictions of the TLK model, and the observed behavior of electrochemically deposited metals onto HOPG.

Using atomic resolution STM, the surface structure of the HOPG at both step edges and monolayer deep thermally etched pits has been reported. Bard, et al.<sup>26</sup> reported STM images which revealed the “usual” atomic structure for HOPG away from the step or pit edge both on the upper and lower layer of the HOPG. However, at the edges the STM images showed a perturbed structure resulting in a corrugation of the edge itself. This corrugation appeared as an increase in the apparent height ( $\sim 2$  Å) of the upper layer of the HOPG surface, which was attributed to a difference in the work function at the edges that

occur because of the unoccupied  $sp^2$  orbital of the carbon atoms at the edge sites.  $Sp^2$  orbitals react very rapidly with oxygen or other functionalities, and could also be the cause of the height increases seen with STM experiments. Functionalities at the edges may provide a more stabilized environment for the Au particles adsorbed on the surface. The thermodynamic free energy of the particles must be reduced enough relative to the lower plane to overcome the decrease in the electron transfer rates associated with the out-of-plane phase. Furthermore, this stabilization of the particles at the edge sites allows these particles to remain on the surface for long periods of time.

## ACCOMPLISHMENTS

Localized activity at surfaces of corroding specimens was project focus during FY 2001. We presented three papers at international symposia detailing our work in this area. Additionally, we submitted many manuscripts for peer-review and publication in journals read by corrosion scientists and engineers. The base project and techniques developed within have been successfully marketed to the Local and National SNF communities and the DOE Office of Transportation, corrosion of Li-based cathode materials. Several technologies are rapidly being developed that will help DOE Office of Environmental Management (DOE-EM) develop cost-saving cleanup technologies.

## Publications

### In Preparation or Submitted

Boxley, C. J., H. S. White, P. J. Pinhero, and T. E. Lister, “Electrodeposition of Au on HOPG,” submitted to *J. Physical Chemistry B.*, January 2002.

Boxley, C. J., H. S. White, P. J. Pinhero, and T. E. Lister, “Pinning of Au Nanoclusters at Electron Dense HOPG Sites,” in preparation for submittal to *Science* October 2001.

Bruhn, D. F., C. R. Breckenridge, M. N. Tsang, C. S. Watkins, W.E. Windes, F. F. Roberto, R. N. Wright, and P. J. Pinhero, “Gamma and Ultraviolet Irradiation Of Microbes From Spent Nuclear Fuel Storage Pool Environments,” in preparation for

submittal to *J. Environ. and Industr. Microbiol.* October 2001.

Bruhn, D. F., P. J. Pinhero, F. F. Roberto, S. M. Frank, and S. G. Johnson, "Microbial Biofilm Growth on Irradiated Experimental Breeder Reactor (EBR-II) Fuel Cladding in a Radiation Rich Environment," in preparation for submittal to *Appl. Environ. Microbiol.*, October 2001.

Lister, T. E., and P. J. Pinhero, "The Effect of Localized Electric Fields on the Detection of Dissolved Sulfur Species from Type 304 Stainless Steel Using a Scanning Electrochemical Microscope," submitted to *J. Phys. Chem.*, October 2001.

Pinhero, P. J. and C. S. Watkins, "Bioinhibition of Aluminum Alloy 6061 by Bacteria," manuscript in preparation for submittal to *Corrosion* October 2001.

Pinhero, P. J., and T. E. Lister, "Dynamical Observation of Passive Film Evolution on Type 304 Stainless Steel with Scanning Electrochemical Microscopy," submitted to *J. Electrochem. Soc.* October 2001.

Pinhero, P. J., T. E. Lister, and C. R. Breckenridge, "Characterization of Environmental Bacteria by Environmental Scanning Electron Microscopy and Noncontact Atomic Force Microscopy," manuscript in preparation for submittal to *J. Environ. and Industr. Microbiol.*, October 2001.

### Accepted or Published

Lister, T. E., and P. J. Pinhero, "In-vivo Atomic Force Microscopy of Surface Proteins Within

*Deinococcus radiodurans*," *Langmuir*, Vol. 17, 2001, p. 2624.

Lister, T. E., R. N. Wright, P. J. Pinhero, and W. D. Swank, "Corrosion of Thermal Spray Haselloy C-22 Coatings in Dilute HCl," *J. Thermal Spray Technol.*, accepted May 2001.

Mizia, R. E., T. E. Lister, P. J. Pinhero, J. N. Dupont, and C. V. Robino, "Corrosion Performance of a Gadolinium Containing Stainless Steel," *Corrosion/2001*, accepted April 2001.

Pinhero, P. J., T. E. Lister, C. S. Watkins, D. F. Bruhn, and S. M. Frank, "Localized Biocorrosion in Spent Nuclear Fuel Cladding Analogues," *EUROCORR 2001*, accepted June 2001.

### Presentations

Lister, T. E., C. S. Watkins, P. J. Pinhero, and R. E. Mizia, "Corrosion Testing of Gd-Doped Intermetallics Considered as Materials for Constructing Nuclear Waste Storage Containers," *2001 Materials Research Society National Meeting, San Francisco, CA, April 16–20, 2001.*

Pinhero, P. J., D. F. Bruhn, F. F. Roberto, S. M. Frank, and S. G. Johnson, "Biofilm Development on Irradiated Stainless Steel Fuel Claddings in a Hot Cell Environment," *2001 Materials Research Society National Meeting, San Francisco, CA, April 16–20, 2001.*

Pinhero, P. J., T. E. Lister, C. S. Watkins, D. F. Bruhn, and S. M. Frank, "Localized Biocorrosion in Spent Nuclear Fuel Cladding Analogues," *EUROCORR 2001*, in press (2001).

## REFERENCES

1. C. H. Paik, H. S. White, and R. C. Alkire, *J. Electrochem. Soc.*, Vol. 147, 2000, p. 4120.
2. S. E. Werner, C. A. Johnson, N. J. Laycock, P. T. Wilson, and B. J. Webster, *Corros. Sci.* Vol. 40, 1998, p. 465.
3. T. P. Darby and C. M. Wayman, *J. of Crystal Growth*, Vol. 28, 1975, p. 41.
4. C. M. Wayman and T. P. Darby, *J. of Crystal Growth*, Vol. 28, 1975, p. 53.

5. R. Nishitani, A. Kasuya, S. Kubota, and Y. Nishina, *J. Vac. Sci. Technol. B*, Vol. 9, 1991, p. 806.
6. A. Hammiche, R. P. Webb, and I. H. Wilson, *J. Vac. Sci. Technol. B*, Vol. 12, 1994, p. 1413.
7. H. Hovel, Th. Becker, A. Bettac, B. Reihl, M. Tschudy, and E. J. Williams, *J. Appl. Phys.*, Vol. 81, 1997, p. 154.
8. B. Blum, R. C. Salvarezza, and A. J. Arvia, *J. Vac. Sci. Technol. B*, Vol. 17, 1999, p. 2431.
9. J. D. McBride, B. van Tassel, R. C. Jachmann, and T. P. Beebe, Jr., *J. Phys. Chem. B*, Vol. 105, 2001, p. 3972.
10. W. Li, J. A. Virtanen, and R. M. Penner, *Applied Physics Letters*, Vol. 60, 1992, p. 1181.
11. A. Wawro, A. Kasuya, R. Czajka, N. Horiguchi, and Y. Nishina, *Surface and Coatings Technology* Vol. 67, 1994, p. 173.
12. H. Rohrer, *Microelectronic Engineering*, Vol. 27, 1995, p. 3.
13. W. Li, G. S. Hsiao, D. Harris, R. M. Nyffenegger, J. A. Virtanen, and R. M. Penner, *J. Phys. Chem.*, Vol. 100, 1996, p. 20103.
14. J. C. Hulthen and R. P. Van Duyne, *J. Vac. Sci. Technol. A*, Vol. 13, 1995, p. 1553.
15. P. P. Nguyen, D. H. Pearson, R. J. Tonicci, K. Babcock, *J. Electrochem. Soc.*, Vol. 145, 1998, p. 247.
16. K. T. Itaya, *E. Surface Science* Vol. 201, 1988, p. L507.
17. S. A.; Hendricks, Y.; Kim, A. J. Bard, *J. Electrochem. Soc.* Vol. 139, 1992, p. 2818.
18. M. A.; Diaz, G. H.; Kelsall, N. J. Welham, *J. Electroanal. Chem.* Vol. 361, 1993, p. 25.
19. R. T.; Potzschke, C. A.; Gervasi, S.; Vinzelberg, G.; Staikov, W. Lorenz, *J. Electrochimica Acta* Vol. 40, 1995, p. 1469.
20. J. V.; Zoval, R. M.; Stiger, P. R.; Biernacki, R. M. Penner, *J. Phys. Chem.* Vol. 100, 1996, p. 837.
21. H.; Martin, P.; Carro, A.; Hernandez Creus, S.; Gonzalez, R. C.; A. Salvarezza, *J. Arvia, Langmuir* Vol. 13, 1997, p. 100
22. U.; Schmidt, M.; Donten, J. G. Osteryoung, *J. Electrochem. Soc.*, Vol. 144, 1997, p. 2013.
23. G.; Oskam, P. C. Searson, *J. Electrochem. Soc.* Vol. 147, 2000, p. 2199.
24. J. H. Gallego, C. E.; Castellano, A. J.; Calandra, A. J. Arvia, *J. Electroanal. Chem.*, Vol. 66, 1975, p. 207.
25. H. Martin, P. Carro, A.H. Creus, S. Gonzalez, G. Andreasen, R.C. Salvarezza, A.J. Arvia, *Langmuir*, Vol. 16, 2000, p. 2915.
26. H.P. Chang, A.J. Bard, *Langmuir*, Vol. 7, 1991, p. 1143.